Characterisation of Two Calmodulin-Related Calcium Sensors, CaBP7 and CaBP8

Hannah Victoria McCue

Thesis submitted in accordance with the requirements of the University of Liverpool for the degree of Doctor in Philosophy

September 2011

Abstract

The CaBPs are a family of small EF-hand-containing calcium binding proteins with limited homology to calmodulin (CaM). The family comprises seven genes with alternative splicing giving rise to a greater number of protein variants. Two distinct groups exist within the CaBP family based on differences in their cation binding properties and domain organization: CaBPs 1-5 and CaBP7 & 8. CaBPs 1-5 interact with a number of known CaM target proteins but generally exert unique regulatory roles and have been implicated in the regulation of numerous Ca^{2+}-channels. A number of interacting binding partners have also been identified which do not overlap with those of CaM and knockout studies have revealed non-redundant roles for CaBP4 and CaBP5. Much less is known about the functions of CaBP7 and CaBP8 with only a direct interaction with phosphatidylinositol 4-kinase III β (PI4KIIIβ) having been characterized in detail. The research presented in this thesis focused on the less well characterised members of this protein family, CaBP7 and CaBP8.

Bioinformatic analyses revealed that CaBP7 and CaBP8 form a distinct group of calcium sensors from the rest of the CaBP family and are highly conserved throughout evolution. Examination of CaBP sequences present in species representing important evolutionary nodes indicated that the CaBP family first arose with the appearance of early vertebrates. The primordial CaBP family members, CaBP1S and CaBP8, were identified in lamprey, the closest living relative to the common vertebrate ancestor. The expansion in the number of CaBP proteins from lamprey to mammals largely coincides with a whole genome duplication event occurring before the divergence of cartilaginous fish. A transient expansion of the group encompassing CaBPs1-5 between the divergence of cartilaginous fish and the emergence of bony fish is also apparent.

Examination of the targeting mechanisms of CaBP7 and CaBP8 demonstrated that these proteins form a unique class of calcium sensors which associate with cellular membranes via a C-terminal tail anchor. The membrane topology of CaBP7 and

CaBP8 was found to be characteristic of the tail anchored class of integral membrane proteins and was consistent with the previously reported interaction with the cytosolic enzyme PI4KIIIβ. Further examination of their subcellular distributions revealed that CaBP7 and CaBP8 localise to the trans-Golgi network and to vesicles which were positive for markers of the late endosomal and lysosomal pathway. This is the first reported instance of a CaM-related calcium sensor localising to membranes of acidic compartments.

CaBP7 also co-localised with markers of late endosomes and lysosomes in dividing cells. These CaBP7 positive vesicles redistributed to the vicinity of the interzonal microtubules and opposite poles of the spindle during cytokinesis. In accordance with previous reports, knockdown of CaBP7 in HeLa cells resulted in an increase in the number of binucleate cells, inferring that CaBP7 plays an important role in the regulation of cytokinesis. CaBP7 was shown to co-localise with VAMP7, a protein known to be important for Ca^{2+}-regulated lysosomal exocytosis and also for the completion of cytokinesis. In addition CaBP7 localised to VSVG positive vesicles which have been previously shown to directly dock and fuse with the plasma membrane at the midzone. Lysosomes are emerging as important platforms for Ca^{2+}-signalling, and proteins important for the release of lysosomal Ca^{2+} stores have also been implicated in mitosis. This may suggest a role for CaBP7 in the regulation of Ca^{2+} signalling processes at the lysosomal membrane during both interphase and in dividing cells.

Finally the use of nuclear magnetic resonance (NMR) spectroscopy led to the partial backbone and side chain assignment of a 100 amino acid N-terminal fragment of CaBP7. Using this data the secondary structure of this fragment was calculated and closely resembled that of Ca^{2+}-bound CaM and CaBP1S N-termini. Spectra for apo CaBP7 were distinct from that of Ca^{2+}-saturated CaBP7 implying that the protein undergoes a significant conformational change upon Ca^{2+} binding. In addition, the use of native PAGE demonstrated a shift in mobility of CaBP7 1-100 upon addition of Ca^{2+} but not Mg^{2+}. Continued NMR analysis of CaBP7 will be required for the determination of a high-resolution structure for this protein.

Acknowledgements

First and foremost I would like to thank my two excellent supervisors, Dr Lee Haynes and Prof Bob Burgoyne who have offered invaluable guidance and support throughout my PhD. I was privileged to be Lee Haynes' first PhD student and he has taught me an enormous amount during my time in Red Block. I would like to give particular thanks to Prof Alexei Tepikin for allowing me to use the microscopes in Blue Block, Dr Andy Herbert for sharing his knowledge of protein expression and NMR, and Dr Dave Rooks for his help constructing phylogenetic trees. Also, Prof Lu-Yun Lian, Dr Sylvie Urbé, Dr Ian Prior, Dr Steve Royle, Dr Pryank Patel and Dr Marie Phelan for reagents and help provided during the course of this project. I also acknowledge the Wellcome Trust for providing generous funding for my Masters degree and PhD. Huge thanks to all the people who helped me proofread this thesis – Martin Smith, Ewan Harney, Matt Edmonds, Liam Cheeseman, Mark Skidmore, Eileen McCue and of course Lee Haynes. I would like to thank everyone in Red Block, past and present, including Alan, Jeff, Helen B, Leanne, Vicky, Matt, James, Dayani, Xi and Sudhanvah. Special thanks goes to two fantastic friends who I met during my time in the lab, Ciara Walsh and Helen Jones – thanks for all your support and for listening to my many rants.

I have made some incredible friends during my time as a postgraduate and it is these people who have helped to keep me sane through the past four years. Thanks goes to Liam for the many times he has helped me to unwind after a frustrating week in the lab. To Ewan for listening to me whinge, sharing my taste in music and for his advice to not use the word discombobulate in my thesis (oops!). To Martin for providing me with a distraction from work in the postgraduate society and also for his amazing generosity. To Gyuri Lur, Jonathan Woodsmith, and Dave Rooks, for the laughs and the drunken nights out. To my fellow PhD peers and ex-housemates Rob and Dan for all the chats and fun times on Allerton Road. To Matt R and Matt G for indulging my love of old board games and introducing me to some not-so politically correct new ones! To my best friends Sara and Jill who have provided tremendous support throughout everything from St Hilda's to undergrad to the end of my PhD. Thanks also to all the people whose names are too many to mention here but who have helped make my time as a PhD student such a wonderful experience.

Finally, a HUGE thank you goes to my family, in particular my Mum who has always provided unconditional love and support. She has listened to me rant on and on about my work and was always there to help me through and calm me down when it all got too much. I couldn't have done this without you.

Publications

Work presented in this thesis has been published in part in the following papers:

McCue HV, Burgoyne RD, Haynes LP.(2011) Determination of the membrane topology of the small EF-hand Ca2+-sensing proteins CaBP7 and CaBP8. *PLoS One.***6**(3):e17853.

McCue HV, Haynes LP, Burgoyne RD. (2010) Bioinformatic analysis of CaBP/calneuron proteins reveals a family of highly conserved vertebrate Ca2+ -binding proteins. *BMC Res Notes.***3**:118.

McCue HV, Burgoyne RD, Haynes LP. (2009). Membrane targeting of the EF-hand containing calcium sensing proteins CaBP7 and CaBP8. *Biochem Biophys Res Commun***380**(4):825-31

Table of Contents

Abbreviations

$[Ca^{2+}]$	Ca^{2+} concentration
$[Ca^{2+}]_i$	Intracellular free Ca^{2+} concentration
2D	Two dimensional
3D	Three Dimensional
ADP	Adenosine diphosphate
AOBS	Acousto-optical beam splitter
AP	Adaptor protein
Asna1	Arsenical pump-driving ATPase
ATP	Adenosine triphosphate
BAPTA	1, 2-bis(o-aminophenoxy)ethane-N, N, N', N'-tetraacetic acid
BFA	Brefeldin A
BLAST	Basic local alignment search tool
BLAT	BLAST-like alignment tool
BSA	Bovine serum albumin
Ca^{2+}	Calcium ion
CaBP	Calcium binding protein
CaBP1L	CaBP1 long isoform
CaBP1S	CaBP1 short isoform
CaBP2L	CaBP2 long isoform
CaBP2S	CaBP2 short isoform
CaM	Calmodulin
CaMKI	Calmodulin kinase I
cAMP	Cyclic adenosine monophosphate
CBFA2	Core binding factor A2
CBL	Calcineurin B-like
CCDS	Consensus coding sequence
CCPN	Collaborative computing project for NMR
CDF	Calcium dependent facilitation
CDI	Calcium dependent inactivation
CHMP	Charged MVB protein
CHO	Chinese hamster ovary
CICR	Calcium-induced calcium-release
Cl^-	Chloride ion
CSI	Chemical shift index
CSNB	Congenital Stationary night blindness
CSV	Constitutive secretory vesicle
C_v	Voltage dependent calcium channel
D2R	Dopamine D2 receptor
DAG	Diacylglycerol
DANGLE	Dihedral angles from global likelihood estimate
DAPI	4', 6-diamidino-2-phenylindole
DMEM	Dulbecco's Modified Eagle Medium

DMSO	Dimethyl Sulphoxide
DNA	Deoxyribonucleic acid
dNTP	Deoxyribonucleotide triphosphate
DREAM	Downstream regulatory element antagonist modulator
EBI	European bioinformatics institute
ECFP	Enhanced cyan fluorescent protein
ECL	Enhanced chemiluminescence
EDTA	Ethylenediamine tetraacetic acid
EF1, EF2, EF3, EF4	EF-hand 1, EF-hand 2, EF-hand 3, EF-hand 4
EGFP	Enhanced green fluorescent protein
EGTA	Ethylene glycol tetraacetic acid
EMBL	European molecular biology laboratory
ER	Endoplasmic reticulum
ERG	Electroretinography
ESCRT	Endosomal sorting complexes required for transport
EYFP	Enhanced yellow fluorescent protein
FBS	Foetal bovine serum
FITC	Fluorescein isothiocyanate
FRET	Fluorescence resonance energy transfer
GABA	γ-amino-butyric acid
GAPDH	Glyceraldehyde 3-phosphate dehydrogenase
GC	Guanylyl cyclase
GCAP	Guanylyl cyclase activating protein
GPCR	G-protein coupled receptor
GST	Glutathione S-transferase
GTP	Guanosine triphosphate
His_6	Hexa-histidine
HRS	Hepatocyte growth factor-regulated tyrosine kinase substrate
HSQC	Heteronuclear single-quantum correlation
IL1RAPL	Interleukin-1 receptor accessory protein-like
IP_3	Inositol 1,4,5-trisphosphate
IP_3R	Inositol 1,4,5-trisphosphate receptor
IPTG	Isopropyl β-D-1-thiogalactopyranoside
ITC	Isothermic titration calorimetry
K^+	Potassium ion
KChIP	Potassium channel interacting protein
KHM	Potassium, HEPES, Magnesium
KPSI	Kilopound per square inch
K_v	Voltage dependent potassium channel
LAMP1	Lysosomal-associated membrane protein 1
LAP	Lysosomal acid phosphatase
LB	Lysogeny Broth
LC3	Light chain 3 of MAP1A/B
LCA	Leber's congenital amaurosis
LGCC	Ligand gated Ca^{2+} channel
LIMP2	Lysosomal integral membrane protein 2

LKU	Lipid kinase unique
LTD	Long term depression
LTP	Long term potentiation
M6PR	Mannose 6-phosphate receptor
MAP1A/B	Microtubule associated protein 1A/B
MAPK	Microtubule associated protein kinase
mCherry	Monomeric cherry fluorescent protein
MDCK	Madin-Darby Canine Kidney
Mg^{2+}	Magnesium ion
mGluR	Metabotropic glutamate receptor
MLCK	Myosin light chain kinase
mOrange	Monomeric orange fluorescent protein
mRNA	Messenger ribonucleic acid
MVB	Multivesicular body
Myo1c	Myosin 1c
N2A	Neuroblastoma 2A
Na^{+}	Sodium ion
NAADP	Nicotinic acid adenine diphosphate
NCBI	National centre for biotechnology information
NCS	Neuronal calcium sensor
NCX	Na^{+}/Ca^{2+} exchanger
NEAA	Non-essential amino acids
NMDA	N-methyl-D-aspartic acid
NMR	Nuclear magnetic resonance
PAGE	Polyacrylamide gel electrophoresis
PBS	Phosphate buffered saline
PBSB	Phosphate buffered saline with BSA
PBST	Phosphate buffered saline with Tween 20
PCR	Polymerase chain reaction
PDB ID	Protein database identification
PH	Pleckstrin homology
pI	Isoelectric point
$PI(3,4,5)P_3$	Phosphatidylinositol 3, 4, 5-trisphosphate
$PI(4,5)P_2$	Phosphatidylinositol 4, 5-bisphosphate
PI3K	Phosphatidylinositol 3-kinase
PI4K	Phosphatidylinositol 4-kinase
PI4P	Phosphatidylinositol 4-phosphate
PKC	Protein kinase C
PLC	Phospholipase C
PM	Plasma membrane
PMCA	Plasma membrane Ca^{2+}-ATPase
PtdIns	Phosphatidylinositol
PTM	Pichia trace metal
PTV	Piccollo bassoon vesicle
RFP	Red fluorescent protein
RNAi	Ribonucleic acid interference

rpm	Revolutions per minute
RyR	Ryanodine receptor
SCP	Sarcoplasmic Ca^{2+} binding protein
SDS	Sodium dodecyl sulphate
SERCA	Sarcoplasmic/endoplasmic reticulum Ca^{2+}-ATPase
siRNA	Short interfering ribonucleic acid
SNAP29	Synaptosomal-associated protein 29
SNARE	Soluble NSF attachment protein receptor
SOC	Super optimal broth with catabolite suppression
SOCC	Store operated Ca^{2+} channel
SP2	Spectrophotometer detection system 2
SRP	Signal recognition particle
SUMO	Small Ubiquitin-like Modifier
TA	Tail anchor
TAE	Tris base, acetic acid, EDTA
TEV	Tobacco etch virus
TGN	Trans-Golgi network
TIRF	Total internal reflection fluorescence
T_m	Melting temperature
TMD	Transmembrane domain
TOM20	Translocase of outer mitochondrial membranes 20 kDa
TPC	Two pore channel
TRP	Transient receptor potential
U	Unit of enzyme activity
UTR	Untranslated region
UV	Ultraviolet
VAMP7	Vesicle associated membrane protein 7
VGCC	Voltage-gated Ca^{2+} channel
VILIP	Visinin-like protein
VSVG	Vesicular stomatitis virus G
WGD	Whole genome duplication
ΔG	Change in Gibb's free energy

Chapter 1:

Introduction

1.1. An Overview of Calcium Signalling

The calcium ion (Ca^{2+}) is involved in the regulation of almost all cellular processes making it the most versatile intracellular messenger known to date (Berridge *et al*., 2000, Clapham, 2007). It modulates a plethora of cellular functions over time scales ranging from microseconds to years (Petersen *et al*., 2005). It is this promiscuity that makes calcium signalling integral to all living processes.

In most cells, calcium signalling events are initiated by an increase in cytoplasmic Ca^{2+}. At resting levels the concentration of intracellular (cytoplasmic) free Ca^{2+} ($[Ca^{2+}]_i$) in cells is estimated at ≈100 nM, but, when opened, channels on the plasma membrane (PM) and endoplasmic reticulum (ER) can elevate $[Ca^{2+}]_i$ to over 1 µM (Bootman *et al*., 2001). Due to unique combinations of channels, ATPases and Ca^{2+} sensors, each cell type possesses different calcium signalling properties. Resting $[Ca^{2+}]_i$ is maintained by membrane pumps and ion exchangers which remove Ca^{2+} from the cytosol and transport it either out of the cell, or into intracellular stores (Clapham, 2007) (Figure 1.1). Some Ca^{2+}-binding proteins, restricted to specific cellular locations, are also important in buffering $[Ca^{2+}]_i$.For instance, in the ER where $[Ca^{2+}]$ is high, the Ca^{2+} buffer, calreticulin, can bind 20 mol of Ca^{2+} per mol of protein which greatly increases the capacity of the ER as an intracellular Ca^{2+} store (Michalak *et al*., 2009). $[Ca^{2+}]_i$ is therefore strictly regulated using numerous different mechanisms.This tight regulation prevents persistent and potentially cytotoxic elevations in $[Ca^{2+}]_i$, whilst increasing the dynamic range of Ca^{2+} signals.

Elevations of $[Ca^{2+}]_i$ result from both influx of extracellular Ca^{2+} at the PM and release of Ca^{2+} from intracellular stores (Figure 1.1). Cells possess a variety of families of PM Ca^{2+} influx channels, each with unique mechanisms of activation. Voltage-gated Ca^{2+} channels (VGCCs) are activated by depolarisation of the PM and are usually found in excitable cells (Lukyanetz, 1997). Ligand-gated Ca^{2+} channels (LGCCs) are activated by binding of a specific ligand to the extracellular domain of the channel (Barritt, 1999). These are usually found in secretory cells and on nerve terminals and include the well-known NMDA receptor. Finally, store operated Ca^{2+}

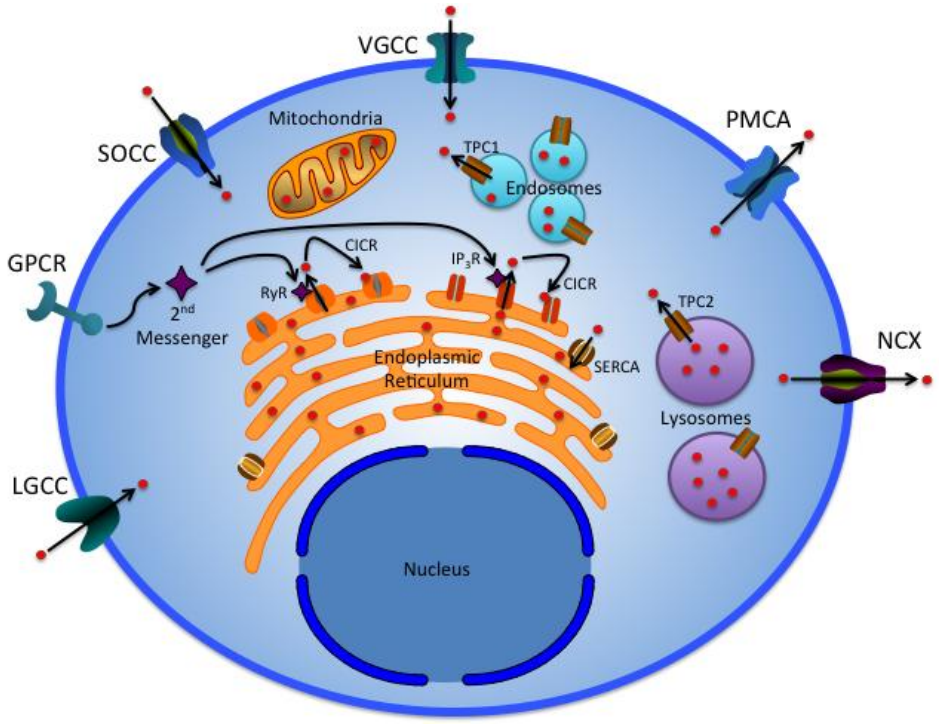

Figure 1.1. An Overview of calcium Signalling. Ca^{2+} influx into the cell is mediated by voltage-gated Ca^{2+} channels (VGCC), Ligand-gated Ca^{2+} channels (LGCC), or store operated Ca^{2+} channels (SOCC). Binding of extracellular agonists to G-protein coupled receptors (GPCRs) stimulates the production of second messengers such as IP_3 and cyclic ADP ribose which bind to and activate IP_3Rs and RyRs on the ER. Both IP_3Rs and RyRs are sensitive to increases in $[Ca^{2+}]_i$, allowing the signal to be propagated through the process of calcium-induced calcium-release (CICR). SOCCs on the PM are opened upon activation of ER IP_3Rs. Ca^{2+} signals are attenuated by several mechanisms including: transport of cytoplasmic Ca^{2+} into the ER by the sarco/endoplasmic reticulum Ca^{2+}-ATPase (SERCA) or efflux of Ca^{2+} from the cell by either the PM Ca^{2+}-ATPase (PMCA) or the Na^+/Ca^{2+} exchanger (NCX). Other organelles such as the mitochondria, lysosomes and endosomes also sequester Ca^{2+}. Ca^{2+} from endosomes and lysosomes is released via the NAADP-sensitive two pore channels, TPC1 and TPC2, respectively.

channels (SOCCs) are activated in response to the depletion of intracellular Ca^{2+} stores (Smyth *et al*., 2006). These are thought to be one of the most ubiquitous types of Ca^{2+} channels (Bootman *et al*., 2001).

Ca^{2+} release from intracellular stores is triggered by messenger activation of channels on the ER or by activation of the mitochondrial permeability transition. The mitochondrial permeability transition pore opens under conditions of mitochondrial Ca^{2+} overload coupled with oxidative stress, elevated phosphate, or adenine nucleotide depletion. This results in extensive mitochondrial swelling, eventual rupture and subsequent release of intermembrane components, including

stored Ca^{2+}. This results in the induction of apoptosis pathways and, ultimately, cell death (Halestrap, 2009).

Release of Ca^{2+} from the ER occurs through two families of ion channels, inositol trisphosphate receptors (IP_3Rs) and ryanodine receptors (RyRs). IP_3Rs are found ubiquitously whereas RyRs are predominantly restricted to excitable cell types. These receptors are large tetrameric complexes and contain cytosolic domains which possess a number of modulatory sites. Binding of extracellular agonists to G-protein coupled receptors (GPCRs) stimulates the production of second messengers such as inositol trisphosphate (IP_3) and cyclic ADP ribose which bind to and activate IP_3Rs and RyRs, respectively.The binding of ligand increases the sensitivity of the channels to $[Ca^{2+}]_i$. Both types of receptor are also sensitive to local increases in $[Ca^{2+}]_i$, resulting in calcium-induced calcium-release (CICR) where increases in $[Ca^{2+}]_i$ induce further release from intracellular stores. At higher $[Ca^{2+}]_i$, the sensitivity of both IP_3Rs and RyRs decreases and the channels begin to close once again (Clapham, 2007), accounting for the classic bell-shaped Ca^{2+} dose response curve for both classes of channel.

A less well-understood mechanism of intracellular Ca^{2+} release is modulated by NAADP via two pore channels (TPCs) on the membranes of acidic subcellular compartments. TPCs are relatively novel members of the voltage gated ion channel superfamily. Three TPC genes have been reported although TPC3 is absent in most primates and some rodent species. TPC2 mRNA is detectable in most human tissues with higher levels observed in the liver and kidneys. TPC2 has been shown to underpin NAADP-induced Ca^{2+} release from lysosomal stores, whereas TPC1 and TPC3 are localised to endosomal membranes and may permit NAADP-mediated Ca^{2+} release from these classes of acidic Ca^{2+} stores. Stimulation of TPC2 with NAADP in the range of 10 nM - 10 µM induces Ca^{2+} release whereas higher NAADP concentrations do not elicit a response suggesting that high ligand concentrations desensitize the channels (Calcraft *et al.*, 2009).

Specific changes occur in the cell based on the type of Ca^{2+}-signal that is generated. This depends upon the route of entry into the cell, the local site of action and the

modulation of the signal. Unique Ca^{2+} signals can therefore be generated within distinct locations and organelles in the cell. Regulation of the amplitude, frequency and duration of Ca^{2+} spikes is also important with some Ca^{2+}-dependent processes responding only at optimal frequencies of Ca^{2+} oscillations (Thomas *et al*., 1996). It is these parameters which allow this simple metal ion to carry out such a wide range of essential physiological functions.

Ca^{2+} microdomains are formed from elementary Ca^{2+} release events which have been named according to the particular release channel involved. Events involving IP_3Rs are named 'blips' and 'puffs' whereas in muscle cells, which primarily employ RyRs, these events are called 'quarks' and 'sparks'. A Ca^{2+} 'blip' or 'quark' occurs due to the opening of single IP_3Rs or RyRs, respectively, and gives rise to a Ca^{2+} signal lasting ≈200 ms with an amplitude of less than 30 nM. These signals usually spread no further than 1 - 2 μm. The coordinated release of Ca^{2+} from a cluster of IP_3Rs (or RyRs) is termed a Ca^{2+} 'puff' (or 'spark') which persists for ≈500 ms, has a peak amplitude of ≈200 nM and extends less than 6 μm. Finally, if the Ca^{2+} released in a 'puff' event is sufficient to activate a neighbouring cluster of IP_3Rs this can give rise to a Ca^{2+} 'wave' which can spread rapidly throughout the cytoplasm. The spread of these different types of Ca^{2+} signal depends upon their ability to overcome Ca^{2+} buffering and uptake mechanisms. These mechanisms act to restrict Ca^{2+} signals and therefore modulate the activity of the channels involved in signal generation (Berridge *et al*., 2000, Laude and Simpson, 2009). Removal of Ca^{2+} from the cytosol prevents both CICR of IP_3Rs and RyRs, and the stimulation of SOCCs, thereby terminating the Ca^{2+} signal.

Ca^{2+} acts as a second messenger regulating many different processes including secretion, muscle contraction, fertilisation, gene transcription and cell proliferation (Bootman *et al*., 2001). In order for this ion to carry out such a wide range of functions it must be able to activate downstream signalling pathways. To do this a variety of specific Ca^{2+}-binding proteins have evolved. As introduced previously, certain Ca^{2+}-binding proteins have a very high affinity for Ca^{2+} and will be saturated even under resting conditions. These proteins are involved in the buffering of $[Ca^{2+}]_i$ rather than signal transduction. Other proteins act as Ca^{2+} sensors and participate in

signal transduction, binding Ca^{2+} and becoming activated in response to local or global elevations in $[Ca^{2+}]_i$at specific cellular locations (Schwaller, 2009). In general Ca^{2+}-buffering proteins exhibit little conformational change on Ca^{2+} binding. In contrast, Ca^{2+}-sensors undergo significant conformational shifts and thereby expose unique binding sites for specific target proteins and nucleic acids.

1.2. Ca^{2+} Binding Motifs

The effects of increased $[Ca^{2+}]_i$ are mediated indirectly through the actions of various Ca^{2+}-binding proteins. Each Ca^{2+}-binding protein possesses unique properties which allow it to decipher different types of Ca^{2+} signal and elicit the relevant biochemical response. As such, Ca^{2+}-binding proteins must be able to respond to short-lived or local $[Ca^{2+}]_i$ fluxes and have therefore evolved to bind and respond very rapidly to changes in $[Ca^{2+}]_i$ (Schwaller, 2009). The majority of Ca^{2+}-binding proteins belong to a family of homologous proteins containing Ca^{2+} chelating EF-hand motifs, however, other Ca^{2+} binding domains also exist such as the C2 domain (Rizo and Sudhof, 1998) and the endonexin fold (Kourie and Wood, 2000).

C2 domains, also known as Ca^{2+} and lipid binding domains, are named for their homology with the second conserved regulatory domain of protein kinase Cβ and consist of 130 amino acids in an eight-stranded antiparallel β sandwich. Ca^{2+} is bound along one edge of the structure by three Ca^{2+} chelating loops containing aspartate residues. Ca^{2+}-bound C2 domains bind to negatively charged phospholipids and therefore Ca^{2+} binding can act as an electrostatic switch that allows soluble C2 domain containing proteins to associate with membranes. C2 domain containing proteins are common in signal transduction and membrane trafficking, and include phosphatidylinositol 3-kinases (PI3Ks), protein kinase C (PKC), synaptotagmins, RIM proteins and rabphillin 3A (Rizo and Sudhof, 1998). The affinities of C2 domains vary, as do the number of Ca^{2+}-binding sites with some C2 domain proteins having evolved divergent functions which do not require Ca^{2+} binding activity (Clapham, 2007, Rizo and Sudhof, 1998).

The endonexin fold domain is a 34 kDa conserved domain found in the C-termini of proteins of the annexin family of Ca^{2+}/phospholipid binding proteins (Kourie and Wood, 2000). This domain consists of four Ca^{2+}-binding repeats (eight in annexin VI) of an ~70 amino acid sequence. The annexins form a diverse family of Ca^{2+}-binding proteins which form voltage-dependent Ca^{2+} channels in lipid bilayers and are found throughout all eukaryotic kingdoms (Kourie and Wood, 2000). The N-termini of annexins are significantly more variable than the endonexin fold-containing C-termini and it is this region which permits this class of proteins to function in a diverse range of cellular processes. Annexins have reported roles in endo- and exocytosis, regulation of the cytoskeleton, and membrane conductance and organisation (Fatimathas and Moss, 2010).

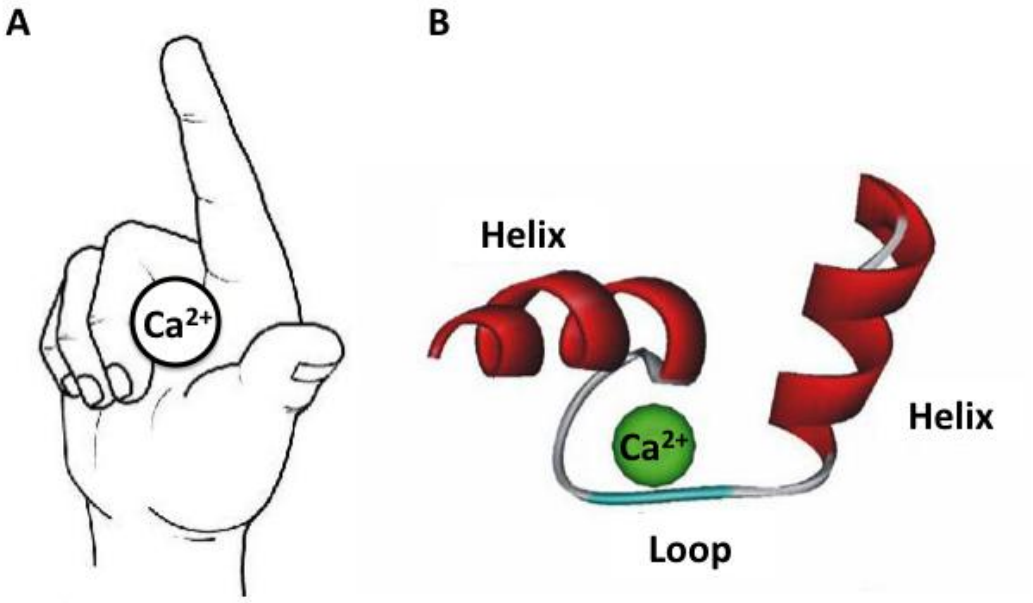

Figure 1.2. **The EF-hand motif has a typical helix-loop-helix structure.** A) The structure of an EF-hand is said to resemble the forefinger and thumb of a hand with Ca^{2+} held at the base of the two digits. B) Ribbon representation of the structure of the first EF-Hand from calmodulin with a bound Ca^{2+} ion (adapted from (Burgoyne, 2007)).

1.3. EF-hand motifs

This thesis will focus on the EF-hand family of Ca^{2+} binding proteins - one of the largest protein families containing a single type of motif. Analysis of the human genome alone has identified 242 proteins containing EF-hand domains and over 600

have been identified in total from various different species (Schwaller, 2009). The EF-hand motif derives its name from the E and F helices of parvalbumin, the protein in which the motif was first discovered. A twelve amino acid linking loop between the two helices forms the Ca^{2+} binding site and gives the motif a characteristic helix-loop-helix structure (Figure 1.2). In the canonical EF-hand, residues 1, 3, 5, 7, 9, and 12 of the binding loop chelate Ca^{2+}. This forms a pentagonal bi-pyramidal array of seven oxygen ligands. Residues 1, 3 and 5 have side-chain oxygens and are usually aspartate residues. Residue 12 is nearly always a glutamate which provides a bidentate oxygen ligand from its two side-chain caboxylate oxygens. Residue 7 coordinates Ca^{2+} with a main chain oxygen and residue 9 hydrogen-bonds with a water molecule to provide the final oxygen ligand (Nelson and Chazin, 1998). This canonical motif is found in most EF-hand proteins, however, some atypical binding loops have been described, although the relevance to their structure and function is not yet known (Gifford *et al*., 2007).

The EF-hand superfamily can be divided into two subsets: the Ca^{2+}-buffers and the Ca^{2+}-sensors. The key differences between the two classes are their Ca^{2+} affinities and their ability to undergo shifts in conformation (Nelson and Chazin, 1998). Ca^{2+}-buffers usually have high Ca^{2+} binding affinities and do not undergo a significant conformational change upon Ca^{2+} binding. They constitute a smaller subset of proteins and help to modulate Ca^{2+} signals spatially and temporally, helping the transmission of the signal through the cell, or sequestering the ion from the cytoplasm. Calbindin D9k is a high affinity Ca^{2+}-buffer that has roles in Ca^{2+} uptake and transport. Upon Ca^{2+} binding, calbindin D9k undergoes only minor conformational changes which are key for maintaining its function. Larger conformational changes would result in the exposure of hydrophobic regions which would reduce its Ca^{2+} affinity and hence alter its binding capacity (Kordel *et al*., 1993). Similarly, parvalbumin, which has roles in the quenching of Ca^{2+} signals in contracting muscle cells, does not undergo a change in conformation upon Ca^{2+} binding. Parvalbumin may also protect against Ca^{2+} toxicity in non-muscle cells and act to sequester Ca^{2+} ions away from the cytosol preventing the activation of signal transducers such as calmodulin (CaM). The roles of parvalbumin require specific

Ca^{2+} binding characteristics but a Ca^{2+}-induced conformational change in the protein would likely adversely influence these properties (Pauls *et al*., 1996).

Although Ca^{2+} buffers play important regulatory roles in intracellular calcium signalling, the majority of EF-hand containing proteins are Ca^{2+}-sensors which are responsible for the activation of downstream signalling pathways in response to changes in $[Ca^{2+}]_i$ (Gifford *et al*., 2007). Ca^{2+}-sensors generally exhibit a large shift in conformation, often exposing hydrophobic surfaces which provide a means to interact with binding partners (Nelson and Chazin, 1998). EF-hand containing Ca^{2+}-sensors will be the focus of this thesis and will therefore be discussed in more detail in the following sections.

1.4. Factors Affecting Ca^{2+}-binding to EF-hand motifs

The core structure of EF-hand motifs is generally well conserved with the flanking regions containing more variation. This variation gives rise to dissociation constants ranging from 10^{-7} to 10^{-5} $molL^{-1}$(Gifford *et al*., 2007). The relative stability of the Ca^{2+}-bound form ("on" form) and the Ca^{2+} unbound form ("off" form) of a Ca^{2+}-sensor determines its overall affinity for Ca^{2+}. The stability of the protein is defined by the energy change upon the transition from a Ca^{2+}-bound state to an unbound state – the "off rate". In general, the more stable the Ca^{2+}-bound form, the greater the energy difference between the two forms. If a protein is unstable in the Ca^{2+}-free form, the protein will have a greater Ca^{2+} binding affinity (Gifford *et al*., 2007). CaM can be used as an example of this: the C-terminal EF-hands have a higher affinity for Ca^{2+} than the N-terminal domain which is thought to be due to the greater instability of the C-terminal domain in its Ca^{2+}-free form. The residues of the flexible linker between the two domains have been suggested to be the cause of this instability: the linker increases the stability of the Ca^{2+}-free state therefore decreasing the Ca^{2+}-affinity. Domain linking regions and other regions flanking the EF-hands can therefore influence the stability of the Ca^{2+}-unbound state of a protein and may help to fine tune the Ca^{2+}-affinity of EF-hand motifs (Gifford *et al*., 2007). In addition to this, dissociation kinetics are important for the control of Ca^{2+} sensor function in order to transduce a signal at the correct time and for the desired duration. In the process of skeletal muscle contraction, the Ca^{2+} released from the

sarcoplasmic reticulum initially binds to troponin C which triggers contraction by the tropomyosin complex. After a brief lag period, the Ca^{2+} then starts to bind to parvalbumin which sequesters it away from troponin C and inactivates contraction. The kinetics of Ca^{2+} dissociation are therefore important for the proper execution of this process (Renner *et al*., 1993, Pechere *et al*., 1977). The 9^{th} position in the Ca^{2+}-binding loop of the EF-hand motif is thought to be important in determining this dissociation rate. Substitutions at this position, to test different amino acid side chains of varying size and charge, have been shown to affect the dissociation rate but not the Ca^{2+}-affinity. Long or acidic side chains at position 9 of the binding loop were found to cause slower dissociation rates due to steric hindrance or electrostatic barriers, respectively (Renner *et al*., 1993). Ca^{2+} buffers have slower dissociation rates and therefore remain bound to Ca^{2+} for longer.

In addition to Ca^{2+},EF-hands can also bind other similar sized divalent and trivalent ions. As most of these ions exist at only very low concentrations in the cell, this does not usually pose a problem. Free magnesium ions (Mg^{2+}), however, are present at estimated cellular concentrations of 0.5 - 5.0 mM (Romani and Scarpa, 1992) and binding of this ion can decrease the Ca^{2+} affinity of many EF-hand containing proteins (Gifford *et al*., 2007). Each individual EF-hand can be categorised based on their specificity for Ca^{2+} or Mg^{2+}. Sites which bind to either Ca^{2+} or Mg^{2+} are known as structural sites whereas sites which have a higher affinity for Ca^{2+} are known as regulatory sites. In order to discriminate over the 10^2 - 10^4 -fold excess of Mg^{2+} in the cell, the structure of regulatory EF-hands prevents formation of the required six-fold co-ordination in the preferred smaller binding site. Despite this specificity, many regulatory sites still bind to Mg^{2+} under resting conditions, although usually form only a four-fold co-ordination. This therefore has no effect on the overall conformation of the protein. This can be observed in CaM where the conformation of the ion free form is almost identical to that of the Mg^{2+}-bound form (Gifford *et al*., 2007, Ohki *et al*., 1997).

Conversely, structural sites have a much higher affinity for Mg^{2+} and, in many cases, Mg^{2+} binding can regulate the protein's Ca^{2+}-binding affinities. In contrast to the effect of Mg^{2+}-binding to regulatory sites, Mg^{2+}-binding to structural sites can also

induce conformational changes and in some cases can bring about functions distinct from those carried out upon Ca^{2+}-binding (Gifford *et al*., 2007, Aravind *et al*., 2008). DREAM (or KChIP3) represents a key example of this. Mg^{2+}-binding stabilises the monomeric form of DREAM and is required for its interaction with specific 'DRE' DNA target elements which results in the transcriptional repression of prodynorphin and c-fos genes. Binding of Ca^{2+} causes a conformational change and subsequent dimerization of DREAM, which disrupts DNA binding and releases transcriptional repression (Osawa *et al*., 2005). Mg^{2+} is therefore physiologically important for the regulation of EF-hand proteins. This cation can serve a structural purpose to stabilise the Ca^{2+}-free form allowing Ca^{2+}-independent interactions to occur and can also modulate the Ca^{2+}-binding affinity of individual EF-hands.

EF-hand motifs nearly always occur in pairs and this is presumed to be important for protein stabilization, increasing Ca^{2+}-affinity and allowing cooperativity of Ca^{2+}-binding. In support of this, no proteins containing a single EF-hand motif have been identified to date and even if one of the EF-hands in a pair is non-functional the symmetry of their structure is often maintained. For example, EF2 in the invertebrate protein, sarcoplasmic Ca^{2+}-binding protein (SCP), has an insertion which inactivates this EF-hand yet it is still paired with the functional EF1 motif and the two-fold symmetry is approximately preserved (Vijay-Kumar and Cook, 1992). There is huge diversity in the packing of EF-hands in Ca^{2+} binding proteins with proteins containing anything from 2 to 12 motifs (Grabarek, 2006). This diversification is further increased by the ability of some EF hands to dimerise. For example the S100 proteins can dimerise to generate a unit comprising four EF-hands or in calpain the unpaired 5^{th} EF-hand can dimerise with other calpain monomers to give a unit containing ten EF-hands (Nelson and Chazin, 1998). The majority of the EF-hand family of proteins, however, contain two pairs of EF-hands as in CaM and troponin C (Grabarek, 2006). Phylogenetic studies have suggested that the EF hand protein family may have derived from a four EF-hand ancestor gene through tandem gene duplication. In support of this theory, CaM, a ubiquitous protein containing four EF-hand motifs, is conserved in all eukaryotic cell types (Niki

et al., 1996) and many other EF-hand containing Ca^{2+} sensors have been discovered with a high degree of homology to this protein.

1.5. Calmodulin

CaM was discovered in 1970 and is a small (148 amino acids) acidic protein (pI ~3.9) containing four EF-hand motifs. CaM is the most ubiquitous Ca^{2+} binding protein and is involved in the regulation of many essential physiological processes including cell motility, exocytosis, cytoskeletal assembly and modulation of intracellular Ca^{2+} and cAMP concentrations. This protein has been highly conserved throughout evolution as it is found in all eukaryotes and is 100% identical across all vertebrates at the amino acid level (Toutenhoofd and Strehler, 2000). Although CaM appears first in eukaryotic organisms, CaM-like proteins have also been identified in bacteria (Friedberg and Rhoads, 2001). Its ubiquitous nature and ability to interact with and regulate multiple protein targets has meant that CaM is the most extensively studied Ca^{2+} sensor and can often serve as a useful prototype for understanding other members of the EF-hand protein family.

Signal transduction through EF-hand containing proteins typically occurs following a Ca^{2+}-induced conformational change. This is exemplified by CaM, in which Ca^{2+} binding brings about a conformational change that exposes hydrophobic residues and mediates binding to target proteins. The first two EF-hands of CaM form an N-terminal globular domain which is joined by a flexible linker to a highly homologous C-terminal region encompassing the third and fourth EF-hands (Figure 1.3A). The highly flexible linker between the two domains can be drastically reoriented upon binding to target proteins and is an essential property of CaM which permits this protein to interact with a diverse array of interacting partners (Figure 1.3B) (Ikura and Ames, 2006). The C-terminal pair of EF-hands has a much higher affinity for Ca^{2+} than the N-terminal pair, allowing the two domains to behave independently at varying Ca^{2+} concentrations. In the absence of Ca^{2+} the N-terminal domain adopts a closed conformation, whereas the C-terminal domain exhibits a semi-open conformation. Under these conditions a hydrophobic patch is revealed in the C-terminal domain which is accessible to solvent and may allow CaM to interact with target proteins at resting Ca^{2+} levels (Chin and Means, 2000).

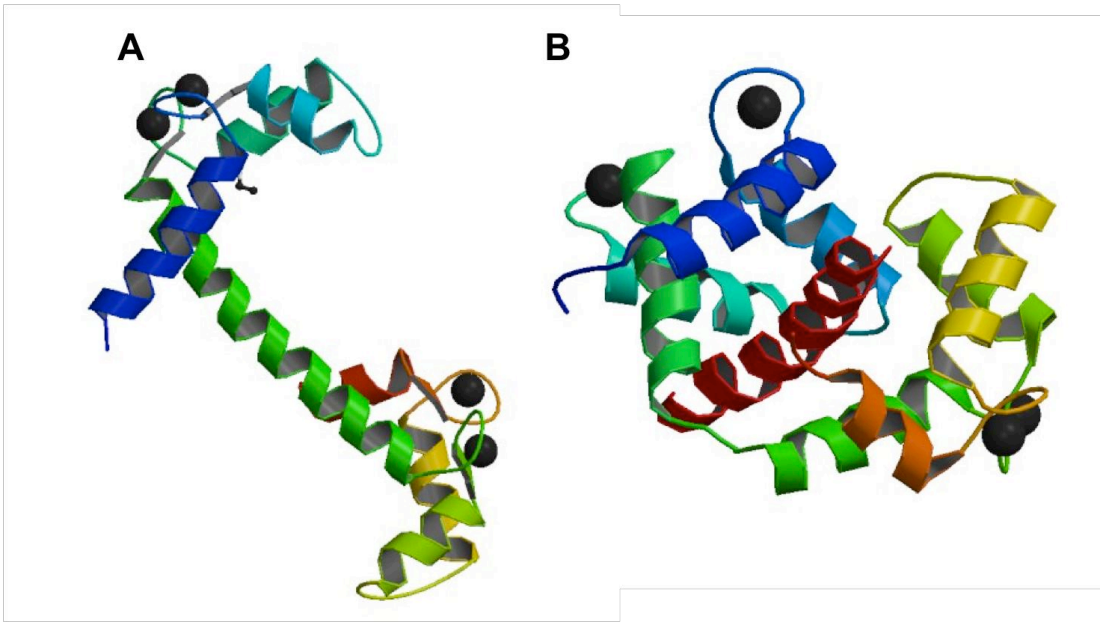

Figure 1.3.The structure of Ca^{2+}-bound CaM. A)The crystal structure of CaM in its Ca^{2+}-loaded form (PDB ID code 1CLL (Chattopadhyaya *et al*., 1992)) with four Ca^{2+} ions (black spheres) bound to the four EF-hands. The central linker alpha helix between the two EF-hand pairs is shown in green. B) The solution nuclear magnetic resonance (NMR) structure of Ca^{2+}-bound CaM complexed with a peptide representing the calmdoulin binding domain of calmodulin kinase I (CaMKI; PDB ID code 2L7L (Gifford *et al*., 2011)). CaM binding to the alpha-helical CaMKI peptide (Red) induces changes in the CaM linker domain (green) which allow its N- and C- terminal domains to wrap around the peptide helix.

Upon elevation of $[Ca^{2+}]_i$, Ca^{2+} is co-ordinated by the Ca^{2+}-binding loops leading to a large shift in conformation of the E and F helices to a much more open arrangement thus exposing hydrophobic residues to solvent (Figure 1.3A) (Chin and Means, 2000). This unfolding of CaM upon Ca^{2+}-binding releases considerable free energy ($\Delta G \approx 133$ (Hopkins Jr and Gayden, 1989)) and it is this ability to convert the Ca^{2+}-binding event into biochemical energy which permits Ca^{2+} sensors to transduce cellular signals (Chin and Means, 2000). Exposure of hydrophobic residues permits binding of CaM to target binding partners and this in turn raises the affinity of CaM for Ca^{2+} ten-fold and sensitizes the complex to further changes in $[Ca^{2+}]_i$. CaM interacts with many effectors which are involved in phosphorylation and also regulates Ca^{2+} pumps, ion channels, ryanodine receptors and some IP_3R isoforms. Each of these interactions occurs under different conditions and CaM's binding partners can be categorised into different classes depending on their mode of interaction under conditions of resting or elevated $[Ca^{2+}]_i$. The ability of CaM to bind differentially to different

effectors depending on the presence of Ca^{2+} suggests that it must possess multiple interaction surfaces to accomplish this (Chin and Means, 2000).

CaM is the archetypal Ca^{2+}-sensor due to its ubiquitous nature and abundant and often paradoxical protein interactions. Ca^{2+} activation of CaM has been found to have a heterogeneous distribution within the cell implying that discrete pools of CaM must exist and emphasizing the importance of spatial and temporal parameters in calcium signalling (Torok *et al*., 2002). How this single protein is able to participate in such a diverse array of cellular processes still remains a central question in cell biology. The interaction of CaM with adenylyl cyclase illustrates this complexity: CaM activates both adenylyl cyclase and cyclic nucleotide phosphodiesterase thereby modulating both the synthesis and degradation of cAMP. In order for productive cAMP signalling to occur, CaM must be modulated both spatially and temporally (Toutenhoofd and Strehler, 2000).

Part of this regulation may occur at the transcript level in higher vertebrates where three non-allelic genes encode the CaM protein. The CaM multigene family is unique in that its three allelic genes do not encode different isoforms but encode the same identical protein. Although it may be expected that three completely identical gene products would give rise to redundancy, their high conservation would seem to argue against this and suggest that there are selective pressures acting to conserve these sequences in vertebrates. Therefore, it stands to reason that the three CaM proteins must target and modulate different populations of interacting partners, possibly at different sites within the cell (Toutenhoofd and Strehler, 2000).

The three CaM genes differ mostly in their promoter regions and in their 5'- and 3'-untranslated regions (UTRs) but have identical intron-exon boundaries implying a common ancestor. During evolution the number of functions for CaM has increased significantly and the advent of three separate genes encoding CaM may have permitted tighter regulation of protein expression through differential expression of the genes and regulation of the various mRNA transcripts at distinct subcellular loci (Friedberg and Rhoads, 2001).

It has been established that there are differences in CaM concentration in different cellular compartments generating distinct pools of CaM which may go some way to explaining how CaM carries out such a diverse array of processes (Persechini and Stemmer, 2002). It has not been established, however, whether the different gene transcripts derive different cellular pools of CaM. CaM could be regulated at a number of different levels. Two distinct pools of CaM have been detected in cells: a soluble 'Ca^{2+} sensitive' fraction and an insoluble 'Ca^{2+} insensitive' fraction (Toutenhoofd and Strehler, 2000). It is thought that CaM may be stored in an inactive form either by binding to molecules which prevent its activity or by phosphorylation to reduce its potency as an activator of target proteins. An appropriate signal such as an elevation in Ca^{2+}, may then release CaM from this inactive pool (Toutenhoofd and Strehler, 2000). Regulation at the spatial level may be inferred by the trafficking of pre-synthesised CaM along cytoskeletal elements to particular subcellular sites (Toutenhoofd and Strehler, 2000). CaM can also be post-translationally modified by a variety of mechanisms including acetylation, trimethylation, carboxylmethylation, proteolytic cleavage and phosphorylation. These modifications may also modulate CaM's activity and target proteins (Ikura and Ames, 2006). Similarly, CaM target proteins can be regulated at the protein level both spatially and temporally and through protein modifications. For instance, phosphorylation of CaM kinase modulates its sensitivity to CaM (Hook and Means, 2001). Regulation of the concentration of both CaM and its relevant target proteins at particular locations within the cell is also significant in determining CaM's activities. A low-affinity binding partner that is expressed at a low concentration in a particular locale is less likely to interact with CaM than a more highly expressed or higher-affinity binding partner. Illustrating this theory, Schaad *et al.*(Schaad *et al*., 1996) reported that NCS-1 is able to replace CaM in interactions with calcineurin (Schaad *et al*., 1996). Subsequent studies, however, could not confirm this as a significant interaction physiologically, and previously reported dissociation constants show that NCS-1 has a three-fold lower binding affinity for calcineurin than CaM (Schaad *et al*., 1996, Hubbard and Klee, 1987). This, together with the fact that CaM is expressed at 5 - 200 fold higher concentrations than NCS-1 in cells, suggests that the physiologically

relevant interaction is between calcineurin and CaM, not NCS-1 (Fitzgerald *et al*., 2008).

At the transcript level, CaM expression may be regulated through the trafficking of different CaM mRNAs to specific cellular compartments for localised translation. Finally, transcriptional control within the nucleus could control which of the multiple CaM genes are expressed thereby fulfilling individual cell and tissue type requirements for CaM (Toutenhoofd and Strehler, 2000).

Various transcripts arise from each of the three CaM genes with varying expression levels depending on the tissue type. This is also apparent in the brain where CaM I and CaM II are highly expressed in the granular cell layer of the cerebellum whereas CaM III is expressed at a much lower level. In the Purkinje cells, however, strong expression of CaM II is observed with lower level expression for CaM I and CaM III. Characteristic subcellular distributions for each mRNA species are also observed in neurons with CaM II mRNA mostly appearing in perikaryal regions, and CaM I and CaM III localised somatodendritically. The promoter regions and 3' UTRs are likely to be important in determining these distinct tissue and subcellular expression patterns (Friedberg and Rhoads, 2001). This regulation may be particularly important in specialised cells such as neurons and complex mechanisms that have evolved to regulate CaM may be related to the enhancement of synaptic plasticity in mammals (Friedberg and Rhoads, 2001). A number of Ca^{2+}-sensing proteins, evolutionarily related to CaM, have been discovered which are enriched or expressed exclusively in the brain. Further duplication and diversification of the CaM gene has given rise to these neuronal Ca^{2+}-sensing proteins which carry out specific neuronal functions in higher organisms (Burgoyne, 2007, McCue *et al*., 2010b, Mikhaylova *et al*., 2011).

1.6. Neuronal Calcium Signalling

Calcium signalling in neurons, like in other cell types, can mediate gene expression, cell growth, development, cell survival, and cell death. In addition, neuronal calcium signalling processes have adapted to modulate the function of important pathways in the brain, including neuronal survival, axon outgrowth, and changes in synaptic strength (Ghosh and Greenberg, 1995). Highly specialised proteins allow the

transduction of Ca^{2+} signals leading both to short term responses, such as the modification of synaptic proteins, and long term responses requiring changes in gene expression (Ghosh and Greenberg, 1995).

It is well established that Ca^{2+} plays a key role in synaptic transmission between neurons, acting as a trigger for neurotransmitter release upon its entry into the presynaptic terminal. Many other specialised roles for Ca^{2+} have also now been identified which are essential for the development and plasticity of the nervous system (Ghosh and Greenberg, 1995). The mechanisms by which changes in $[Ca^{2+}]_i$ in neurons can bring about such diverse and long-lasting responses has become a topic of widespread interest.

Many of these processes have been shown to be largely dependent upon the particular route of Ca^{2+} entry into the cell (Ghosh and Greenberg, 1995). For instance, Ca^{2+} influx through VGCCs can lead to increased survival of embryonic neurons, whereas influx of Ca^{2+} through NMDA receptors in postnatal neurons mediates excitotoxic cell death (Choi, 1988, Franklin and Johnson Jr, 1992). Changes in $[Ca^{2+}]_i$ are mediated, as in other cell types, by influx from either the extracellular space or from intracellular stores such as the ER. The major PM Ca^{2+} channels in neurons are VGCCs and NMDA receptors, however, specific subsets of neurons also express other specialised channels such as the neuronal acetylcholine receptor, type 3 serotonin receptors, AMPA receptors and kainate receptors (Ghosh and Greenberg, 1995, Berridge, 1998). The contributions of the various VGCCs in neurons have been well characterised and the majority of Ca^{2+} currents generated by these channels appear to be mediated by L-, N-, and P-type channels (Ghosh and Greenberg, 1995). Each of these channels seems to have distinct functions and they are expressed in distinct PM domains. N-type channels tend to be quite broadly distributed and have been implicated, along with P-type channels, in the regulation of neurotransmitter release. L-type channels on the other hand, are concentrated at the base of the apical dendrite in hippocampal pyramidal neurons and can regulate Ca^{2+}-dependent signalling events in postsynaptic neurons (Ghosh and Greenberg, 1995).

NMDA receptors are particularly important neuronal Ca^{2+} influx channels due to their critical involvement in processes such as synaptic plasticity and cell death. In contrast to the VGCCs, NMDA receptor activation requires both ligand binding and membrane depolarisation (Ghosh and Greenberg, 1995). Postsynaptic Ca^{2+} signals arising from activation of NMDA receptors give rise to two important processes in synaptic plasticity, long term potentiation (LTP) and long term depression (LTD). LTP and LTD are examples of the way synaptic transmission can change synaptic efficacy and are thought to be important in modulating learning and memory. Importantly, the Ca^{2+} signals that bring about either LTP or LTD differ only in their timing and duration. LTP is triggered by Ca^{2+} signals on the µM scale for a few seconds whereas LTD is triggered by Ca^{2+} signals on the scale of hundreds of nM for longer durations (Burgoyne, 2007, Bear and Malenka, 1994).

Ca^{2+} release from internal stores also contributes significantly to changes in $[Ca^{2+}]_i$. The main Ca^{2+} store in neurons, as in other cell types, is the ER which forms an elaborate network extending throughout the whole cell, from the nuclear membrane into the dendrites and along the axon (Berridge, 1998). As in other cell types Ca^{2+} is released from ER stores by two main mechanisms involving IP_3Rs and RyRs (Berridge, 1998).The extensive ER network is thought to be very important for the function of neurons and has sometimes been described as a 'neuron-within-a-neuron' (Berridge, 1998). The ER can act as a sink for localised Ca^{2+} pulses generated by brief neuronal activity and the Ca^{2+} will gradually dissipate. In this way the ER can buffer a large number of Ca^{2+} spikes. As the load of the ER increases, however, IP_3Rs and RyRs become increasingly sensitized due to the increase in $[Ca^{2+}]_i$ and eventually Ca^{2+} may be released back into the cytosol as a consequence of CICR. Therefore, by acting as a sink for brief elevations of Ca^{2+} release, the ER can keep track of the cumulative Ca^{2+} spikes eventually leading to opening of intracellular channels. This can then lead to the generation of a global signal that reaches the nucleus, causing changes in gene transcription (Berridge, 1998).

The highly polarised nature of neurons means that calcium signalling in this cell type is usually highly localised. For this reason the spatial proximity of molecular targets to a given Ca^{2+} signal greatly influences its outcome (Augustine *et al*., 2003). For

instance the influx of Ca^{2+} through a single Ca^{2+} channel can only be translated into a signal if the relevant Ca^{2+}-sensor is within 50 nm of the channel. At the presynaptic terminal, neurotransmitter release is triggered by the influx of Ca^{2+} through clusters of channels which creates a Ca^{2+}-microdomain. This influx activates Ca^{2+}-sensors which are situated within a fraction of a μm of the channels (Augustine *et al*., 2003). Another example of highly localised neuronal calcium signalling occurs in dendritic spines where ligand-gated channels are targeted to the tip of the spine. Ca^{2+} influx through these channels creates nanodomains or microdomains within the spine head which decay over the approximately 1μm length of the spine. The specific localisation of the ligand-gated channels together with the restricted movement of Ca^{2+} within the thin neck of the spine results in a highly localised Ca^{2+} signal (Augustine *et al*., 2003). Differences in diffusion rates can give rise to large differences in the magnitude and speed of a Ca^{2+} signal. It is therefore important that the Ca^{2+}-sensors involved in a given process have properties that are appropriate for the local Ca^{2+} signal being detected. In accordance with this, families of Ca^{2+}-sensors that are expressed specifically in neurons have been reported. These neuronal Ca^{2+} sensors each possess unique properties which determine their site of action within the neuron and which allow them to carry out highly specialised functions in the nervous system.

1.7. The Neuronal Calcium Sensor Family

Whereas CaM is ubiquitously expressed, the expression of other Ca^{2+}-sensing proteins is restricted to particular cell types. A key example of this is the neuronal calcium sensor (NCS) family of proteins which are primarily expressed in neurons or retinal photoreceptors. The NCS family of proteins are related to CaM but have distinct properties that allow them to carry out non-redundant functions. Members of the NCS protein family have been implicated in the regulation of neurotransmitter release, regulation of receptors and ion channels, control of gene transcription, cell growth and cell survival (Burgoyne, 2007). The NCS proteins are encoded by a family of fourteen genes in mammals with a further level of diversity being generated by alternative splicing. The gene products each contain four EF-hand motifs and display limited similarity (<20%) to CaM (Burgoyne, 2004).

NCS-1, the mammalian homologue of yeast frequenin, is the most widely expressed member of this family and is thought to be the primordial NCS protein. The protein was first discovered in *Drosophila melanogaster* and although initially it was originally described as neuronal specific it has since been demonstrated to exhibit a wider expression profile. An NCS-1 orthologue has been identified in yeast which is essential for survival (Hilfiker, 2003) and there appears to have been a steady increase in the complexity of this protein family throughout evolutionary history. Five distinct classes of NCS protein have now been identified in higher organisms termed classes A-E. Class A comprises NCS-1, which first arose in yeast. Class B consists of the visinin-like proteins (VILIPs), which appeared first in *Caenorhabditis elegans*. Classes C and D first appeared in fish and comprise recoverin and the guanylyl-cyclase-activating proteins (GCAPs), respectively. Finally class E encode the K^+ channel-interacting proteins (KChIPs) which are present in insects and evolutionary subsequent species (Burgoyne, 2004). Mammals have a single NCS-1, five VILIP proteins, a single recoverin, three GCAPs and four KCHIPs. The recoverins and GCAPs are restricted to the retina whereas the rest of the NCS family are expressed in neurons with varying expression profiles (Burgoyne, 2007). Although localisation and expression studies have proven difficult due to cross-reactivity of antibodies, it has been established that certain neurons express several or all of the NCS proteins. The expression pattern for each of the NCS proteins is unique, however, suggesting that despite the high sequence homology within this family, each one is likely to perform distinct functions in specific cell types (Burgoyne and Weiss, 2001).

In contrast with CaM, not all EF-hand motifs in the NCS proteins are functional and the first EF-hand is unable to bind Ca^{2+} in all family members (Figure 1.4). In the case of recoverin and KChIP1 only two of their four EF-hand motifs are functional in Ca^{2+} binding (Burgoyne, 2007, Burgoyne *et al*., 2004). Unlike the extended dumbbell structure of CaM, NCS proteins are compact and globular when bound to Ca^{2+}. The NCS proteins also differ from CaM in that they have covalent modifications which can allow direct association with cellular membranes. KChIP1 and all members of classes A-D are *N*-myristoylated whereas KChIP2 and KChIP3 are palmitoylated

(Figure 1.4). In some cases the membrane association conferred by these moieties only occurs upon Ca^{2+} binding when a sequestered *N*-myristoyl acyl chain is extruded from the protein core after a shift in conformation. For instance VILIP proteins and recoverin are cytosolic at resting Ca^{2+} concentration but localise to the PM or Golgi upon Ca^{2+} elevation. Each of the NCS proteins displays distinct subcellular localisations which in some cases are additionally influenced by the specific phosphoinositides with which their N-termini interact (Burgoyne, 2007).

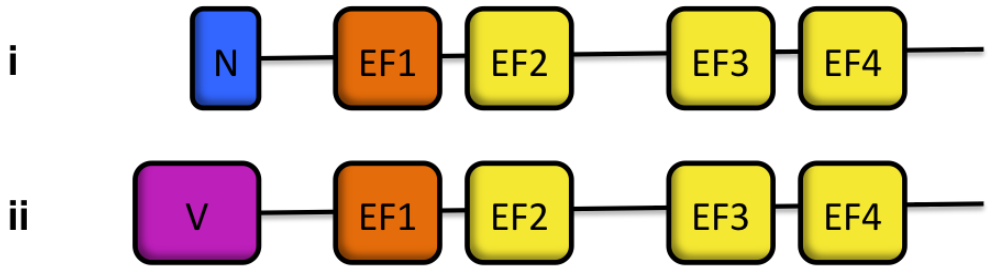

Figure 1.4. Schematic diagram showing the typical domain organisation of the NCS proteins. With the exception of recoverin and KChIP1, the NCS proteins have three functional EF-hands (yellow) (i). EF-1 is non-functional in all NCS proteins (orange). All NCS proteins with the exception of KChIP2 and KChIP3 are *N*-myristoylated (i) (denoted 'N', blue). The KChIPs have a variable N-terminal extension (ii) (denoted 'V', pink) - the source of multiple splice isoforms and different mechanisms of membrane association (either *N*-myristoylation or palmitoylation). (Adapted from (Burgoyne and Weiss, 2001)).

NCS proteins are multifunctional regulators of various proteins involved in processes ranging from vesicular trafficking and ion channel modulation to gene transcription (Burgoyne *et al.*, 2004). NCS-1 has been shown to enhance neurotransmitter release and constitutive exocytosis when overexpressed. Consistent with this function, an interaction with phosphatidylinositol-4 kinase (PI4K) has been reported in both yeast and mammals suggesting that NCS-1 may regulate neuronal secretion through the modulation of phosphatidylinositol-dependent trafficking steps (Hilfiker, 2003). The VILIP or class B proteins modulate various signal transduction pathways including cyclic nucleotide and MAPK signalling. They have been shown to have effects on gene expression and are also

involved in membrane trafficking (Braunewell and Klein-Szanto, 2009). Recoverin and the GCAPs are expressed exclusively in the retina and have important roles in light adaptation. Recoverin interacts with and inhibits the activity of rhodopsin kinase and can prolong phototransduction and enhance visual sensitivity (Sampath *et al*., 2005). GCAPs are the only known activators of retinal guanylyl cyclases (GCs) and are unusual in that they activate GCs when in their Ca^{2+}-free form but GCAP2 and GCAP3 become inhibitors of GCs at higher Ca^{2+} concentrations. GCAP3 is expressed in cone cells whereas GCAP1 and GCAP2 are expressed in rod cells and despite GCAP1 and GCAP2 sharing the same function in the same cell type each protein has different Ca^{2+} binding affinities for GC activation. This means that both proteins are required for GC activation over the full physiological range of $[Ca^{2+}]_i$ thus increasing dynamic range and light sensitivity in the mammalian retina. The GCAPs therefore represent an example of how Ca^{2+} sensors have become adapted to increase the sensitivity of important regulatory mechanisms in specialised cell types (Burgoyne, 2007, Burgoyne and Weiss, 2001, Palczewski *et al*., 2004).

KChIPs have been found to associate with transient voltage-gated potassium channels of the K_v4 family, but the specific functions of these proteins in the brain remains unclear (Wang, 2008). They are expressed predominantly in the brain but KChIP2 is also expressed in the heart and depletion of KChIP2 causes a complete loss of Ca^{2+}-dependent transient outward potassium currents and a susceptibility towards ventricular tachycardia (Kuo *et al*., 2001). Knockouts of KChIP1 have revealed a potential role in the GABAergic inhibitory system (Xiong *et al*., 2009) and KChIP3 knockout mice exhibit reduced responses in acute pain models (Reisch *et al*., 2006) and decreased β-amyloid production (Lilliehook *et al*., 2003). KChIP3, also known as DREAM or calsenilin, is the most comprehensively understood of the KChIPs and has roles identified in transcriptional regulation (Burgoyne *et al*., 2004, Yakovleva *et al*., 2006) and in the processing of presenilins which are important proteins in Alzheimer's disease pathophysiology (Buxbaum *et al*., 1998).

In support of the NCS proteins having essential roles in higher organisms, a number of recent discoveries have implicated these proteins in the pathological processes of various diseases. Apart from the link to Alzheimer's disease through interaction of

KChIP3 with presenilins (Jo *et al*., 2004), the NCS proteins have been linked with other diseases of the nervous system. VILIP1 has been implicated in Alzheimer's disease due to an association with amyloid plaques in diseased brains (Schnurra *et al*., 2001). NCS-1 has been found to be up-regulated in neural tissue from patients with schizophrenia and bipolar disorders (Koh *et al*., 2003) and also interacts with interleukin-1 receptor accessory protein-like (IL1RAPL), a protein which, when mutated, results in X-linked mental retardation (Bahi *et al*., 2003). Apart from links to neurological disorders, NCS protein function has also been implicated in cancer. Recoverin is detected in 68% of small cell and 85% of non-small-cell cancer-associated retinopathy-producing lung carcinomas and was also expressed in ~50% of other tested tumour types including breast and ovarian cancers (Bazhin *et al*., 2004). Recoverin is hypothesized to regulate cancer cell growth in a Ca^{2+}-dependent manner through modulation of receptor kinases and may offer a therapeutic target for the treatment of recoverin expressing tumours (Braunewell, 2005). High expression of VILIP1 has been detected in less aggressive skin tumours in mice but expression was significantly reduced or absent in invasive squamous carcinoma. However, when aggressive tumour cell lines were transfected with VILIP-1 the cancer cells became less invasive hinting at a role for VILIP-1 as a tumour suppressor (Mahloogi *et al*., 2003). The effects that NCS proteins confer in these diseases appear to be dependent on the up- or down-regulation of their expression. As yet, few genetic links have been found between the NCS proteins and these diseases suggesting epigenetic effects may be responsible. Epigenetic effects also have a role in synaptic plasticity and memory formation which are affected in many neurodegenerative disorders such as Alzheimer's disease, X-linked mental retardation and schizophrenia and have also been linked to the regulatory mechanisms carried out by the NCS proteins. A current hypothesis is that the epigenetic deregulation of NCS proteins may contribute to the cognitive impairments seen in many neurodegenerative diseases making the epigenetic regulation of NCS proteins a potential new therapeutic target for these diseases (Braunewell, 2005).

This family of proteins have evolved to carry out specialized neuronal functions which are separate to the functions of CaM. When trying to decipher why these proteins are particularly well adapted for carrying out functions in neuronal populations it is therefore useful to compare their properties to those of CaM. Of particular note is their approximately 10-fold higher affinity for Ca^{2+} compared to CaM. This higher affinity allows the NCS proteins to be activated at low Ca^{2+} concentrations which would ordinarily activate only a fraction of cellular CaM. Expression of Ca^{2+} binding proteins with a range of Ca^{2+} binding affinities increases the dynamic range over which Ca^{2+} can regulate neuronal processes. In this way the cell can respond to very slight or more dramatic changes in $[Ca^{2+}]_i$ depending on which populations of Ca^{2+} sensors are activated under those particular conditions (Burgoyne and Weiss, 2001). As mentioned previously, the individual expression patterns and the subcellular localisation of each of the NCS proteins is also likely to play an important role in their suitability for neuronal cell signalling. The characteristic *N*-myristoylation or palmitoylation modifications, which allow these proteins to associate with membranes, may position them at relevant sites in the cell leading to a faster and more efficient response to Ca^{2+} signals.

The NCS proteins represent a family of neuronal Ca^{2+} binding proteins which have evolved to carry out discrete functions separate to those of CaM. Various members of this protein family arose at different points in evolutionary history and carry out a diverse array of functions. The NCS proteins are a prime example of how the properties of Ca^{2+} binding proteins have been fine-tuned to allow them to regulate specific targets in neuronal signalling pathways.

As an example of how the NCS proteins are adapted to carry out specialised functions, two members of this protein family will be discussed in more detail. NCS-1 represents an important member of the NCS family and has been well characterised functionally. The function of recoverin is less well characterised than for NCS-1, however, the structure of recoverin has been extensively studied. Recoverin's unique structural properties provide an interesting example of how NCS proteins have adapted, in this case to perform important functions in the retina.

1.7.1. NCS-1

NCS-1 the primordial NCS protein has been highly evolutionarily conserved, retaining 59% homology with its yeast orthologue, frequenin. It displays a high Ca^{2+} affinity (≈ 440 nM) compared to CaM (≈ 4 - 20 µM) (Schaad *et al*., 1996) and is able to respond to marginal changes in $[Ca^{2+}]_i$. Like many of the other NCS family members NCS-1 has an *N*-myristoyl group which enables membrane association. Endogenous NCS-1 is therefore predominantly associated with Golgi and trans-Golgi membranes and in some cell lines, has been detected in vesicular structures and at the PM (Hilfiker, 2003). NCS-1 carries out important neuronal functions and, for example, has been found to regulate phosphorylation, trafficking and signalling of D2 dopamine receptors (D2Rs). D2Rs represent an important target for the development of novel therapeutic drugs for the treatment of schizophrenia and, interestingly, NCS-1 can also contribute to the pathology of schizophrenia and has been suggested as an alternative molecular target for antipsychotic drugs (Kabbani *et al*., 2011). Unlike the rest of NCS family, however, NCS-1 is not neuron specific and is expressed in neuroendocrine cells and several non-neuronal cell types at low levels. For example, a study using NCS-1 (-/-) knockout mice identified NCS-1 as a novel regulator of calcium signalling in immature and hypertrophic hearts. This was mediated in part by regulation of IP_3R function (Nakamura *et al*., 2011). In addition NCS-1 is essential for survival in yeast and taken together these facts suggest a more generalized role for NCS-1 (Hilfiker, 2003).

NCS-1 has three functional EF-hand motifs which have differing cation specificities. It is hypothesised that under resting conditions EF2 and EF3 are Mg^{2+} bound, whereas EF4 is a Ca^{2+} specific binding site and remains unoccupied. In resting conditions, when in its Mg^{2+} bound form, NCS-1 adopts a conformation which drastically reduces exposed hydrophobic regions. This may be important in the prevention of non-specific interactions in the absence of an appropriate Ca^{2+}-signal. In the presence of Ca^{2+}, EF2 and EF3 are bound simultaneously followed by binding to EF4 (Aravind *et al*., 2008). The Mg^{2+} bound form of NCS-1 has a 5-fold lower affinity for Ca^{2+} than the apo-form (440 nM versus 90 nM) (Aravind *et al*., 2008). As resting $[Ca^{2+}]_i$ is ≈ 100 nM a Ca^{2+} affinity of 90 nM would not allow NCS-1 to efficiently

revert to its Ca^{2+}-free form. Binding to Mg^{2+} therefore lowers the Ca^{2+} affinity of NCS-1 thereby allowing a more efficient reversal to the Ca^{2+}-unbound state. This implies that Mg^{2+} binding provides significant modulation of NCS-1 and is important in fine-tuning its Ca^{2+} sensing ability (Aravind *et al*., 2008).

Much of the current understanding regarding the function of NCS-1 stems from overexpression or knockout studies. Overexpression in *Drosophila* caused a frequency-dependent facilitation of neurotransmitter release (Pongs *et al*., 1993) and in *Xenopus* caused enhanced spontaneous and evoked transmission at neuromuscular junctions (Olafsson *et al*., 1995). Overexpression was also found to increase Ca^{2+}-dependent exocytosis of dense core granules in PC12 cells (McFerran *et al*., 1998) and to enhance associative learning and memory in *C. elegans* (Gomez *et al*., 2001, Hilfiker, 2003).

Knockout of NCS-1 in *Sacchormyces cerevisiae* is lethal due to its involvement in the activation of Pik1, one of the two yeast PI4Ks. NCS-1 can interact with PI4K in both yeast and in mammals and enhances its activity 3 - 10 fold (Hendricks *et al*., 1999, Taverna *et al*., 2002). The high conservation of both its sequence and function between yeast and mammalian orthologs suggests an important role for NCS-1 in the regulation of phosphoinositides and hence membrane trafficking. Knockout in other organisms, however, is not lethal but does lead to developmental phenotypes. Knockout in *Dictyostelium discoideum* changes the rate of development (Coukell *et al*., 2004) and in *C. elegans* results in impaired learning and memory (Gomez *et al*., 2001). NCS-1 therefore appears to be important in developmental processes in various different organisms and knockdown of one of the NCS-1 genes in *Danio Rerio*, ncs-1, prevents formation of the semicircular canals of the inner ear (Burgoyne, 2007, Hilfiker, 2003). Further investigation identified the involvement of a previously described (Haynes *et al*., 2005, Haynes *et al*., 2007) signalling pathway involving NCS-1, ARF1 and PI4KIIIβ which was found to modulate the secretion of components important for the development of the vestibular apparatus of the inner ear (Petko *et al*., 2009).

Many different binding partners have been identified for NCS-1 and often these interactions and the effects they confer are very similar to those of CaM. Despite this overlap in roles, these Ca^{2+}-sensors have not become redundant due to differences in their Ca^{2+} binding properties (Schaad *et al*., 1996, Fitzgerald *et al*., 2008). NCS-1 has a higher affinity for Ca^{2+} than CaM and therefore may preferentially interact with some binding partners when the Ca^{2+} elevation is too small to activate CaM activity. For example, both CaM and NCS-1 have been shown to interact with and desensitize dopamine D2 receptors but are likely to mediate their effects at different Ca^{2+} levels due to the 10-fold difference in Ca^{2+} affinity between the two proteins (Kabbani *et al*., 2002, Woods *et al*., 2008). NCS-1 does not merely represent an alternative regulator of classical CaM targets, however, and numerous NCS-1 specific binding partners have been identified which have no documented interactions with CaM. These proteins include ILRAPL1, Kv4.2 channels, PI4K, ARF1 and TGFβR1(Haynes *et al*., 2006).

The example of NCS-1 illustrates how evolutionary pressures have fine tuned Ca^{2+} sensors to carry out specialized functions. The individual properties of NCS-1 allow this protein to localise to discrete domains within the cell and interact with distinct target proteins under conditions of Ca^{2+} stimulation which would not activate the archetypal Ca^{2+} sensor, CaM. NCS-1 is not neuronal specific and appears to carry out more generalized functions which have been conserved through evolution. Further adaptive mutations, however, have given rise to many more members of the NCS protein family which can carry out more dedicated functions.

1.7.2. Recoverin

Insights into how calcium signalling has been fine-tuned to allow the evolution of the complex vertebrate nervous system can be gained by studying more accessible regions of the nervous system such as the retina (Polans *et al*., 1996). In particular, photoreceptor cells can be maintained in isolation for biochemical and electrophysiological investigations and the response of photoreceptors to a single photon can be quantified. Therefore, the biochemical steps involved in phototransduction have been extensively studied and comprise a useful model for the examination of how specialised processes in the nervous system are regulated.

Ca^{2+} modulates several stages in phototransduction through the activation of various Ca^{2+} binding proteins and is the key regulator during light adaptation. Retinal NCS proteins that are important in phototransduction, include GCAPs, visinin and recoverin (Polans *et al*., 1996).

Recoverin is found primarily in rod and cone cells of the retina (Braunewell and Klein-Szanto, 2009, Yamagata *et al*., 1990, Dizhoor *et al*., 1991) and is thought to act to prolong the lifetime of photolyzed rhodopsin by inhibiting its rhodopsin kinase mediated phosphorylation and prolonging the light response. Recoverin activity is therefore important for the modulation of light adaptation (Klenchin *et al*., 1995). This function remains controversial, however, with several observations suggesting that this hypothesis may be oversimplified. The interaction of recoverin with rhodopsin kinase was found to occur in a Ca^{2+}-dependent manner, however the binding of Ca^{2+} to recoverin also increases its hydrophobicity and results in its binding to various photoreceptor proteins, not just rhodopsin kinase (Polans *et al*., 1991, Chen *et al*., 1995a). Discrepancies have also arisen regarding the [Ca^{2+}] required for interaction with rhodopsin kinase which may be out of the normal physiological range (Baylor, 1996). In addition, the expected phenotype was not observed in knockout mice which only displayed changes in the response to flashes of light at the end of background illumination but showed no change in the response to general flashes of light as would be expected (Chen *et al*., 1995b). It is possible that other components of the phototransduction pathway could compensate for the loss of recoverin in these mice. Further work is therefore required to deduce the exact role of recoverin in light adaptation (Polans *et al*., 1996).

Despite the ambiguity surrounding the possible function of recoverin, the structure of this protein is the most extensively studied of all the NCS proteins. Unlike the rest of the NCS proteins, recoverin has only two functional EF-hand motifs due to an internal salt bridge in EF4 (Ames *et al*., 1996). X-ray crystallography and nuclear magnetic resonance (NMR) studies have been used to deduce the structure of recoverin in its Ca^{2+}-bound and unbound forms and have revealed unusual properties which are unique to this member of the NCS family (Ames *et al*., 1997, Flaherty *et al*., 1993). Recoverin is composed of two distinct domains separated by a

bent linker and forms a compact structure in the absence of Ca^{2+}. Upon binding of Ca^{2+}, the N-terminal domain comprising EF1 and EF2 rotates through 45^{o} relative to the C-terminal domain and a usually buried *N*-myristoyl group is extruded. This allows the protein to associate with membranes whilst simultaneously revealing a hydrophobic surface which forms the binding pocket for its interaction with rhodopsin kinase (Ames *et al*., 1996). The residues involved in the interaction of the myristoyl group with the hydrophobic pocket are also conserved in other members of the NCS family, however, not all display this 'myristoyl switch'. NCS-1 and KChIP1 are constitutively membrane bound via their permanently extruded *N*-myristoyl groups, but, similar to recoverin, expose a hydrophobic surface upon Ca^{2+} binding which could also be important for their target interactions (Ames *et al*., 1996). Information about the structure of recoverin may go some way to aid understanding of the generally conserved structural features of the NCS proteins. There are subtle differences in the surface residues of the individual proteins, however, that may confer structural variation, giving rise to their ability to interact with a wide range of non-overlapping target proteins.

1.8. The CaBP Family of CaM-related Ca^{2+} Sensors

The Calcium Binding Proteins (CaBPs) are a relatively recently discovered family of Ca^{2+} sensors which first arose in vertebrates (Chapter 3, (McCue *et al*., 2010a)) and are likely to represent another example of how Ca^{2+} sensors have evolved to carry out discrete processes important for the divergence of higher organisms. The CaBPs share sequence homology with CaM and also display a similar structural arrangement of EF-hand motifs. Each of the CaBPs has four EF hand motifs and, like the NCS proteins, display different patterns of EF-hand inactivation when compared to CaM (Figure 1.5). Another key difference between the CaBPs and CaM is a four amino acid extension within their central linking alpha helix, between the C-terminal and N-terminal EF-hand pairs. This has been suggested to allow these proteins to interact with larger targets (Haeseleer *et al*., 2000). The CaBP family can be divided into two subgroups depending on their pattern of EF-hand inactivation: CaBPs 1-5 which have an inactive EF-hand 2 and active EF-hands 1, 3 and 4; and

CaBP7 and CaBP8 which have only two active Ca^{2+}-binding motifs, EF-hands 1 and 2 (Figure 1.5).

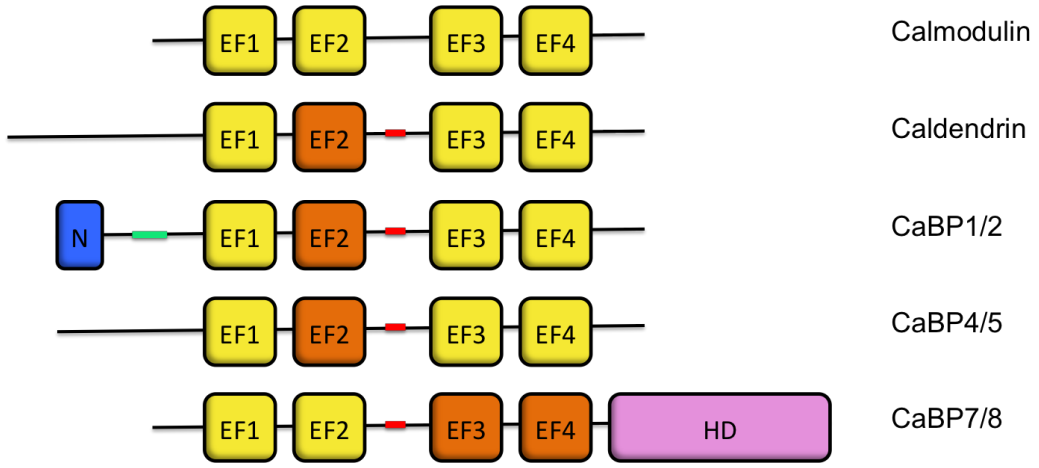

Figure 1.5. Schematic diagram showing the domain structure of CaM and the CaBPs. Functional EF-hand motifs are shown in yellow and non-functional EF-hands are shown in orange. The CaBPs have an extended linker region between their first and second EF-hand pairs (red). CaBP1 and CaBP2 each have an *N*-myristoylation motif (blue, denoted 'N'), and alternative splice sites within their N-termini give rise to long and short splice variants (green). Caldendrin is a longer splice isoform of CaBP1 that does not contain an *N*-myristoylation motif. CaBP7 and CaBP8 possess a 38 amino acid hydrophobic domain at their C-termini (pink, denoted 'HD').

1.8.1. CaBPs 1-5

Five genes encode CaBP1, CaBP2, CaBP3, CaBP4 and CaBP5. CaBP3 differs from the remaining members of this family as it is predicted to have only two active EF-hand motifs: EF-hands 3 and 4. CaBP3 is thought to be a pseudogene, however, as although the mRNA has been detected in cells, no protein product has been found (Haeseleer *et al*., 2000). Three isoforms of CaBP1 (Caldendrin, CaBP1 Long (CaBP1L) and CaBP1 Short (CaBP1S)), and two splice isoforms of CaBP2 (CaBP2 Long (CaBP2L) and CaBP2 Short (CaBP2S)), are also generated through alternative spicing of their respective mRNAs. Caldendrin is the longest isoform of CaBP1 and lacks the *N*-myristoylation motif which is found in other splice isoforms of both CaBP1 and CaBP2. *N*-myristoylation of long and short CaBP1 and CaBP2 isoforms permits their

association with both the PM and Golgi apparatus (Haeseleer *et al*., 2000). CaBP4 and CaBP5 lack this *N*-myristoylation motif and are predominantly cytosolic. The greatest region of divergence between CaBPs 1-5 resides in their N-termini and it is thought that this region may be important for the correct localisation of CaBP1 and CaBP2. As such, the long and short isoforms of CaBP1 show subtle differences in their subcellular localisation. CaBP1L localises predominantly to the Golgi and also displays some cytosolic localisation whereas CaBP1S localises most prominently to the PM and to Golgi structures (Haeseleer *et al*., 2000, McCue *et al*., 2009).

Various proteins have been identified as targets of the CaBP family, some of which are also targets for CaM. The outcomes of such interactions are generally not the same, however. Differences in expression patterns, subcellular targeting mechanisms and Ca^{2+} binding properties of the various members of the CaBP protein family have likely allowed them to carry out highly specialised, non-redundant, regulatory roles.

Much of the work examining the function of CaBP1 has been derived from studies of caldendrin. It is not yet clear whether the different splice isoforms of CaBP1 can carry out the same functions although some differences have been observed (Tippens and Lee, 2007). CaBP1 and caldendrin have roles in the regulation of various different types of Ca^{2+} channels including P/Q-type channels (Lee *et al*., 2002), L-type channels (Zhou *et al*., 2005, Cui *et al*., 2007), IP_3Rs (Haynes *et al*., 2004), and the TRPC5 channel (Kinoshita-Kawada *et al*., 2005). Interactions of CaM with these Ca^{2+}-channels have also been reported, but the regulatory outcome is quite different. In addition, CaBP1 has also been shown to compete with CaM for a number of other interacting binding partners. CaBP1 is able to compete with CaM for binding to the IQ domain of myo1C, a member of the myosin-1 family of motor proteins (Tang *et al*., 2007) and also to presynaptic group III metabotropic glutamate receptors (mGluRs) (Nakajima, 2011). Numerous molecules including, Ca^{2+}, cAMP, PKC, and Munc 18-1, are involved in the fine tuning of presynaptic mGluR function, hence allowing the process of synaptic transmission to be strictly regulated. CaBP1 binding adds a new

level of regulation which is Ca^{2+} dependent and is blocked by PKC dependent phosphorylation of the receptor (Nakajima, 2011).

Unique interactions of Caldendrin with other types of proteins, which are not shared with CaM, have also been reported. Caldendrin, but not CaM, interacts with light chain 3 (LC3) of MAP1A/B, a cytoskeletal protein which is involved in cellular transport processes and in the biogenesis of autophagosomes (Seidenbecher *et al*., 2004, Weidberg *et al*., 2010). In addition, a unique role for Caldendrin in NMDA receptor signalling has been reported via an interaction with a novel neuronal protein, Jacob (Dieterich *et al*., 2008). Upon NMDA receptor activation Jacob is normally recruited to the nucleus through the importin pathway, and results in the stripping of synaptic contacts and drastic alterations in the morphology of the dendritic tree. When there is a sustained synaptodendritic elevation in $[Ca^{2+}]$, caldendrin binds to Jacob to prevent its nuclear trafficking (Dieterich *et al*., 2008). Finally, a Ca^{2+}-dependent interaction between caldendrin and recoverin has been reported and the two proteins were observed to co-localise in the retina (Fries *et al*., 2010).

Limited information has been published on the functions of CaBP2 and CaBP5. CaBP2 was found to stimulate CaM Kinase II activity more strongly than the other CaBPs in *in vitro* studies, however the physiological relevance of this has not been investigated further (Haeseleer *et al*., 2000). CaBP2 and CaBP5 expression has been detected in the retina and in hair cells of the inner ear where it is proposed they may regulate the activity of VGCCs (Rieke *et al*., 2008, Yang *et al*., 2006a). CaBP5 was found to directly interact with the CaM binding domain of $Ca_v1.2$ and co-localised with $Ca_v1.2$ in rod bipolar cells (Rieke *et al*., 2008). CaBP5 was also shown to have a modest inhibitory effect on the inactivation of $Ca_v1.3$ channels in transfected HEK293T cells whereas CaBP2 was unable to exert similar effects (Yang *et al*., 2006a). A crucial role for CaBP5 in the retina is supported by the observation that CaBP5 knockout mice have reduced sensitivity of retinal ganglion cells to light responses implicating CaBP5 in phototransduction pathways (Rieke *et al*., 2008).

CaBP4 is expressed in the retina, localising to synaptic terminals, and has also been detected specifically in hair cells of the inner ear (Yang *et al*., 2006a, Cui *et al*., 2007). CaBP4, like CaBP1 and CaBP5, appears to modulate VGCCs, including $Ca_v1.3$ and $Ca_v1.4$ channels (Cui *et al*., 2007, Yang *et al*., 2006a, Haeseleer *et al*., 2004). The function of CaBP4 is modulated by protein kinase Cζ in the retina, which increases CaBP4 phosphorylation in light-adapted retinas (Lee *et al*., 2007b). This phosphorylation was shown to prolong Ca^{2+} currents through $Ca_v1.3$ channels and suggests that light-stimulated phosphorylation of CaBP4 might help to regulate presynaptic Ca^{2+} signals in photoreceptors (Lee *et al*., 2007b). CaBP4 has also been implicated in neurotransmitter release at synaptic terminals due to its interaction with unc119, a synaptic photoreceptor protein important for neurotransmitter release and maintenance of the nervous system (Haeseleer, 2008). CaBP4 (-/-) homozygous knockout mice exhibit abnormal synaptic morphology and function. These knockout mice have impaired rod and cone function and resemble animals that are deficient in subunits of the $Ca_v1.4$ channel (Haeseleer, 2008).

As in the NCS family of Ca^{2+} sensors, the importance of the CaBPs can be illustrated by their involvement in multiple neuronal diseases. Post-mortem brains of chronic schizophrenics have been shown to exhibit reduced numbers of caldendrin immunoreactive neurons which express the protein at elevated levels. This loss of caldendrin in some neurons and upregulation in others is likely to profoundly change synapto-dendritic signalling in schizophrenic patients (Bernstein *et al*., 2007). Changes in the distribution of caldendrin have also been observed in kainate-induced epileptic seizures in rats. Caldendrin translocated to the post synaptic density only in rats which suffered epileptic seizures and this may implicate the protein in the pathophysiology of the disease (Smalla *et al*., 2003).

CaBP4 has the most well characterised role in disease within this family of proteins. Genetic mutations in this gene have been shown to cause defects in retinal function. Knockout of CaBP4 was shown to cause a phenotype similar to that of incomplete congenital stationary night blindness (CSNB) patients (Haeseleer *et al*., 2004) and mutations in CaBP4 can cause autosomal recessive night blindness (Zeitz

et al., 2006). Patients with mutations in the CaBP4 gene have been identified that display CSNB, however, some patients with mutations display different phenotypes (Zeitz *et al*., 2006). In particular a novel homozygous nonsense mutation has been reported in two siblings, which resulted in severely reduced cone function but only negligible effects on rod function (Littink *et al*., 2009). In addition, a homozygous single base pair mutation in CaBP4 has been found in four family members suffering a from a Leber's congenital amaurosis (LCA)-like disease. The phenotype of LCA is more severe than CSNB and patients symptoms include: involuntary eye movements, severe visual impairment, and severely diminished or absent electroretinography (ERG) measurements (Aldahmesh *et al*., 2010). It appears, therefore, that genetic mutations in CaBP4 cause multiple cone-rod synaptic disorders of varying physiological severity (Littink *et al*., 2009, Littink *et al*., 2010).

1.8.2. CaBP7 and CaBP8

CaBP8 was first discovered in 2001 and originally named Calneuron I (Wu *et al*., 2001). It was identified as a CaM-related protein with homology to the CaBPs. Initial sequence analysis identified some differences between the CaBPs and CaBP8. Whereas the CaBPs share similar sized mRNAs and genomic structure to CaM, CaBP8 mRNA is much larger and displays a different intron-exon organisation (Wu *et al*., 2001). A second protein with a high degree of homology to CaBP8 (or calneuron I) was later discovered and named Calneuron II (referred to here as CaBP7) (Mikhaylova *et al*., 2006). These proteins have been consistently grouped with CaBPs 1-5 due to the homology shared among these proteins and were first referred to as CaBP7 and CaBP8 in 2002 by Haeseleer *et al.*(Haeseleer *et al*., 2002). For simplicity these proteins will be referred to as CaBP7 and CaBP8 for the remainder of this thesis.

CaBP7 and CaBP8 have a different pattern of EF-hand inactivation compared with the rest of the CaBPs, with active EF-hands 1 and 2 and inactive EF-hands 3 and 4 (Mikhaylova *et al*., 2006). Another key difference is that CaBP7 and CaBP8 possess a highly hydrophobic, 38 amino acid extension at their C-terminus, when compared to CaBPs 1-5 (Mikhaylova *et al*., 2006). The functions of CaBP7 and CaBP8 have only recently started to be deduced. Both have been found to associate with PI4KIIIβ and

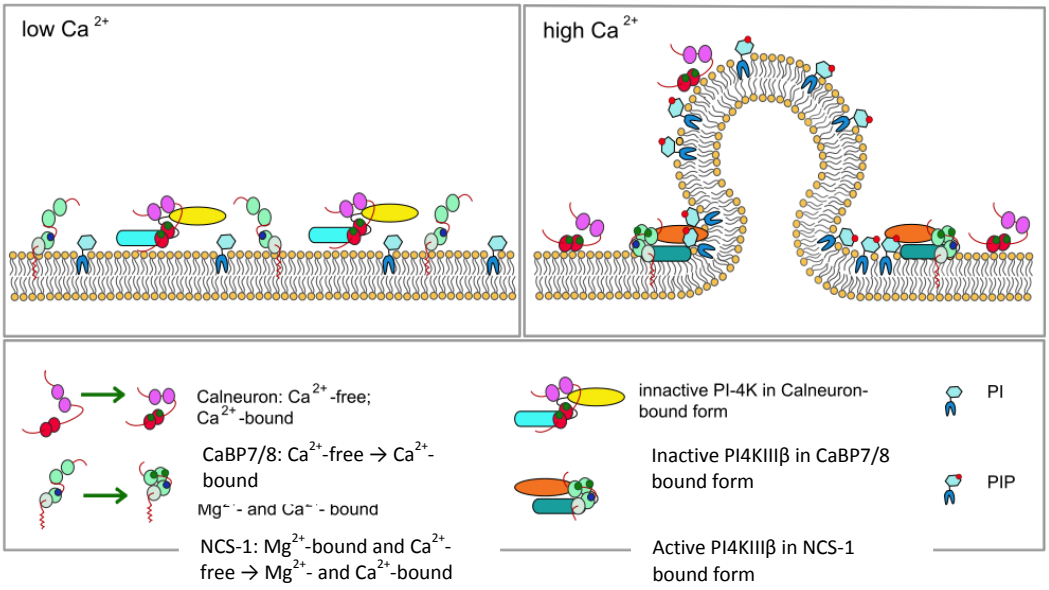

Figure 1.6 Proposed model for the Ca^{2+}-dependent molecular switch between CaBP7/8 mediated inhibition and NCS-1 mediated activation of PI4KIIIβ at the TGN. At low $[Ca^{2+}]_i$ (Left) PI4KIIIβ is predominantly in the CaBP7/8-bound form which inhibits kinase activity and slows TGN to PM trafficking. When $[Ca^{2+}]_i$ becomes elevated (Right) NCS-1 binds Ca^{2+} and is able to compete with CaBP7/8 for binding to PI4KIIIβ. NCS-1 stimulates the activity of PI4KIIIβ and causes a 3 to 4-fold increase in PI4P and PI(4,5)P_2 production which in turn enhances TGN to PM trafficking. CaBP7 and CaBP8 are therefore thought to set the threshold Ca^{2+} concentration at which PI4KIIIβ becomes activated (Adapted from*(Mikhaylova et al., 2009)).*

inhibit its activity at low or resting Ca^{2+} levels (Mikhaylova *et al.*, 2009). Overexpression of the proteins caused a reduction in phosphatidylinositol 4-phosphate (PI4P) levels in COS-7 cells and inhibited Golgi-to-PM trafficking in cortical neuron cultures, implicating them as regulators of cargo release from the Golgi. Overexpression of CaBP7 or CaBP8 also caused enlargement of the trans-Golgi network (TGN) and reduced trafficking of synaptophysin-containing vesicles and piccolo-basson vesicles (PTVs). In accordance with this, knockdown of CaBP8 in cortical neurons caused a reduction in the size of the TGN and a significant increase in the number of axonal PTVs (Mikhaylova *et al.*, 2009). NCS-1 had been previously shown to activate PI4K in a Ca^{2+}-dependent manner (Zhao *et al.*, 2001) and Mikhaylova *et al.* proposed that a molecular switch for the production of phosphoinositides at the TGN is created by the opposing roles of NCS-1 and CaBP7 or CaBP8 (Figure 1.6) (Mikhaylova *et al.*, 2009). At resting Ca^{2+} levels, CaBP7 and

CaBP8 bind to PI4KIIIβ and inhibit PI4P production. At elevated Ca^{2+} levels NCS-1 preferentially binds to PI4KIIIβ, competing with CaBP7 or CaBP8 binding. The enzyme is hence activated, generating PI4P at the TGN and allowing increased TGN-to-PM trafficking (Mikhaylova *et al*., 2009). As part of this study, the ability of CaBP7 and CaBP8 to bind to Ca^{2+} and Mg^{2+} was also assessed. Isothermal Titration Calorimetry (ITC) experiments revealed that CaBP7 and CaBP8, as predicted, have two high affinity Ca^{2+} binding sites, with global affinities of 230 nM and 180 nM, respectively (Mikhaylova *et al*., 2009). No binding to Mg^{2+} was observed in these experiments, consistent with related fluorimetry analyses where no change in fluorescence intensity was detected upon addition of Mg^{2+} to apo-CaBP8 whereas a significant change was observed upon addition of Ca^{2+} (Mikhaylova *et al*., 2009).

Whole cell patch-clamping experiments in bovine adrenal chromaffin cells, cells of a neural lineage, have shown that overexpression of CaBP8 can inhibit Ca^{2+} influx (Shih *et al*., 2009). A similar effect was observed in cells overexpressing a Ca^{2+}-binding deficient mutant but not with a mutant lacking the hydrophobic 38 amino acid C-terminal region. The major VGCCs in bovine chromaffin cells are L-, N-, and P/Q-type channels and through the use of specific VGCC blocking toxins, Shih *et al.* found that the dominant VGCC in these cells were N-type channels (Shih *et al*., 2009). Measurement of Ca^{2+} influx in HEK293T cells co-transfected with the N-type channel and CaBP8 showed an inhibition of Ca^{2+}influx which was not seen in cells transfected with GFP alone. Again, a truncated mutant lacking the hydrophobic C-terminus of CaBP8 was unable to inhibit Ca^{2+}influx through N-type channels (Shih *et al*., 2009). As will be discussed in Chapter 4, the hydrophobic C-termini of CaBP7 and CaBP8 are important for their normal subcellular localisation (McCue *et al*., 2009, McCue *et al*., 2011, Hradsky *et al*., 2011). The data from Shih *et al.* therefore suggest that subcellular localisation but not Ca^{2+}-binding is important for CaBP8 inhibition of Ca^{2+} influx (Shih *et al*., 2009). As previously discussed, CaBPs 1-5 have numerous roles in regulating VGCCs. Shih *et al.* demonstrated that CaBP8 also has an effect on the activity of VGCCs, however, as CaBP8 has been shown to be important in TGN to PM trafficking, it is uncertain whether this effect is exerted through a direct interaction

with VGCCs. It is possible that the observed inhibition results from the inhibition of VGCC transport to the PM thus indirectly preventing Ca^{2+} influx (Shih *et al.*, 2009).

More recently, CaBP7 was identified in a high throughput siRNA screen identifying genes that function during mitosis (Neumann *et al.*, 2010). Knockdown of CaBP7 in HeLa cells resulted in a binucleate phenotype suggestive of a role for CaBP7 during cytokinesis. This phenotype was not observed in HeLa cells stably transfected with an RNAi resistant mouse orthologue of CaBP7 when treated with the same siRNAs, implying that it was not an off-target effect. No other proteins of the CaBP family were identified in this screen (Neumann *et al.*, 2010).

1.9. Important Interacting Binding Partners of the CaBP Family

1.9.1. Voltage-gated Ca^{2+} channels (VGCCs)

VGCCs mediate cellular Ca^{2+} influx in response to membrane depolarisation. Ca^{2+} entering through these channels acts as a second messenger and initiates intracellular events such as contraction, secretion, synaptic transmission and gene expression. There are multiple types of Ca^{2+} current which are designated L-, N-, P/Q-, R- or T-type depending upon physiological and pharmacological criteria (Catterall, 2000). L-type currents are categorised as high voltage activation (HVA) channels, which exhibit slow voltage-dependent inactivation, are regulated by cAMP dependent phosphorylation, and are inhibited by dihydropyridines. L-type channels were therefore named for their 'long-lasting' currents. In comparison, T-type currents are generated through low voltage activated (LVA) channels, which inactivate rapidly, and are insensitive to pharmacological channel blockers. T-type channels are named for their 'transient' kinetics. N-, P/Q- and R-type channels are all HVA channels and are distinguished from L-type channels through their sensitivity to various peptide toxins: N-type channels are blocked by ω-conotoxin GVIA; and P/Q-type channels are sensitive to ω-agatoxin IVA. Finally R-type channels are resistant to all known Ca^{2+} channel blockers (Catterall, 2000).

VGCCs are made up four principal components: a transmembrane, pore-forming α_1 subunit, which dictates the functional and pharmacological properties of the channel; a cytoplasmic β subunit, which influences the channel inactivation

properties; a membrane anchored $\alpha_2\delta$ subunit; and transmembrane glycoprotein γ subunit. These subunits exist in different combinations depending on the channel type (Catterall, 2000, Minor and Findeisen, 2010) and various isoforms exist for each of the subunits. The most important subunit for channel function and characterisation, however, is the α_1 subunit. Expression of the α_1 subunit alone is sufficient to produce functional Ca^{2+} channels, however, the additional subunits are required to regulate the kinetics, voltage dependence and trafficking of the channel (Catterall, 2000, Bichet *et al*., 2000). The α_1 subunit shares structural homology to Na^+ and K^+ channels and each is composed of six transmembrane segments (S1-S6) and a membrane associated loop between S5 and S6. The S4 segment acts as the voltage sensor for the channel, and S5 and S6, with the associated loop, form the pore lining. Glutamate residues in the pore loop are required to confer Ca^{2+} selectivity (Catterall, 2000).

Different types of Ca^{2+} currents are defined by the specific α_1 subunits that the channel is assembled from. Ten distinct α_1 subunits have been identified and are divided into structurally and functionally related families: L-type currents are mediated by the Ca_v1 family; P/Q-, N- and R-type channels are mediated by the Ca_v2 family; and T-type channels are mediated by the Ca_v3 family. There are multiple subunits mediating L-type currents ($Ca_v1.1$ - $Ca_v1.4$) and T-type currents ($Ca_v3.1$ - $Ca_v3.3$), whereas single subunits have been identified which generate P/Q-, N- and R-type currents ($Ca_v2.1$, $Ca_v2.2$ and $Ca_v2.3$ subunits, respectively). Further diversity is generated through different isoforms of the β, γ, and $\alpha_2\delta$ subunits (Catterall, 2000, Minor and Findeisen, 2010).

Ca^{2+} entering through VGCCs influences many intracellular signalling pathways through the activation of various Ca^{2+} sensors. Some Ca^{2+} sensors are highly localised to the regions surrounding the channels and act as feedback regulators of channel function. For example the L-type, $Ca_v1.2$ channel is regulated by direct binding of CaM. CaM binds to the IQ domain in the C-terminus of $Ca_v1.2$, eliminates Ca^{2+} dependent inactivation (CDI) and causes Ca^{2+} dependent facilitation (CDF) of channel activity (Asmara *et al*., 2010).

As discussed earlier, CaBPs 1-5 have emerged as important regulators of L- and P/Q-type VGCCs (Lee *et al*., 2002, Zhou *et al*., 2004, Zhou *et al*., 2005, Haeseleer *et al*., 2004, Few *et al*., 2005, Tippens and Lee, 2007, Findeisen and Minor, 2010, Oz *et al*., 2011). The first interaction of L-type channels with the CaBPs was reported between CaBP4 and $Ca_v1.4$ channels in 2004 (Zhou *et al*., 2004). CaBP4 shifted the activation range of $Ca_v1.4$ to more hyperpolarised voltages which led to enhanced Ca^{2+} influx (Haeseleer *et al*., 2004). Since this initial observation, numerous interactions of CaBP1, CaBP4 and CaBP5 with the L-type channels, $Ca_v1.2$ and $Ca_v1.3$, have also been reported (Zhou *et al*., 2005, Tippens and Lee, 2007, Zhou *et al*., 2004, Findeisen and Minor, 2010, Oz *et al*., 2011). Like CaM, CaBP1 and CaBP5 were shown to inhibit CDI and promote CDF (Rieke *et al*., 2008, Zhou *et al*., 2004, Zhou *et al*., 2005, Findeisen and Minor, 2010). CaBP1 and CaBP4 were also shown to suppress CDI of $Ca_v1.3$ in inner hair cells where CDI is weak or absent and CaBP5 had similar effects in transfected HEK293T cells (Cui *et al*., 2007). This property of inner hair cells is thought to allow the audition of sustained sounds (Yang *et al*., 2006a). A stronger inhibitory effect has been described for CaBP1 than CaBP4, however, suggesting that CaBP1 may be the key Ca^{2+} sensor involved in this process (Cui *et al*., 2007). In contrast, CaBP1 modulation of the P/Q-type, $Ca_v2.1$ channel, enhances CDI and does not support CDF (Lee *et al*., 2002, Few *et al*., 2005). Interestingly, the interactions of CaBP1 with both $Ca_v1.2$ and $Ca_v2.1$ channels do not require functional EF-hand motifs suggesting that these interactions are Ca^{2+}-independent (Few *et al*., 2005, Findeisen and Minor, 2010).

The interaction of $Ca_v2.1$ with CaBP1 appears to be fine tuned by the presence or absence of an *N*-myristoylation signal. Wild type CaBP1L, which possesses an *N*-myristoyl group, enhances inactivation and shifts the activation range of the channel to more depolarising voltages (Lee *et al*., 2002). An *N*-myristoylation site mutant, however, was unable to support these effects, but instead modulated the channels with similar effects to CaM which promotes facilitation of the channel (Few *et al*., 2005). Differential modulation of L-type channels depending on the splice isoform of CaBP1 has also been observed. CaBP1 has been shown to completely inhibit inactivation of $Ca_v1.2$ channels (Zhou *et al*., 2005), but caldendrin causes a more modest suppression and signals through a different set of molecular

determinants (Tippens and Lee, 2007). This suggests that the sub cellular localisation of CaBP1 is important for its function and there are likely to be individual roles for the various splice isoforms.

In depth analysis of the interactions between CaBP1 and $Ca_v1.2$ channels have revealed that CaBP1 binds to the N-terminus, the S3-S4 linker region and the IQ domain at the C-terminus of $Ca_v1.2$ (Findeisen and Minor, 2010). CaBP1 can compete with CaM for binding to the IQ domain, however, interaction with the N-terminus and the S3-S4 linker region appear to be the crucial determinants for the regulatory function of CaBP1 on CDI. Interestingly Caldendrin, which causes a more modest suppression of CDI, does not bind to the N-terminus of $Ca_v1.2$ (Tippens and Lee, 2007).

1.9.2. Transient Receptor Potential Channels

Transient receptor potential (TRP) channels mediate the influx of extracellular Na^+ and Ca^{2+} into the cytoplasm. In excitable cells this influx depolarizes the PM and is important for the generation of action potentials. In non-excitable cells, membrane depolarisation by TRP channels stimulates voltage dependant channels (Ca^{2+}, K^+ and Cl^- channels). TRP channels have important functions mediating vision, taste, olfaction, hearing, touch, thermo-sensation, and osmo-sensation, and mutation or deregulation of TRP channels has been associated with various diseases (Song and Yuan, 2010).

TRP genes are found in organisms ranging from archaea to plants and animals, and in mammals are expressed in brain, heart, lung and other tissues. TRP proteins are transmembrane proteins which form cation channels with varying cation selectivities. Their topology is composed of six transmembrane domains (TMD) with a pore forming domain between TMD 5 and 6. The functional TRP channel is composed of a homo- or hetero-tetramer of TRP proteins, each subunit of which, contributes to the ion selectivity of the pore. The TRP superfamily is divided into two groups based on sequence and topological homology and these two groups are further subdivided into various TRP sub-classes. Group 1 comprises TRPC, TRPV,

TRPM, TRPA and TRPN, and group 2 comprises, TRPP and TRPML (Song and Yuan, 2010).

CaBP1 was found to interact with TRPC5 (Kinoshita-Kawada *et al*., 2005), a member of the TRPC family of channels which have been implicated in neurite extension, growth cone morphology and synaptogenesis in hippocampal neurons. The TRPC subfamily contains 7 genes which can be grouped depending on their sequence and functional characteristics. Group 1 contains TRPC1, 4 and 5. TRPC1 is widely expressed in many tissues and forms heteromeric channels with TRPC4 and TRPC5, whereas TRPC4 and TRPC5 can form homomeric channels. Together, TRPC1, 4 and 5 form non-selective cation channels which are activated by signalling through trimeric $G_{q/11}$ proteins which activate a phosolipase C (PLC) mediated pathway. The exact signalling mechanism is not fully understood, however (Song and Yuan, 2010, Beech, 2007).

Kinoshita-Kawada *et al.* demonstrated that the activity of TRPC5 channels in *Xenopus* ooctyes is dependent on the presence of Ca^{2+} (Kinoshita-Kawada *et al*., 2005). They also reported a direct interaction of CaBP1 with TRPC5 and showed that co-expression resulted in inhibition of TRPC5 activity. CaM also interacts with TRPC5 but does not have an inhibitory role and binds to TRPC5 at sites in close proximity, but not identical, to those bound by CaBP1 (Kinoshita-Kawada *et al*., 2005, Beech, 2007).

Biological functions for TRPC5 have been identified including roles mediating Ca^{2+} entry and excitation in smooth muscle, and as a regulator of neuronal growth cone extension. In addition, the TRPC5 gene is located on a region of the X chromosome which has been linked to X-linked mental retardation (Beech, 2007).

1.9.3. Inositol 1,4,5-trisphosphate Receptors

IP_3 and diacylglycerol (DAG) are second messengers which are produced as a result of hydrolysis of phosphatidylinositol 4,5-bisphosphate ($PI(4,5)P_2$) by PLC. IP_3 induces Ca^{2+} release from intracellular Ca^{2+} stores such as the ER. This is mediated by IP_3Rs, which are an IP_3-gated Ca^{2+} release channel. The conversion of IP_3 signals into Ca^{2+} signals is important for many cellular functions including cell proliferation,

differentiation, fertilisation, secretion, light transduction and brain function (Mikoshiba, 2007, Yang *et al*., 2002a).

There are three types of IP_3Rs in human, IP_3R1-3. Each type of IP_3R has different IP_3 binding and modulation properties. All three share a similar structure with five major domains: 1) an N-terminal IP_3-binding suppressor domain, 2) the IP_3 domain, 3) the central modulatory domain, 4) the channel forming domain, and 5) the C-terminal gate-keeper domain. IP_3R subunits assemble into either homo- or hetero-tetramers to form functional Ca^{2+}-release channels (Mikoshiba, 2007).

IP_3Rs are regulated by various endogenous ligands such as ATP and, importantly Ca^{2+} itself. Ca^{2+} release from IP_3Rs is enhanced at low levels of Ca^{2+} through CICR whereas, at higher $[Ca^{2+}]_i$, IP_3R activity is inhibited. CICR allows amplification and regenerative propagation of Ca^{2+} signals and is a property which is also shared by RyRs suggesting that it is a key feature for the regulation of intracellular calcium signalling (Mikoshiba, 2007).

An interaction of proteins of the CaBP family with IP_3Rs was first described by Yang *et al.* in 2002 (Yang *et al*., 2002a). This study reported a Ca^{2+}-dependent interaction of CaBP1S and a C-terminal CaBP1 fragment, encompassing the four EF-hand domains, with all three IP_3R isoforms (Yang *et al*., 2002a). Patch-clamping experiments in *Xenopus* ooctyes with different combinations of agonist in the pipette solutions revealed that CaBP1S, the C-terminal fragment of CaBP1, CaBP2S and CaBP5 were all able to enhance IP_3R mediated Ca^{2+} release independently of IP_3. CaBP4 was not tested in these experiments and CaM had no effect on IP_3R activity. These results indicated that there could be an alternative activation mechanism for IP_3Rs which does not require IP_3. This mechanism may be important for inducing CICR from IP_3Rs when the phosphoinositide signalling pathway has not been engaged (Yang *et al*., 2002a). Haynes *et al.*(Haynes *et al*., 2004) later reported a direct, Ca^{2+}-dependent, interaction between CaBP1L and IP_3R1. Conversely, this study found that overexpression of CaBP1L in PC12 cells inhibited IP_3R mediated Ca^{2+} release in response to agonists selective for purinergic receptors (Haynes *et al*., 2004). The discrepancies between the two studies may have arisen due to differences in the

activities of the CaBP1 splice isoforms used or could be due to differences in the experimental systems. Interestingly an earlier study also reported an inhibitory effect of CaBP1 on CICR release through an IP_3 independent mechanism (Kasri *et al*., 2003) and Kasri *et al.*(Kasri *et al*., 2004) reported an inhibitory effect of both CaBP1S and CaBP1L in COS cells. CaM also binds to and inhibits IP_3R, however, it has 100-fold lower binding affinity and elicits a weaker inhibitory effect than CaBP1 (Kasri *et al*., 2004). It was suggested that CaBP1 function may be important for the tight regulation of IP_3Rs in neurons where CaM may predominantly regulate RyRs (Kasri *et al*., 2004).

1.9.4. Phosphatidylinositol 4-kinases

PI4Ks are essential for the production of most phosphoinositide derivatives of phosphatidylinositol (PtdIns) (Balla and Balla, 2006). They catalyse the production of PI4P from PtdIns which is the first step in the synthesis of $PI(4,5)P_2$ and PtdIns (3,4,5)-trisphosphate ($PI(3,4,5)P_3$). $PI(4,5)P_2$ is the main substrate of PLC which generates the important second messengers, IP_3 and DAG. $PI(4,5)P_2$ also has important roles in the regulation of several ion channels and enzymes such as phospholipase D. $PI(3,4,5)P_3$ is generated from $PI(4,5)P_2$ through the action of PI3Ks and regulates a range of pathways including cell metabolism and an anti-apoptotic pathway. The production of important signalling phosphoinositides is therefore acutely dependent on the function of PI4Ks (Balla and Balla, 2006).

There are four identified PI4Ks in mammalian cells which are divided into two classes depending on their sensitivity to wortmanin, which is a potent PI3K inhibitor (Graham and Burd, 2011). Type III PI4Ks are sensitive to wortmanin and include PI4KIIIα and PI4KIIIβ. Type II PI4Ks are insensitive to wortmanin and include PI4KIIα and PI4KIIβ. Type III PI4Ks are structurally related to PI3Ks sharing a high degree of homology between their catalytic domains and explaining their shared sensitivity to wortmanin. A number of other domains are conserved between yeast and mammalian PI4KIIIβ orthologues including a lipid kinase unique (LKU) domain, the frequenin/NCS-1 binding domain, and the rab GTPase binding site (Hom2 domain). PI4KIIIα contains an LKU domain, a pleckstrin homology (PH) domain and a proline-rich domain which are conserved between the yeast and mammalian orthologues.

Type II PI4Ks are smaller proteins with little sequence homology to Type III PI4Ks and contain two catalytic domains, one of which harbours a cysteine-rich insert that is palmitoylated allowing these proteins to localise to membranes and orientate the kinase domains close to the PtdIns substrate (Balla and Balla, 2006).

Each type of PI4K therefore resides at a distinct subcellular compartment due to different targeting mechanisms which allow them to conduct specific non-redundant roles in vesicle trafficking and Golgi function (Balla and Balla, 2006). These kinases control signalling events through the production of PI(4,5)P_2 at the PM and nucleus, regulate endocytosis and determine the fate of endocytosed cargo by directing membrane proteins for degradation, and regulate the lipid composition of cellular membranes. PI4Ks are therefore important not simply for the production of PI4P, as the precursor of PI(4,5)P_2, but also for the correct functioning of numerous downstream signalling pathways (Balla and Balla, 2006).

As discussed above, CaBP7 and CaBP8 have been shown to interact directly with PI4KIIIβ and regulate vesicle trafficking from the TGN through inhibition of PI4P and PI(4,5)P_2 production (Mikhaylova *et al*., 2009). Mammalian PI4KIIIβ is predominantly Golgi localised and is recruited to this organelle via an interaction with the small GTP-binding protein Arf1 (Graham and Burd, 2011). PI4KIIIβ also interacts with and is regulated by NCS-1 but it is unknown if this contributes to the recruitment of PI4KIIIβ to the Golgi (Zhao *et al*., 2001, Balla and Balla, 2006). The details of how PI4KIIIβ affects Golgi function are not fully understood, however, products of PI4KIIIβ activity, along with Arf1 and other GTPases such as Rab11 are likely to recruit several effectors which promote the budding and release of Golgi-derived transport vesicles. PI4Ks have also been found in secretory granules and synaptic vesicles and PI4KIIIβ has been implicated in the modulation of regulated exocytosis. It has been proposed, therefore that PI4KIIIβ may play important roles in the transport and exocytosis of synaptic vesicles (Balla and Balla, 2006).

1.10. Differential Tissue expression of the CaBPs

The CaBPs have typically been described as neuronal Ca^{2+} sensors. CaBP1 is widely expressed in the brain and retina, whereas CaBPs 2-5 have been described as retina

specific proteins (Haeseleer *et al*., 2000). CaBP7 and CaBP8 are also highly expressed in the brain and *in situ* hybridization in rat brain highlighted differential expression when the two proteins were compared. CaBP7 is restricted to the CA3 region of the hippocampus, entorhinal cortex, the antero-dorsal and entero-ventral thalamus and the inferior and superior colliculus (Mikhaylova *et al*., 2006). In contrast, CaBP8 has a more widespread distribution in the brain with intense hybridization signals detected throughout the cerebellum, cortex and hippocampus (Mikhaylova *et al*., 2009). These expression patterns along with the reported interactions with important neuronal effectors such as the VGCCs suggest an important role for the CaBP family in the regulation of neuronal function. More recently, however, evidence has begun to emerge that suggests a more widespread expression for many of the CaBP proteins.

A study examining the expression of CaBP mRNAs in gastrointestinal smooth muscle identified significant levels of CaBP1L but not caldendrin, CaBP2, CaBP4, CaBP5 or CaBP7 (Ohya and Horowitz, 2002). CaBP1 has also been detected in type II taste cells isolated from taste buds in mice (Rebello *et al*., 2011). In addition, a 5-fold down-regulation of CaBP5 expression was detected in a microarray examining the platelet expression profile of a patient with a mutation in the transcription factor, core binding factor A2 (CBFA2) which causes abnormal platelet aggregation (Sun *et al*., 2007). This study suggests that CaBP5 is normally expressed in platelets and is not restricted to the retina. The discovery that CaBP7 expression in HeLa cells is essential for efficient cytokinesis is also suggestive of a more widespread distribution of this protein in dividing cells (Neumann *et al*., 2010).

The Human Protein Atlas project (http://www.proteinatlas.org/) is a publicly accessible database containing data about the normal expression and cellular distribution of proteins in 46 different human tissues. Immunohistochemistry data was available for CaBP5 and CaBP8 in this database. Moderate to strong CaBP5 immunostaining was detected in most normal tissues with the exception of pneumocytes, renal glomeruli, ovarian stromal cells and smooth muscle cells. CaBP8 showed moderate staining in neuronal cells and strong positive staining in a subset of glial cells as would be expected, but also gave moderate cytoplasmic or

membranous staining in basal layers of squamous epithelium, gall bladder, renal glomeruli, Leydig cells, myocytes and a subset of bone marrow poietic cells. A second online database, Genenote (http://bioinfo2.weizmann.ac.il/cgi-bin/genenote/home_page.pl), which uses microarrays to examine gene expression in normal human tissues, also contains data for CaBP1, CaBP4, CaBP7 and CaBP8. This data suggested that CaBPs are expressed in non-neuronal tissues (thymus, bone marrow, spleen, heart, skeletal muscle, kidney, lung, liver, pancreas, and prostate), and in the cases of CaBP4 and CaBP8, at similar expression levels to that found in the brain or spinal cord.

1.11. Summary of CaBP Expression and Function

The CaBPs are emerging as important regulators of various neuronal functions. The numerous reported interactions of CaBPs 1-5 with VGCCs suggest that these proteins may perform important roles regulating synaptic function and plasticity through the regulation of Ca^{2+} influx into neurons. Interactions with other important Ca^{2+} channels such as IP_3Rs and TRPC5 channels also support an important role for these proteins in the fine-tuning of calcium signalling in higher organisms. In contrast to the numerous roles of the CaBPs in the regulation of ion channels, interactions with proteins important for cellular transport have also been detected and an interaction with presynaptic mGluRs is suggestive of an important regulatory role in neurotransmission. CaBP7 and CaBP8 are the most divergent members of the CaBP family and may constitute a separate family of Ca^{2+} sensors in their own right. The only well-characterised function of these proteins is the regulation of TGN to PM trafficking through an interaction with PI4KIIIβ. Roles in the modulation of VGCCs and during cytokinesis have also been postulated, but it is not known how CaBP7 and CaBP8 exert their effects in these processes.

Characterisation of the CaBP family to date has largely focused on their functions in neuronal cell types, however emerging data suggests that CaBP protein expression may not be restricted to the central nervous system. In particular, a requirement for CaBP7 for efficient cytokinesis in HeLa cells is suggestive of an important role for this protein in dividing cells. It therefore seems that the current knowledge of CaBP function may only be the tip of the iceberg. Further investigative work will be

required to elucidate the full impact of the CaBPs upon calcium signalling in vertebrates and higher organisms.

1. 12. Aims and objectives

The aim of this study was to characterise CaBP7 and CaBP8 using a variety of different techniques. Four main research issues were addressed:

- The evolutionary origin of the CaBP family was examined and used to deduce whether CaBP7 and CaBP8 constitute a unique family of Ca^{2+} sensors separate from the rest of the CaBP family.

- The subcellular localisation and targeting mechanism of CaBP7 and CaBP8 was examined in neuronal and non-neuronal cell types.

- An investigation was carried out into a potential role for CaBP7 in cytokinesis.

- NMR spectroscopy was employed to investigate the structural differences between the two classes of CaBP proteins: CaBPs 1-5 and CaBP7 & 8. CaBP4 and CaBP7 were selected as representative proteins of these two classes.

Chapter 2:

Materials and Methods

2.1. Bioinformatics

The GenBank database accession numbers for human CaBP proteins (http://www.ncbi.nlm.nih.gov/sites/entrez) used for bioinformatics analyses were: Caldendrin (NM_001033677) CaBP1L (NM_031205), CaBP1S (NM_004276), CaBP2S (NM_031204), CaBP2L (NM_016366), CaBP4 (NM_145200), CaBP5 (NM_019855), CaBP7 (NM_182527), CaBP8 (AY007302), CaM (AAA35635). BLAST 2.2.22 at NCBI (http://blast.ncbi.nih.gov/blast.cgi) was used to perform BLASTP searches of these sequences restricted to particular organisms: *Danio rerio, Xenopus tropicalis, Anolis carolinenesis, Gallus gallus, Monodelphis domestica, Mus musculus, Pan troglodytes,* and *Homo sapiens.* Further searches using TBLASTN were performed against the reference genomic sequence and reference mRNA sequence databases to identify missing CaBP sequences not found in BLASTP searches. The genomes of the deuterostomes, *strongylocentrotus purpuratus, ciona intestinalis* and *branchiostoma floridae* and the jawless fish, Lamprey (*Petromyzon marinus)*,were searched using the BLAT facility at http://genome.ucsc.edu/cgi-bin/hgBlat?command=start. A TBLASTN search of the elephant shark (*Callorhinchus milli*) genomic sequences was carried out at http://esharkgenome.imcb.a-star.edu.sg/. Exon sequences from the human CaBPs were found by searching for each gene in the CCDS database at http://www.ncbi.nlm.nih.gov/CCDS/CcdsBrowse.cgi. Sequence identity between elephant shark and human exon sequences was calculated using ClustalW (http://www.ebi.ac.uk/Tools/msa/clustalw2/). The accession numbers of zebrafish (*Danio Rerio*) protein sequences used for analysis were: CaM: (NP_955864), CaBP1 (NP_001002414), CaBP2 (NP_001025439), CaBP4 (XP_001338361), CaBP5 (NP_956992), CaBP7 (XP_683885), CaBP8 (XP_690899). There were additional duplicated protein sequences identified in zebrafish which were: CaBP1 (NP_001005962), CaBP2 (XP_688066), CaBP5 (NP_00108568), CaBP7 (XP_001920190) and CaBP8 (XP_001343041).

Multiple sequence alignments were compiled using the ClustalX function (Conway Institute, UCD, Dublin) within the BioEdit Sequence Alignment Editor 6.0.5 (Tom Hall, Ibis Therapeutics, Carlsbad, California;

http://www.mbio.ncsu.edu/BioEdit.bioedit.html), using the BLOSUM62 matrix and default settings. The positions of the EF-hand motifs were identified by comparison to the EF-hand consensus sequence (Moncrief *et al*., 1990) and alignment with CaM. Identity values between different protein sequences were generated using the Sequence Identity Matrix option in BioEdit.

The open reading frames of human CaBP7 and CaBP8 were identified from their mRNA transcripts (NM_001017440.2 and NM_031468.3 respectively) using BioEdit and the sequences surrounding their multiple start sites were examined to identify the presence of a Kozak consensus sequence.

A phylogenetic tree was constructed using the human and zebrafish CaBP protein sequences based on alignments created using ClustalW (EMBL-EBI). The variable N-termini of the proteins were removed to aid construction of the tree and the alignment of the C-termini of CaBP7 and CaBP8 with the rest of the CaBPs was adjusted to give a more realistic representation of homology in this region. The maximum likelihood method was used to create the tree using the Phylip suite of programs (www.phylip.com). Seqboot.exe was used to make 2000 bootstrapped data sets from the alignment and proml.exe was then used to find the phylogeny estimate for each of these data sets using the maximum likelihood method for protein amino acid sequences. CaM was used as the out-group to root the tree. The outtree file from proml.exe was input into consensus.exe to generate a consensus tree. The final Consensus tree was drawn using TreeView (http://darwin.zoology.gla.ac.uk/~rpage/treeviewx/download.html).

Percentage sequence conservation within defining regions of the CaBPs (CaBP1L 16-75, CaBP2L 1-56, CaBP4 1-120, CaBP7 189-215 and CaBP8 193-219) in various species compared to human was assessed by creating pairwise sequence alignments using ClustalW and viewing the result summary to obtain the identity values.

2.2. Molecular Biology

2.2.1. PCR

DNA sequences for insertion into plasmids were prepared using PCR subcloning from existing plasmids. 100 µl PCR reaction mixes contained 20 µl 5x PCR reaction buffer, 5% v/v DMSO, 0.2 mM dNTPs, 0.5 µM forward and reverse primers, 0.5 µg template DNA and 1 U Phusion® polymerase (New England Biolabs, Hertfordshire, UK) and distilled water to 100 µl. The following PCR conditions were used:

1 cycle:	98°C	1 minute
35 cycles:	98°C	30 seconds
	*T_m-5°C	30 seconds
	72°C	15 seconds per kilobase
1 cycle:	72°C	5 minutes
	30°C	1 minute

* The annealing temperature used was 5°C below the lowest melting temperature (T_m) of the primer pair.

2.2.2. Restriction Endonuclease Digestion

Complimentary overhangs on plasmids and inserts for subcloning were generated by digestion with the appropriate restriction endonucleases as detailed in table 2.1, section 2.2.4. Digestion reactions containing 4 µl of the appropriate 10x buffer (New England Biolabs), 1 U of each required enzyme (New England Biolabs) and 1 µg of DNA in a total of 40 µl distilled water, were incubated at 37°C for 60 minutes. Digested products were separated by agarose gel electrophoresis and purified by gel extraction where necessary.

2.2.3. Agarose gel electrophoresis and gel extraction

For visualization and purification of PCR products or digested DNA products, DNA was separated by agarose gel electrophoresis using a gel composed of 1% w/v agarose dissolved in TAE buffer (40 mM Tris base pH 8.0, 20 mM acetic acid, 1 mM EDTA). 0.5 µl/ml Sybr Safe (Invitrogen, Paisley, UK) was included in the gels to stain the DNA. 10% sucrose was added to the samples and run alongside HyperLadder™ I

DNA molecular weight markers (Bioline, Sheffield, UK) at 60-80 V. After electrophoresis, DNA fragments were purified from agarose gels by visualisation using a UV transilluminator and excision of the required bands. DNA was extracted from the excised bands using a gel extraction kit (NBS biologicals Ltd, Cambridgeshire, UK). Briefly, excised bands were dissolved into the supplied binding buffer and released DNA then bound to an ion exchange column. The bound DNA was then washed and eluted in 30-50 µl elution buffer.

2.2.4. Ligation

For subcloning of prepared DNA inserts into linearised acceptor vectors, ligation reactions were used to generate circular plasmid constructs. 50 ng of acceptor vector was used with a 1:3 molar ratio of vector:insert and mixed with 2 µl 10x T4 DNA ligase reaction buffer (New England Biolabs) and 400 U T4 DNA ligase (New England Biolabs) in a final volume of 20 µl made up with deionised water. The reaction was incubated at room temperature for 15 - 30 minutes then 5 µl removed and used to transform chemically competent XL-1 *E. coli* cells.

Table 2.1 lists the plasmids which were made by subcloning, with the PCR primers and plasmid template used in PCR reactions, and the restriction enzymes used to generate complementary overhangs for ligation reactions.

Table 2.1. Plasmids made by subcloning

Plamid Name	Primers	Restriction Sites	Template Plasmid
mCherry^{CaBP7TMD}	Sense: 5′ - ATATAAGCTTTGCTCATCTGCGCCTTCGCC - 3′ Antisense: 5′ - CCGCGGCTACTTCATGCCACTGCGATAT - 3′	Hind III SacII	mCherry-CaBP7
mCherry-CaBP7-myc	Sense: 5' - ATATAAGCTTTAATGCCGTTCCACCCGGTG - 3' Antisense: 5′ - ATATCCGGGCCCGCGGCTACAGATCTTCTTCAGAAATAAGTTTTTG TTCCTTCATGCCACTGCGCAGCACCTGGTT - 3′	Hind III SacII	mCherry-CaBP7
mCherry-CaBP8-myc	Sense: 5' - ATATAAGCTTTAATGCCGTTCCACCATGTG - 3' Antisense: 5′ - ATATCCGGGCCCGCGGCTACAGATCTTCTTCAGAAATAAGTTTTT GTTCCTCCATGCCGCTCCGGAGTATCTGGTT - 3′	Hind III SacII	mCherry-CaBP8
SUMOPRO-optimised CaBP7 1-188	Sense: 5′ - ATATTCTAGATCAGCTCTTACGCACACA - 3′ Antisense: 5′ - ATATCTCGAGTCACAGGCTCTTACGCACACA - 3′	BsaI XhoI	TrcHisA-Optimised CaBP7 1-188

A number of protein expression plasmids were generated during the course of this project which were not used to generate any of the final data. Details for these plasmids are therefore not described here with the exception of TrcHisA-optimised CaBP7 1-188 as this was used as a template to subclone SUMOPRO-optimised

CaBP7 1-188. The names of the remaining plasmids can be found in table 6.1, chapter 6, section 6.2.1.

2.2.5. Transformation of chemically competent *E. coli*

To amplify DNA constructs by plasmid miniprep or maxiprep methods, competent *E. coli,* prepared in-house, were transformed with 5 µl of ligation reaction or 0.5 µl of the relevant plasmid for amplification. The DNA was incubated with 50 µl chemically competent cells on ice for 30 minutes before being subjected to a heat shock of 45 seconds at 42^{o}C. The cells were then returned to ice for a further 2 minutes followed by addition of 450 µl SOC medium (2% w/v tryptone, 0.5% w/v yeast extract, 8.56 mM NaCl, 2.5 mM KCl, 10mM $MgCl_2$, 20mM glucose) and incubation at 37^{o}C for 1 hour with continuous shaking at 250 rpm. The transformed *E. coli* were spread onto sterile LB agar plates (1.5% w/v agar, 1% w/v tryptone, 0.5% w/v yeast extract, 8.56 mM NaCl) containing the appropriate antibiotic for the selection of positive transformants of the plasmid in question. The transformation plates were incubated at 37^{o}C overnight and colonies selected for further analysis or proliferation.

2.2.6. Purification of Plasmid DNA

To analyse *E. coli* transfomants of newly ligated plasmids, single colonies were selected and grown overnight at 37^{o}C, with shaking, in 5 ml LB media (1% w/v tryptone, 0.5% w/v yeast extract, 8.56 mM NaCl) containing the appropriate antibiotic. The cultures were then pelleted by centrifugation (12 000 x g, 10 minutes) and plasmid DNA extracted using a spin column miniprep kit (NBS biologicals Ltd) according to the manufacturer's protocol. Briefly, cells were lysed with an alkaline solution containing sodium dodecyl sulphate (SDS) and immediately neutralized by addition of acetate which precipitates both the SDS and genomic DNA. After centrifugation (12 000 x g, 5 minutes) to pellet precipitated material, the supernatant was transferred to a silica gel based spin column to bind the DNA. Bound DNA was washed to remove impurities and then eluted in 30 - 50 µl Tris based elution buffer. Purified plasmid DNA could then be analysed by restriction endonuclease digestion and agarose gel electrophoresis (see section 2.2.2).

For large scale plasmid preparations 150 ml LB media containing the appropriate antibiotic was inoculated with a single colony from the transformation plate and incubated overnight at 37^{o}C with shaking at 250 rpm. Plasmid DNA was extracted from the cultures using a QIAfilter HiSpeed Plasmid Maxi Kit (Qiagen, West Sussex, UK) according to the manufacturer's instructions. The concentration of purified plasmid DNA was determined from the absorbance of the DNA sample at 260 nm.

2.2.7. Generation of plasmids by mutagenesis

A number of plasmids were generated using site directed mutagenesis of existing expression vectors. These plasmids are listed in Table 2.2, along with the relevant mutagenesis primers and the original plasmid which was used as a template.

Reactions for site directed mutagenesis contained 5 µl 10x PCR reaction buffer, 50 ng template DNA, 125 ng forward and reverse mutagenesis primers, 0.2 mM dNTPs and 1 U *PfuTurbo* (Invitrogen). The following PCR conditions were used:

Step 1:	95^{o}C	30 seconds	
Step 2:	95^{o}C	30 seconds	
	55^{o}C	1 minutes	
	68^{o}C	6 minutes	(1 minute per kilobase)

Step 2 was repeated for a different number of cycles depending on the type of mutation:

x12 for a single base change

x16 for a single amino acid change

x18 for multiple amino acid changes

The reactions were subsequently cooled on ice for 2 minutes then treated with Dpn1 (New England Biolabs), to digest the parental template DNA, for 1 hour at 37^{o}C. 1 µl of the Dpn1 digested material was transformed into chemically competent *E. coli* as described in section 2.2.5. Plasmids were checked and amplified as for subcloned plasmids (sections 2.2.5-2.2.6).

Table 2.2. Plasmids made by mutagenesis.

Plasmid Name	Mutagenesis Primers	Template Plasmid
CaBP7^{TMDKKK}	Sense: 5'- TGCGCCTTCGCCATCAAGAAGAAGATCAGT GTCATGCTC – 3' Antisense: 5' – GAGCATGACACTGATCTTCTTCTTGATGGCGAAGGCGCA – 3'	mCherry-CaBP7
CaBP8^{TMDKKK}	Sense: 5' – TGCGCCTTTGCTATGAAGAAGAAGATCAGTGTCATGCTG-3' Antisense: 5' – CAGCATGACACTGATCTTCTTCTTCATAGCAAAGGCGCA – 3'	mCherry-CaBP8
mCherry-CaBP7 EF1'	Sense: 5' – TTCATCTCCAAGCAGCAGCTGGGCACAGCCATG -3' Antisense: 5' – CATGGCTGTGCCCAGCTGCTGCTTGGAGATGAA-3'	mCherry-CaBP7
mCherry-CaBP7 EF2'	Sense: 5' – CAAGTGGACTTTGAGCAGTTTGTGACCCTTCTG-3' Antisense: 5' – CAGAAGGGTCACAAACTGCTCAAAGTCCACTTG-3'	mCherry-CaBP7
mCherry-CaBP7 EF1' EF2'	Sense: 5' – CAAGTGGACTTTGAGCAGTTTGTGACCCTTCTG-3' Antisense: 5' – CAGAAGGGTCACAAACTGCTCAAAGTCCACTTG-3'	mCherry-CaBP7 EF1'
mCherry-CaBP8 EF1'	Sense: 5' – TTCATCTCCAAGCAGCAGCTGGGCATGGCCATG -3' Antisense: 5' – CATGGCCATGCCCAGCTGCTGCTTGGAGATGAA-3'	mCherry-CaBP8
mCherry-CaBP8 EF2'	Sense: 5' – CAGGTGGATTTTGATCAATTCATGACCATTCTT -3' Antisense: 5' – AAGAATGGTCATGAATTGATCAAAATCCACCTG-3'	mCherry-CaBP8
mCherry-CaBP8 EF1' EF2'	Sense: 5' – CAGGTGGATTTTGATCAATTCATGACCATTCTT -3' Antisense: 5' – AAGAATGGTCATGAATTGATCAAAATCCACCTG-3'	mCherry-CaBP8 EF1'
mCherry-CaBP7 lyso	Sense: 5' – GATGAGCTGAAGCGGGCGGCCGCCGACACCTTCTGCGAG-3' Antisense: 5' – CTCGCAGAAGGTGTCGGCGGCCGCCCGCTTCAGCTCATC-3'	mCherry-CaBP7
mCherry-CaBP8 lyso	Sense: 5' – GAGTTGAAGCACATTGCCGCTCATGCCTTCCGAGAC-3' Antisense: 5' – GTCTCGGAAGGCATGAGCGGCAATGTGCTTCAACTC-3'	mCherry-CaBP8
mCherry-CaBP7 (RNAi resistant)	Sense: 5' – GACATAGAGAACATAATTATGACAGAGGAGGAG-3' Antisense: 5' – CTCCTCCTCTGTCATAATTATGTTCTCTATGTC-3'	mCherry-CaBP7
mCherry-CaBP7 1-188 (RNAi resistant)	Sense: 5' – GACATAGAGAACATAATTATGACAGAGGAGGAG-3' Antisense: 5' – CTCCTCCTCTGTCATAATTATGTTCTCTATGTC-3'	mCherry-CaBP7 1-188
mCherry-CaBP7 EF1' EF2' (RNAi resistant)	Sense: 5' – GACATAGAGAACATAATTATGACAGAGGAGGAG-3' Antisense: 5' – CTCCTCCTCTGTCATAATTATGTTCTCTATGTC-3'	mCherry-CaBP7 EF1' EF2'

2.2.8. Commercially synthesized genes and insertion into expression vectors

A number of customized genes were ordered from either Integrated DNA Technologies (IDT, Glasgow, UK) or GeneArt (Invitrogen). The required protein sequences were sent to either IDT or GeneArt and the corresponding gene synthesized with optimized codon usage for expression in the relevant organism. A codon optimized variant of CaBP7 1-188 was obtained from IDT in order to improve the DNA sequence for translation in *E. coli*. This was used to produce recombinant CaBP7 1-188 and CaBP7 1-100 proteins. A codon optimized variant of CaBP4 was ordered from GeneArt for the same reasons.

These genes were synthesized with restriction sites at their 3' and 5' ends to allow cloning into the relevant expression plasmid. For instance, CaBP7 1-188 was

synthesized with a 3' Xho1 site and a 5' BglII site to allow direct ligation into pTrcHisA. The restriction sites used are listed in table 2.3. Synthesised genes were cloned into their relevant expression vector by digestion of the acceptor and donor vectors with the relevant restriction enzymes, gel purification and subsequent ligation of the vector and insert as described in sections 2.2.2 – 2.2.4.

Table 2.3 Plasmids made from custom synthesized genes

Plasmid name	Donor plasmid	Restriction Sites
TrcHisA-optimised CaBP7 1-188	IDT optimised CaBP7 1-188	XhoI BglII
SUMOPRO-optmised CaBP4	GeneArt optimised CaBP4	BsaI XhoI

2.2.9. CaBP7 shRNA and other plasmids

CaBP7 shRNA and scrambled shRNA were ordered from origene (Cambridge, UK) from the HuSH-29 range of pre-designed human shRNA plasmids. The sequence for the scrambled shRNA was: 5'-GCACTACCAGAGCTAACTCAGATAGTACT-3'. The sequence for the CaBP7 specific shRNA was: 5'-GACATGGATGGTGATGGTCAAGTGGACTT-3'. The plasmid encodes a 29-mer shRNA under control of a human U6 promoter. The plasmid also encodes GFP under control of a cMV promoter to verify transfection efficiency.

Table 2.4 lists any other plasmids that were used in this thesis.

Table 2.4. Other plasmids.

Plamid name	Obtained from
Caldendrin-mCherry	Dr L. Haynes, University of Liverpool
CaBP1L-EYFP	Dr L. Haynes, University of Liverpool
CaBP1L-mCherry	Dr L. Haynes, University of Liverpool
CaBP1S-mOrange	Dr L. Haynes, University of Liverpool
CaBP1S-EYFP	Dr L. Haynes, University of Liverpool
CaBP2-mCherry	Dr L. Haynes, University of Liverpool
CaBP4-mCherry	Dr L. Haynes, University of Liverpool
CaBP5-mCherry	Dr L. Haynes, University of Liverpool
CaBP7-mCherry	Dr L. Haynes, University of Liverpool
CaBP8-mCherry	Dr L. Haynes, University of Liverpool
mCherry-CaBP7	Dr L. Haynes, University of Liverpool
mCherry-CaBP8	Dr L. Haynes, University of Liverpool
EYFP-CaBP7	Dr L. Haynes, University of Liverpool
EYFP-CaBP8	Dr L. Haynes, University of Liverpool
mCherry-CaBP7 1-188	Dr L. Haynes, University of Liverpool
mCherry-CaBP8 1-192	Dr L. Haynes, University of Liverpool
$CaBP5^{CaBP7TMD}$-mCherry	Dr L. Haynes, University of Liverpool
$CaBP5^{CaBP8TMD}$-mCherry	Dr L. Haynes, University of Liverpool
LAMP1-EYFP	Dr L. Haynes, University of Liverpool
Rab5A-EYFP	Dr L. Haynes, University of Liverpool
LC3-EYFP	Dr L. Haynes, University of Liverpool
EGFP- VAMP7	A gift from Prof T. Galli
VSVG-GFP ts045	A gift from Dr J. Presley
Optimised CaBP7 1-188	Customised synthesis from IDT
Optimised CaBP4	Customised synthesis from GeneArt
ECFP-C1	Clontech, Saint-Germain-en-Laye, France
CaBP7 shRNA	Origene, Cambridge, UK
Scrambled shRNA	Origene, Cambridge, UK

2.2.10. DNA sequencing

All cloning was verified by automatic sequencing carried out by "DNA sequencing and services" in Dundee, UK.

2.3. Cell culture and transfection

All cell culture reagents used to maintain cell lines were purchased from Invitrogen. Cells were cultured in 75 cm^2 flasks at 37^oC in a humidified atmosphere of 5% CO_2/95% air.

Cells for transfection were seeded onto 24-well or 6-well trays at a density of ~$4x10^5$. Cells for imaging were grown on coverslips in 24 well trays or on glass bottomed dishes (MatTek corporation, Massachusetts, USA). Transfection mixtures contained the DNA plasmids to be transfected with 3 µl GeneJuice® transfection reagent per 1 µg DNA, made up to either, 100 µl for each well of a 24 well plate, or 300 µl for each well of a 6 well plate, with Opti-MEM® serum free media. The reaction mixtures were incubated for 15 - 20 minutes at room temperature to allow the lipid and DNA complexes to associate then added drop-wise to the cells. Cells were maintained for 24 hours post transfection before use unless otherwise indicated. Cells for fixation without further processing were washed three times in phosphate buffered saline (PBS; 137 mM NaCl, 2.7mM KCl, 10 mM Na_2PO_4, 2 mM NaH_2PO_4, pH 7.4) then fixed in 4% formaldehyde in PBS at room temperature for 10 minutes. Cells were then washed a further three times in PBS, the coverslips rinsed gently with deionized H_2O and dried, then the coverslips mounted onto glass slides using ProLong® Gold antifade mounting reagent (Invitrogen) and left to dry at room temperature overnight before imaging.

2.3.1. HeLa cell culture

HeLa cells were maintained in Dulbecco's modified Eagle's medium (DMEM) supplemented with 5% foetal bovine serum (FBS), 1% non-essential amino acids (NEAA) and 1% penicillin-streptomycin.

2.3.2. N2A cell culture

Neuroblastoma 2A (N2A) cells were cultured in DMEM supplemented with 10% FBS and 1% penicillin-streptomycin. To stimulate differentiation prior to transient transfection, N2A cell media was exchanged for DMEM supplemented with 2% FBS, 1% penicillin-streptomycin, and 20 µM retinoic acid.

2.4. Immunofluorescence

Table 2.5. List of antibodies used for immunofluorescence and their dilutions.

Antibody	Description	Supplier	Dilution
α -Tubulin (DM1A)	Mouse monoclonal	Abcam (Cambridge, UK)	1 in 500
c-myc	Rabbit polyclonal	Sigma (Missouri, USA)	1 in 100
CaBP7	Rabbit polyclonal	Santa Cruz (California, USA)	1in 200
Calnexin	Rabbit polyclonal	Sigma (Missouri USA)	1 in 200
CD63	FITC conjugated Mouse monoclonal	Abcam (Cambridge, UK)	1 in 00
CD63	Mouse monoclonal	Biodesign International (Maine, USA)	1 in 200
HRS	Rabbit polyclonal	Dr Sylvie Urbé (University of Liverpool, UK)	1 in 1000
LAMP1	Mouse monoclonal	Abcam (Cambridge, UK)	1 in 400
M6PR	Rabbit polyclonal	Prof Paul Luzio (University of Cambridge, UK)	1 in 500
p230	Mouse polyclonal	BD Biosciences (Oxford, UK)	1 in 200
Rab11	Rabbit polyclonal	Zymed (California, USA)	1 in 500
RFP	Rabbit polyclonal	Dr Ian prior (University of Liverpool, UK)	1 in 100
SNAP29	Rabbit polyclonal	Sigma (Cambridge, UK)	1 in 50
Syntaxin6	Mouse monoclonal	Abcam (Cambridge, UK)	1 in 200
TOM20	Mouse monoclonal	BD Biosciences (Oxford, UK)	1 in 1000
VAMP7	Mouse monoclonal	Abcam (Cambridge, UK)	1 in 500

Cells were washed three times in PBS then fixed in 4% formaldehyde in PBS at room temperature for 10 minutes. Cells were washed a further three times in PBS then permeabilised using 0.2% triton X-100 in PBS for 6 minutes at room temperature. Cells were washed three times in PBS to remove detergent then twice in PBS containing 5% BSA (PBSB). Cells were then incubated with primary antibody at the dilutions indicated in table 2.5, for 1 hour at room temperature in PBSB. Cells were washed three times in PBS and twice in PBSB prior to incubation with the relevant fluorophore conjugated secondary antibody (1 in 75 dilution for FITC conjugates, 1 in 400 dilution for Alexa Fluor conjugates) for 1 hour at room temperature except in the case of directly FITC conjugated anti-CD63 primary antibody. Cells were washed again three times in PBS, rinsed with deionized H_2O, dried and mounted onto glass slides using ProLong® Gold antifade reagent (Invitrogen). Where nuclei were visualized, ProLong® Gold antifade reagent supplemented with DAPI (Invitrogen) was used.

2.5. Confocal Microscopy

Table 2.6. Fluorophores used in confocal microscopy and the excitation and emission wavelengths used.

Fluorophore	Excitation (nm)	Emission (nm)
ECFP	405	450-500
EYFP	488	520-570
EGFP	488	505-615
mCherry	594	610-710
FITC	488	500-540
Alexa 594	594	590-710
Alexa 405/DAPI	405	450-500
Alexa 568	594	560-720
mCherry and FITC	594 488	610-710 500-540

2.5.1. Fixed cell imaging

Imaging of transfected and/or immunostained cells was carried out using a Leica AOBS SP2 microscope (Leica microsystems, Heidelberg, Germany) using a 63x oil

immersion objective with a 1.4 numerical aperture. In most cases the pinhole was set to Airy1 to give the optimum signal to noise ratio and hence minimum thickness confocal section for the excitation laser used. The wavelengths used for excitation of fluorophores and the emission ranges collected are listed in table 2.6.

2.5.2. Live cell imaging

All live cell imaging experiments with the exception of the experiment using Lysotracker™ Blue, were carried out using a Leica AOBS SP2 microscope using a 63x oil immersion objective with a 1.4 numerical aperture. Cells were maintained at room temperature throughout each experiment as indicated in section 2.6.2.

Imaging of Lysotracker™ Blue DND-22 (Invitrogen) uptake was carried out using a Zeiss LSM510 confocal system. Cells were incubated for 30 minutes in media containing 50 nM Lysotracker™ Blue DND-22 at 37^{o}C. Loading media was then exchanged for fresh media and the fluorescence signal imaged. Lysotracker™ Blue fluorescence was measured by excitation with a UV laser line at 351 nm.

2.5.3. Image analysis

All Images were processed using the CorelDraw software package (Corel Corporation, Ottawa, Canada) or ImageJ Java-based imaging software (NIH, USA).

2.6. Cell assays

2.6.1. VSVG assay

For colocalisation of ts045 VSVG-GFP at the TGN cells were co-transfected with various wild type and mutant, colour tagged, CaBP7 and CaBP8 constructs along with ts045 VSVG-GFP. Cells were incubated at 37^{o}C for 4 hours post-transfection then transferred to 40^{o}C overnight. Cells were subsequently transferred to 20^{o}C for 2 hours to trap ts045 VSVG-GFP at the TGN before fixation.

2.6.2. Fluorescence Protease Protection Assay

HeLa cells were plated onto glass bottomed dishes and triply transfected with 1 µg of each of three constructs: ECFP-C1, either EYFP-CaBP7 or EYFP-CaBP8, and either CaBP7-mCherry or CaBP8-mCherry. Protease protection of the fluorescent colour

tag was examined using a previously described method (Lorenz *et al*., 2006). 24 hours post-transfection cells were washed three times in KHM buffer (20 mM HEPES pH7.2, 110 mM potassium acetate, 2 mM magnesium chloride) at room temperature. The cell chamber was set up for perfusion on the microscope stage and the microscope focused on one or two transfected cells. Imaging was started during this pre-permeabilisation stage with one frame collected every 8 seconds. Each of the three colour channels was recorded in series to avoid potential bleed-through. Cells were perfused with KHM buffer containing 40 µM digitonin until the cytosolic ECFP fluorescence started to dissipate. Perfusion was then switched to KHM buffer alone until the ECFP fluorescence had disappeared (approximately 10 - 60 sec) then switched to KHM buffer containing 4 mM trypsin (Sigma). Images were recorded until the EYFP signal was lost.

2.6.3. Biochemical Protease Protection Assay

HeLa cells were plated at a density of ~$4x10^5$ on 6-well trays and duplicate wells transfected with 3 µg of either: mCherry-C1, mCherry-CaBP7 or CaBP7-mCherry. 24 hours post-transfection cells were washed twice in KHM buffer. One well from each condition was then treated with 40 µM digitonin in KHM buffer for 1 minute at room temperature to selectively permeabilise the PM. After permeabilisation cells were treated with 4 mM trypsin in KHM buffer for 5 min at room temperature. The cells were then washed and solubilised into 300 µl Laemmli buffer, then the samples boiled for 5 minutes. The remaining wells were not treated with digitonin or trypsin but were also lysed into 300 µl Laemmli buffer and boiled. 25 µl volumes of each sample were analysed by SDS-PAGE and western blotting using a rabbit polyclonal RFP antibody (Table 2.7).

2.6.4. Antibody accessibility experiments

Cells plated onto glass coverslips were transfected with 1 µg of either mCherry-CaBP7-myc or mCherry-CaBP8-myc. 24 hours post-transfection cells were washed and permeabilised in one of two ways: Control cells were fixed in 4% formaldehyde in PBS then all cellular membranes non-selectively permeabilised by incubation with 0.2% Triton-X-100 in PBS for 6 minutes. For selective permeabilisation of the PM, cells were first treated with 40 µM digitonin in KHM buffer for one minute before

fixation using 4% formaldehyde in PBS. Cells from both conditions were processed for immunofluorescence using either a monoclonal anti-c-myc antibody or a rabbit polyclonal anti-RFP antibody (Table 2.5).

2.7. SDS PAGE and Western blotting

Cells transfected on a 6 well tray were solubilised into 300 µlLaemmli buffer, boiled for 5 minutes and proteins resolved by SDS PAGE. Typically either fixed 12% or 15% acrylamide gels or pre-cast Novex 8-16% Tris-glycine gradient gels (Invitrogen) were used. 5 µl SeeBlue® plus 2 prestained standard molecular weight protein markers (Invitrogen) were loaded alongside protein samples. SDS PAGE gels were run at 140 V for approximately 90 minutes. Gels were stained with SimplyBlue™ SafeStain (Invitrogen) or transferred to nitrocellulose membranes by transverse electrophoresis for 1 hour at 80 V. Nitrocellulose membranes were stained with Ponceau-S solution (Sigma) to confirm successful protein transfer. Membranes were washed with PBS to remove the stain then blocked in blocking buffer (5% milk in PBS) for 1 hour. This was followed by incubation for 1 hour with primary antibody in blocking buffer at the concentration indicated in table 2.7. The membrane was then washed three times in PBS plus 0.1% Tween 20 (PBST) and once in PBS before incubation with the appropriate horseradish peroxidase-conjugated secondary antibody (Sigma) (1 in 400) in blocking buffer. Membranes were subsequently washed once in PBST followed by two washes in PBS. A high salt wash using 0.5 M NaCl in PBS was then performed for 30 minutes at room temperature followed by a 15 minute wash in dH_2O before blots were developed by incubation for ~2 minutes with ECL Plus Western Blotting Detection Reagents (GE Healthcare, Buckinghamshire, UK). Blots were imaged on a ChemiDoc XRS system (BioRad, California, USA).

Table 2.7. List of antibodies and their dilutions used for western blotting.

Antibody	Description	Supplier	Dilution
α-Tubulin	Mouse monoclonal	Abcam (Cambridge, UK)	1 in 500
CaBP7	Rabbit polyclonal	Santa Cruz (California, USA)	1in 200
GAPDH	Mouse monoclonal	Sigma (Missouri, USA)	1 in 1000
RFP	Rabbit polyclonal	Dr Ian prior (University of Liverpool, UK)	1 in 200

2.8. Protein expression and purification

Recombinant proteins made for any purpose other than NMR were expressed from BL21 cells grown in superbroth media (0.5% w/v NaCl, 1.5% w/v tryptone, 2.5% w/v yeast extract) supplemented with the appropriate antibiotics for the expression plasmid (appendix, table A1) and BL21 strain used (Table 6.1, chapter 6). Isotopically labelled proteins for NMR were made by growing the expression bacteria in M9 minimal media (50 mM sodium phosphate buffer, 22 mM potassium phosphate buffer, 8.5 mM NaCl, pH 7.2) supplemented with 1 mM $MgSO_4$, 50 µM $CaCl_2$, 23 mM NH_4Cl, 22 mM glucose and 100 µl PTM_1 salts (24 mM $CuSO_4$.5H2O, 0.534 mM NaI, 17.8 mM $MnSO_4.5H_2O$, 0.827 mM $NaMoO_4.2H_2O$, 0.323 mM H_3BO_3, 2.1 mM $CoCl_2.6H_2O$, 147 mM $ZnCl_2$, 234 mM $FeSO_4.7H_2O$, 1.64 mM biotin, 188 mM H_2SO_4) per litre. Media was also supplemented with appropriate antibiotics for the expression plasmid and specific BL21 strains used. Unlabelled ammonium chloride was substituted with ^{15}N labelled ammonium chloride (ISOTEC®, Sigma) in single and double labelled protein preparations. Unlabelled glucose was substituted with ^{13}C labelled glucose (ISOTEC®, Sigma) in double labelled protein preparations. Single labelled but not double labelled protein preparations were supplemented with 0.5 g ^{15}N labelled ISOGRO ® (ISOTEC®, Sigma) per 1 litre minimal media. ISOGRO® is an algal lysate-derived complex labelled growth medium which supports acceleration of host cell metabolism.

Expression bacteria were grown at 37^{o}C until an OD_{600} of 0.8 - 1.0 was achieved. Protein expression of various glutathione S-transferase (GST) and His_6-tag fusion proteins was induced using IPTG according to the parameters listed in chapter 6, section 6.2.1, table 6.1. Standard BL21 (DE3) cells were taken from lab stocks. A range of BL21 variants were tested as in Chapter 6, section 6.2.1, table 6.1. These included Rosetta™ (DE3) competent cells (Merck,Darmstadt, Germany), BL21-CodonPlus® (DE3)-RIL cells (Agilent Technologies, California, USA), BL21-CodonPlus® (DE3)-RP cells (Agilent Technologies), and ArcticExpress (DE3)-RIL competent cells (Agilent Technologies). After induction bacteria were harvested by centrifugation at 2400 x *g* for 10 mins. Pellets were resuspended in binding buffer, either: 50 mM Tris pH 7.0 for GST fusion proteins; or 50 mM sodium phosphate buffer pH 7.0, 300 mM NaCl (Talon buffer) for His fusion proteins. Both buffers were supplemented with protease inhibitors (Complete mini protease inhibitor cocktail tablets, Roche, Basel, Switzerland). Cells were lysed using a cell disrupter (Constant Systems Ltd, Daventry, UK) set at 27 KPSI then centrifuged at 100 000 x *g* in a Beckman L80K ultracentrifuge for 1 hour at 4^{o}C to separate soluble and insoluble fractions.

Glutathione cellulose resin (Bioline) was used to affinity purify GST fusion proteins. Talon™ metal affinity resin (Takara, Saint-Germain-en-laye, France) or HiTrap™ IMAC FF columns (GE Healthcare) charged with $NiSO_4$, were used to affinity purify His tagged proteins. For purification with unpacked resin, the resin was prewashed in the appropriate binding buffer then incubated with clarified bacterial lysate for 1 hour at 4^{o}C. The resin was then washed extensively (> 30 resin volumes) in binding buffer. To elute bound protein from the resin the appropriate binding buffer was supplemented with 10 mM reduced glutathione for GST fusion proteins or 500 mM imidazole for His_6-tagged proteins. For purification using HiTrap™ columns (GE Healthcare), the clarified lysate was loaded onto the column using a syringe. The column was then washed extensively with binding buffer (> 5 column volumes) followed by binding buffer supplemented with 25 mM imidazole (> 5 column volumes) to remove non-specifically bound protein. Protein remaining on the column was eluted in 3 ml fractions using binding buffer supplemented with 500

mM imidazole. Protein expression and yield was checked by SDS PAGE and gels stained with SimplyBlue™ SafeStain (Invitrogen).

Affinity tags were cleaved using commercially available proteases according to the manufacturer's instructions. PreScission Protease (GE Healthcare) was used to cleave GST tags, Tobacco etch virus (TEV) protease (Invitrogen) was used to cleave the His_6-tag from proteins expressed from the TrcHisTEV plasmid, and the SUMO Protease, ULP1, was used to cleave His_6-SUMO tags (made in-house by Dr Andy Herbert). ULP1 is compatible for use in a range of different buffers and was generally used in the buffer subsequently used for NMR experiments. The SUMO Protease protocol was adjusted to perform the cleavage with recombinant protein immobilized on affinity resin as described in chapter 6, section 6.2.

Where proteins were purified using a HiTrap™ column, imidazole was removed by dialysis into an appropriate compatible NMR buffer. After dialysis the His_6-SUMO-tag was cleaved by incubating the protein with 2 U of SUMO Protease per mg of test protein at room temperature for 2 - 3 hours. This protein sample was then re-applied to a new HiTrap™ column to remove free His_6-SUMO tag and ULP-1 protease, along with any uncleaved fusion protein. Protein from this repass step was then concentrated into a 500 µl final volume using vivaspin ultrafiltration columns (GE Healthcare) with an appropriate molecular weight cut off significantly below the size of the protein to be purified.

Protein concentration was calculated by measuring the absorbance at 280 nm using the theoretical molar extinction coefficient (ExPASy, ProtParam http://web.expasy.org/protparam/). The Concentration of protein samples used to record NMR spectra were typically in the range of 50 - 200 µM.

Apo CaBP7 1-100 was made by dialyzing the uncleaved protein into 20 mM HEPES pH 7.0, 50 mM NaCl, 2 mM octylglucoside, 5 mM EDTA, 5 mM EGTA. The His_6-SUMO tag was cleaved after dialysis as described above and cleaved protein diluted into EDTA/EGTA-free buffer using a vivaspin ultrafiltration column until the

EDTA/EGTA concentrations were below 50 µM. Protein was re-applied to a HiTrap™ column to remove the free SUMO, protease and uncleaved fusion protein and subsequently concentrated using a new vivaspin ultrafiltration column.

2.9. NMR Spectroscopy

Samples for NMR were prepared in their respective buffers in 90% H_2O/10% D_2O. Spectra were acquired on Bruker AVANCE II+ 600 MHz and 800 MHz spectrometers fitted with 5 mm triple resonance TCI cryoprobes. NMR experiments for ^{1}H, ^{15}N and ^{13}C backbone and side-chain assignments included 2D ^{1}H-^{15}N HSQC, ^{1}H-^{13}C HSQC, 3D HNCO, HN(CA)CO, CBCANH, CBCA(CO)NH, HBHANH and (H)CCH-TOCSY. Descriptions of these experiments can be found in chapter 6, section 6.2.5, table 6.3. All NMR spectra were acquired and processed by Dr Andrew Herbert (NMR Centre for Structural Biology, University of Liverpool). The parameters used in the experiments for CaBP7 1-100 backbone and side chain assignments are listed in table 2.8. NMR data was processed using Bruker Topspin 2.1 and analysed using the Analysis program from the collaborative computing project for NMR (CCPN) (Vranken *et al*., 2005)

The buffers used for individual NMR experiments are indicated in chapter 6, table 6.2. Titrations of octylglucoside and $CaCl_2$ were performed by adding appropriate volumes of pH matched 1 M stock solutions to give the concentrations indicated on individual spectra in chapter 6. Identical acquisition parameters were used for each spectrum in a titration series.

Table 2.8 Parameters used in the NMR experiments for CaBP7 1-100 backbone and side chain assignments.

Experiment	Parameters
^{1}H-^{15}N-HSQC (2D)	sw ^{15}N = 20ppm; o3p=116.0 ppm; td f1 = 256
HNCO (3D)	sw ^{15}N = 20ppm; sw ^{13}C = 14ppm; o3p = 116.0; o2p = 176; td f1 = 128; td f2 = 128
HN(CA)CO (3D)	sw ^{15}N = 20ppm; sw ^{13}C = 14ppm; o3p = 116.0; o2p = 176; td f1 = 128; td f2 = 128
HNCACB (3D)	sw ^{15}N = 20ppm; sw ^{13}C = 70ppm; o3p = 116.0; o2p = 42; td f1 = 256; td f2 = 128
CBCA(CO)NH (3D)	sw ^{15}N = 20ppm; sw ^{13}C = 70ppm; o3p = 116.0; o2p = 42; td f1 = 256; td f2 = 128
HBHA(CO)NH (3D)	sw ^{15}N = 20ppm; sw ^{1}H (f1) = 8ppm; o3p = 116.0; td f1 = 256; td f2 = 128
HCCH-TOCSY (3D)	sw ^{13}C = 75ppm; sw ^{1}H (f1) = 6ppm; o2p = 28.5; td f1 = 256; td f2 = 128
^{1}H-^{13}C-HSQC (2D)	sw ^{13}C = 75ppm; td f1 = 512; o2p = 28.5

*f1 = ^{1}H dimension; f2 = ^{13}C dimension; f3 = ^{15}N dimension; sw = spectral width; o2p = offset in ppm for the ^{13}C dimension; o3p = offset in ppm for ^{15}N dimension; td = time domain (number of points in that dimension).

2.10. Gel mobility assay

Gel mobility shift assays were performed by resolving non-boiled protein samples in SDS-free loading buffer on native PAGE gels and assessing the shift in apparent molecular weight in the presence of different chelators and cations. The stacking gel contained 250 mM Tris pH 6.8, 4% acrylamide and the separating gel contained 750 mM Tris pH 7.5, 18% acrylamide. The loading buffer contained 50 mM Tris pH 7.5, 10% glycerol, 10% sucrose, 2 mM EDTA, 2 mM EGTA. To investigate Ca^{2+} binding, 10mM $CaCl_2$ was added to the loading buffer. To investigate Mg^{2+} binding, 10 mM $MgCl_2$ was added to the loading buffer. The running buffer consisted of 500 mM Tris, 385 mM glycine. Gels were run at 140 V for approximately 90 mins then stained with SimplyBlue™ SafeStain (Invitrogen) according to the manufacturer's protocol.

Chapter 3:

Bioinformatic Analysis of the CaBP Family of Ca^{2+}-Sensors

3.1. Introduction

Many aspects of cellular function are regulated by changes in $[Ca^{2+}]_i$(Berridge *et al*., 2000) and diverse families of proteins with specific Ca^{2+}-binding motifs have evolved to mediate responses to such $[Ca^{2+}]_i$ fluxes (Clapham, 2007). These highly specialised calcium sensors undergo conformational changes upon Ca^{2+}-binding allowing them to interact with different binding partners depending on their Ca^{2+} loading status. This in turn allows them to regulate unique signalling pathways in response to changes in $[Ca^{2+}]_i$(Ikura and Ames, 2006).

Calcium signalling controls numerous fundamental aspects of cellular physiology and this, in part, is brought about by variation in the amplitude, timing and spatial localisation of the Ca^{2+} signal itself (Boulware and Marchant, 2008, Bootman *et al*., 2001). Further diversification of these physiological outcomes is generated by the existence of multiple Ca^{2+}-sensors that each have finely tuned properties to allow them to regulate specific target proteins (Ikura and Ames, 2006, Burgoyne, 2007).

The ubiquitous and highly conserved Ca^{2+}-sensor, CaM, which is present in all eukaryotes, is the best studied Ca^{2+}-sensing protein (Chin and Means, 2000). Each CaM molecule can bind four Ca^{2+} ions via four canonical EF-hand motifs. The EF-hand motif, first identified in parvalbumin, has now been identified in an array of other proteins, some of which are highly related and constitute distinct families (Moncrief *et al*., 1990, Grabarek, 2006). Examples of the EF-hand containing families include the S100 proteins in vertebrates (Donato, 2001) and the calcineurin B-like (CBL) proteins in plants (Batistic and Kudla, 2009, Weinl and Kudla, 2009).

In neurons changes in $[Ca^{2+}]_i$ have many important effects which occur on timescales ranging from microseconds to many minutes (Berridge, 1998). For this reason, Ca^{2+}-sensing protein families which are expressed specifically in neuronal cell types have been of particular interest in the calcium signalling field (Burgoyne, 2007). Two families of neuronal Ca^{2+}-binding proteins have become more widely studied in recent years: The NCS proteins (Burgoyne, 2007, Burgoyne and Weiss, 2001) and the CaBP family (Haeseleer *et al*., 2000, Haeseleer *et al*., 2002,

Seidenbecher *et al*., 1998, Laube *et al*., 2002, Mikhaylova *et al*., 2006). These Ca^{2+}-sensors have emerged as important regulators of neuronal function and have been implicated in processes such as neuronal exocytosis, neurotransmission, phototransduction and neurite outgrowth (Zheng *et al*., 2005, Nakajima, 2011, Maeda *et al*., 2005, Sampath *et al*., 2005, Weiss *et al*., 2010, Dieterich *et al*., 2008).

Understanding precisely how these proteins appeared and expanded during evolution could give important functional clues about how they may have contributed to the generation of increasingly complex organism architecture and behaviour. For instance, the earliest orthologue of the NCS proteins, frequenin or NCS-1, was detected as a single gene in fungal genomes (Hendricks *et al*., 1999). There has been a progressive expansion of this gene family through evolution, with three NCS proteins expressed in *Caenorhabditis elegans* and four genes encoded by *Drosophila melanogaster.* Increasing diversification of these genes split the family into further subtypes. *D. melanogaster* encodes two frequenins, a neurocalcin and a single KChIP. Zebrafish (*Danio rerio)* have two NCS-1 orthologues, eight VILIPs, a recoverin, eight GCAPs and five KChIPs. All mammals have a highly conserved set of fourteen NCS genes that encode one NCS-1, five VILIPs, one recoverin, three GCAPS and four KChIPs (Burgoyne and Weiss, 2001). In addition to the numerous genes encoded by this protein family, the KCHIPs are expressed as multiple splice isoforms in neurons (Pruunsild and Timmusk, 2005). Analogously, the plant CBL proteins also show an increase in gene number through evolution with only one CBL gene found in algae compared to ten found in higher plants (Weinl and Kudla, 2009). These findings suggest that the expansion of Ca^{2+}-binding protein families during evolution may have contributed to increased signalling complexity in higher organisms.

Here, a thorough analysis of the evolution of the CaBP family of neuronally expressed Ca^{2+}-sensors is presented. This family is thought to comprise of the five CaBP genes originally described by Haeseleer *et al.*(Haeseleer *et al*., 2000) together with the independently discovered calneuron I and calneuron II (Wu *et al*., 2001, Mikhaylova *et al*., 2006). Based on their shared homology to CaM, the calneurons were suggested to belong to the same family as CaBPs 1-5 and thus are alternatively

referred to as CaBP7 (calneuron II) and CaBP8 (calneuron I)(Haeseleer *et al*., 2002). Others have suggested that the calneurons in fact constitute a distinct family that is unrelated to the other CaBPs (Mikhaylova *et al*., 2006). For the purposes of these analyses these proteins will henceforth be referred to as CaBP7 and CaBP8.

3.2. Results

3.2.1. Human CaBP family

There are six genes encoding the human CaBP family of proteins, *CABP1, CABP2, CABP4, CABP5, CABP7 and CABP8*. Two of these genes, CABP1 and CABP2, give rise to multiple splice isoforms. The *CABP1* gene generates three different proteins (CaBP1S, CaBP1L and caldendrin) whereas the *CABP2* gene generates two proteins (CaBP2S and CaBP2L). A seventh gene, *CABP3*, which partially overlaps with the *CABP5* gene, also exists but is only found in genomic sequences and expression of the protein has never been detected. *CABP3* is therefore thought to be a pseudogene and has not been included in the bioinformatic analyses. Note that a sixth gene product was originally discovered but later found to belong to an unrelated subfamily of Ca^{2+}-binding proteins. This explains the absence of a CaBP6 variant in the CaBP family of proteins (Haeseleer *et al*., 2002).

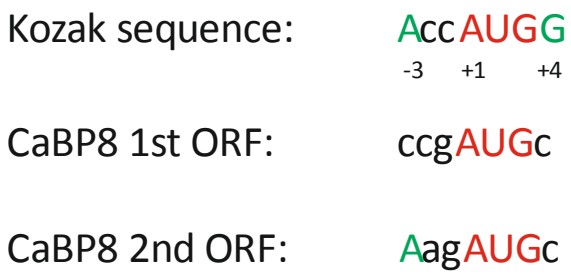

Figure 3.1. RNA sequences surrounding the start codon of the open reading frames (ORF) for the proposed two isoforms of CaBP8. The second ORF is more similar to the consensus kozak sequence and has a conserved purine at the -3 position found in the majority of eukaryotic mRNAs. This sequence can be regarded as an adequate kozak site whereas CaBP8 ORF1 lacks both a purine at -3 and guanosine at +4 and therefore represents a weak transcriptional start consensus site.

Alternative transcripts of *CABP8* can be found in the Genbank database for *Homo sapiens* and a number of other species which could potentially encode for short and long CaBP8 variants. Examination of these transcripts revealed that the start codon in the long variant was not located within a Kozak consensus sequence and was therefore unlikely to be efficiently translated (Figure 3.1). Consistent with this there is presently no evidence supporting the expression of a long CaBP8 variant. The long form was therefore not included in any further analyses.

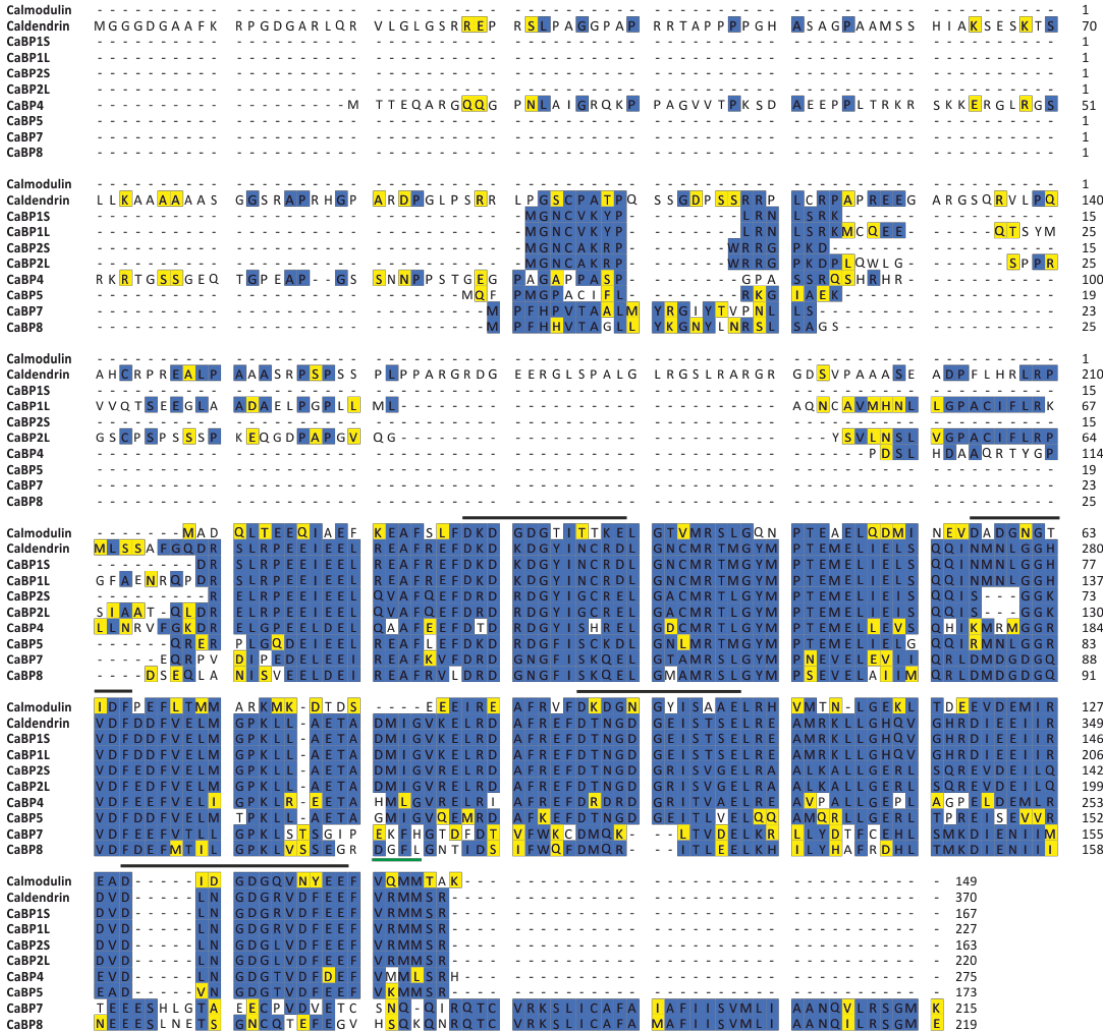

Figure 3.2 - Alignment of the sequences of human calmodulin and CaBP proteins. Protein sequences were compiled and aligned using ClustalW. Residues that are identical in more than one protein are highlighted in blue and residues with similar properties are highlighted in yellow. The black lines above the sequences indicate the position of the predicted 12 amino acid coordinating loop within the EF-hands. In EF-hand motifs where insertions or deletions have rendered the co-ordinating loopinactive in Ca^{2+} binding, the black bars appears longer or shorter than the canonical 12 amino acid loop. The green bar beneath the sequence indicates the position of the linker region in the CaBPs that is extended in comparison to CaM.

A multiple sequence alignment of the human CaBP protein sequences along with human CaM is shown in figure 3.2. Residues that are either identical or similar in at least two of the sequences are highlighted in the alignment. Bold black lines above the sequences indicate the positions of the four EF-hand domains and illustrate the similarity in domain structure amongst proteins of this family and also with CaM. CaM, however, possesses a shorter linker region between the N-terminal and C-terminal EF-hand pairs (underlined in green in figure 3.2). In the CaBPs the linker is extended by 4 amino acids and there is a high level of identity within this region. It has been speculated that this linker extension permits the CaBPs to interact with targets distinct from those recognized by CaM (Haeseleer *et al*., 2000).

The C-terminal portion of the protein sequences, containing the four EF-hand domains, is the most conserved, with the N-terminal region being most divergent. Some of the EF-hand motifs have undergone deletions or substitutions within their consensus sequence, most likely rendering them inactive for divalent cation binding. EF-hand 2 in CaBPs 1-5 is predicted to not bind cations due to deletions or substitutions in the Ca^{2+}-binding loop. Biochemical and structural analyses of CaBP1S have indeed confirmed that the substitutions within the loop of EF-hand 2 in this protein prevent coordination of divalent cations at this position (Haeseleer *et al*., 2000, Wingard *et al*., 2005, Li *et al*., 2009, Park *et al*., 2011).

The pattern of EF-hand inactivation in CaBP7 and CaBP8 differs from the other CaBP family members. Analysis of their protein sequences predicts they will have functional EF-hands 1 and 2 but there is a three amino acid deletion in EF-hand 3, and EF-hand 4 has undergone both substitutions and insertions. EF-hands 3 and 4 in these two proteins are therefore predicted to be inactive in divalent cation binding.

Table 3.1 shows the percentage sequence identities between the various human CaBP proteins and CaM. CaBP1S, CaBP2S and CaBP5 exhibit the highest sequence similarities with CaM at ~37% identity. The identities in table 3.1 therefore highlight that the CaBPs show only limited homology with CaM. Most of the CaBPs possess a significantly extended N-terminal region when compared to CaM and

correspondingly the CaBPs with the longest N-termini exhibit the least sequence identity with CaM.

CaBP7 and CaBP8 have the lowest comparative identities within the CaBP family. Despite exhibiting 63.0% identity with one another, the highest identity observed with any other CaBP member is only 24.0% between CaBP7 and CaBP2S. The comparative identities within caldendrin and CaBPs 1-5, however, suggest a higher relatedness, ranging from 30.8% to 72.6%. These values are suggestive of the existence of two distinct sub-groups within the CaBP family – one encompassing caldendrin and CaBPs 1-5, the other comprising CaBP7 and CaBP8. In support of this theory there are obvious differences in the sequence and domain structure of CaBP7 and CaBP8. Aside from the differences in their central linker region and pattern of EF-hand inactivation, CaBP7 and CaBP8 also possess a 38 amino acid extension at their C-terminus when compared with CaM and all other CaBP family members. This C-terminal extension is highly hydrophobic and, as will be discussed in chapter 4, has been found to be important for membrane targeting (McCue *et al*., 2009, McCue *et al*., 2011).

Table 3.1. Percentage sequence identity of residues across the various human CaBPs and CaM protein sequences that are shown in Figure 3.1.

	Caldendrin	CaBP1S	CaBP1L	CaBP2S	CaBP2L	CaBP4	CaBP5	CaBP7	CaBP8
CaM	16.7	36.6	27.1	37.8	28.5	22.9	36.7	20.0	20.7
Caldendrin		42.4	45.1	32.1	35.1	31.5	30.8	12.1	13.5
CaBP1S			73.5	72.6	54.9	36.3	64.9	21.7	23.2
CaBP1L				53.5	56.7	33.1	50.4	18.0	19.1
CaBP2S					74.0	40.0	58.1	24.0	21.9
CaBP2L						36.5	46.4	20.2	18.3
CaBP4							34.5	16.4	16.1
CaBP5								23.3	21.6
CaBP7									63.0
CaBP8									

3.2.2. The CaBPs first arose with the appearance of vertebrates

To gain insight into the evolutionary origins of the CaBP family, NCBI BLAST searches were performed against each of the human CaBP protein and nucleotide sequences. *D. melanogaster* and *C. elegans* were used as representative invertebrate species

but no proteins with significant homology greater than CaM were detected. Figure 3.3 illustrates the 8 major nodes in the evolution of chordates and, where genomic sequencing data was publicly available, BLAST searches were conducted for an organism representing every node. Detailed searches for specific organisms were carried out using the databases for specific genome projects as detailed in the materials and methods chapter, section 2.1. Genome searches of early deuterostomes such as sea urchin (*Strongylocentrotus purpuratus*), sea squirt (*ciona intestinalis*) and amphioxus (*Branchiostoma floridae*), representing the first two nodes in figure 3.3, did not reveal any candidate CaBP homologues. The top hits were CaM or CaM-like proteins. Lampreys (*Petromyzon marinus*), belonging to the superclass Agnatha (jawless fish), are thought to be the closest living organism to our vertebrate ancestor (Figure 3.3). The genome project for the lamprey is not yet complete, however, specific BLAT and BLAST searches of the available lamprey genome databases revealed partial sequences of two proteins most closely related to human CaBP1S and CaBP8 with 80.2% and 61.4% coverage respectively (Table 3.2 a and b).

Searches in the elephant shark (*Callorhinchus milli*) genome, which was used as a representative organism for the cartilaginous fish node (Figure 3.3), also identified a number of DNA contigs encoding fragments of the CaBPs. Three contigs were found with homology to human CaBP1, CaBP2 and CaBP5 (Table 3.3). The two contigs with homology to CaBP1 and CaBP5 appeared to follow on from each other and corresponded to exons 3 and 4 of human CaBP1S or CaBP5 (Table 3.3). When the exons were assembled together the protein had 46.1% coverage (Table 3.2a) and 90.0% homology compared to the full-length human CaBP1S protein sequence. The third contig encoded a short region with greatest homology to human CaBP2. This region corresponded to the same region encoded by one of the other contigs but was not identical in sequence (Table 3.3). This suggests that the elephant shark must have at least two proteins with homology to CaBP1 and CaBP2 and possibly a third protein with homology to CaBP5. As CaBPs 1-5 are so similar in their core sequence, it is very difficult to deduce whether the fragment with homology to CaBP5 is indeed an exon from the same protein as one of the other fragments, or

belongs to a completely separate CaBP protein. This issue could be clarified if a contig map were available for the elephant shark genome.

In addition, nine DNA contigs were identified which encoded fragments of CaBP7 and CaBP8. The coding regions within each of these contigs corresponded to the exons of human CaBP7 and CaBP8 (Table 3.3). Fragments encoding all CaBP8 exons were discovered and all exons except the first, N-terminal, exon were discovered for CaBP7. This gave a total coverage of 83.3% and 100% (Table 3.2b) for CaBP7 and CaBP8 respectively.

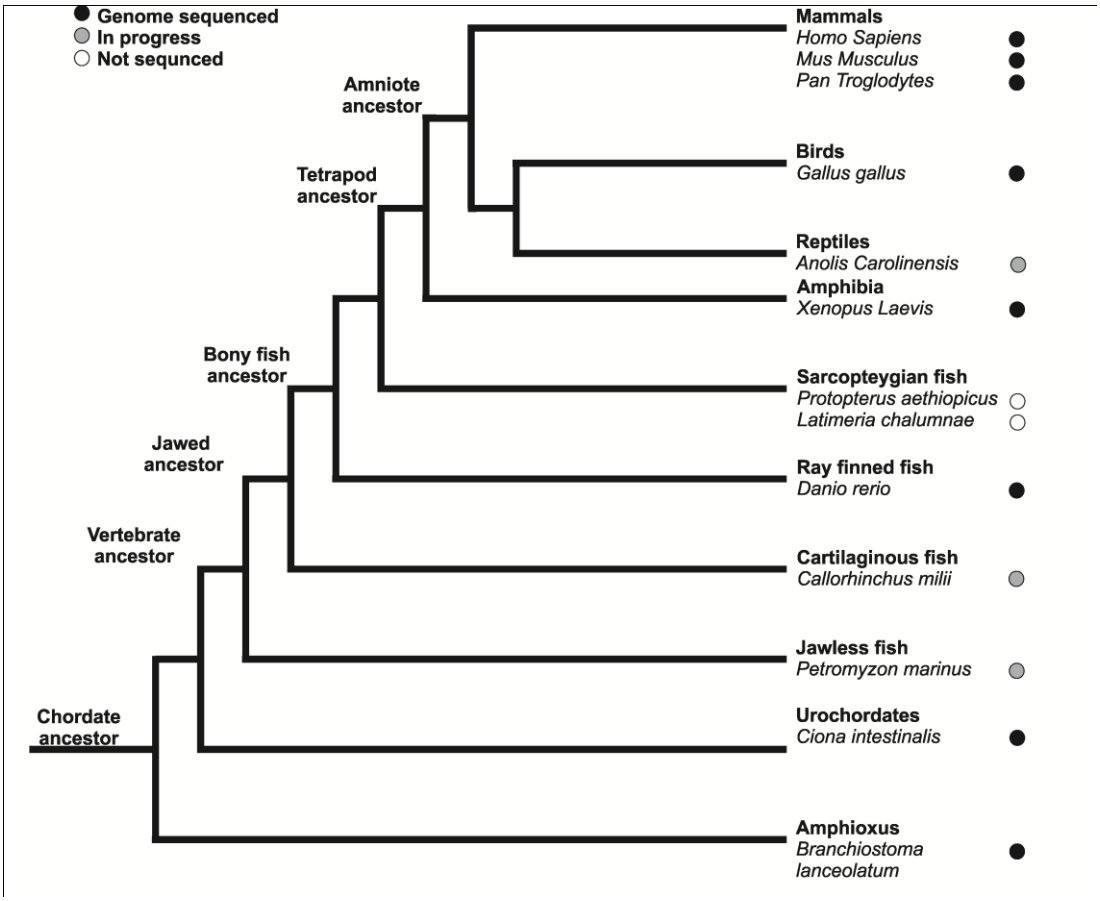

Figure 3.3. Cladogram illustrating the evolution of chordates. A representative species is shown for each major taxonomic group. The shaded circles indicate whether the genome of these species has been sequenced, is partially sequenced or has not yet been sequenced.

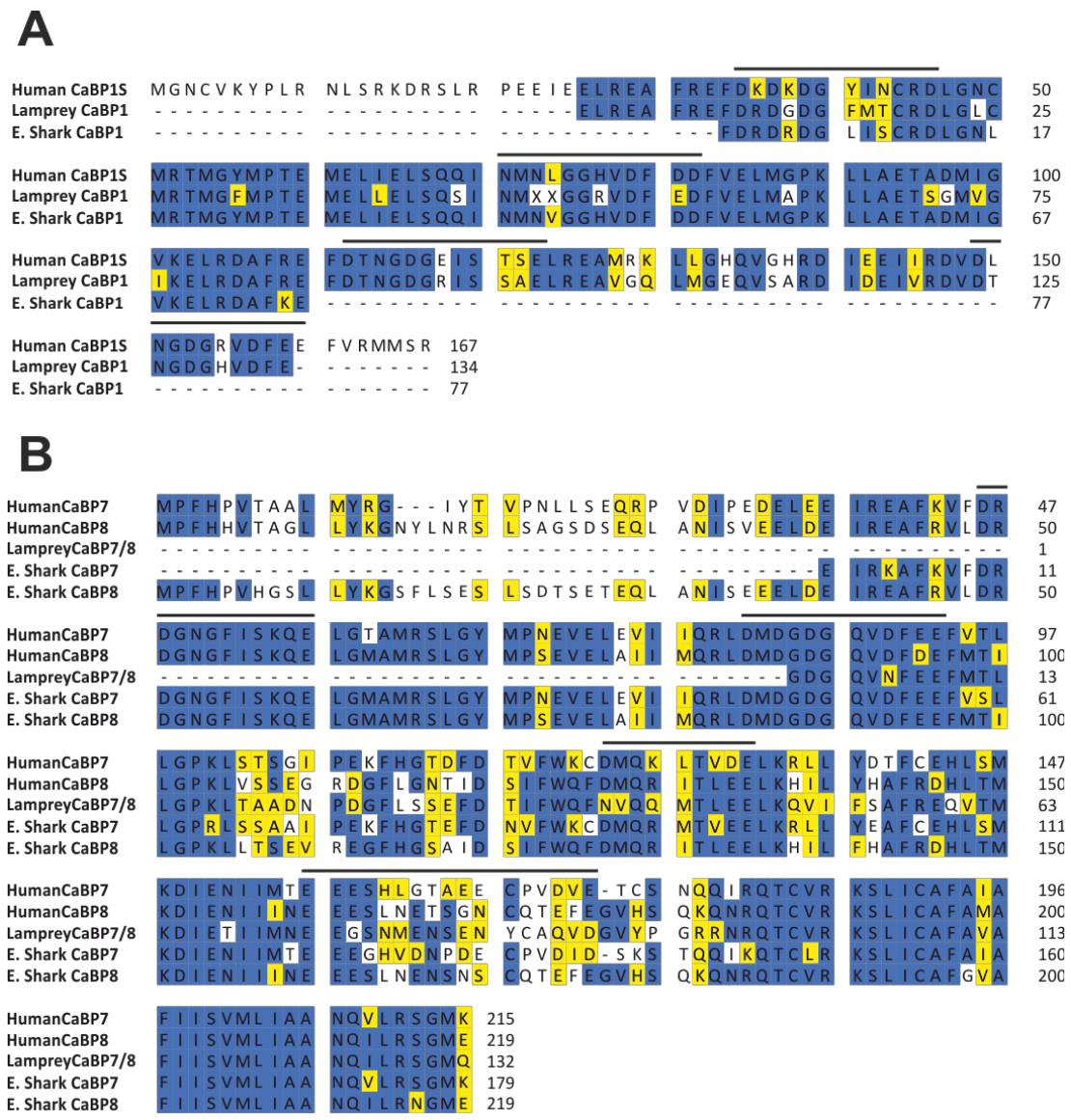

Figure 3.4. Alignment of the sequences of human, lamprey and elephant shark CaBP proteins. A) Alignment of human, lamprey and elephant shark CaBP1 sequences. B) Alignment of human, lamprey and elephant shark CaBP7 and CaBP8 sequences. Protein sequences were compiled and aligned using ClustalW. Residues that are identical in more than one protein are highlighted in blue and residues with similar properties are highlighted in yellow. The lines above the sequences indicate the position of the predicted 12 amino acid coordinating loop within the EF-hands.In EF-hand motifs where insertions or deletions have rendered the co-ordinating loopinactive in Ca^{2+} binding, the black bars appears longer or shorter than the canonical 12 amino acid loop.

Figure 3.4 A and B depict multiple sequence alignments for the translated lamprey and elephant shark CaBP1S, CaBP7 and CaBP8 sequences along with the corresponding human sequences. These sequences were constructed using the fragments identified in BLAST/BLAT searches based on the exon structure of the human CaBPs. The bold black lines above the sequences mark the position of the four EF-hands. Despite the C-terminal half of the elephant shark CaBP1S being missing, the same predicted pattern of EF-hand inactivation could be seen in both the lamprey CaBP sequences and the elephant shark CaBP7 and CaBP8 sequences when compared to humans. Therefore the function and specificity of these motifs has remained highly conserved since the evolution of early vertebrate species. Tables 3.2a and 3.2b show the percentage coverage for each of the CaBPs along with the percentage identity to their human orthologues within the aligned sequence. The lamprey and elephant shark CaBP1 have 76.0% and 90.0% homology to human CaBP1S respectively, illustrating that this protein has remained highly conserved from early vertebrates to higher mammals. The elephant shark CaBP7 and CaBP8 have 84.0% and 87.0% homology to their human counterparts, respectively. The CaBP in lamprey corresponding to either CaBP7 or CaBP8 has between 61.0 - 65.0% homology with the human protein sequences but is most similar to human CaBP8.

The sequencing projects for both the lamprey and elephant shark are still ongoing. The elephant shark genome is complete to only 1.4X coverage, which may explain the fragmentary nature of the data for this organism. The lamprey genome, however, has been completed to 5.9X coverage and therefore it can be predicted with greater confidence that there are indeed only two ancestral CaBPs in the earliest vertebrate organisms representing CaBP1 and CaBP8. CaBP7 arises later during the evolution of cartilaginous fish along with at least one other protein with homology to CaBPs 1-5. The remaining CaBPs may have arisen later still, after the separation of cartilaginous fish and bony fish. However, it is not possible to definitively prove this until sequencing of the elephant shark genome or another fish of this class is completed to a higher degree of coverage.

Table 3.2a. Percentage coverage and percentage identity between the CaBP1 protein sequences found in lamprey and elephant shark compared to human.

	CaBP1S	
	% coverage	% Identity
Lamprey CaBP1	80.20%	76
Elephant Shark CaBP1	46.10%	90

Table 3.2b. Percentage coverage and percentage identity between the CaBP7 and CaBP8 protein sequences found in lamprey and elephant shark compared to human.

	CaBP7		CaBP8	
	% coverage	% Identity	% coverage	% Identity
Lamprey CaBP7/8	61.40%	56	60.3	**65**
Elephant Shark CaBP7	83.30%	**84**	81.7	66
Elephant Shark CaBP8	102%	63	100	**87**

Shaded cells indicate the highest sequence identity for that particular orthologue.

The teleost fishes, the zebrafish (*D. Rerio*) and the pufferfish (*Tetraodon nigroviridis)* were used as representative organisms of the Ray-finned fish node, which are the closest to the bony fish ancestor (Figure 3.3). The full complement of the CaBP family was identified in these genomes suggesting an expansion of the CaBP family at the separation of cartilaginous and bony fish.

The sarcopterygian fish node, comprising organisms such as lungfish (*Protopterus aesthiopicus*) and the coelacanth (*Latimeria chalumnae*), would be closest to the tetrapod ancestor; however, neither genome has yet been completed (Figure 3.3). It would be expected that these organisms should also contain a full complement of the CaBP proteins. The teleost fish are therefore the closest sequenced organisms before the divergence of tetrapods. The rest of these analyses will focus on zebrafish sequences due to the completeness of the genome and because all the CaBP proteins can be detected in this organism.

Table 3.3. Protein sequence fragments identified in BLAST searches against the elephant shark genome along with the sequence of the corresponding exon in human and the percentage identity between the two sequences.

Contig	Sequence	Homology	Exon	Human Exon Sequence	% Identity
AAVX01573327.1	FDRDRDGLISCRDLGNLMRTMGYMPTEMELIELSQQINMN	CaBP5	3	ELREAFLEFDKDRDGFISCKDLGNLMRTMGYMPTEMELI ELGQQIRMN	87
AAVX01478821.1	VGGHVDFDDFVELMGPKLLAETADMIGVKELRDAFKE	CaBP1	4	LGGHVDFDDFVELMGPKLLAETADMIGVKELRDAFRE	94
AAV01407556.1	VGGRVNFEDFVE*MAPKLLAETADMIGIK	CaBP2	5	SGGKVDFEDFVELMGPKLLAETADMIGVRELRDAFRE	78
AAVX01108357.1	EIRKAFKVFDRDGNGFISKQELGMAMRSLGYMPNEVELEVIIQRLDMD	CaBP7	2	EIREAFKVFDRDGNGFISKQELGTAMRSLGYMPN EVELEVIIQRLDMD	95
AAVX01059912.1	GDGQVDFEEFVSLLGPRLSSAAIPEKFHGTEFDNVFWK	CaBP7	3	GDGQVDFEEFVTLLGPKLSTSGIPEKFHGTDFDTVFWK	81
AAVX01059912.1	CDMQRMTVEELKRLLYEAFCEHLSMKDIENIIMTEEEGHVDNPDECPVDIDSK	CaBP7	4	CDMQKLTVDELKRLLYDT FCEHLSMKDIENIIMTEEESHLGTAEECPVDVET	71
AAVX01124961.1	STQQIKQTCLRKSLICAFAIAFIISVMLIAANQVLRSGMK	CaBP7	5	CSNQQIRQTCVRKSLICAFAIAFIISVMLIAANQVL RSGMK	80
AAVX01563725.1	MPFHPVHGSLLYKGSFLSESLSDTSETEQLANISEEELD	CaBP8	1	MPFHHVTAGLLYKGNYLNRSLSAGSDSEQLANISVEELD	66
AAVX01190659.1	EIREAFRVLDRDGNGFISKQELGMAMRSLGYMPSEVELAIIMQRLDMDG	CaBP8	2	EIREAFRVLDRDGNGFISKQELGMAMRSLGY MPSEVELAIIMQRLDMDG	98
AAVX01097552.1	DGQVDFEEFMTILGPKLLTSEVREGFHGSAIDSIFW	CaBP8	3	DGQVDFDEFMTILGPKLVSSEGRDGFLGNTIDSIFWQ	77
AAVX01062942.1	QFDMQRITLEELKHILFHAFRDHLTMKDIENIIINEEESLNENSNSCQTEFEG	CaBP8	4	FDMQRITLEELKHIL YHAFRDHLTMKDIENIIINEEESLNETSGNCQTEFEG	90
AAVX01282372.1	VHSQKQNRQTCVRKSLICAFGVAFIISVMLIAANQILRNGME	CaBP8	5	VHSQKQNRQTCVRKSLICAFAMAFIISVMLIAA NQILRSGME	92

3.2.3. Zebrafish CaBP proteins

All six CaBP genes corresponding to those found in humans were found in the teleost fish, zebrafish. (Figure 3.5 and Table 3.4 and 3.5). A whole genome duplication event is proposed to have occurred in ray-finned fish after their divergence from tetrapods and before the diversification of teleost fish (Brunet *et al*., 2006). In accordance with this two separate genes were found in zebrafish for all of the CaBPs except CaBP4. The zebrafish sequences with the highest similarity to their human counterparts were selected to simplify further comparison. Table 3.4 shows the percentage identity between zebrafish and human orthologues. Values in bold and underlined indicate the percentage identity between identified orthologues. No distinct splice isoforms for any of the CaBPs were identified in zebrafish and table 3.4 shows that zebrafish CaBP1 and CaBP2 are most like human CaBP1S and CaBP2L, respectively. Most family members display over 60.0% identity with their human orthologue with the exception of CaBP4, which displays 44.7%. These values illustrate the strong evolutionary conservation of the CaBP protein sequences, particularly in the case of CaBP8, which shows 93.1% sequence identity with its human counterpart (Table 3.4 and Figure 3.5).

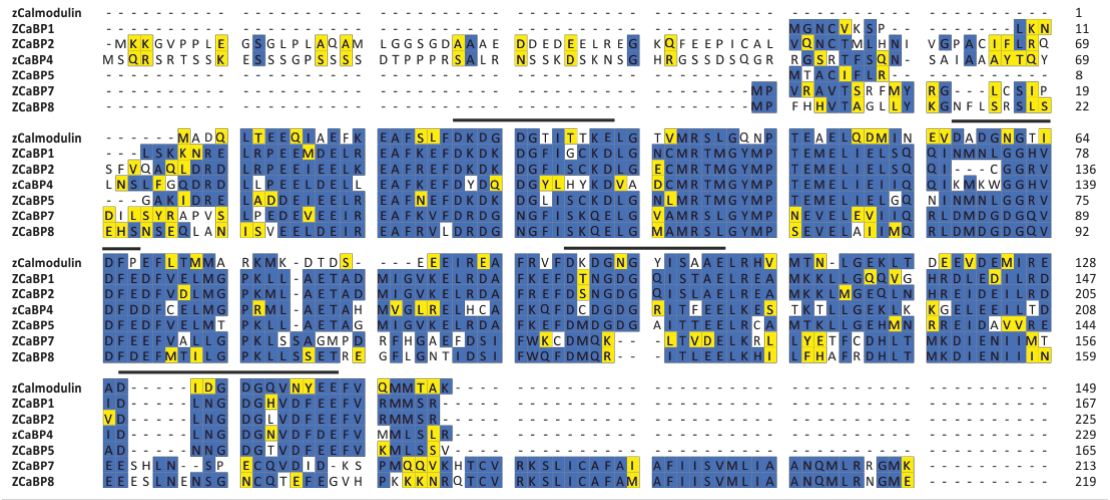

Figure 3.5. Alignment of the sequences of zebrafish (*Danio rerio*) calmodulin and CaBP proteins. Protein sequences were compiled and aligned using ClustalW. Residues that are identical in more than one protein are highlighted in blue and residues with similar properties are highlighted in yellow. The lines above the sequences indicate the position of the predicted 12 amino acid coordinating loop within the EF-hands. In EF-hand motifs where insertions or deletions have rendered the co-ordinating loopinactive in Ca^{2+} binding, the black bars appears longer or shorter than the canonical 12 amino acid loop.

Table 3.4. Comparison of the percentage sequence identity of zebrafish (Z) CaBPs in relation to the human protein sequences.

		Zebrafish						
		ZCaM	**ZCaBP1**	**ZCaBP2**	**ZCaBP4**	**ZCaBP5**	**ZCaBP7**	**ZCaBP8**
	CaM	**100**	35.5	29.6	24.0	38.7	20.1	21.1
	Caldendrin	16.7	37.0	36.2	28.0	30.4	13.3	13.5
	CaBP1S	36.6	**86.8**	54.3	40.7	66.6	24.3	24.2
	CaBP1L	27.1	63.8	44.2	32.9	50.0	19.5	19.8
Human	**CaBP2S**	37.8	62.0	52.2	41.7	54.4	23.0	20.5
	CaBP2L	28.5	50.2	**60.6**	39.6	46.8	20.3	19.1
	CaBP4	22.9	35.4	38.1	**44.7**	34.5	16.7	17.3
	CaBP5	36.7	62.1	51.7	38.4	**73.5**	23.8	22.8
	CaBP7	20.1	22.1	18.1	17.8	22.0	**77.2**	60.2
	CaBP8	20.7	22.9	18.0	19.2	21.0	59.3	**93.1**

Values in bold and underlined indicate the percentage identity between identified orthologues.

Table 3.5. Percentage sequence identity between the various zebrafish (Z) CaBP and CaM proteins shown in Figure 3.4.

	ZCaBP1	**ZCaBP2**	**ZCaBP4**	**ZCaBP5**	**ZCaBP7**	**ZCaBP8**
ZCaM	35.5	29.6	24.0	38.7	19	21.0
ZCaBP1		56.5	42.9	66.2	22.7	23.7
ZCaBP2			42.2	48.9	18	19.1
ZCaBP4				38.8	16.2	10.2
ZCaBP5					22.3	22.0
ZCaBP7						59.3
ZCaBP8						

As observed in the human proteins, certain EF-hand motifs within zebrafish CaBPs are predicted to be inactive and this followed the pattern observed in the human sequences (Figure 3.6 and Table 3.6). In addition to mutations which completely block cation chelation, some EF-hands possess a single amino acid substitution which alters the cation specificity of the motif. This is determined by the amino acid at the 12th position of the EF-hand loop. For instance, the primary sequence of EF1 in CaM is DKDGDGTITTKE. The glutamate (E) at position 12 predicts the motif to be a high affinity Ca^{2+}-binding site. However if this amino acid is substituted for aspartate (D), the Ca^{2+} affinity of the binding site is diminished (Hobson *et al*., 2005) and the motif will instead exhibit a preference for binding Mg^{2+}. EF1 in CaBP1 is predicted to co-ordinate Mg^{2+} in preference to Ca^{2+} because of one such E→D substitution. It has been confirmed in structural analyses that this EF-hand is indeed

constitutively Mg^{2+} bound whereas EF3 and EF4, which have glutamate at position 12, can bind both Ca^{2+} and Mg^{2+}(Wingard *et al*., 2005)(Li *et al*., 2009). Human CaBP5 also has an aspartate at this position in EF1, which is therefore predicted to bind Mg^{2+} in preference to Ca^{2+}.

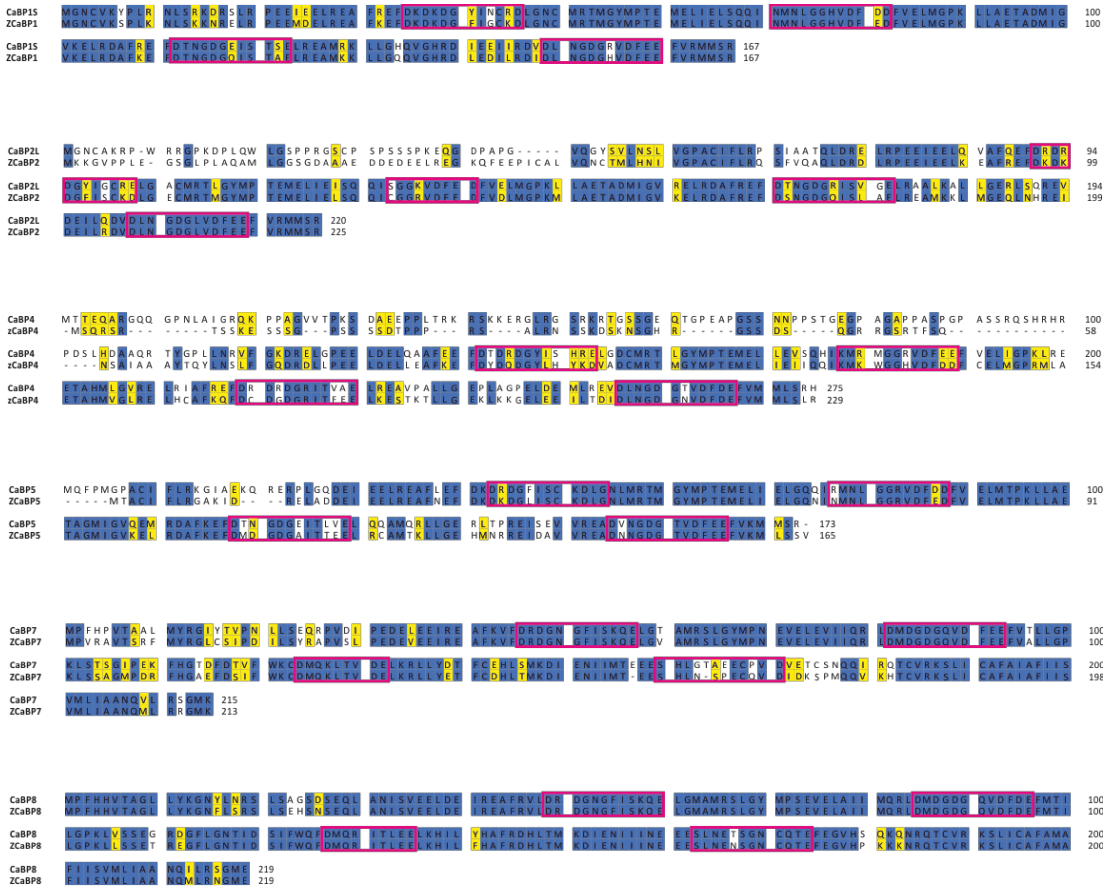

Figure 3.6. Alignment of sequences of the individual zebrafish CaBPs and their corresponding human orthologues. Protein sequences were compiled and aligned using ClustalW. Residues that are identical in more than one protein are highlighted in blue and residues with similar properties are highlighted in yellow. Pink boxes indicate the position of the predicted 12 amino acid coordinating loop within the EF-hands.In EF-hand motifs where insertions or deletions have rendered the co-ordinating loopinactive in Ca^{2+} binding, the pink boxes appears longer or shorter than the canonical 12 amino acid loop.

The conservation of cation binding properties for each of the EF-hand motifs in zebrafish and human CaBPs was examined (Table 3.6). The same pattern of EF-hand inactivation was observed for both species with an inactive EF2 motif in CaBPs 1-5 and inactive EF3 and EF4 motifs in CaBP7 and CaBP8. Varying degrees of conservation were seen across the EF-hand motif sequences as a whole and differences could be observed in the amino acid present at position 12 of the EF-hand loop between human and zebrafish proteins. In general the most conserved

Table 3.6. Comparison of the EF hands in zebrafish and human CaBPs.

	EF1			EF2			EF3			EF4		
	Zebrafish	**Human**	**Conserved**	**Zebrafish**	**Human**	**Conserved**	**Zebrafish**	**Human**	**Conserved**	**Zebrafish**	**Human**	**Conserved**
CaBP1	D	D	75%	D	D	92% (N)	E	E	83%	E	E	92%
CaBP2	D	E	50%	D	D	78% (N)	E	E	67%	E	E	100%
CaBP4	D	E	42%	D	E	58% (N)	E	E	67%	E	E	92%
CaBP5	D	D	58%	D	D	83% (N)	E	E	58%	E	E	92%
CaBP7	E	E	100%	E	E	100%	E	E	100% (N)	I	D	58% (N)
CaBP8	E	E	100%	E	E	100%	E	E	100% (N)	E	E	92% (N)

The table indicates whether the amino acid at position 12 of the EF-hand Ca^{2+}-coordinating loop is aspartate (D) or glutamate (E) and the percentage sequence identity between zebrafish and human EF-hand loop sequences. In the conserved column it is indicated if the EF hand is predicted to be non-functional (N).

EF-hand was EF4. CaBP7 and CaBP8 both have 100% sequence conservation within their first 3 EF-hands even though EF3 is predicted to be non-functional in Ca^{2+}-binding. EF4 in CaBP7 and CaBP8 is the least conserved but retains 92.0% conservation in CaBP8. This high degree of conservation in non-functional EF-hands suggests they must play an alternative functional role and may be important for the maintenance of correct protein structure.

Excluding those EF-hand motifs with inactivating mutations, the specificity for Ca^{2+} was conserved with the exception of EF1. The Ca^{2+}/Mg^{2+} binding properties of CaBP1 and CaBP5 remained the same between humans and zebrafish. The same properties are also observed in the lamprey and elephant shark CaBP1 sequences. Zebrafish CaBP2 and CaBP4 both have an aspartate at position 12 of EF1 in comparison to the corresponding residue in humans which is a glutamate. This suggests there has been an increase in the number of specific Ca^{2+}-binding EF-hand motifs from zebrafish to human.

3.2.4. CaBP7 and 8 form a distinct family of calcium sensing proteins to CaBPs 1-5

In order, the most conserved proteins of the CaBP family are: CaBP8, CaBP1S and CaBP7 (Tables 3.2a, 3.2b and 3.4). Interestingly these three proteins, in particular CaBP1S and CaBP8, were also the primordial CaBP family members.

A phylogenetic tree was constructed based on the protein sequences of human and zebrafish CaBPs using CaM as the root (Figure 3.7). For the purposes of this analysis the highly variable N-termini, which in some cases varies between splice isoforms, was excluded as they are less well conserved suggesting this region has experienced less functional evolutionary pressure. Only the core “CaM-like” domain was therefore used for comparison. The 38 amino acid extensions at the C-termini of CaBP7 and CaBP8 were also retained for this analysis as this region exhibits a high degree of similarity between the two proteins despite being absent from other CaBPs. The resulting phylogenetic tree implies that CaBP7 and CaBP8 form a completely different group of calcium sensors to CaBPs 1-5. This hypothesis is

consistent with the idea that the two primordial CaBPs, CaBP1 and CaBP8, arose independently of each other and with the appearance of vertebrates. Gene duplications have driven subsequent expansion of the two separate families of Ca^{2+}-sensors. Within the class of proteins encompassing CaBPs1-5, CaBP2 and CaBP4 form a distinct subgroup from CaBP1 and CaBP5. Importantly all members of this group show some relatedness to CaBP1 as would be expected.

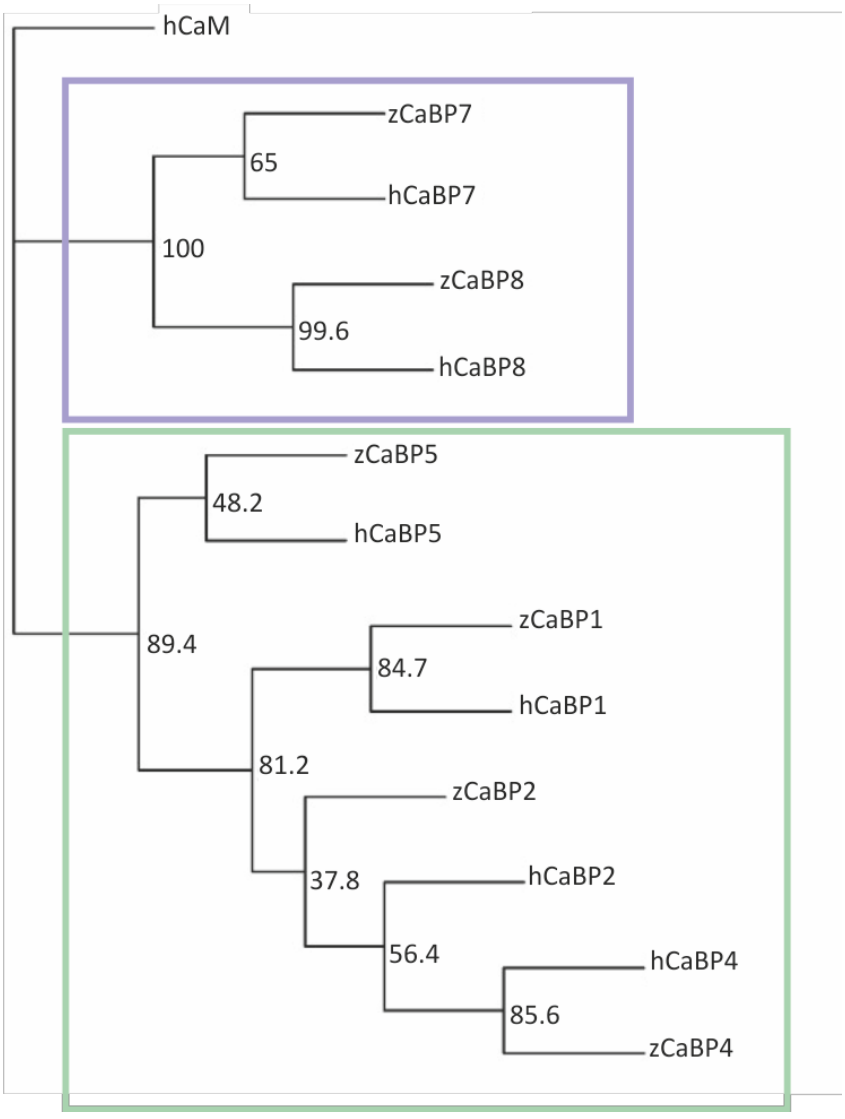

Figure 3.7. Phylogenetic tree depicting relatedness of the human and zebrafish CaBP proteins. A consensus maximum likelihood tree based on the alignment of the CaBPs was generated and rooted to human calmodulin (hCaM). The percentage of 2000 bootstrap replicates supporting the topology is given at each node. The purple box indicates the subfamily encompassing CaBP7 and CaBP8. The Green box indicates the subfamily encompassing CaBPs1-5.

3.2.5. CaBP proteins of other species and evolutionary changes

Table 3.7. The CaBP protein compliment found in each major vertebrate taxonomic group.

Scientific Name	Common Name	Vertebrate Class	CaBP
Lamprey	Lamprey	Jawless fish	1, 7
Callorhinchus milii	Elephant Shark	Cartilaginous fish	1*, 2*, 7, 8
Danio Rerio	Zebrafish	Bony fish	1a, 1b, 2a, 2b, 4, 5a, 5b 7a, 7b, 8a, 8b
Xenopus laevis	Frog	Amphibian	1, 4, 7, 8
Anolis carolinensis	Green Anole	Reptile	1, 2, 4, 5, 8
Gallus gallus	Chicken	Bird	1, 2, 4**, 7, 8
Monodelphis domestica	Opossum	Marsupial	1, 2, 4, 5, 7, 8
Mus musculus	Mouse	Mammal	1, 2, 4, 5, 7, 8
Pan troglodytes	Chimpanzee	Mammal	1, 2, 4, 5, 7, 8
Homo sapiens	Human	Mammal	1, 2, 4, 5, 7, 8

a and b represent teleost CaBP duplicates

* This was the highest homology observed based on the very fragmentary data available

** Data derived from primary literature searches rather than genome blast

The most obvious differences between the zebrafish and human CaBP family are the lack of long CaBP1 and short CaBP2 splice variants in zebrafish, and variation within the N-termini of CaBP2 and CaBP4. The sequences of the CaBPs from various tetrapod species representing amphibians, reptiles, birds, marsupials and placental mammals were compared and a number of evolutionary changes can be observed. Table 3.7 shows the compliment of CaBP proteins found in representative animals from each of these vertebrate classes. The lamprey, elephant shark and zebrafish are also included for comparison. All mammals appear to have the full compliment of CaBP proteins, however there appear to be variations in the numbers seen in amphibians, reptiles, and birds. The green anole lizard is missing only CaBP7 but as the genome is not yet complete, the sequence for this protein may yet be discovered. The amphibian, *Xenopus laevis*, appears to lack CaBP2 and CaBP5 and the avian, *Gallus gallus*, was missing sequences with homology to CaBP4 and CaBP5.

It is possible that these genes have been lost during the course of evolution, however these findings should be treated tentatively. Despite the apparent absence of a CaBP4 sequence in the completed *Gallus gallus* genome, Lee *et al.* have reported the presence of CaBP4 mRNA and antibody staining of expressed CaBP4 protein in chicken cochlear hair cells (Lee *et al*., 2007c).

The extended N-terminal domain of caldendrin, which is derived from alternative splicing of the CaBP1 gene, is encoded in mammals but not found in any other genomes. The N-termini of the CaBP proteins is the most variable region between CaBP family members and the N-terminal domains which define each of CaBP1, CaBP2, and CaBP4 have been compared across species to examine the different patterns of evolutionary change (Figure 3.8). The C-terminal 38 amino acid extension, which is specific to CaBP7 (CaBP7 178-215) and CaBP8 (CaBP8 181-219), has also been included in this analysis. The domain that defines CaBP1L (CaBP1L 16-75) was not present in zebrafish but was found in all tetrapods. The sequence conservation in this region compared with human caldendrin was relatively high across all species ranging from 68.0% in amphibians to 98.0% in chimpanzee. The variable N-terminal domain of CaBP2L (CaBP2L 1-56) was detected at very low sequence conservation in zebrafish but was not found in available avian or amphibian genomic databases. Interestingly, this region was 100% conserved in the reptile, the green anole, but showed varying degrees of conservation in mammals ranging from around 60.0% in the opossum and mouse to 96.0% in the chimpanzee. The variable N-terminal region of CaBP4 (CaBP4 1-120) was found in all species from zebrafish onwards apart from chicken with a progressive convergence in sequence identity with the human protein, ranging from 22.5% in zebrafish to 99.0% in chimpanzee. It is possible that chicken do in fact express both the long form of CaBP2 and CaBP4, however, sequence information for this organism appears incomplete and is contradicted by published results (Lee *et al*., 2007c). The C-terminal domains of CaBP7 and CaBP8 can be seen across all organisms examined and exhibit a high degree of sequence conservation throughout evolutionary history. This is demonstrated by the 89% identity seen between the CaBP8 C-terminus in human and lamprey, one of the most closely related living organisms to

our vertebrate ancestor. The high sequence identity of these defining regions of CaBP1L, CaBP7 and CaBP8 across numerous species implies that these proteins must have an important vertebrate specific function.

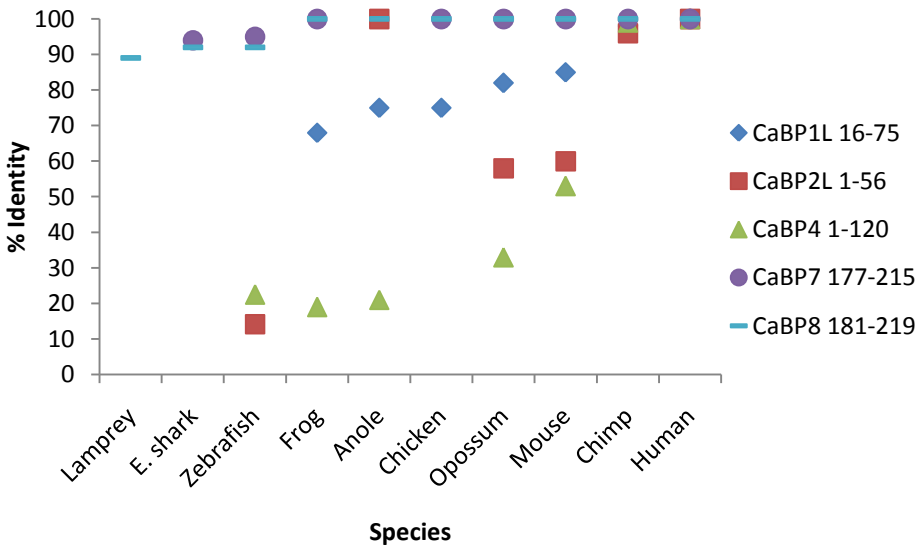

Figure 3.8. Relative sequence identity of domains specific to particular CaBPs between selected vertebrates and the corresponding human sequence. The percentage identity compared to human is plotted for the indicated domains in the indicated species. Where no symbol is present no orthologous protein or domain could be found from BLAST searches.

3.2.6. Evolutionary expression of target proteins for the CaBP family

A number of target proteins are now known for the CaBP family of proteins. It is of interest to examine whether any of these targets co-evolved with the CaBPs during the evolution of vertebrates. Several CaBPs have been suggested to regulate various VGCCs (Zhou *et al*., 2005, Cui *et al*., 2007, Yang *et al*., 2006a, Shih *et al*., 2009, Lee *et al*., 2002, Zhou *et al*., 2004, Haeseleer *et al*., 2004, Tippens and Lee, 2007, Lee *et al*., 2007a). VGCCs related to the major VGCC types found in vertebrates are also found in invertebrates. For instance, *D. melanogaster* and *C. elegans* possess genes encoding VGCCs that are orthologues of the mammalian VGCC α subunits which are regulated by the CaBPs. Invertebrate species possess only three VGCC genes, however, each representing one of the three families of VGCC found in mammals: L-type, non-L-type and T-type channels (Jeziorski *et al*., 2000). Whole genome

duplication events have subsequently resulted in the expansion of the three VGCC families. In mammals four L-type, three non-L-type and three T-type channel genes can be found (Jeziorski *et al*., 2000). The earliest evidence for the expansion of the VGCCs was reported in the cartilaginous fish *Discopyge ommata* which expresses at least two L-type channel subtypes (Horne *et al*., 1993). This expansion in the number of VGCCs in vertebrates may explain the evolutionary pressures selecting for a more diverse family of Ca^{2+}-sensing proteins to regulate them. The VGCCs are critical for the functioning of the mammalian central nervous system. Therefore the expansion of this family of channels and the proteins which modulate them has likely influenced the evolution of complex vertebrate nervous systems.

The IP_3R, another known target for CaBP1 (Haynes *et al*., 2004, Yang *et al*., 2002a, Kasri *et al*., 2004), is also found in invertebrate species (Zhang *et al*., 2007, Iwasaki *et al*., 2002) but only one isoform is expressed. Three IP_3R isoforms can be detected in both *Xenopus* and *D. rerio* whereas primitive deuterostomes possess only one (Zhang *et al*., 2007, Iwasaki *et al*., 2002, Ashworth *et al*., 2007). Therefore there has been an expansion in the number of IP_3R isoforms between the evolution of vertebrates and the diversification of teleost fish. This expansion in the number of IP_3R isoforms is consistent with a requirement to co-evolve specific regulatory proteins that compliment newly emergent functions. In accordance with this theory, both CaBP2 and CaBP5 were also shown to regulate IP_3Rs in *Xenopus* oocytes but differences in their regulatory properties have not yet been studied (Yang *et al*., 2002b).

Caldendrin has been reported to interact with jacob protein (Dieterich *et al*., 2008) which, interestingly, is also a vertebrate specific protein. Although only the shorter splice variant of CaBP1, CaBP1S, is present in early vertebrates, jacob has been demonstrated to bind to the basic EF-hand core in the absence of the extended N-terminus of caldendrin. It is therefore possible that in lower vertebrates jacob is regulated by CaBP1S.

The only known interacting partner for CaBP7 and CaBP8, apart from a possible regulatory role for N-type VGCCs, is PI4KIIIβ(Mikhaylova *et al*., 2009, Shih *et al*., 2009). This protein is not, however, a vertebrate specific protein and a single PI4KIIIβ can be detected in all the major eukaryotic taxa from protists to mammals (Brown and Auger, 2011). PI4KIIIβ is regulated by other, non-vertebrate, specific proteins, in particular, NCS-1 (de Barry *et al*., 2006) and therefore regulation by CaBP7 and CaBP8 may represent an adaptation of function of these calcium sensors in order to impart an additional new and vertebrate specific regulation of PI4KIIIβ and intracellular vesicular trafficking from the TGN.

3.3. Discussion

This phylogenomic study of the CaBP family of calcium sensors has highlighted a number of key findings about the evolution and classification of these proteins. Firstly, the CaBPs first arose with the appearance of vertebrates, around 550 million years ago (Shu *et al*., 1999). No orthologues of the CaBPs could be found in invertebrates apart from CaM-like proteins but partial sequences of two CaBP proteins with significant homology to CaBP1S and CaBP8 were found in the lamprey, *P. marinus*, the most closely related living organism to our early vertebrate ancestor. Secondly, based on the relative sequence identity and conservation, pattern of EF-hand inactivation, and phylogenetic analysis, CaBP7 and CaBP8 appear to form a completely distinct family of proteins to CaBPs 1-5. This suggests the existence of two primordial CaBP genes arising independently of each other at the vertebrate node; one of which gave rise to CaBPs1-5 and another to CaBP7 and CaBP8.

A number of whole genome duplication (WGD) events are proposed to have occurred in the vertebrate lineage which led to the expansion of gene families (Brunet *et al*., 2006, On *et al*., 2008, Jaillon *et al*., 2004). The first of these WGD events occurred early in vertebrate evolution around the time of the divergence of lamprey and hagfish lineages. The two CaBP genes found in lamprey may have

arisen during this WGD through the duplication of CaM and CaM-like genes and subsequent domain shuffling to generate divergent novel proteins.

The second WGD event occurred prior to the divergence of cartilaginous fish. In accordance with this at least four CaBP genes can be detected in the cartilaginous fish, the elephant shark; two corresponding to CaBP7 and CaBP8 and two corresponding to CaBPs1-5. A third WGD event occurred specific to the bony fish, before the emergence of teleost fish and as such, duplicate genes are found for all six of the CaBP genes in zebrafish.

Therefore the appearance of the two genes encoding CaBP7 and CaBP8 in mammals can be easily explained through the duplication of the primordial CaBP8 gene found in lamprey. However, four genes encoding CaBPs1-5 are found in humans and many tetrapods, whereas only two genes were definitively identified in the elephant shark. As the full complement of CaBP proteins is found in zebrafish, this suggests a transient expansion of this family from two genes in cartilaginous fish to four genes in the bony fish ancestor. Unfortunately the actual complement of CaBP proteins found in our tetrapod ancestor cannot currently be examined as no genomes of sarcopterygian fish have been fully sequenced to date and thus the teleost fish are the closest representatives. It is also possible that there are more as yet undiscovered CaBP genes in both lamprey and elephant shark which were not detected due to the incomplete nature of the available genomic data. A clearer picture will become available upon the completion of these genome projects and through the sequencing of the sarcopterygian fish, the coelacanth, which is currently underway (http://www.broadinstitute.org/scientific-community/science/projects/mammals-models/vertebrates-invertebrates/coelacanth/coelacanth).

All CaBPs display limited homology to CaM and thus it is assumed that this family of proteins arose through gene duplication and further diversification of CaM or CaM-like genes. CaM is present in all eukaryotic organisms and exhibits a high degree of sequence conservation throughout evolutionary history. Vertebrates such as

humans, rat, and *Xenopus*, have evolved multiple CaM genes but interestingly, all of these genes give rise to an identical protein product (Karabinos and Bhattacharya, 2000). Invertebrates however, possess either a single CaM gene or two CaM genes that encode different isoforms. Two CaM genes are found in amphioxus as well as two genes encoding CaM-like proteins (Karabinos and Bhattacharya, 2000). If amphioxus is used as an example of the chordate ancestor, it could be assumed that a WGD event occurring before the diversification of the jawless fish would have given rise to an excess of CaM isoforms. It is possible that various CaM-related Ca^{2+}-binding protein families may have arisen as a result of such an event.

It is thought that the high conservation of the CaM protein sequence across multiple genes in the same organism has occurred because of the diversity of its target proteins (Moncrief *et al*., 1990). Other Ca^{2+}-sensors, which show more variation in protein sequence throughout their evolution, have developed more specialized functions. Certain families of Ca^{2+}-sensors, such as the NCS proteins (Burgoyne, 2007) in animals and the CBL proteins (Batistic and Kudla, 2009, Weinl and Kudla, 2009) in plants, show a progressive increase in complexity through evolution, with an increase in the number of distinct genes. There is a general increase in the number of NCS genes with increasing complexity from one in fungi to fourteen in mammals (Burgoyne and Weiss, 2001). These proteins are expressed predominantly in retinal photoreceptors or in neurons. The expansion of CaM-related Ca^{2+}-sensing protein families has likely allowed the evolution of specific proteins to carry out functions unique to a particular cell or tissue type. This diversification allows the fine-tuning of processes usually regulated by CaM and may have contributed significantly to the neuronal complexity observed in mammals. As such, the CaBP proteins have been found to share a number of interacting binding partners with CaM, (Zhou *et al*., 2005, Cui *et al*., 2007, Yang *et al*., 2006a, Shih *et al*., 2009, Lee *et al*., 2002, Zhou *et al*., 2004, Haeseleer *et al*., 2004, Tippens and Lee, 2007, Lee *et al*., 2007a, Haynes *et al*., 2004, Yang *et al*., 2002a, Kasri *et al*., 2004) in addition to a number of unique interactions (Dieterich *et al*., 2008, Nakajima, 2011, Seidenbecher *et al*., 2004). The CaBPs sometimes have different modulatory effects to those seen with CaM, however, illustrating that they

are not simply redundant regulators of CaM targets (Few *et al*., 2005). Interestingly, investigations into the functions of the genes which are retained after duplication events have observed an enrichment in development, signalling, behaviour and regulation related genes (Brunet *et al*., 2006).

Like the NCS proteins, the CaBP proteins are predominantly expressed in the retina and brain (Haeseleer *et al*., 2000, Mikhaylova *et al*., 2006). CaBP4 and CaBP5 regulate different VGCCs in retinal photoreceptors and have been shown to play non-redundant roles in phototransduction in mammals based on studies in knockout mice (Haeseleer *et al*., 2004, Rieke *et al*., 2008). Mutations in CaBP4 in humans have also been shown to cause congenital visual disorders (Littink *et al*., 2009, Zeitz *et al*., 2006, Aldahmesh *et al*., 2010). CaBP4 was found in bony fish, amphibians, reptiles, birds and mammals but CaBP5 was missing from the *G. gallus* and *X. laevis* genomes. CaBP4 was the least well conserved of all the CaBP proteins, with significant differences in its N-terminus between zebrafish and human suggesting there may be some species specific differences in the regulation of photoreceptor function. This may also explain the absence of CaBP5 from amphibians and birds.

The pattern of active and inactive EF hands in all CaBPs remained the same in zebrafish compared to human CaBPs. There were, however, some differences in the cation binding specificity of EF1 in CaBP2 and CaBP4. In zebrafish these proteins had D at position 12 in the EF-hand loop whereas in humans this residue is E. The zebrafish CaBP2 and CaBP4 are therefore predicted to bind Mg^{2+} at EF1 whereas in humans this EF-hand motif is specific for Ca^{2+}-binding. CaBP1 and CaBP5 are both predicted to bind Mg^{2+} at EF1 in both zebrafish and human proteins and this has been confirmed by structural analyses in CaBP1 (Wingard *et al*., 2005, Li *et al*., 2009). This increase in the number of Ca^{2+} specific binding sites in CaBP2 and CaBP4 from zebrafish to humans could have important structural and functional consequences. Structural studies of CaBP1 have shown that binding of Mg^{2+} to EF1 has a global effect on the conformation of the protein compared to the cation-free apo form, and is suggested to stabilize the protein in Ca^{2+} independent interactions

(Wingard *et al*., 2005). More limited conformational changes were observed upon binding of Ca^{2+} to the remaining EF-hands. CaBP2 and CaBP4 would potentially lack an intermediate Mg^{2+}-stabilized conformation between the apo and Ca^{2+} bound forms and therefore might be predicted to interact differently with target proteins. More comprehensive structural studies into the effect of D → E substitutions at position 12 of the EF1 loop are needed to better understand the functional consequences of these differing cation specificities.

The CaBPs have somewhat overlapping roles, with multiple proteins from this family capable of modulating the same target proteins. They also share some common targets with CaM such as the VGCCs. It has also been shown, however, that the physiological effects of the CaBPs on the VGCCs, differ from those of CaM, and knockout studies of CaBP4 and CaBP5 suggest non-redundant roles for these proteins (Catterall and Few, 2008, Zhou *et al*., 2005, Cui *et al*., 2007, Yang *et al*., 2006a, Shih *et al*., 2009, Lee *et al*., 2002, Zhou *et al*., 2004, Haeseleer *et al*., 2004, Tippens and Lee, 2007, Lee *et al*., 2007a, Maeda *et al*., 2005, Rieke *et al*., 2008). This is in agreement with the idea that the CaBPs evolved to provide a further level of regulation to fine tune the modulatory activities of CaM. The evolution of CaBP target proteins was examined to determine if there was any correlation between appearance of targets and the appearance of the CaBPs. Jacob protein is the only interacting partner of the CaBPs that is reported to also be vertebrate specific. The VGCCs and the IP_3Rs arose before the emergence of vertebrates; however, drastic changes occurred in these families of proteins which were specific to the vertebrate clade. Once again as a result of WGDs, there was an expansion in the number of both VGCCs and IP_3Rs which originated in an early vertebrate ancestor (Iwasaki *et al*., 2002, Zhang *et al*., 2007, Jeziorski *et al*., 2000). It is possible, therefore, that this sudden increase in complexity in these families provided the evolutionary pressures necessary to select for new families of calcium sensing proteins.

The existence of at least two CaBPs in all vertebrates and the high sequence conservation, of particularly CaBP1S, CaBP7 and CaBP8, suggests that they have functionally important and non-redundant roles. The only characterized target for

CaBP7 and CaBP8 is PI4KIIIβ. Both proteins bind to and inhibit this enzyme which is required to generate PI4P, an essential lipid for vesicular trafficking from the TGN (Mikhaylova *et al*., 2009). PI4K has similar roles in yeast (Walch-Solimena and Novick, 1999) and flies (Polevoy *et al*., 2009) and therefore this inhibitory control is a more recent mechanism which has evolved in vertebrates specifically. Given the presence of both CaBP7 and CaBP8 from cartilaginous fish onwards and their extreme sequence conservation from elephant shark to humans (84% and 87%, respectively), it is highly unlikely that these two proteins perform redundant roles. It will be important to identify other, non-redundant functions for these proteins in order to fully appreciate the evolutionary pressures which have led them to be so strongly conserved in vertebrates. To date the only knockout studies of the CaBP genes are CaBP4 and CaBP5 knockout mice (Maeda *et al*., 2005, Rieke *et al*., 2008). Knockouts of the other four CaBP genes would prove useful to test the functional redundancy of these proteins.

3.3.1. Conclusions

These analyses are consistent with the CaBPs forming two separate classes of proteins with CaBPs 1-5 in one group and CaBP7 and CaBP8 in the other. The first appearance of both these classes of proteins can be traced back to the emergence of the vertebrates. CaBP1S and CaBP8 can be identified in the lamprey genome suggesting these were the primordial ancestors in the two classes of CaBPs. A subsequent WGD event before the divergence of cartilaginous fish gave rise to CaBP7, which, along with CaBP8, has remained remarkably highly conserved throughout vertebrate evolution. At least one other CaBP gene with homology to CaBPs1-5 was also discovered in the genome of the cartilaginous fish, the elephant shark. A full complement of the CaBPs can be found in teleost fish suggesting that there has been a transient increase in the number of genes corresponding to CaBPs1-5 between the emergence of cartilaginous fish and the divergence of bony fish. The appearance and subsequent expansion of these two independently arising families of calcium sensing proteins also correlates with an observed increase in complexity in the families from which the CaBP target proteins originate. The

increase in gene number and, in mammals, splice variants, has likely allowed the fine tuning of processes otherwise regulated by CaM in invertebrates, and may have contributed significantly to the increased complexity of higher organisms.

Chapter 4:

Subcellular Localisation and Membrane Targeting Mechanism of CaBP7 and CaBP8

4.1. Introduction

The calcium ion influences a diverse array of processes ranging from fertilisation to cell death, gene transcription to ion channel function, and phospholipid metabolism to protein trafficking (Berridge, 2009). The existence of a multitude of different Ca^{2+}-sensing proteins is intrinsic to the cell's ability to exert such a wide range of physiological effects in response to a simple cation. Each Ca^{2+}-sensor exhibits unique Ca^{2+}-binding properties and specific tissue, cellular and subcellular distributions, which give rise to specific and non-redundant physiological roles for each protein. Ca^{2+} signals vary in timing, magnitude, and spatial localisation, and depending on the precise combination of these parameters, can activate distinct Ca^{2+}-sensors. The often restricted subcellular localisation of Ca^{2+}-binding proteins is therefore fundamental to their ability to respond to specific patterns of Ca^{2+} signal and thereby generate selective changes in cellular activity.

Members of the CaM superfamily of EF-hand containing Ca^{2+}-binding proteins display broad diversity in their cation binding properties and subcellular targeting mechanisms. For example, members of the NCS protein family have a high affinity for Ca^{2+} when compared to CaM and exhibit specific subcellular localisation patterns. Many are able to associate with membranes via post-translational lipidation (Haynes and Burgoyne, 2008). Eleven of the fourteen NCS proteins are N-terminally myristoylated and palmitoylation has also been found to play an important role in membrane targeting of the KChIPs (Burgoyne, 2004, Takimoto *et al*., 2002). Despite many of the NCS proteins sharing the same post-translational modification, myristoylation has been shown to affect these proteins in distinct ways. In the case of NCS-1 itself, the myristoyl tail is permanently extruded from the protein core directing persistent membrane association of the protein. Other NCS proteins, in contrast, possess a reversible 'myristoyl switch' (Decordier *et al*., 2008). Hippocalcin, neurocalcin-δ, the VILIPs and recoverin all sequester their myrsitoyl chain within a hydrophobic pocket when not bound to Ca^{2+}. Upon Ca^{2+}-binding, these proteins undergo a conformational change which promotes extrusion of the myrsitoyl group and therefore Ca^{2+}-dependent membrane association (Haynes and Burgoyne, 2008). The function of the myristoyl group in the constitutively

membrane bound GCAP subfamily, is less well understood but recent research has suggested that GCAP2 possesses a reverse myristoyl switch which is exposed in the absence of Ca^{2+} to allow membrane association, but sequestered inside the protein when Ca^{2+}-bound(Schroder *et al*., 2011, Theisgen *et al*., 2011). No switch mechanism has been demonstrated for GCAP1 and the myristoyl group appears to be permanently buried within a hydrophobic pocket within the protein, where it plays a role in stabilizing the protein rather than in membrane association (Stephen *et al*., 2007). The NCS proteins therefore illustrate how Ca^{2+}-sensors have diversified through evolution to localise to different subcellular compartments through subtly different mechanisms. Importantly, the lipid moieties responsible for the membrane association of these proteins has also been found to be required for correct protein function (O'Callaghan *et al*., 2003, Chandra *et al*., 2011).

The CaBP subfamily of CaM related proteins have recently emerged as important regulators of ion channels and intracellular trafficking enzymes (Haeseleer *et al*., 2000, Mikhaylova *et al*., 2006, McCue *et al*., 2010b). To date a number of CaBP isoforms have been shown to bind to specific target proteins and regulate non-redundant cellular processes (Dieterich *et al*., 2008, Haynes *et al*., 2004, Kasri *et al*., 2004, Nakajima, 2011, Haeseleer *et al*., 2004, Oz *et al*., 2011, Cui *et al*., 2007, Mikhaylova *et al*., 2009), although scant functional data exists for both CaBP2 and CaBP5. CaBP1 has three splice variants, two of which, CaBP1S and CaBP1L, associate with membranes following *N*-myristoylation on a glycine residue at position 2 in each protein. This myristoyl group has been shown to be essential for some of the regulatory roles mediated by CaBP1 (Few *et al*., 2005, Kasri *et al*., 2004). The less well characterised, CaBP2 also carries an N-terminal myristoylation consensus motif. Other members of the CaBP family, CaBP4, CaBP5, and the third isoform of CaBP1, caldendrin, do not possess any obvious consensus motifs for post-translational lipidation and consistent with this the proteins are predominantly cytosolic (Dieterich *et al*., 2008, Haeseleer *et al*., 2004, Rieke *et al*., 2008, McCue *et al*., 2009). Although these proteins lack the means to directly associate with specific subcellular compartments, they will likely become targeted upon interaction with other specifically localised proteins. As such a Ca^{2+} dependent interaction between

caldendrin and myristoylated recoverin has been reported which in turn permits Ca^{2+}-induced translocation of caldendrin to subcellular membranes (Fries *et al*., 2010). Although it has been difficult to visualize *in vivo*, CaBP4 and CaBP5 interact with integral membrane VGCCs and therefore are also able to localise to membranes through interactions with their specific binding partners (Haeseleer *et al*., 2004, Rieke *et al*., 2008).

Normal targeting of Ca^{2+}-sensing proteins to their appropriate subcellular compartments has been shown to be indispensible for biological function. Understanding the precise mechanisms underlying the localisation of these proteins is therefore important for understanding how different Ca^{2+} signals are decoded to generate a variety of physiological outcomes. Ca^{2+}-sensors have evolved a myriad of subcellular targeting strategies which have permitted the fine tuning of specific cellular pathways. CaBP7 and CaBP8 provide an additional example of the evolutionary diversification of targeting mechanisms amongst Ca^{2+}-sensing proteins. These proteins contain no consensus motifs for post-translational acylation yet initial examination of the localisation of the overexpressed proteins in N2A cells revealed a distinct membrane localisation for both proteins (section 4.2.1 and (McCue *et al*., 2009)). The aim of this chapter was to examine the exact subcellular localisation of CaBP7 and CaBP8, and the mechanism by which these proteins are able to associate with cellular membranes.

4.2. Results

4.2.1. Localisation of human CaBP isoforms in N2A cells

All members of the CaBP family exhibit the greatest expression levels in neuronal tissues (Haeseleer *et al*., 2000, Wu *et al*., 2001, Mikhaylova *et al*., 2006) and therefore initial characterisation of their subcellular localisation was carried out in a neuronal cell line. N2A cells are a model neuroblastoma cell line that can be differentiated to a neuronal like morphology upon retinoic acid treatment (Pankratova *et al*., 1994). N2A cells were transfected with colour tagged constructs encoding each of the CaBPs, and images taken 24 hours after retinoic acid treatment (Figure 4.1). The *N*-myristoyl groups of CaBP1L, CaBP1S, and CaBP2 allow

these proteins to target to membranes. As such, CaBP1L, CaBP1S and CaBP2 localised to both the PM and to a perinuclear region resembling the Golgi apparatus (Figure 4.1B-D). CaBP1L also exhibited stronger cytoplasmic localisation than CaBP1S illustrating that there are differences in the targeting of the two splice isoforms of CaBP1 even though both associate with membranes via *N*-myristoylation at an identical consensus sequence.

None of the remaining CaBPs possess consensus sequences for post-translational lipidation and caldendrin, CaBP4 and CaBP5 exhibited a predominantly cytosolic localisation, as expected (Figure 4.1A, E and F). Caldendrin also appeared to concentrate in specific areas of the nucleus resembling nucleoli (Dundr and Misteli, 2001). CaBP7 and CaBP8, despite lacking consensus motifs for acylation, both localised to membranes in N2A cells (Figure 4.1G-H). Both proteins localised predominantly to a perinuclear compartment resembling the Golgi apparatus, intracellular vesicles and, in some cells, the PM. This unexpected membrane association prompted further investigation into the precise subcellular localisation of CaBP7 and CaBP8 and the mechanism by which they are targeted.

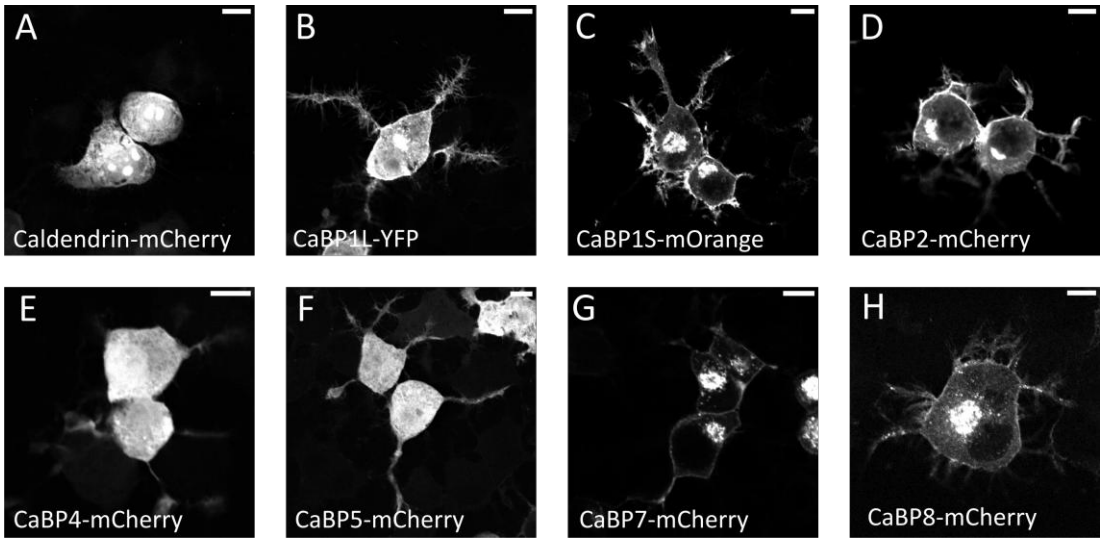

Figure 4.1. Intracellular distribution of fluorescently tagged human CaBP isoforms. The indicated constructs were used to determine the localisation of caldendrin, CaBP1S, CaBP1L, CaBP2, CaBP4, CaBP5, CaBP7 and CaBP8 expressed exogenously in retinoic acid differentiated N2A cells. Scale bars = 10 μm.

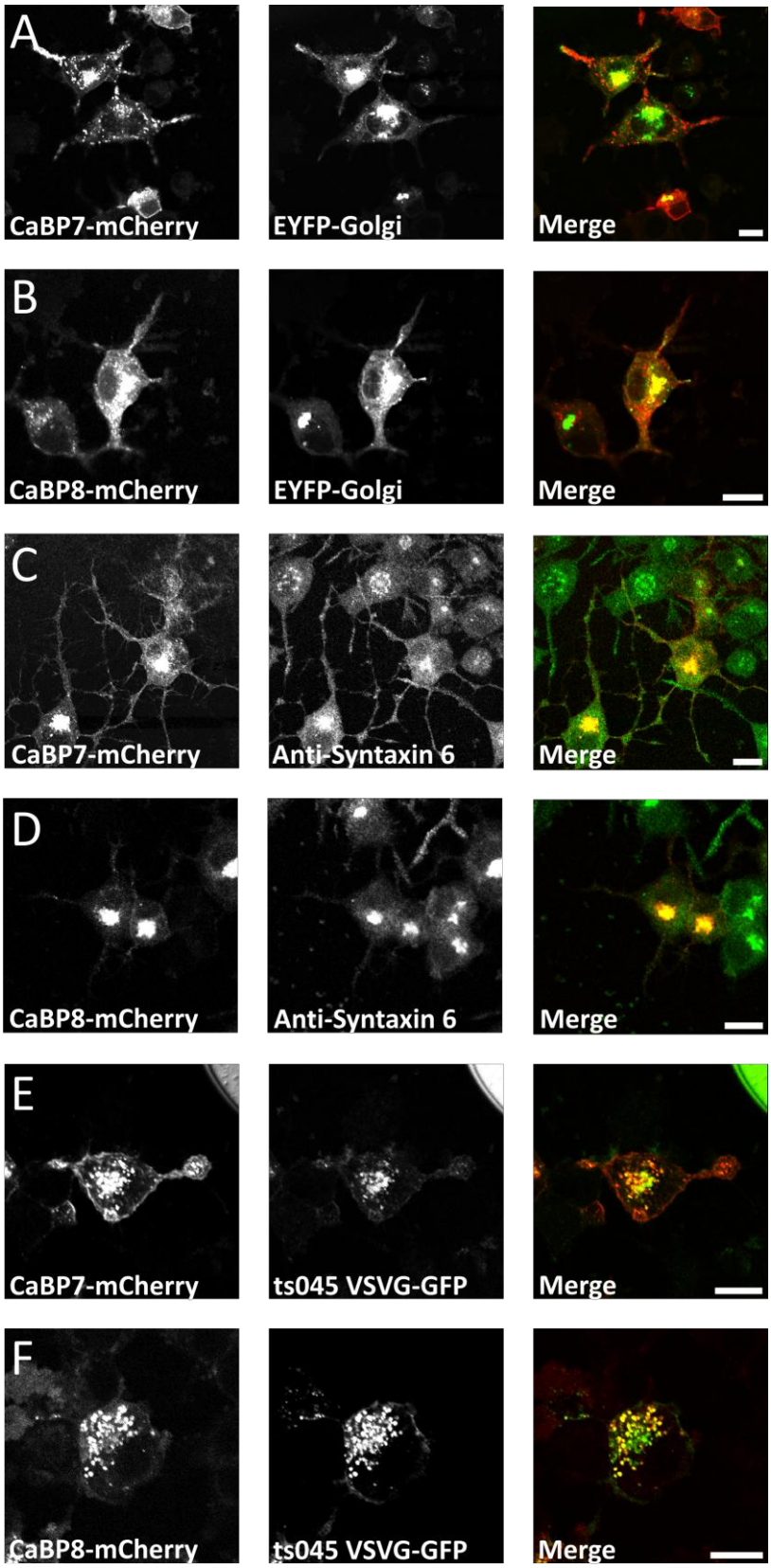

Figure 4.2. Co-localisation of CaBP7 and CaBP8 with TGN markers in differentiated N2A cells. Localisation of CaBP7 and CaBP8 (red) with an EYFP tagged cis/medial Golgi marker (A,B, green) or the TGN specific markers, anti-syntaxin 6 (C,D, FITC, green) and ts045 VSVG-GFP (E,F, green) was examined. Regions of co-localisation appear yellow in the merged images. Scale bars = 10 µm.

4.2.2. CaBP7 and CaBP8 colocalise with TGN markers in N2A cells.

The localisation of CaBP7 and CaBP8 to the Golgi-apparatus was confirmed by co-transfecting differentiated N2A cells with the mCherry tagged proteins along with a YFP tagged cis/medial Golgi marker, EYFP-Golgi (Figure 4.2A and B). Only partial co-localisation was observed, however, and since CaBP1L and CaBP1S have previously been determined to localise to the TGN, markers of this Golgi compartment were next investigated. Two TGN specific markers, syntaxin 6 (Teng *et al*., 2001) and the constitutive secretory cargo, vesicular stomatitis virus-G protein (VSVG) (Pelham, 2001)), were used to examine TGN localisation of CaBP7 and CaBP8. N2A cells overexpressing mCherry tagged CaBP7 or CaBP8, immunostained with a specific syntaxin 6 antibody highlighted extensive co-localisation of both CaBPs with the TGN marker (Figure 4.2C and D). To investigate the co-localisation of the proteins with VSVG, a temperature sensitive GFP tagged mutant of the cargo protein (ts045 VSVG-GFP) was exploited. Ts045 VSVG-GFP exhibits a temperature sensitive reversible folding defect which traps the protein in the ER at 40°C. Cells were maintained at 40°C overnight post-transfection and subsequently transferred to 20°C to permit correct folding of the protein and hence trafficking from the ER to the TGN. Maintenance of cells at 20°C blocked further trafficking from the TGN. Cells overexpressing either CaBP7 or CaBP8 showed extensive co-localisation with ts045 VSVG-GFP at the TGN under these conditions (Figure 4.2E and F) which is consistent with anti-syntaxin 6 colocalisation.

4.2.3. Identification of putative C-terminal TMDs in CaBP7 and CaBP8

Examination of the primary sequence of CaBP7 and CaBP8 revealed that both proteins were predicted to possess a TMD at their extreme C-termini (http://www.ch.embnet.org/software/TMPRED_form.html). In CaBP7 this spanned residues 189-205, and in CaBP8, residues 193-209. Both TMDs were 17 amino acids long, the optimal length for TGN localisation in preference to PM targeting which generally requires an extended transmembrane helix (Watson and Pessin, 2001). The remaining CaBPs were also examined for the presence of putative TMDs. Only CaBP1L and CaBP2 were predicted to contain a TMD although the confidence scores in these instances were significantly lower than observed for CaBP7 and CaBP8.

Since it has been previously shown that N-terminal myristoylation is essential for membrane localisation of CaBP1L and CaBP2, characterisation of the putative TMDs of CaBP7 and CaBP8 became the focus of this work.

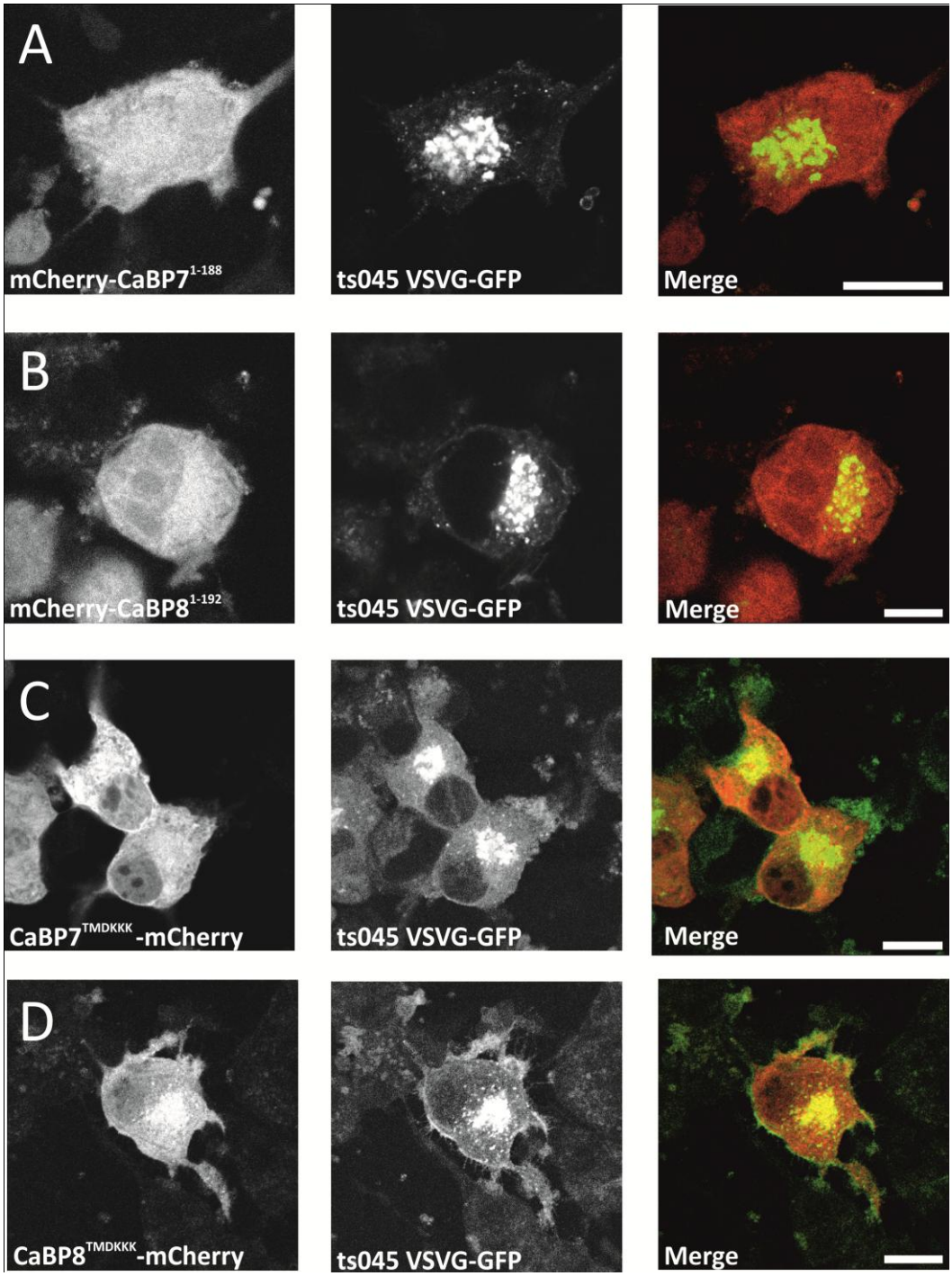

Figure 4.3. Analysis of the function of the putative TMD of CaBP7 and CaBP8 in differentiated N2A cells. Cells were transfected with ts045 VSVG-GFP (green) as a TGN marker and either mCherry-CaBP7$^{1–188}$ or mCherry-CaBP8$^{1–192}$ TMD deletion mutants (A,B, red); CaBP7^{TMDKKK}-mCherryor CaBP8^{TMDKKK}-mCherryTMD triple lysine mutants (C,D, red). Co-localisation appears yellow in merged images. Scale bars = 10 µm.

4.2.4. The predicted TMDs of CaBP7 and CaBP8 are required for correct membrane localisation

Truncation mutants of CaBP7 and CaBP8 were created which terminated at the amino acid directly preceding the start of the predicted TMD in order to investigate the requirement of this region for membrane targeting. Figures 4.3A and B show the subcellular localisation of the proteins expressed from these constructs (mCherry-CaBP7$^{1\text{-}188}$ and mCherry-CaBP8$^{1\text{-}192}$) along with VSV-G as a marker for the TGN. Removal of the TMD from CaBP7 and CaBP8 ablated membrane association and resulted in a predominantly cytosolic localisation with loss of co-localisation with TGN specific markers. Other variants of CaBP7 and CaBP8, used to further test the function of the predicted TMDs, were generated by mutating the central three amino acids of this region to lysine residues (mCherry-CaBP7^{TMDKKK} and mCherry-CaBP8^{TMDKKK}). This was predicted to abolish TMD function (http://www.ch.embnet.org/software/TMPRED_form.html) and when overexpressed in N2A cells, the triple lysine mutants exhibited increased cytosolic localisation compared to the full-length wild-type proteins that was more pronounced for CaBP7^{TMDKKK} than for CaBP8^{TMDKKK} (Figure 4.3C and D). Collectively these data indicated that disruption of the predicted TMDs of CaBP7 and CaBP8 caused extensive mislocalisation of both proteins to the cytosol.

4.2.5. CaBP7 and CaBP8 TMDs alone are sufficient to target normally cytosolic proteins to the TGN

To investigate properties of the TMDs in isolation, these sequences were fused to normally cytosolic proteins. Chimaeric constructs encoding the C-terminus of both CaBP7 (residues 189-215) or CaBP8 (residues 193-219) fused to either CaBP5-mCherry (CaBP5^{CaBP7TMD}-mCherry and CaBP5^{CaBP8TMD}-mCherry) or mCherry alone (mCherry^{CaBP7TMD}) were made. In contrast to the normally cytosolic localisation of wild-type CaBP5 (Figure 4.1F), both CaBP5^{CaBP7TMD}-mCherryand CaBP5^{CaBP8TMD}-mCherry colocalised extensively with the TGN marker ts045 VSVG-GFP (Figure 4.4A and B). Similarly, the TMD of CaBP7 fused to mCherry was able to direct a pool of this chimaeric protein to the TGN (Figure 4.4C). These observations indicate that the

putative TMDs of CaBP7 and CaBP8 alone are sufficient to accurately target proteins to membranes of the TGN.

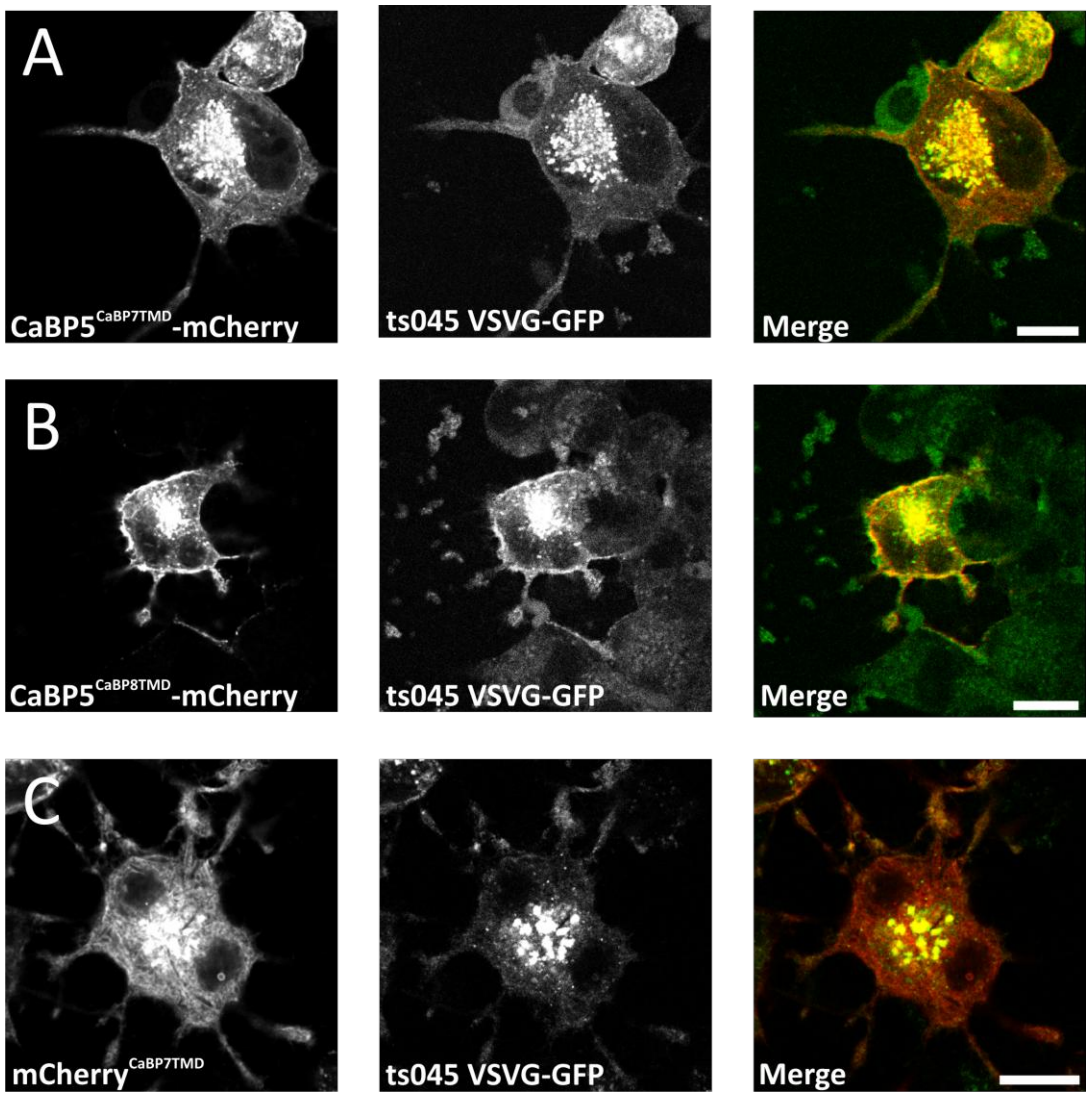

Figure 4.4. Analysis of CaBP5 and mCherry chimaeric constructs in retinoic acid differentiated N2A cells. CaBP5^{CaBP7TMD}-mCherry or CaBP5^{CaBP8TMD}-mCherrychimaeras (A,B, red), or mCherry^{CaBP7TMD} (C, red) were co-expressed with ts045 VSVG-GFP (green) as a TGN marker. Regions of co-localisation appear yellow in merged images. Scale bars = 10 μm.

4.2.6. The position of the fluorescent colour tag does not affect targeting of CaBP7 or CaBP8

The putative TMDs of CaBP7 and CaBP8 are positioned 10 amino acids from the carboxy-terminus of the proteins. Neither protein possesses a signal peptide and since the TMD exits the ribosome very close to translation termination during synthesis, these proteins are unlikely to be inserted into membranes co-translationally as is the case for the majority of membrane proteins. This finding

suggested that CaBP7 and CaBP8 may be members of a special class of membrane protein, the tail anchored (TA) proteins, which are inserted into membranes post-translationally. This class of membrane protein is defined by the occurrence of a single transmembrane domain less than 30 amino acids from the carboxy-terminus (Borgese *et al*., 2003). Extension of the region C-terminal to the TMD beyond 30 amino acids can result in a shift from post-translational to co-translational membrane insertion, with the protein instead being processed as a classical type II membrane protein. (Brambillasca *et al*., 2006). As all the constructs examined thus far have encoded a C-terminal colour tag, and therefore artificially extended the C-termini of each protein beyond the 30 amino acid threshold, it was important to investigate whether the position of the colour tag affected the correct targeting of CaBP7 and CaBP8. CaBP7 and CaBP8 were re-cloned into an N-terminally tagging vector and the constructs co-expressed with their C-terminally tagged counterparts. Figures 4.5A and B illustrate that the position of the colour tag, whether C-terminal or N-terminal, does not alter the localisation of CaBP7 and CaBP8 and the two colour tagged fusion proteins in each case completely co-localised.

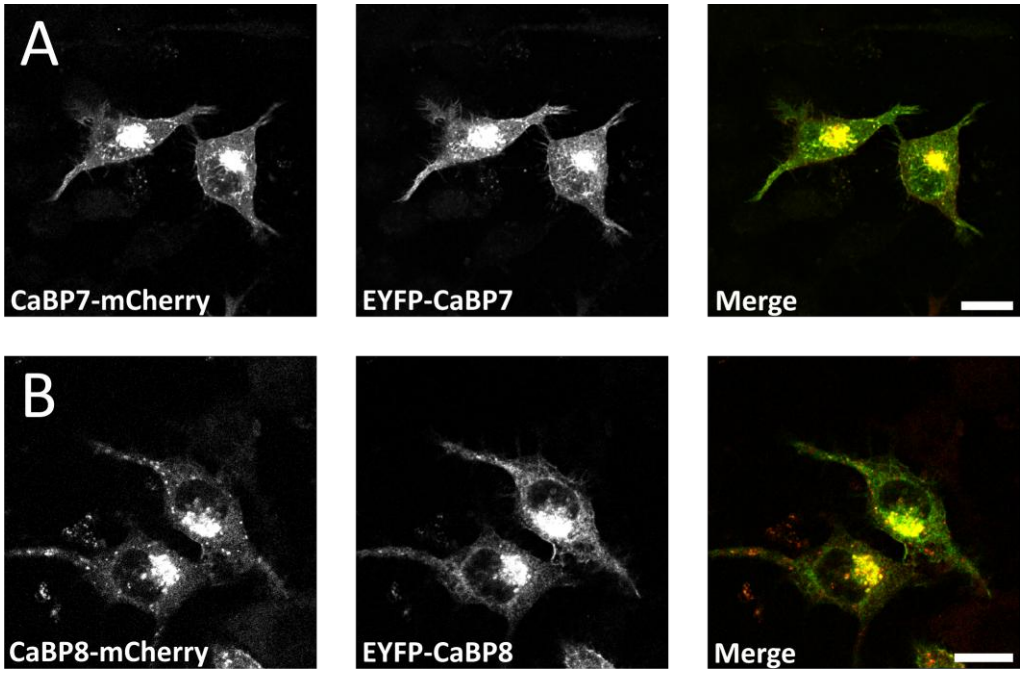

Figure 4.5. The effect of the position of the colour tag fused to CaBP7 and CaBP8. C-terminally mCherry tagged CaBP7 (red, A) and CaBP8 (red, B) were co-expressed with N-terminally EYFP tagged variants of the same proteins (green, A,B). Regions of co-localisation appear yellow in merged images. Scale bars = 10 µm.

4.2.7. Localisation of human CaBP isoforms in HeLa cells

A high throughput siRNA screen in HeLa cells reported a phenotype upon knockdown of CaBP7 (Neumann *et al*., 2010) suggesting that its expression may not be restricted to neuronal cell types. This prompted further investigation into whether HeLa cells expressed CaBP7 endogenously. Figures 4.6A and B show immunostaining and an immunoblot using an anti-CaBP7 antibody illustrating that HeLa cells do express an anti-CaBP7 reactive endogenous protein of the correct molecular weight for CaBP7. Endogenous CaBP7 appears to localise to numerous vesicles throughout the cell which concentrate in a perinuclear region. This finding agreed with exogenous CaBP7 localisation in N2A cells although the punctate structures appeared less numerous in N2A cells and tended to accumulate more tightly in the region of the TGN (Figure 4.1G vs. Figure 4.6A). As HeLa cells have a preferable morphology for studying subcellular localisation in detail, this cell system was adopted for the remainder of these analyses.

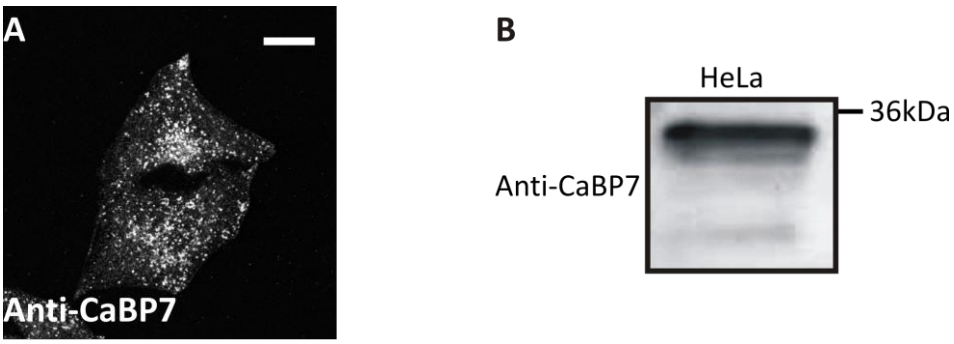

Figure 4.6. Expression of endogenous CaBP7 in HeLa cells. A) HeLa cells immunostained with a CaBP7 specific antibody and detected with an Alexa 568 conjugated anti-rabbit secondary antibody. B) Western blot detection of endogenous CaBP7 expression in HeLa cell lysate using the same CaBP7 specific antibody. (marker = 36 kDa). Scale bar = 10 µm

All human CaBP isoforms were individually transfected into HeLa cells to check their localisation in a non-neuronal cell line compared to that observed in N2A cells (Figure 4.7). As in N2A cells, caldendrin, CaBP4 and CaBP5 all displayed a diffuse, cysosolic distribution (Figure 4.7A, E and F), with caldendrin accumulation in discrete regions of the nucleus resembling nucleoli. As expected for *N*-myristoylated proteins, CaBP1L, CaBP1S and CaBP2 all localised to the PM and subcellular membranes resembling the Golgi apparatus and other punctate structures (Figure 4.7B, C and D). CaBP1L again exhibited greater cytosolic fluorescence than CaBP1S (Figure 4.7C). Exogenously expressed CaBP7 and CaBP8 localised, similarly to endogenous CaBP7 (Figure 4.6A), to punctate structures throughout the cytosol which appeared to cluster in a perinuclear region resembling the TGN (Figure 4.7 G and H). mCherry-CaBP7 and mCherry-CaBP8 showed partial colocalisation with the TGN specific marker p230 in many cells (Figure 4.8A and C) whereas in others almost no TGN localisation was observed (Figure 4.8B and D) and instead the protein was found only on vesicular structures.

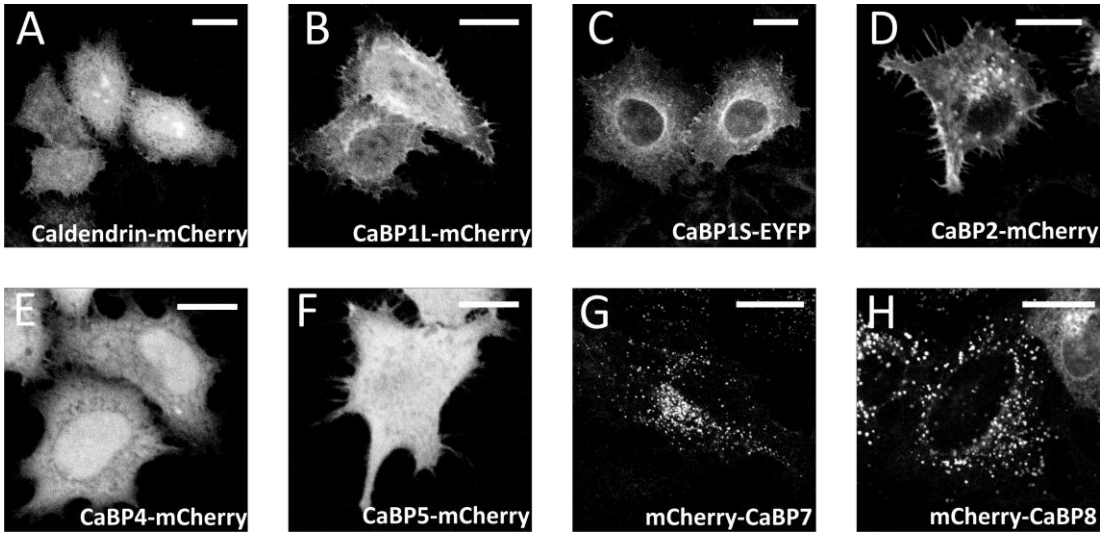

Figure 4.7. Intracellular distribution of fluorescently tagged human CaBP isoforms in HeLa cells. The indicated constructs were used to determine the localisation of caldendrin, CaBP1S, CaBP1L, CaBP2, CaBP4, CaBP5, CaBP7 and CaBP8 expressed exogenously in HeLa cells. Scale bars = 10 µm.

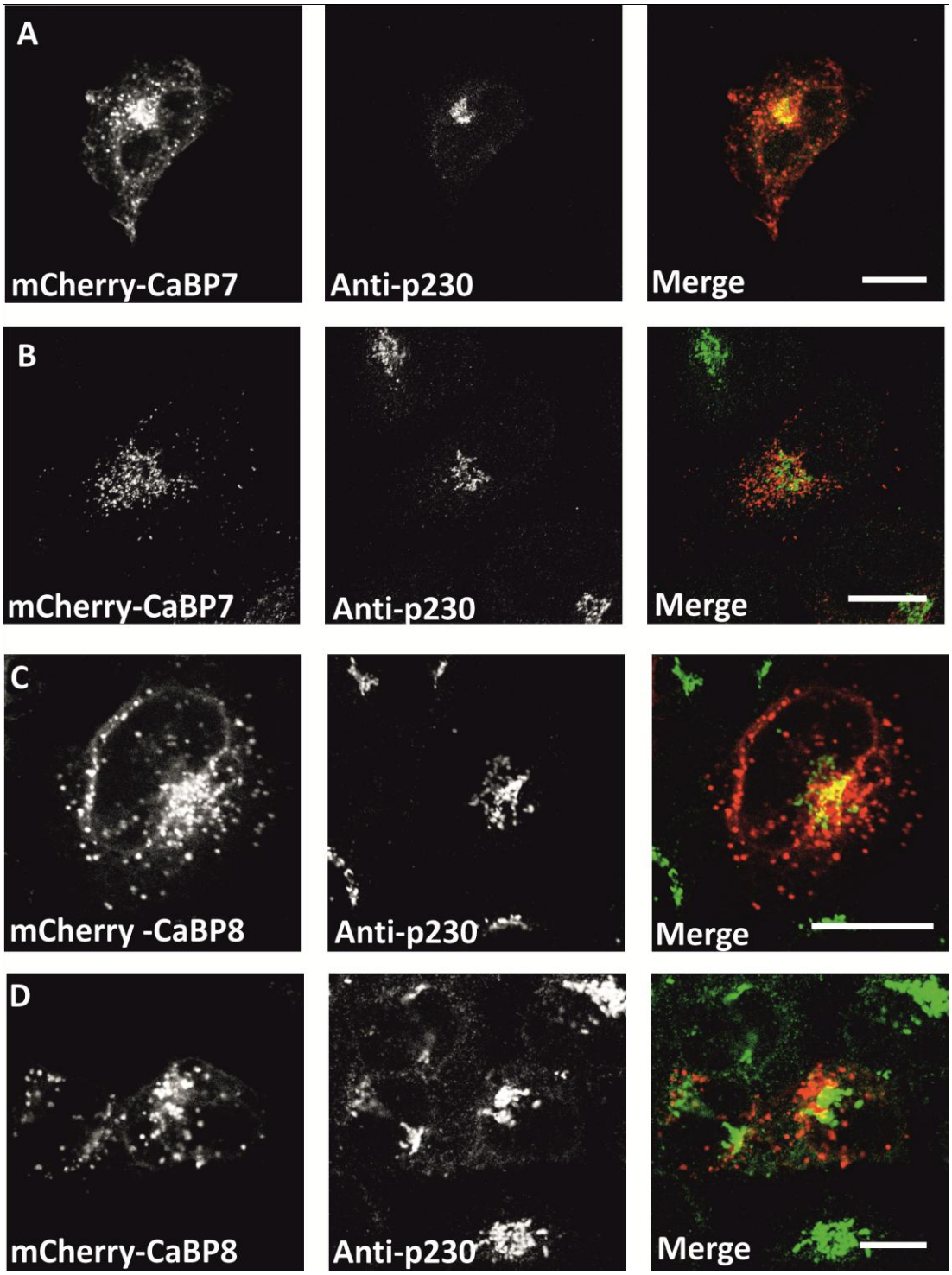

Figure 4.8. Localisation of fluorescently tagged CaBP7 and CaBP8 in HeLa cells compared with the TGN marker p230. A and B) Exogenously expressed mCherry-CaBP7 (red) and immunostained p230 (Anti-p230, FITC, green). C and D) Exogenously expressed mCherry-CaBP8 (red) and immunostained p230 (Anti-p230, FITC, green). A and C) show examples where the exogenous protein (red) and the TGN marker, p230 (green), overlap in localisation (yellow). B and D) show examples where there is little or no overlap in localisation of the exogenous protein (red) and the TGN marker p230 (green). Scale bars = 10 µm.

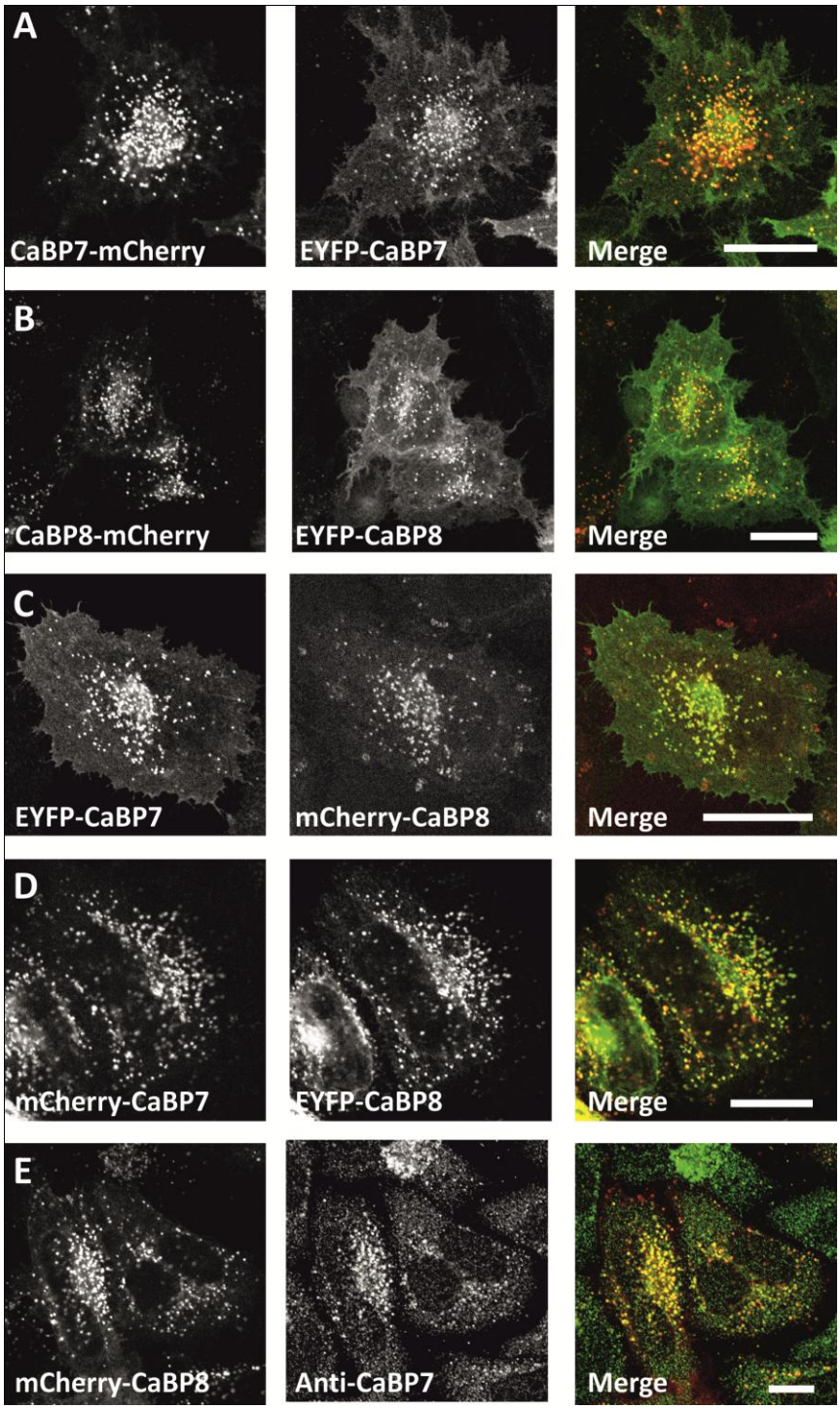

Figure 4.9. Localisation of fluorescently tagged CaBP7 and CaBP8 in HeLa cells. A) Exogenously expressed C-terminally tagged CaBP7-mCherry (red) and N-terminally tagged EYFP-CaBP7 (green). B) Exogenously expressed C-terminally tagged CaBP8-mCherry (red) and N-terminally tagged EYFP-CaBP8 (green). C and D) Exogenously co-expressed N-terminally EYFP- (green) or mCherry- (red) tagged CaBP7 and CaBP8. E) Exogenously expressed N-terminally tagged mCherry-CaBP8 (red) and immunostained endogenous CaBP7 (Anti-CaBP7, FITC, green) in HeLa cells. Co-localisation appears yellow in merged image. Scale bars = 10 µm.

The localisation of exogenous and endogenous CaBP7 and CaBP8 in HeLa cells was further examined by co-transfection of cells with different combinations of N- and C-terminally tagged constructs. Figure 4.9A and B demonstrate that, as seen in N2A cells, the position of the colour tag did not affect the localisation of exogenously expressed CaBP7 and CaBP8. Complete co-localisation was observed in co-transfections of N- and C-terminally tagged variants of each protein. Co-expression of N-terminally tagged CaBP7 and CaBP8 (Figure 4.9C and D) resulted in extensive overlap in the localisation of the two proteins to the same vesicular structures. The different colour tags also failed to influence the co-localisation of the two proteins. Staining of CaBP8 transfected cells with anti-CaBP7 confirmed that exogenous CaBP8 protein co-localised to the same vesicles as endogenous CaBP7 (Figure 4.9E). Collectively these data confirmed that tagging of CaBP7 and CaBP8 at either the C- or N-terminus had no impact on normal protein localisation and that CaBP7 and CaBP8 localise to the same subcellular membranes.

4.2.8. Trypsin protection analysis of CaBP7 and CaBP8 membrane topology

CaBP7 and CaBP8 have a similar architecture to TA proteins, with a putative TMD 10 amino acids from their extreme C-termini. TA proteins typically have a cytosolically oriented N-terminus and short luminal C-terminus (Figure 4.10Ai). Trypsin protection assays were used in order to confirm whether this was also the membrane topology of CaBP7 and CaBP8. A number of alternative arrangements were also possible including: 1) N- and C- termini facing the cytosol, with only partial membrane insertion of the TM helix (Figure 4.10Aii), or 2) A luminal N-terminus and cytosolic C-terminus (Figure 4.10Aiii). It was important to distinguish between these different topologies in order to characterise CaBP7 and CaBP8 as true TA proteins and also to provide a topological basis for the published interaction with the cytosolic Golgi-associated enzyme, PI4KIIIβ (Mikhaylova *et al*., 2009).

To address this issue an imaging based protocol was employed whereby HeLa cells were triply transfected with ECFP (as a soluble marker) and CaBP7 or CaBP8 tagged at either the N-terminus with EYFP or the C-terminus with mCherry. This approach was based on a well-characterised method for studying the topology of membrane

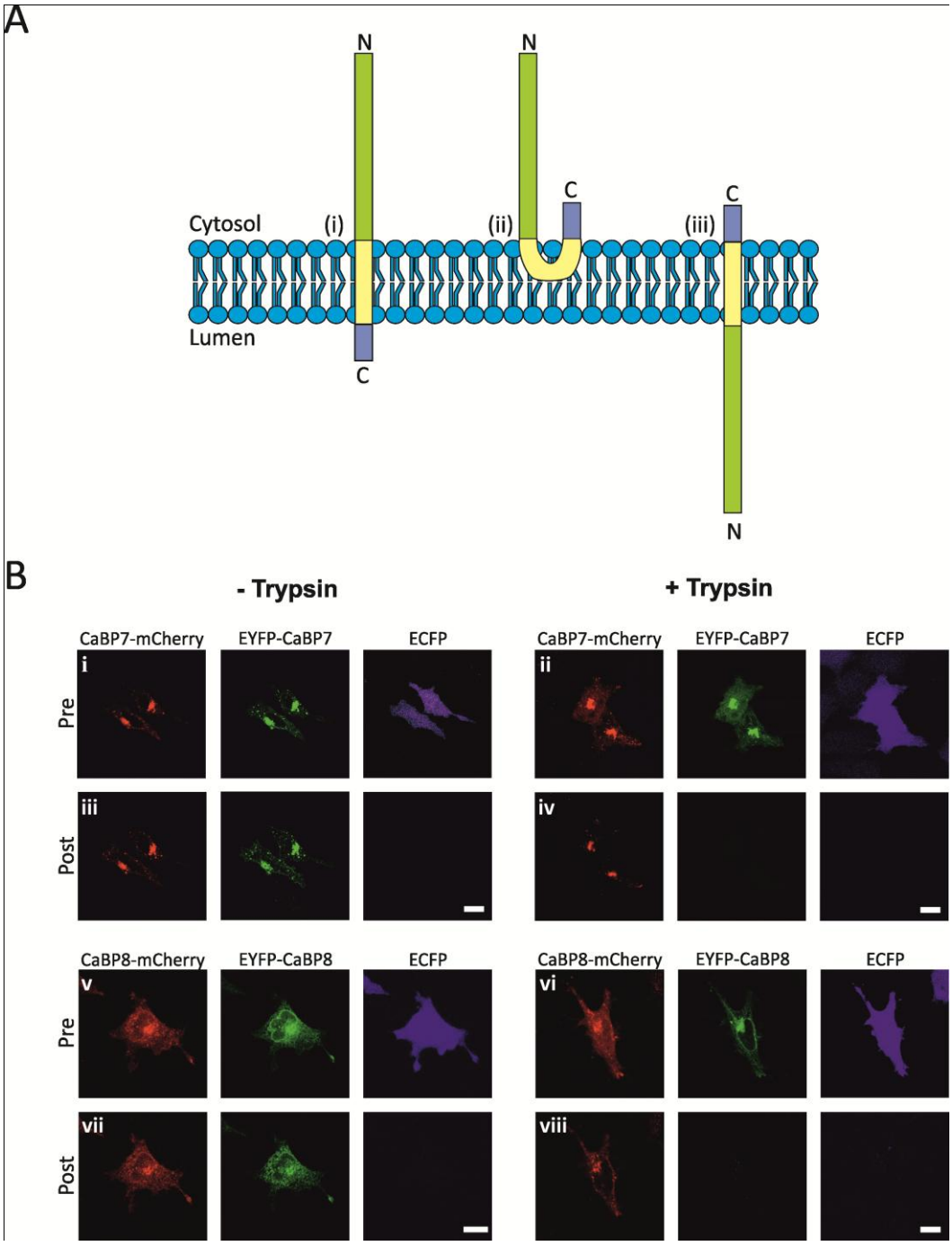

Figure 4.10. Possible CaBP7 and CaBP8 membrane topologies and representative fluorescence protease protection assay images. A) Potential membrane topologies for CaBP7 and CaBP8 across biological membranes: (i) Type II membrane protein orientation; (ii) Peripheral membrane protein orientation; (iii) Type I membrane protein orientation. Protein domains are: Green – N-terminal domain; Yellow – Transmembrane domain and Purple – C-terminal domain. The lipid bilayer is shown in blue. (From (McCue *et al.*, 2011)) B) HeLa cells transfected with ECFP (blue) and N- and C-terminally tagged: CaBP7-mCherry (red) and EYFP-CaBP7 (green) or CaBP8-mCherry (red) and EYFP-CaBP8 (green). 'Pre' denotes before digitonin application; 'Post' denotes following digitonin (40 µM) and ± trypsin (4 mM) treatment. Controls are shown before (i and v) and after (iii and vii) digitonintreatment but without trypsin treatment for CaBP7 and CaBP8 respectively. Experimental cells are shown prior to digitonin application (ii and vi) and following both digitonin and trypsin treatment (iv and viii) for CaBP7 and CaBP8 respectively. Scale bars = 10 µm.

proteins resident on various organelles including the Golgi apparatus (Lorenz *et al*., 2006). Digitonin was applied to the cells to selectively permeabilise the PM. Loss of cytosolic ECFP fluorescence was used to monitor permeabilisation. Perfusion was then switched to media containing trypsin which could now access the cytosol and degrade any proteins not protected within intracellular membranes. EYFP and mCherry fluorescence intensity at the TGN was monitored over time to assess the susceptibility of their environment to trypsin digestion. Using Figure 4.10A as a guide it can be reasoned that if the topology matches that depicted in (i), the N-terminal fluorescent tag should be exposed to trypsin digestion in the cytosol and the fluorescence signal lost, whereas the C-terminal tag should remain protected inside the lumen of the TGN. If the topology is as depicted in Figure 4.10A(ii), both colour tags should be digested upon trypsin treatment. Finally if the protein adopts the same topology as in Figure 4.10A(iii), the C-terminal fluorescent signal, not the N-terminal fluorescent signal, would be lost.

In control experiments, cells were perfused with KHM buffer until a steady fluorescence baseline was achieved (CaBP7: Figure 4.10B(i), CaBP8: Figure 4.10B(v)). Cells were permeabilised with digitonin but not subsequently challenged with trypsin (CaBP7: Figure 4.10B(iii), CaBP8: Figure 4.10B(vii)). The loss of ECFP fluorescence confirmed that the PM had been effectively compromised and there was no significant loss of EYFP or mCherry fluorescence at the TGN in the absence of trypsin. Representative fluorescence intensity traces are show in figure 4.11A (CaBP7) and 4.11C (CaBP8).

In cells treated with both digitonin and trypsin, there was a time dependent loss of the N-terminal EYFP signal in both CaBP7 and CaBP8 transfected cells (CaBP7 pretreatment: Figure 4.10B(ii), versus CaBP7 post digitonin/trypsin treatment: figure 4.10B(iv), and CaBP8 pretreatment: figure 4.10B(vi), versus CaBP8 post digitonin/trypsin treatment: figure 4.10B(viii)). In contrast, the C-terminal mCherry signal was preserved in both CaBP7 and CaBP8 expressing cells (Figure 10B and representative traces in Figure 4.11B (CaBP7) and Figure 4.11D (CaBP8)). The results

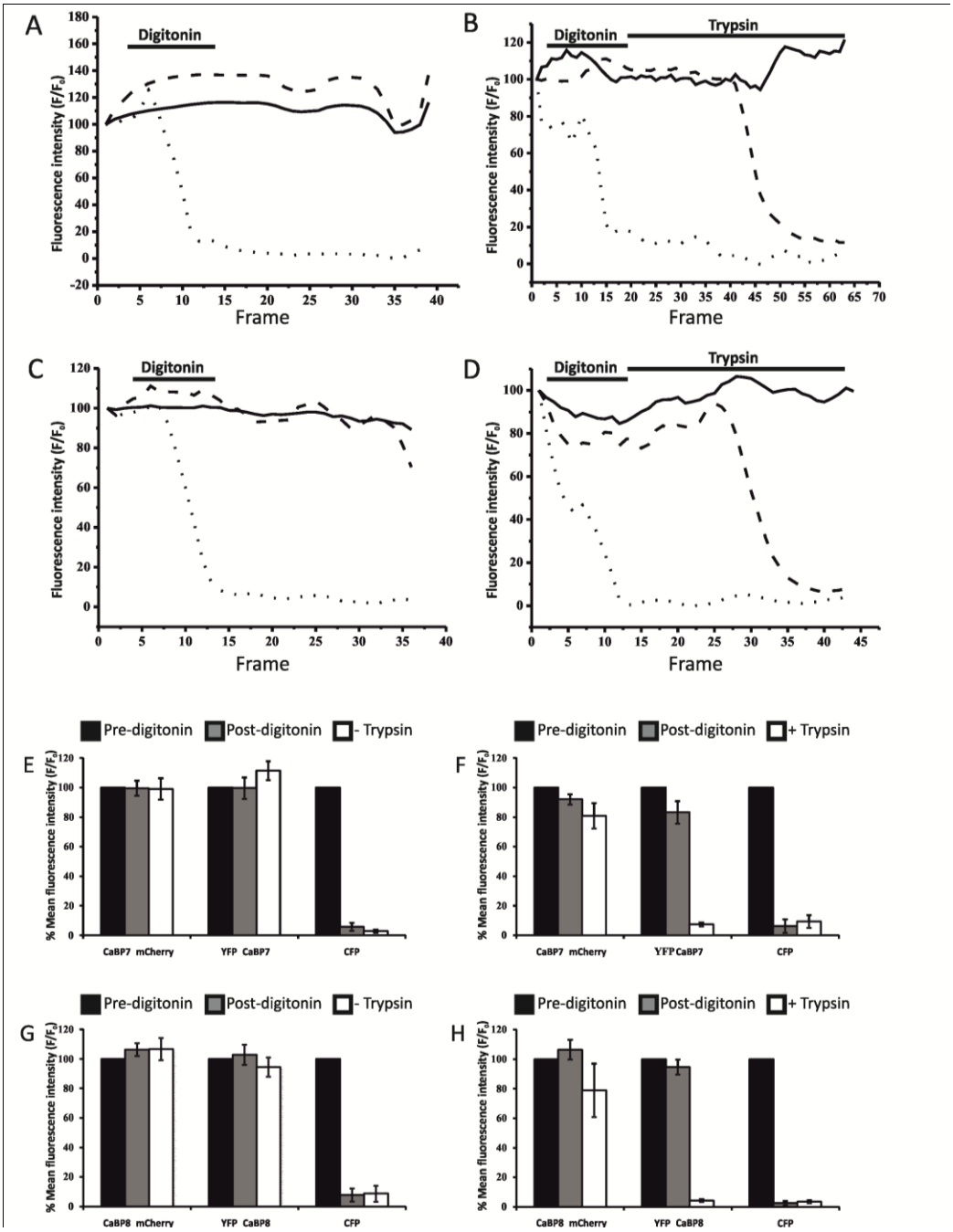

Figure 4.11. Example fitted curves from individual fluorescence protease protection assays. A and C) Control experiments without trypsin treatment for CaBP7 and CaBP8 respectively. B and D) CaBP7 and CaBP8 treated with both digitonin (40µM) and trypsin (4 mM). Solid lines represent C-terminally mCherry tagged CaBP7 or CaBP8, dashed lines represent N-terminally EYFP tagged CaBP7 or CaBP8 and dotted lines represent ECFP fluorescence. Frame rate = 1 frame/8 seconds. E-G) Histograms for averaged fluorescence protease protection assay results. E and G) Control experiments without trypsin treatment for CaBP7 and CaBP8 respectively. F and H) CaBP7 and CaBP8 treated with both digitonin (40µM) and trypsin (4 mM). Key: Black = before treatment with digitonin, Grey = after treatment with digitonin, White (Controls E and G) = End of experiment with no trypsin treatment, White (F and H) = End of experiment post-trypsin treatment. (E) n=7 cells, (F) n=12 cells, (G) n=7 cells, (H) n=7 cells. Data are plotted as mean ± SEM. $F/F_0$is the mean fluorescence intensity (F) at a given time point divided by the mean fluorescence intensity at the start of the experiment (F_0).

from multiple independent experiments were averaged (Figure 4.11E-H) and demonstrated specific protection of the C-terminal mCherry tag and degradation of the N-terminal EYFP tag upon treatment with trypsin (Figure 4.11F (CaBP7) and Figure 11H (CaBP8)). These data were consistent with a cytosolic N-terminus, susceptible to trypsin digestion, and a luminal C-terminus, protected from proteolysis within the TGN lumen – the topology typical of TA proteins. This data also confirmed that CaBP7 and CaBP8 possess a TMD which spans the membrane at the TGN.

To further validate the results of this imaging assay, biochemical assays were carried out to confirm the topology of CaBP7. HeLa cells were transfected with CaBP7 tagged with mCherry at either the C-terminus or the N-terminus and challenged with trypsin in the manner outlined above. In these experiments, protection of the colour tags was monitored by western blotting with an mCherry specific antibody (Anti-RFP, figure 4.12). Control lysate from cells transfected with mCherry alone and not treated with trypsin gave a clear immunoreactive band at ~26 kDa as expected for free mCherry protein (Figure 4.12, mCherry (-)). Lysates from control cells transfected with either N-terminally (Figure 4.12, mCherry-CaBP7 (-)) or C-terminally (Figure 4.12, CaBP7-mCherry (-)) mCherry-tagged CaBP7 gave an immunoreactive band at ~50 kDa. Consistent with the imaging studies, when cells were treated with digitonin and trypsin, the signal from cell lysates transfected with mCherry-CaBP7 was lost (Figure 4.12, mCherry-CaBP7 (+)) suggesting that this tag was oriented towards the cytosol and therefore susceptible to proteolysis. In contrast, the immunoreactive band from cell lysates transfected with CaBP7-mCherry (Figure 4.12, CaBP7-mCherry (+), indicated by the arrow) shifted in molecular weight to ~30 kDa. This suggested that the full-length fusion protein was being partially degraded at its cytosolically exposed N-terminus whereas the TMD and mCherry tag remained protected within the membrane and lumen of the TGN. Therefore an N-terminally truncated protein with apparent molecular mass of 30kDa was generated. Quantitation by densitometry indicated that the protein remaining in trypsin treated mCherry-CaBP7 samples was 25±11.9% of that present in trypsin treated CaBP7-mCherry samples (n=3 independent experiments, ±SEM).

These results are consistent with a cytosolic N-terminus and luminal C-terminus CaBP7 topology.

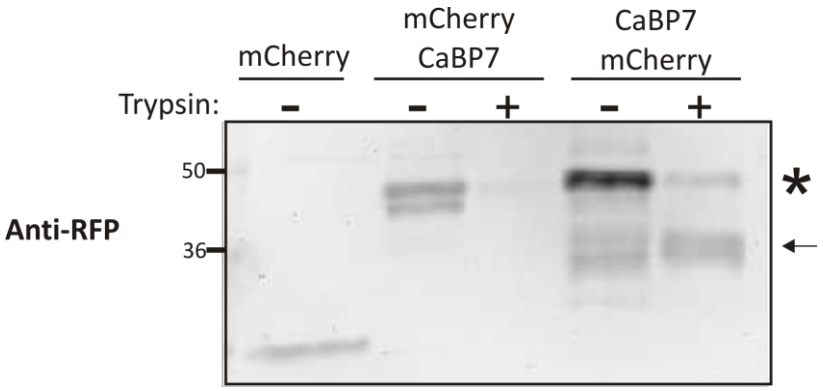

Figure 4.12. Biochemical protease protection assay. HeLa cells expressing mCherry control protein, mCherry-CaBP7 or CaBP7-mCherry were permeabilised using 40 µM digitonin followed by incubation ± 4 mM trypsin. Cells were lysed, protein resolved on SDS-PAGE and mCherry detected by immunoblotting with polyclonal anti-RFP antibody. (*) - Denotes full length mCherry-CaBP7 or CaBP7-mCherry; (←) - Denotes the major proteolytic fragment generated from CaBP7-mCherry following trypsin digestion. Molecular weight standards (kDa) are shown on the left side of the image.

4.2.9. Antibody accessibility experiments to assess the membrane topology of CaBP7 and CaBP8

As discussed earlier, fusion of peptide tags longer than 30 amino acids to the C-terminal end of a TA protein has been shown to cause aberrant processing of the resultant chimera as a type-II membrane protein, with the protein being inserted into the membrane co-translationally, rather than post-translationally (Borgese *et al*., 2003, Borgese *et al*., 2007, Kutay *et al*., 1995, Kim *et al*., 1997). For this reason further experiments were performed to assess whether fusion of a large fluorescent protein tag at the C-terminus of CaBP7 or CaBP8 had caused them to adopt an incorrect membrane topology. The c-myc epitope tag is only 10 amino acids in length and could therefore be fused to the C-termini of CaBP7 and CaBP8 without exceeding the experimentally determined 30 amino acid limit for correct TA protein processing. Epitope accessibility was then used to assess the position of both the myc tag and the N-terminus of the protein in relation to the membrane (Kuroda *et al*., 1996). Cells were transfected with either mCherry-CaBP7-myc or mCherry-CaBP8-myc and subsequently treated with either digitonin, to selectively

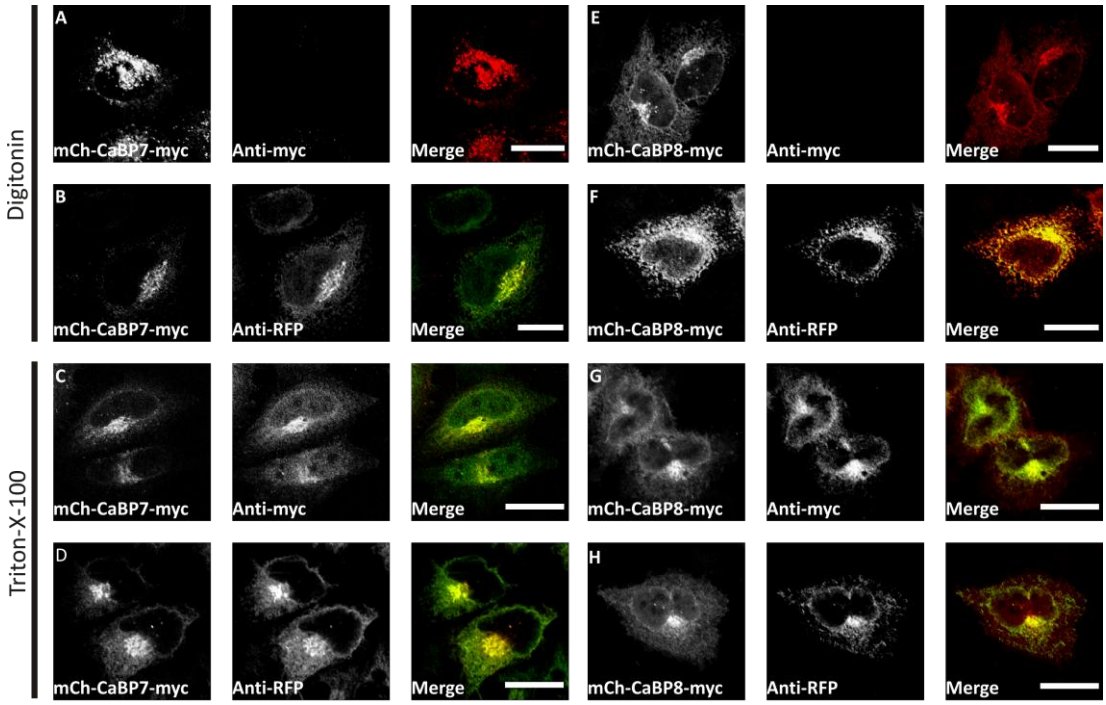

Figure 4.13. Epitope accessibility analysis of C-terminally myc tagged CaBP7 and CaBP8. A,B,E and F) Digitonin permeabilisation - HeLa cells expressing mCherry-CaBP7-myc or mCherry-CaBP8-myc (mCh-CaBP7-myc and mCh-CaBP8-myc, red) were treated with digitonin to selectively permeabilise the PM, fixed and processed for immunofluorescence with an anti-c-myc antibody (Anti-myc, FITC, green. A: mCh-CaBP7-myc, red. E: mCh-CaBP8-myc, red.) or an anti-RFP antibody (Anti-RFP, FITC, green. B: mCh-CaBP7-myc, red. F: mCh-CaBP8-myc, red.). C, D, G and H) Triton-X-100 permeabilisation - HeLa cells expressing mCh-CaBP7-myc or mCh-CaBP8-myc were fixed, treated with Triton-X-100 to permeabilise all cellular membranes and processed for immunofluorescence with an anti-c-myc antibody (Anti-myc, green. C: mCh-CaBP7-myc, red. G: mCh-CaBP8-myc, red.) or an anti-RFP antibody (Anti-RFP, green. D: mCh-CaBP7-myc, red. H: mCh-CaBP8-myc, red.). Regions of colocalisation appear yellow in overlay images. Scale bars = 10 µm.

permeabilise the PM, or with Triton X-100 to permeabilise all cellular membranes. Fixed, permeabilised cells were incubated with either anti-RFP or anti-myc and the subsequent staining pattern assessed to deduce the membrane topology. Following digitonin permeabilisation of the PM, mCherry fluorescence was present but no anti-myc immunofluorescence was detectable (Figure 4.13A, mCh-CaBP7-myc and Figure 4.13E, mCh-CaBP8-myc) indicating that the myc antibody did not have access to the C-terminus of the protein. In similarly treated cells, anti-RFP immunofluorescence was detected demonstrating that the N-terminus of the protein was cytosolic and the mCherry tag freely accessible to the RFP antibody. In control cells, non-selectively permeabilsed with Triton X-100, immunofluorescence

from both anti-RFP and anti-myc was observed. Therefore, consistent with the trypsinisation assays (Section 4.2.8), the C-terminal myc-tag was resident within a sub-cellular membrane bounded compartment that was only accessibile to anti-myc following Triton permeabilisation of all cellular membranes. The N-terminal mCherry tag was freely accessible to anti-RFP antibody after PM-selective permeabilisation using digitonin. Collectively, these data indicate that CaBP7 and CaBP8 adopt the membrane topology of true TA proteins.

4.2.10. Localisation of CaBP7 and CaBP8 Chimeras in HeLa cells

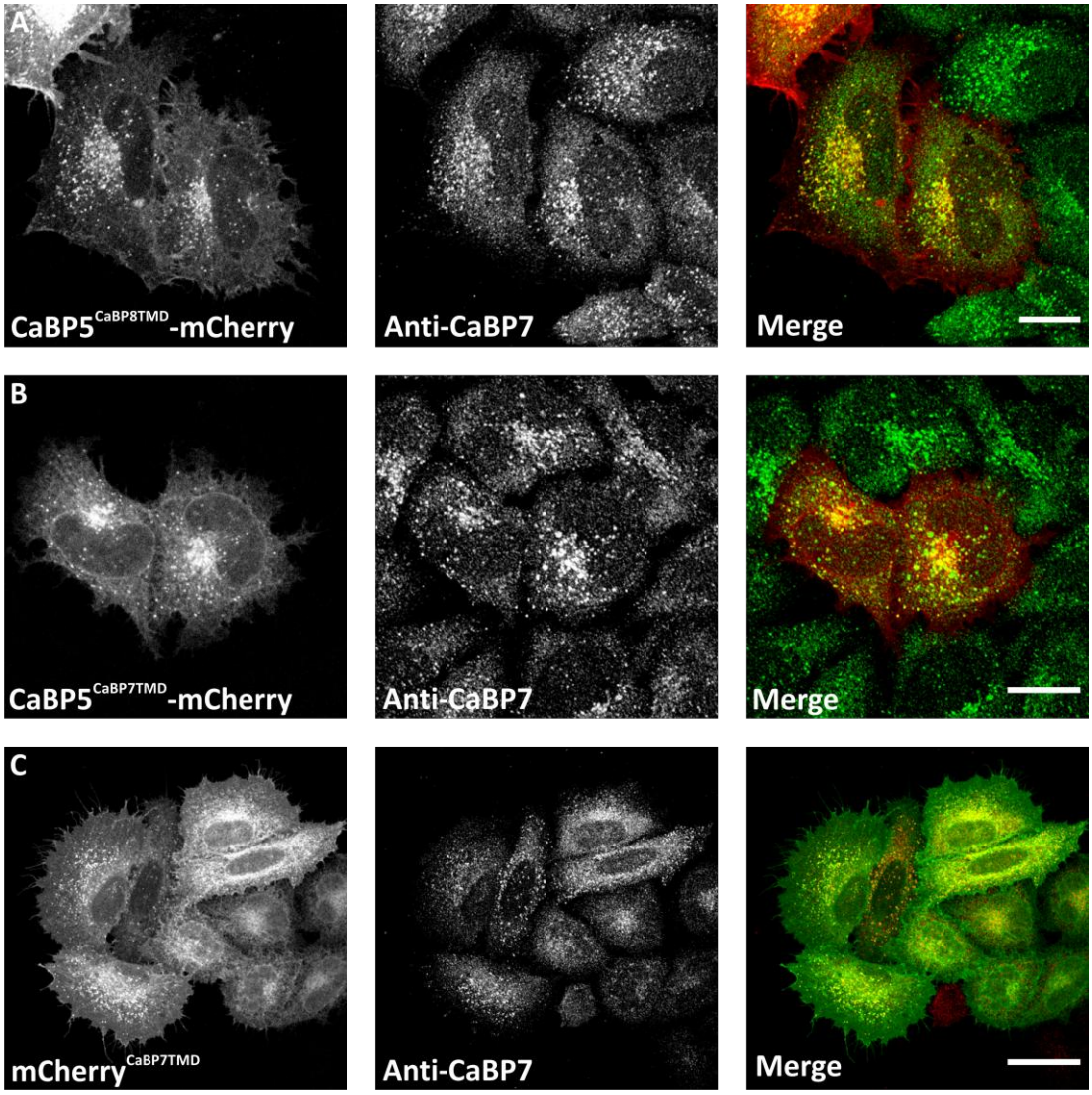

Figure 4.14. Analysis of localisation of CaBP5 and mCherry chimaeric constructs in HeLa cells. HeLa cells exogenously expressing or CaBP5^{CaBP8TMD}-mCherry chimaeras (A,B, red), or mCherry-^{CaBP7TMD} (C, red) immunostained with a CaBP7 antibody (Anti-CaBP7, FITC, green) to detect endogenous protein (NB Anti-CaBP7 is specific to the N-terminus of the protein so does not detect the transmembrane domain fused to either CaBP5 or mCherry). Regions of co-localisation appear yellow in merged images. Scale bars = 10 µm.

As previously indicated, exogenously expressed CaBP7 and CaBP8 localise to the same structures in HeLa cells. It was found that HeLa cells express CaBP7 endogenously and anti-CaBP7 immunostaining confirmed that exogenous and endogenous protein localised to the same subcellular compartments (section 4.2.7). Chimeras of the TMD of either CaBP7 or CaBP8 fused to normally cytosolic proteins also localised like the full length wild-type protein in N2A cells (section 4.2.5). The localisation of these chimeras was also assessed in HeLa cells to ensure that the proteins were not processed differently in this non-neuronal cell line (Figure 4.14). Cells were immunostained with anti-CaBP7 to confirm that the proteins resided in the same compartments as endogenous CaBP7. CaBP5^{CaBP7TMD}-mCherryand CaBP5^{CaBP8TMD}-mCherry exhibited extensive colocalisation with endogenous CaBP7 on intracellular vesicles (Figure 4.14A and B). Chimeras had increased cytosolic fluorescence and some localisation to the PM. mCherry^{CaBP7TMD} localised to anti-CaBP7 labelled vesicles in some cells, but in others a more reticular pattern of fluorescence was observed (Figure 4.14C). The observed partial colocalisation with endogenous protein suggested that a proportion of the chimearic protein was being targeted correctly in HeLa cells.

Trypsin protection and antibody accessibility experiments confirmed that CaBP7 and CaBP8 belong to the TA class of integral membrane proteins (section 4.2.8). As such, these proteins must be inserted into membranes post-translationally rather than co-translationally. Typically, TA proteins are initially inserted into membranes of either the ER or the mitochondria (Borgese *et al*., 2001). The reticular-like pattern of localisation of mCherry^{CaBP7TMD} suggested that CaBP7 and CaBP8 are initially inserted into the ER membrane and then subsequently trafficked to the TGN and to post-Golgi vesicles. For this reason, the extent of co-localisation of full-length mCherry-CaBP7 (Figure 4.15A and B) or mCherry^{CaBP7TMD} (Figure 4.15C and D) with the mitochondrial marker, TOM20, or the ER marker, calnexin was assessed. In these cells full length CaBP7 labelled vesicular structures which were untagged by either antibody. mCherry^{CaBP7TMD} did not co-localise with the mitochondrial marker but did exhibit partial co-localisation with calnexin, consistent with an ER localisation for a pool of the chimaera (Figure 4.15C and D).

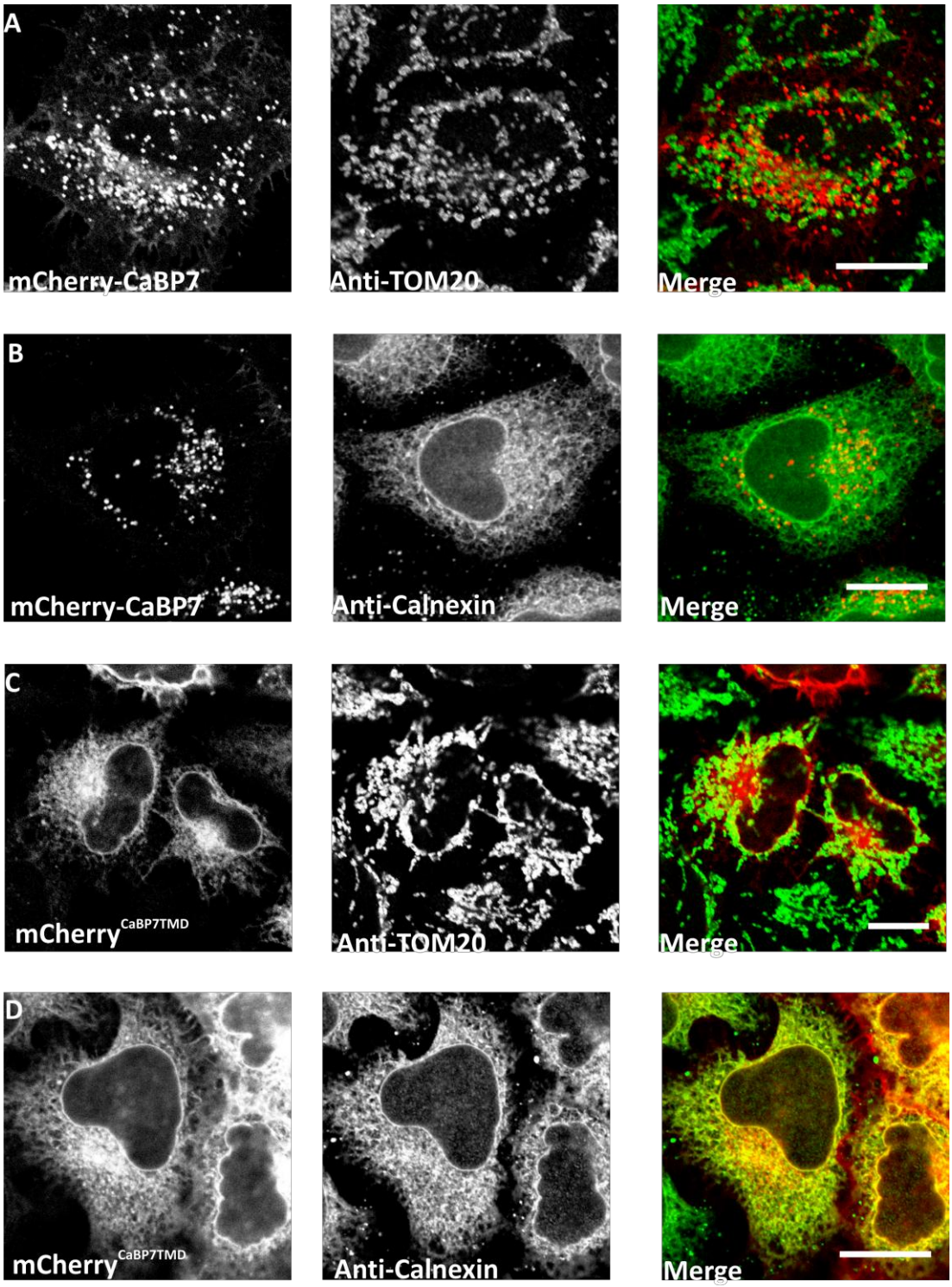

Figure 4.15. Analysis of localisation of mCherry-CaBP7 or mCherry^{CaBP7TMD} compared with markers of the mitochondria and the ER. HeLa cells exogenously expressing mCherry-CaBP7 (A, B, red), or mCherry-^{CaBP7TMD} (C, D, red) immunostained with either the mitochondrial marker TOM20 (anti-TOM20, A, C, FITC, green) or the ER marker, calnexin (anti-calnexin, B, D, FITC, green). Regions of co-localisation appear yellow in merged images. Scale bars = 10 µm.

4.2.11. Identification of CaBP7 and CaBP8 positive vesicles in HeLa cells

As shown in figure 4.8, CaBP7 and CaBP8 displayed partial co-localisation with the TGN specific marker p230, but also localised to discrete puncta throughout the cell cytosol. The identity of these punctate structures was examined by performing co-transfections of mCherry tagged CaBP7 and CaBP8 with EYFP tagged markers of defined subcellular compartments (Figure 4.16). No co-localisation with the early endosome marker, Rab5a (Figure 4.16A and D), or the autophagosome marker, LC3β (Figure 4.16B and E), was observed, however there was extensive co-localisation of CaBP7 and CaBP8 with the lysosomal marker LAMP1 (Figure 4.16C and F).

To further characterise this localisation, cells were transfected with mCherry-CaBP7 (as a model for both CaBP7 and CaBP8), and immunostained with antibodies to various markers of endosomes and lysosomes (Figure 4.17). No-colocalisation was observed with the endosomal and multivesicular body (MVB) marker, HRS, or the recycling endosome marker, Rab11 (Figure 4.17A and B). Colocalisation with late endosome/lysosome markers, LAMP1 and CD63, was observed, although in both cases there was a population of CaBP7-positive vesicles which did not label with the antibodies and vice versa (Figure 4.17D and E). Lysosomes are typically characterised by the absence of mannose-6-phosphate receptors (M6PR). Consistent with this, immunostaining of mCherry-CaBP7 overexpressing cells with M6PR antibody indicated that there was no co-localisation between the two proteins (Figure 4.17C). This is in agreement with the co-localisation observed with exogenously expressed LAMP1-YFP in figure 4.16. Cells co-immunostained with anti-CaBP7 and either anti-LAMP1 or anti-CD63 confirmed that endogenous CaBP7 co-localised with the same markers as the exogenously expressed protein (Figure 4.18A and B). mCherry-CaBP7 completely colocalised with the acidotropic dye, LysoTracker™ Blue (Figure 4.18C), consistent with the presence of CaBP7 on acidic organelles.

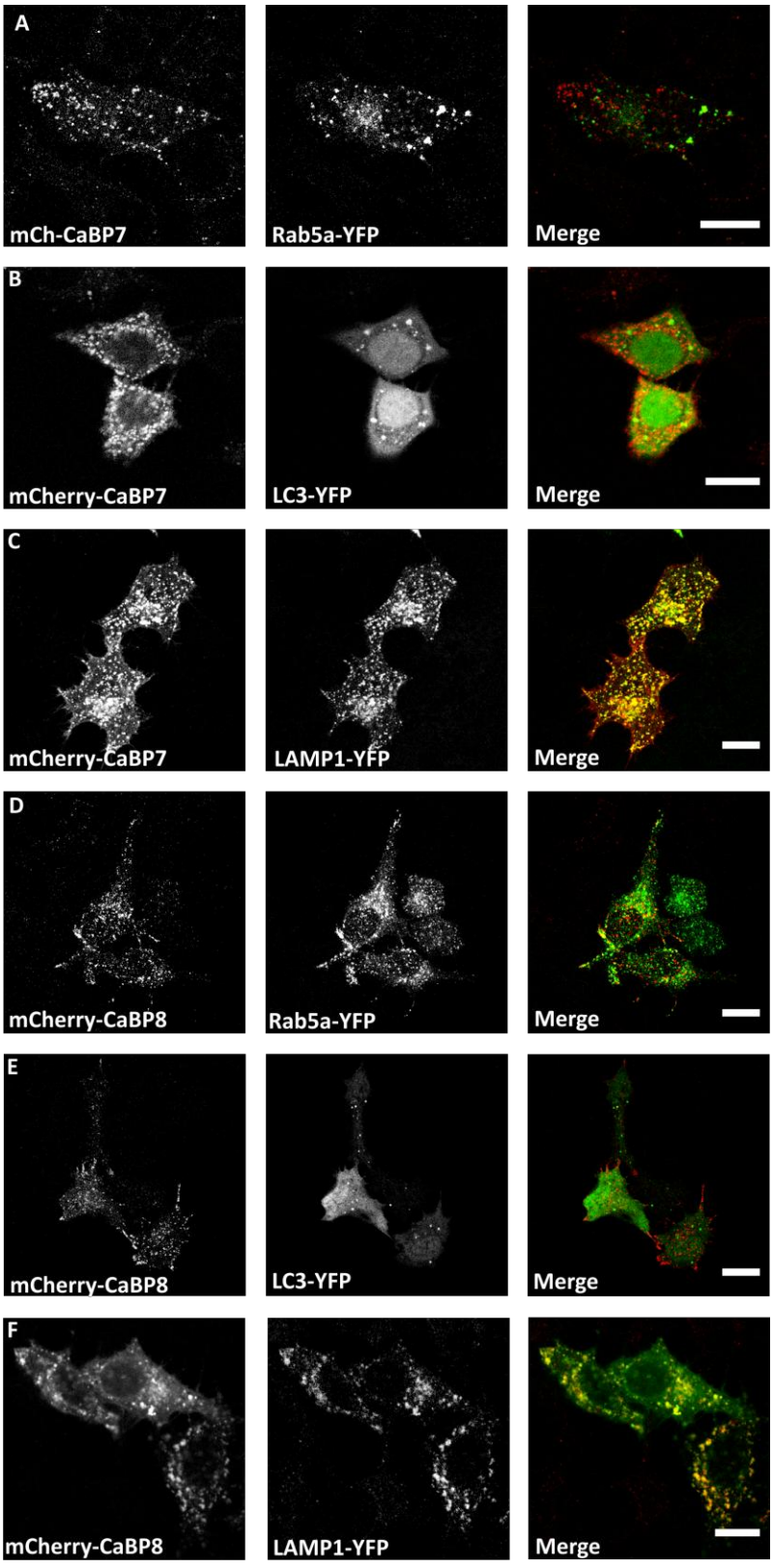

Figure 4.16. Analysis of localisation of mCherry-CaBP7 or mCherry-CaBP8 in HeLa cells co-expressing fluorescently tagged markers of various organelles. HeLa cells exogenously expressing mCherry-CaBP7 (A, B, C, red), or mCherry-CaBP8 (D, E, F, red) with EYFP fusions of either: the early endosomal marker, Rab5A (A and D; Rab5A-YFP, green), the autophagosome marker, LC3β (B and E; LC3-YFP, green), or the lysosomal marker, LAMP1 (C and F; LAMP1-YFP, green). Regions of co-localisation appear yellow in merged images. Scale bars = 10 µm.

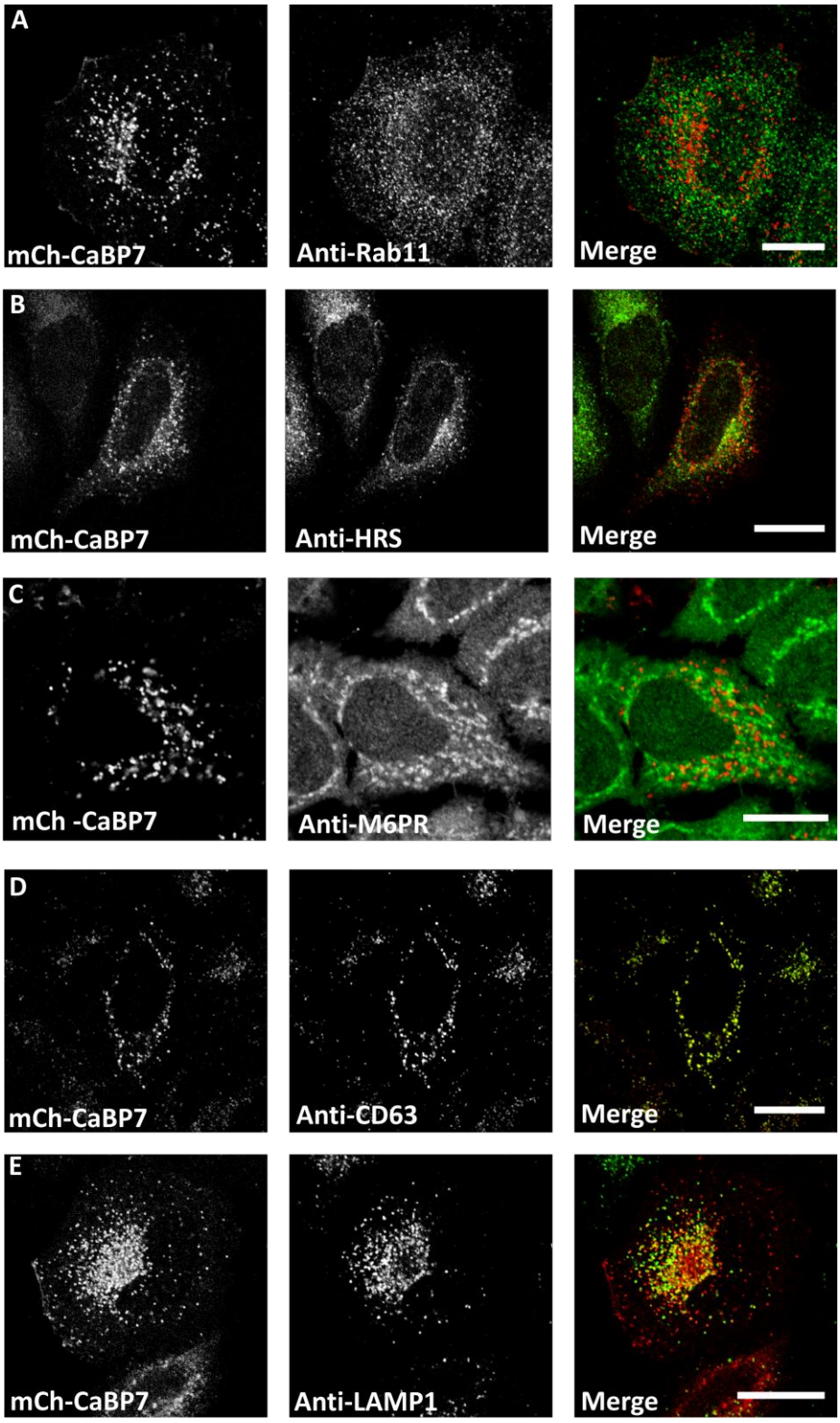

Figure 4.17. Analysis of localisation of mCherry-CaBP7 compared with markers of various intracellular compartments. The figure shows HeLa cells exogenously expressing mCherry-CaBP7 (mCh-CaBP7) immunostained for A) the recycling endosome marker, Rab11 (Anti-Rab11, FITC, green), B) the endosome and MVB marker, HRS (anti-HRS, FITC, green), C) the endosome marker, M6PR (anti-M6PR, FITC, green), D) the late endosome and lysosome marker, CD63 (Anti-CD63, FITC, green), E) the late endosome and lysosome marker, LAMP1 (Anti-LAMP1, FITC, green). Regions of co-localisation appear yellow in merged images. Scale bars = 10 µm.

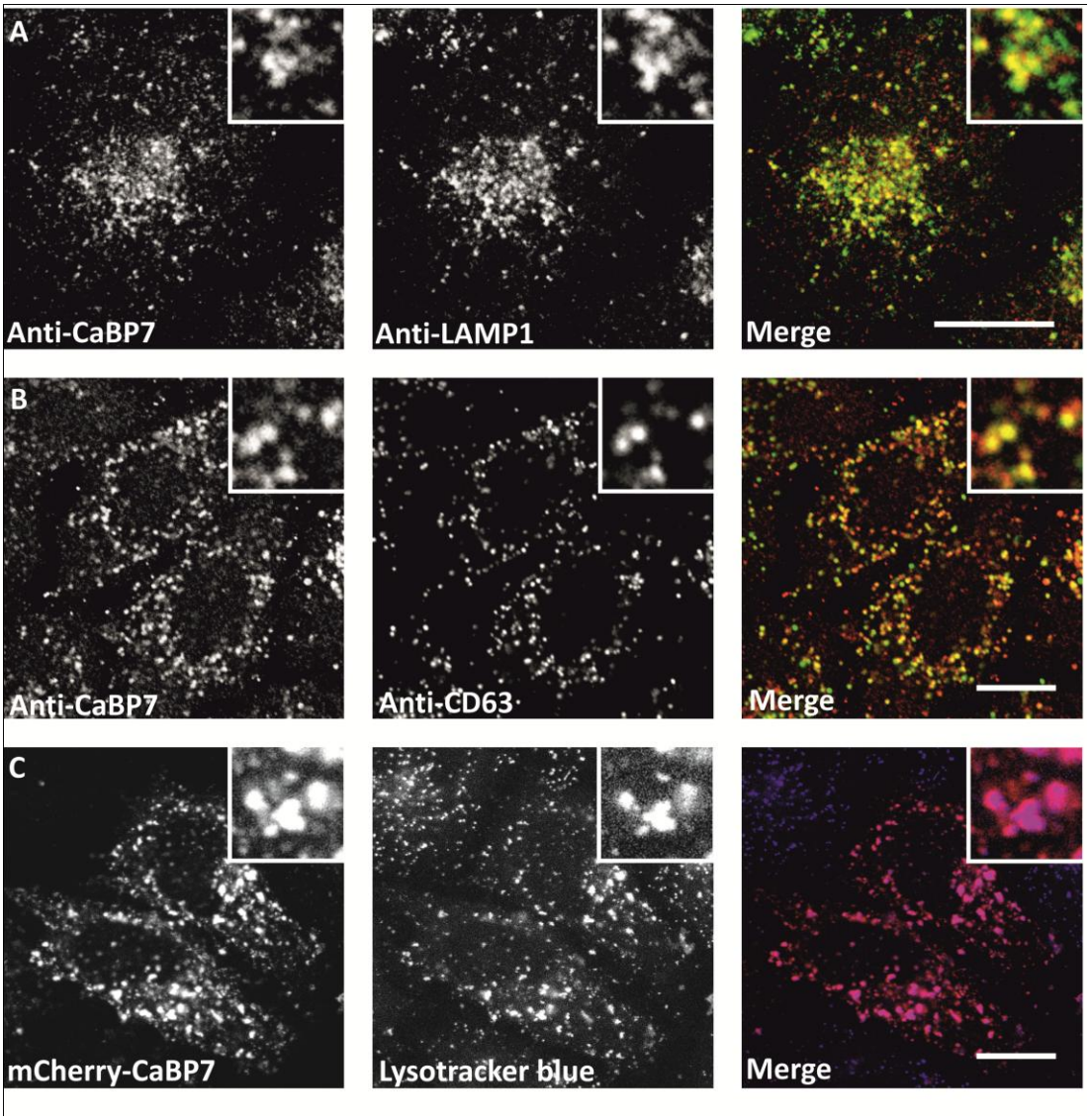

Figure 4.18. Co-localisation of endogenous CaBP7 or exogenous, mCherry-CaBP7 with various lysosmal markers. A) HeLa cells co-immunostained with antibodies to CaBP7 (anti-CaBP7, Alexa 568, red) and the lysosomal marker LAMP1 (anti-LAMP1, FITC, green). B) HeLa cells co-immunostained with antibodies to CaBP7 (Anti-CaBP7, Alexa 568, red) and the lysosomal marker CD63 (Anti-CD63, FITC, green). C) HeLa cells exogenously expressing mCherry-CaBP7 (red) after a 30 minute incubation with Lysotracker™ Blue to stain acidic compartments. Zoomed regions of interest are shown in the top right corner of each image. Regions of co-localisation appear yellow in merged images for A and B and pink in the merged image for C. Scale bars = 10 µm.

VAMP7 is a tail anchored v-SNARE protein which is resident on late endosomal and lysosomal membranes (Martinez-Arca *et al*., 2003). The localisation of CaBP7 was therefore compared with that of both endogenous and exogenously expressed VAMP7 as a representative TA protein with a similar localisation (Figure 4.19). Extensive overlap was observed in the localisation of overexpressed CaBP7 and

VAMP7 in HeLa cells (Figure 4.19A) and the same was observed when cells were immunostained for the endogenous proteins (Figure 4.19B).

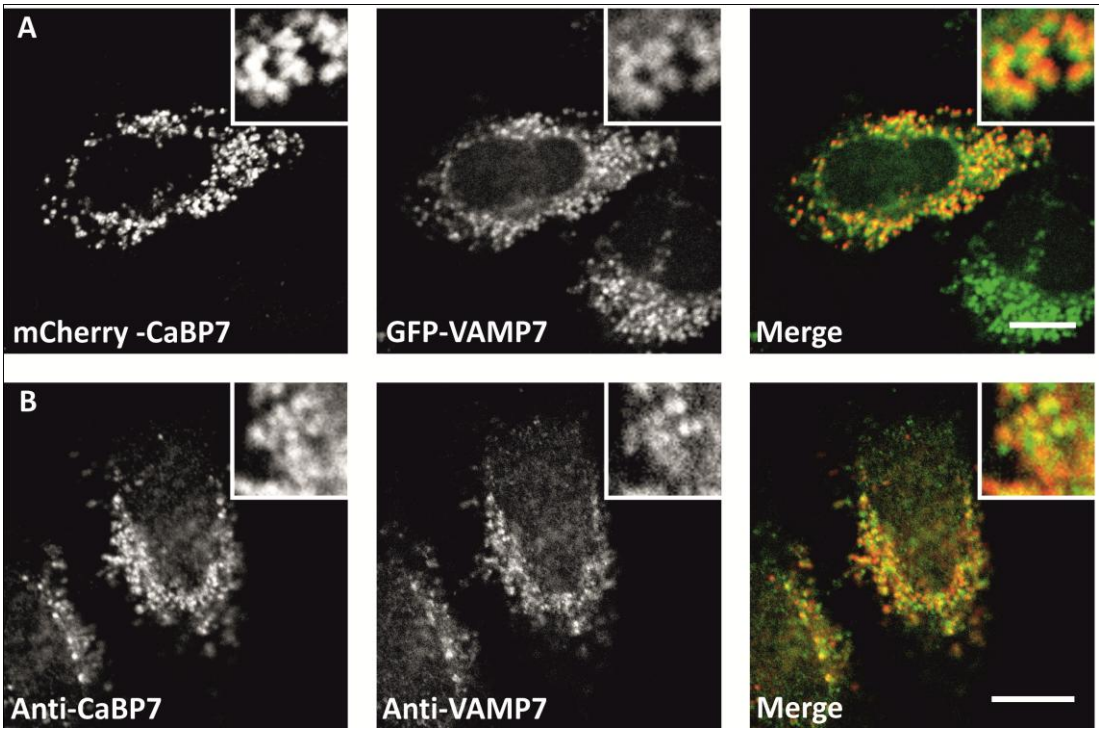

Figure 4.19. Co-localisation of exogenous and endogenous CaBP7 with the late endosomal and lysosomal TA protein, VAMP7. A) HeLa cells exogenously co-expressing mCherry-CaBP7 (Red) and GFP-VAMP7 (Green). B) HeLa cells immunostained for endogenous CaBP7 (Alexa 568, red) and VAMP7 (FITC, green). Zoomed regions of interest are shown in the top right corner of each image. Regions of co-localisation appear yellow in merged images. Scale bars = 10 µm.

It was previously shown (Figure 4.2), that CaBP7 and CaBP8 co-localise with ts045 VSVG-GFP at the TGN and in vesicles in N2A cells. Co-localisation of CaBP7 with this marker in vesicles was also examined in HeLa cells. Cells transfected with the temperature sensitive VSVG mutant, ts045 VSVG-GFP, were incubated at a permissive temperature (37°C) for VSVG trafficking from the TGN. Complete overlap was observed in the localisation of ts045 VSVG-GFP with endogenous CaBP7 (Figure 4.20A). VSVG is believed to be a marker of the constitutive secretory pathway, however, this is at odds with the apparent localisation of CaBP7 to late endosomal and lysosomal compartments. To further investigate this, HeLa cells overexpressing ts045 VSVG-GFP were immunostained with the late endosome and lysosome

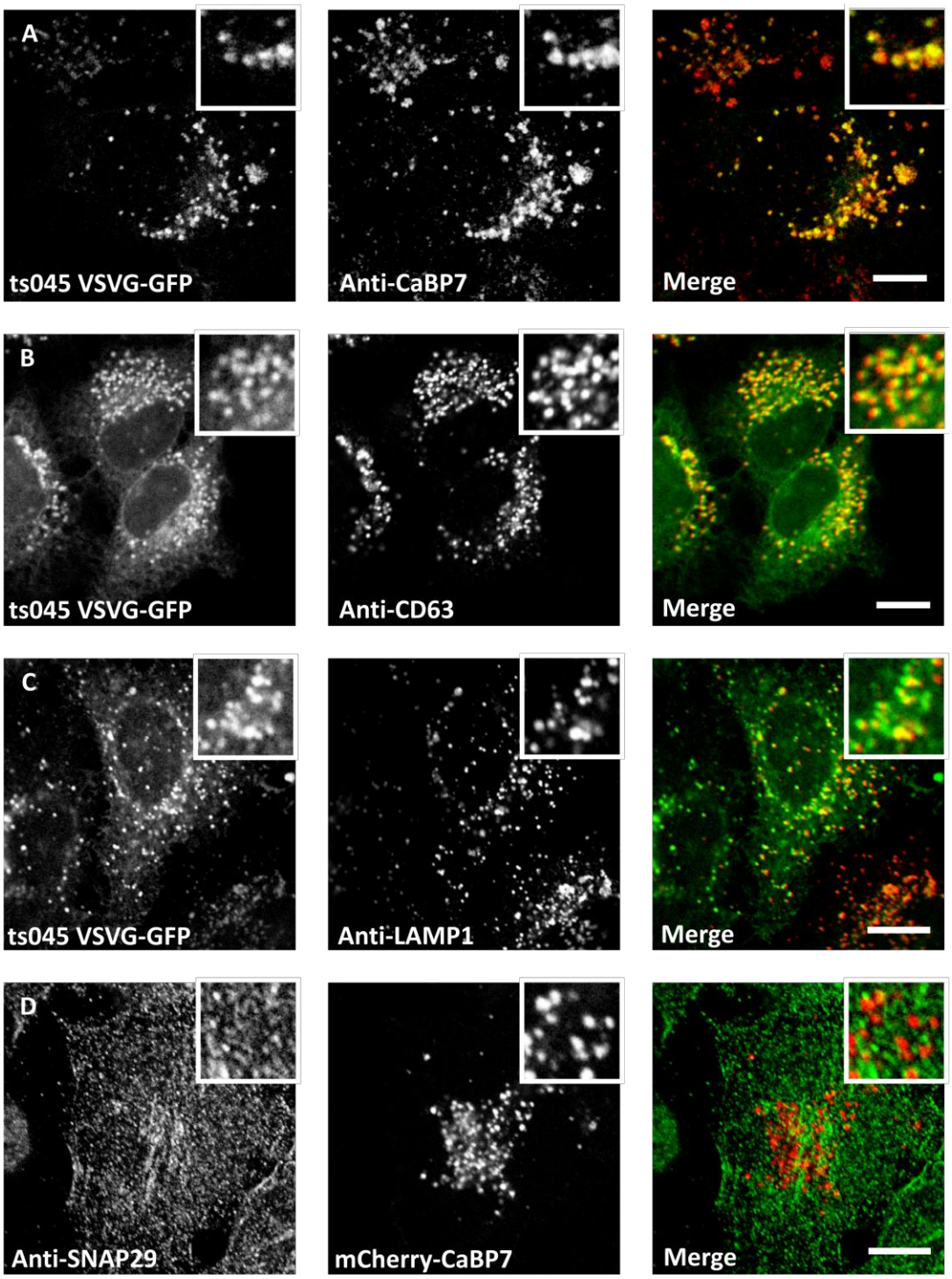

Figure 4.20. Co-localisation of CaBP7 with VSVG but not with a potential marker of constitutive secretory vesicles. A) HeLa cells exogenously expressing ts045 VSVG-GFP (Green) immunostained for endogenous CaBP7 (Anti-CaBP7, Alexa 568, red). B) HeLa cells exogenously expressing ts045 VSVG-GFP (Green) immunostained for the late endosome and lysosome marker, CD63 (Anti-CD63, Alexa 594, red). C) HeLa cells exogenously expressing ts045 VSVG-GFP (Green) immunostained for the late endosome and lysosome marker, LAMP1 (Anti-LAMP1, Alexa 594, red). D) HeLa cells exogenously expressing mCherry-CaBP7 (Red) immunostained with the constitutive secretory vesicle marker, SNAP29 (Anti-SNAP29, FITC, green). Zoomed regions of interest are shown in the top right corner of each image. Regions of co-localisation appear yellow in merged images. Scale bars = 10 µm.

markers, CD63 and LAMP1 (Figure 4.20B and C). Interestingly, extensive co-localisation was also observed with these markers suggesting that VSVG does not localise exclusively to the TGN and constitutive secretory vesicles (CSVs). In an extension of these investigations, cells overexpressing mCherry-CaBP7 were immunostained with a potential endogenous marker of CSVs, SNAP29 (Figure 4.20D). SNAP29 is a post-Golgi SNARE protein which has been shown to be required for constitutive secretion (Gordon *et al*., 2010). SNAP29 has been shown previously to localise to the TGN, PM and cytosol (Wong *et al*., 1999, Su *et al*., 2001, Feldmann *et al*., 2009), however there are no reports of endogenous SNAP29 immunostaining in HeLa cells. Figure 4.20D illustrates immunostaining of SNAP29 in HeLa cells which is consistent with a localisation to the PM and PM ruffles. SNAP29 was also observed in small punctate structures distributed throughout the cytosol which may represent a pool of CSVs. No co-localisation of SNAP29 with overexpressed mCherry-CaBP7 was observed suggesting that CaBP7 does not localise to the same population of vesicles as SNAP29.

4.2.12. Dependency of CaBP7 and CaBP8 localisation upon Ca^{2+}-binding

The dependence of CaBP7 and CaBP8 localisation on functional Ca^{2+}-binding activity was assessed using mCherry-tagged mutants which were defective in Ca^{2+}-binding at either EF1, EF2 or both functional EF-hand motifs. These mutants were created by site directed mutagenesis of the wild-type constructs to mutate the glutamate at the 12^{th} position in each of the Ca^{2+}-binding loops to a glutamine residue. This type of mutation has been proven to abolish Ca^{2+}-binding in a number of EF-hand containing Ca^{2+}-binding proteins (Faurobert *et al*., 1996, Hasdemir *et al*., 2005, Weiss *et al*., 2000). Each of the EF-hand mutants was co-transfected into HeLa cells with the corresponding wild-type protein tagged with EYFP. Figure 4.21 illustrates that each of the mutant proteins displays complete overlap in localisation to the same vesicular structures as the corresponding wild-type protein This indicates that targeting to these vesicles is unlikely to be Ca^{2+} dependent.

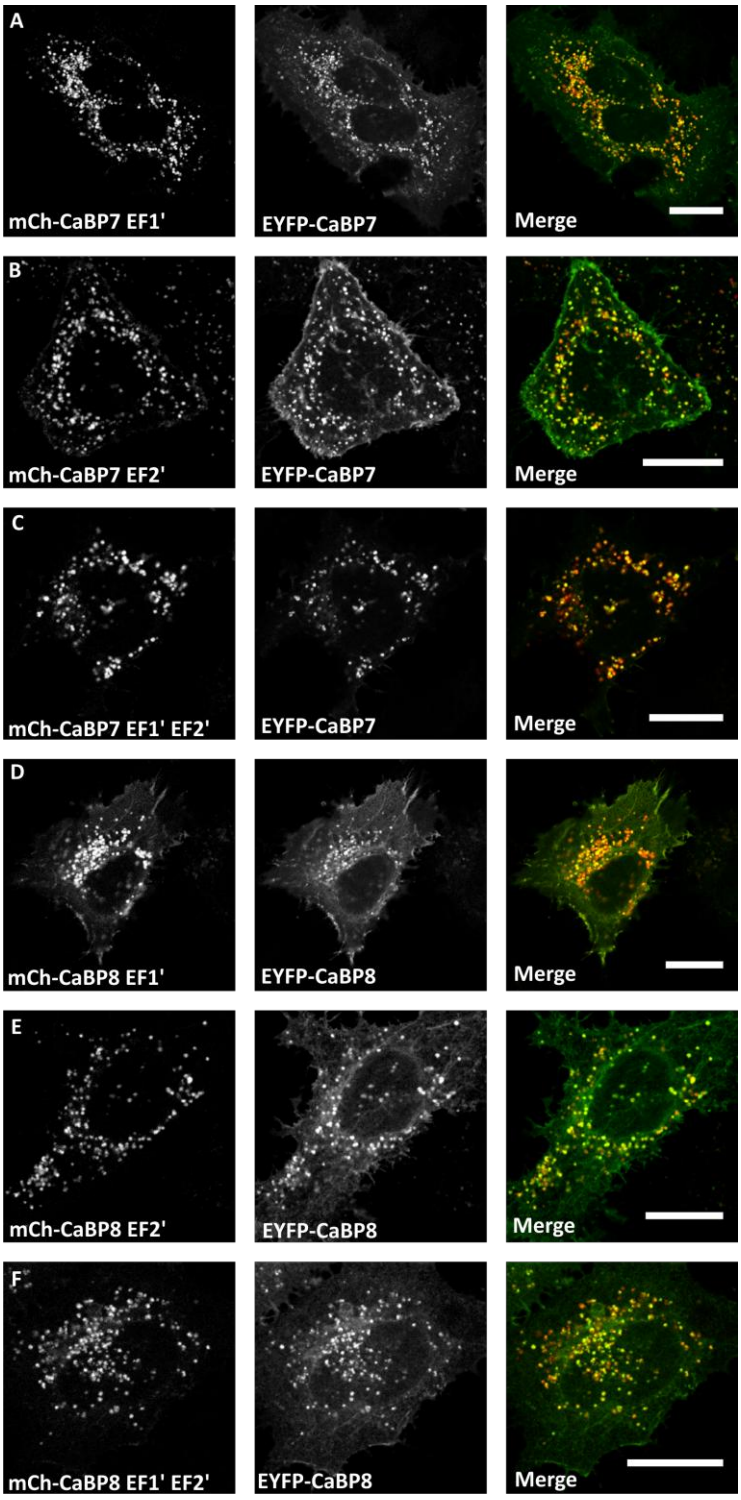

Figure 4.21. Localisation of exogenously expressed Ca^{2+}-binding deficient mutants of CaBP7 and CaBP8 compared with the wild-type proteins. A-C) HeLa cells exogenously co-expressing wild-type EYFP-CaBP7 (green) with either A) a CaBP7 mutant which cannot bind Ca^{2+} at EF1 (mCh-CaBP7 EF1', red), B) a CaBP7 mutant which cannot bind Ca^{2+} at EF2 (mCh-CaBP7 EF2', red) or D) a CaBP7 mutant which cannot bind Ca^{2+} at either EF1 or EF2 (mCh-CaBP7 EF1' EF2', red). D-F) HeLa cells exogenously co-expressing wild-type EYFP-CaBP8 (green) with either D) a CaBP8 mutant which cannot bind Ca^{2+} at EF1 (mCh-CaBP8 EF1', red), E) a CaBP8 mutant which cannot bind Ca^{2+} at EF2 (mCh-CaBP8 EF2', red) or F) a CaBP8 mutant which cannot bind Ca^{2+} at either EF1 or EF2 (mCh-CaBP8 EF1' EF2', red). Regions of co-localisation appear yellow in merged images. Scale bars = 10 µm.

4.2.13. Localisation of potential lysosomal targeting mutants of CaBP7 and CaBP8

The primary sequences of CaBP7 and CaBP8 were searched for motifs which could be responsible for targeting to lysosomal membranes. Sorting information for known lysosomal membrane proteins is encoded in their short cytoplasmic tails. LIMP2 utilises a dileucine motif, whereas LAMP1, LAMP2, CD63, LIMP1 and LAP all utilise tyrosine motifs of the form Y-X-X-Φ, where X is any amino acid and Φ is a hydrophobic residue (Obermuller *et al*., 2002). CaBP7 and CaBP8 each possess a number of potential dileucine and tyrosine motifs which may each contribute towards effective lysosomal targeting. Only one tyrosine motif appears at the same position in both CaBP7 and CaBP8 when compared in multiple sequence alignments although the exact sequence of the motif is not identical. In CaBP7, the sequence LLYDTF is located 47 amino acids from the start of the TMD and consists of both dileucine and tyrosine sorting motifs. In CaBP8 the corresponding sequence, ILYHAF, resides 48 amino acids from the start of the TMD. The effect of mutating the potential lysosomal targeting motifs was examined by changing LLY to AAA in CaBP7 and LY to AA in CaBP8. Protein localisation was unaffected by these mutations as illustrated by extensive overlap of each mutant with the corresponding wild-type protein (Figure 4.22A and B). In addition, the tyrosine sorting mutants colocalised with antibody staining for the late endosome/lysosomal markers CD63 and LAMP1 (Figure 4.22C and D). These data indicated that mutation of potential tyrosine motifs in CaBP7 and CaBP8 had no significant effect upon their localisation to lysosomes. As previously described in section 4.2.10, the TMD alone was sufficient to target normally cytosolic proteins to the same subcellular compartments as labeled by the wild-type protein. It therefore follows that any targeting motifs preceding the TMD are unlikely to have a substantial effect upon targeting of these proteins to lysosomal membranes. Tyrosine motifs along with the dileucine motifs present in these proteins may however confer more subtle effects in modulating the targeting efficiency of these proteins. The trafficking dynamics of the tyrosine mutants compared to the wild-type proteins was not examined in detail here.

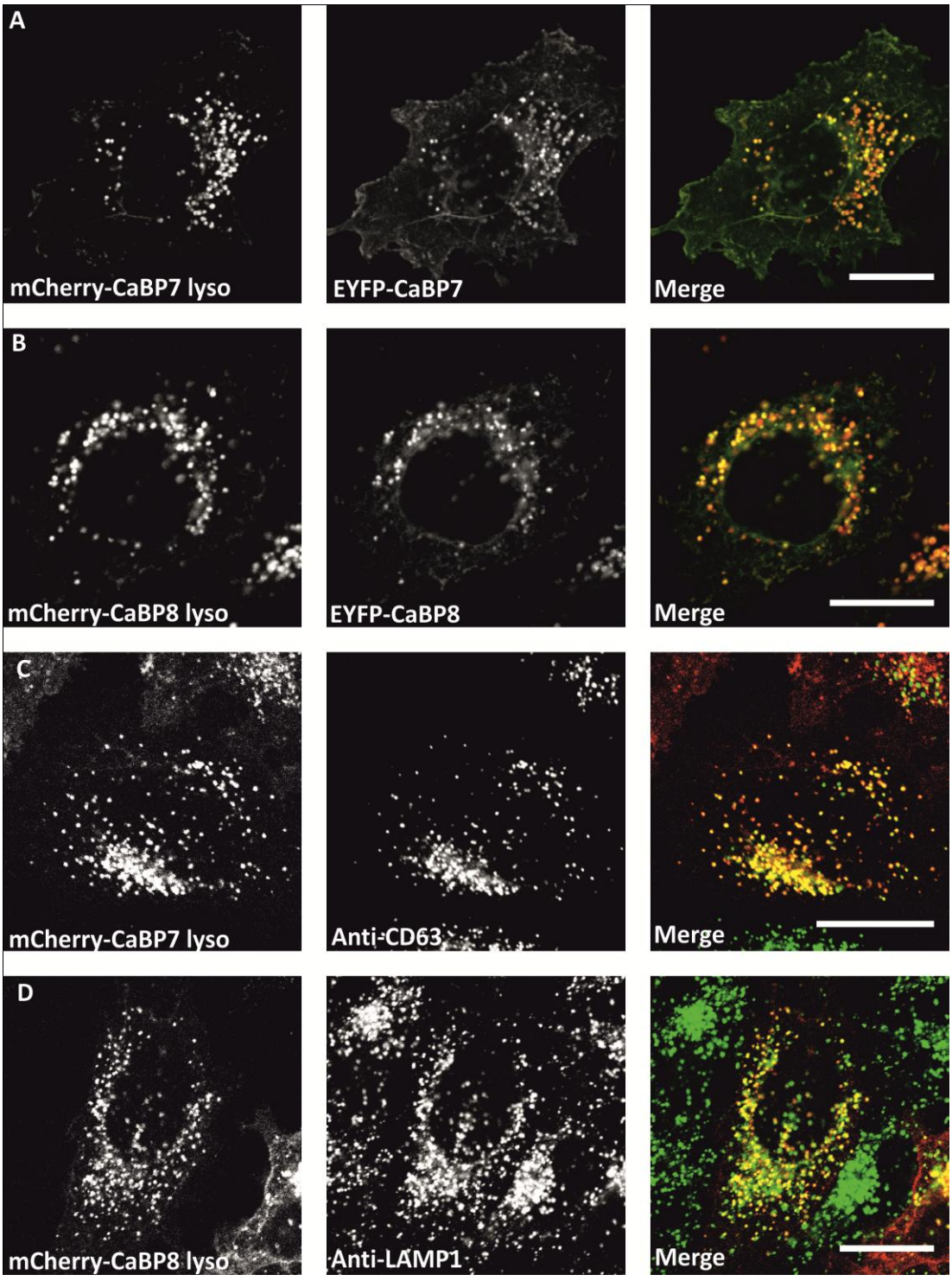

Figure 4.22. Localisation of exogenously expressed tyrosine motif mutants of CaBP7 and CaBP8 compared with the wild-type proteins and lysosome specifc markers. A) HeLa cells co-expressing a CaBP7 tyrosine mutant tagged with mCherry (mCherry-CaBP7 lyso, red) and wild-type CaBP7 protein tagged with YFP (EYFP-CaBP7, green). B) HeLa cells co-expressing a CaBP8 tyrosine mutant tagged with mCherry (mCherry-CaBP8 lyso, red) and wild-type CaBP8 protein tagged with YFP (EYFP-CaBP8, green). C) HeLa cells expressing mCherry-CaBP7 lyso and immunostained with the late endosome and lysosome specific marker, CD63 (Anti-CD63, FITC, green). D) HeLa cells expressing mCherry-CaBP8 lyso and immunostained with the late endosome and lysosome specific marker, LAMP1 (Anti-LAMP1, FITC, green). Regions of co-localisation appear yellow in merged images. Scale bars = 10 µm.

4.3. Discussion

The findings in this chapter highlight the importance of the single transmembrane segment found in the extreme C-termini of CaBP7 and CaBP8 for normal protein localisation in both neuronal and non-neuronal cell types. In differentiated N2A cells, CaBP7 and CaBP8 localised to membranes of the TGN as evidenced by co-localisation with TGN specific markers. The existence of a 17 amino acid TMD was initially identified through examination of the primary amino acid sequence of the proteins using the online TMD prediction server, TMPred. The location of the putative TMDs 10 amino acids from the C-termini of the proteins suggested that CaBP7 and CaBP8 might belong to a specific sub-class of integral membrane protein, the TA proteins. The relevance of the predicted TMDs for correct protein targeting was assessed by the design of specific TMD mutants. CaBP7 and CaBP8 lacking their TMDs were completely cytosolic and unable to associate with cellular membranes. As the removal of the C-terminus could have potentially affected protein-folding leading to mislocalisation, the properties of these domains were investigated further. Substitution of the central three amino acids within the TMD to lysine residues was predicted, using the TMPred algorithm, to completely abolish TMD function. Proteins containing this mutation targeted less efficiently than their wild-type counterparts when expressed in N2A cells. The lysine mutants exhibited an increase in cytosolic localisation coupled to diminished membrane association which was more severe for CaBP7^{TMDKKK} than for CaBP8^{TMDKKK}. These data verified that the putative TMDs were necessary for the normal subcellular localisation of CaBP7 and CaBP8. It is possible that amino acid sequences flanking the TMD are responsible for mediating the residual membrane association observed for CaBP8. As such, the minimal domain requirement for PM trafficking of the TA protein, syntaxin 1A, includes the TMD and a number of positively charged residues preceding the TMD. Truncation mutants encoding the TMD and lacking the flanking charged residues distributed in a pattern resembling the ER (Hong, 2005).

To evaluate whether the TMDs alone were sufficient to correctly target the proteins to subcellular membranes, chimeras of normally cytosolic proteins fused to the TMD containing C-termini of CaBP7 and CaBP8 were generated. CaBP5 chimeras

were able to localise to subcellular compartments with a distribution strongly resembling that of wild-type CaBP7 and CaBP8. Direct fusion of the TMD of CaBP7 to mCherry also efficiently targeted the fluorescent protein to subcellular membranes. Cumulatively, these data illustrated that the hydrophobic C-termini of CaBP7 and CaBP8 are necessary and sufficient for correct membrane targeting of these proteins and that both proteins appear to possess a functional TMD at a location in the peptide which is consistent with TA protein architecture.

To rigorously demonstrate that CaBP7 and CaBP8 possess a membrane-spanning domain and classify them as true TA proteins, a series of experiments were performed to assess their membrane topology. Trypsin protection assays in HeLa cells transfected with CaBP7 or CaBP8 tagged N- or C-terminally with fluorescent protein variants demonstrated that only C-terminal tags were afforded protection from proteolysis. This observation implied that the N-termini of the proteins reside within the cytosol and were freely accessible to trypsin digestion whereas the C-termini were shielded from proteolysis within the lumen of the TGN. These data confirm that the TMDs of CaBP7 and CaBP8 fully insert across the lipid bilayer and that the proteins adopt the standard TA topology with a relatively long cytosolic N-terminus and short luminal C-terminus.

Addition of a 26 kDa GFP-based fluorescent tag to the C-terminus of TA proteins has the potential to cause aberrant processing and membrane insertion of the protein. Positioning of the TMD less than 30 amino acids from the carboxyl terminus in TA proteins dictates that these proteins are inserted into membranes post-translationally. Extending the C-terminus of TA proteins so that the TMD is no longer in such close proximity to the extreme C-terminus may result in the protein being inserted co-translationally as a type II membrane protein. To ensure that the results of trypsin protection assays were not an artefact of extending the C-termini of the proteins, variants of CaBP7 and CaBP8 with a N-terminal mCherry tag and a C-terminal myc tag were generated. Addition of the myc tag extended the C-termini of CaBP7 and CaBP8 to only 20 amino acids so should not affect the post-translational membrane insertion of either protein. The accessibility of the mCherry

tag and the myc epitope in cells transfected with these variants was assessed under different membrane permeabilisation conditions. As expected, in controls where total cellular membranes were non-specifically permeabilised using Triton X-100, both tags were accessible to their respective antibodies. However, when the PM was selectively permeabilised with digitonin, only the N-terminal mCherry tag was accessible and no anti-myc immunostaining was detectable. Hence, in accordance with trypsin protection data, CaBP7 and CaBP8 have a cytosolically accessible N-terminal domain, a single transmembrane-spanning segment and a luminal C-terminal tail, and can be classified as true TA proteins. CaBP7 and CaBP8 might therefore be inserted into membranes post-translationally via a dedicated TA specific mechanism (Borgese *et al*., 2003).

Tethering of CaBP7 and CaBP8 to membranes through a C-terminal tail anchor represents a novel example of how CaM-related Ca^{2+}-sensing proteins have evolved distinct targeting strategies to permit their sorting into specific target organelles. The Ca^{2+}-sensing protein subfamily comprising CaBP7 and CaBP8 appears to have arisen with the divergence of vertebrate species (McCue *et al*., 2010a) and, interestingly, examination of the number of TA proteins in yeast and humans indicates an expansion of this type of protein during the evolution of higher organisms: 55 TA proteins can be identified in yeast (Beilharz *et al*., 2003), but over 300 are present in humans (Kalbfleisch *et al*., 2007). TA proteins represent 2.02% of all coding open reading frames in the human genome (Borgese and Righi, 2010) and have been implicated in many important aspects of cell physiology including mitochondrial function, apoptosis and vesicular trafficking (Stefer *et al*., 2011).

Insertion of most transmembrane proteins into biological membranes requires the activity of protein-conducting channels which facilitate the translocation of the exoplasmic domain and integration of the hydrophobic transmembrane segment into the lipid bilayer (Hong, 2005). Translocon proteins themselves must also become integrated into the ER membrane and so the question arises concerning how this machinery can be initially inserted in the absence of any assistance (Brambillasca *et al*., 2006). Interestingly, sec61β and sec61p, are key components of

the translocon machinery and are also TA proteins (Favaloro *et al*., 2010, Falcone *et al*., 2011). TA proteins are conserved throughout evolution and may represent one of the most primitive mechanisms for membrane association. Therefore this class of protein may have arisen before the evolution of translocon channels. As such, a number of prokaryotic TA proteins and at least one eukaryotic TA protein, cytochrome b5, can insert unassisted into protein-free lipid bilayers (van Dalen and de Kruijff, 2004, Brambillasca *et al*., 2005). Various studies have examined the requirement of co-factors during post-translational membrane insertion of TA proteins and at least three distinct pathways have been described (Rabu *et al*., 2009, Borgese and Fasana, 2011). The membrane insertion pathway for a particular TA protein appears to be dictated by the degree of hydrophobicity within the transmembrane helix (Kalbfleisch *et al*., 2007). Based on the hydrophobicity scores of the TMDs of CaBP7 and CaBP8 (50.7 and 48.1 (Kyte and Doolittle, 1982), respectively) it can be speculated that they might utilise either the Asna-1 (Stefanovic and Hegde, 2007) or signal recognition particle (SRP) (Abell *et al*., 2004) mediated pathway for membrane insertion. As such, a recent study has reported a direct interaction of CaBP8 and Asna-1 (Hradsky *et al*., 2011). This interaction was confirmed through heterologous co-immunoprecipitation experiments, co-purification of co-expressed recombinant proteins, proximity ligation assays and bioluminescence resonance energy transfer (BRET). Weak immunoprecipitation of Sec61β, a subunit of the Sec61 protein translocation channel which is associated with the SRP complex, was also observed (Hradsky *et al*., 2011). Whether these proteins are required for membrane insertion of CaBP7 or CaBP8 has not yet been investigated.

The CaBP7 and CaBP8 membrane topology determined in this study is consistent with a reported interaction with the cytosolic enzyme PI4K, an important regulator of TGN to PM trafficking (Mikhaylova *et al*., 2009). NCS-1 is also an important effector in this pathway but associates with the TGN membrane via an *N*-myristoyl group. CaBP7 and CaBP8 inhibit the activity of PI4K at resting $[Ca^{2+}]_i$ causing a decrease in $PI(4,5)P_2$ production and a concomitant decrease in TGN to PM trafficking. Upon $[Ca^{2+}]_i$ elevation, NCS-1 competes with CaBP7 or CaBP8 for binding

to PI4K and activates the enzyme thereby increasing TGN to PM trafficking (Mikhaylova *et al*., 2009). Both NCS-1, and CaBP7/CaBP8 are therefore able to localise to the same subcellular compartment and regulate the same effector despite being targeted through unique membrane association mechanisms. This raises the question of why distinct membrane association mechanisms, which ultimately target related Ca^{2+}-binding proteins to the same organelle, have evolved. One hypothesis is that the diversification in membrane targeting permits different Ca^{2+}-sensors to associate with different membrane microdomains. In addition, although related Ca^{2+}-sensors may co-localise when at the TGN, their post-Golgi trafficking routes are often unique suggesting that they may associate with distinct classes of transport vesicle and/or sorting machineries. Differences in membrane targeting mechanisms could therefore influence the wider cellular distribution of particular Ca^{2+}-sensors to different subcellular platforms thereby specifying the target-proteins available for interaction.

No other CaM-related small EF hand containing Ca^{2+}-binding proteins have been reported to localise via a tail anchor suggesting this may be a feature unique to CaBP7 and CaBP8. Other unrelated EF-hand containing proteins, however, have been reported which target in this manner. The mitochondrial Rho GTPases, Miro-1 and Miro-2 each have two GTPase domains separated by a linker containing a pair of EF-hands and are localised to the outer mitochondrial membrane by a C-terminal tail anchor (Fransson *et al*., 2006). Members of the TA family of membrane proteins are specifically directed to either the ER or to the mitochondrial outer membrane for membrane insertion depending on the composition of their TMD. As such some TA proteins display a dual localisation and are able to target to both organelles (Borgese *et al*., 2001). No colocalisation was observed between mCherry-CaBP7 and antibodies for specific mitochondrial or ER markers. $mCherry^{CaBP7TMD}$, however, in addition to targeting in a similar distribution to wild-type CaBP7 in many cells, accumulated in a reticular pattern in other cells, where it co-localised with calnexin, an ER resident marker. Although this accumulation is likely to be an effect of overexpression, it hints that CaBP7 might first be inserted post-translationally into the ER membrane and subsequently trafficked through the Golgi to the TGN and

other vesicular structures. As such, other TA proteins are found in compartments of the secretory and endocytic pathways and include members of the SNARE family of proteins (Hong, 2005).

Data presented in this chapter has since been confirmed by the work of Hradsky *et al.* (Hradsky *et al*., 2011). This groupinvestigated the membrane topology of overexpressed CaBP8 at the PM by assessing the accessibility of an N- or C-terminally fused GFP tag to a GFP antibody in live, unpermeabilised cells. In accordance with the data presented in this chapter, CaBP8 possessed a cytosolic N-terminus and an extracellular C-terminus. PM localisation of CaBP7 and CaBP8 appears to be an artefact of overexpression, however, as when HeLa cells are immunostained for endogenous CaBP7, no signal is detected at the PM (Figure 4.6). Additionally, Hradsky *et al.* repeated the fluorescence protease protection assays, as presented in this chapter, and were able reproduce the same effect. Hradsky *et al.* also made a number of TMD mutants to deduce the minimal domain requirement for correct subcellular targeting of CaBP7 and CaBP8. mCherry fused to the 17 amino acid TMD predicted by TMPred was able to correctly localise a pool of CaBP7 and CaBP8 to the TGN but many cells exhibited a diffuse cytosolic localisation or ER localisation in COS-7 cells. Hradsky *et al.* suggested that a longer TMD segment might be required for correct localisation and found that fusion of a proposed 23 amino acid TMD (CaBP8 192-214) was able to improve Golgi recruitment of CaBP8 compared to the 17 amino acid fusion. In accordance with the data shown in this chapter, Hradsky *et al.* found that fusion of the full length C-terminal region of CaBP8 containing the TMD was able to efficiently localise GFP to the Golgi. The ER localisation of the 17 amino acid TMD GFP fusion is consistent with the ER localisation of the C-terminal domain mCherry fusion presented in this chapter. This is in agreement with initial CaBP7 and CaBP8 insertion into the ER and subsequent trafficking to Golgi and post-Golgi compartments. In accordance with this Hradsky *et al.* found that treatment of cells overexpressing CaBP8 with brefeldin A to disrupt ER to Golgi transport caused CaBP8 to accumulate in the ER. The work of Hradsky *et al.* is therefore consistent with the data presented in this thesis. There is, however, some discrepancy about the length of the TMD. Hradsky

et al. suggest that the length of the TMD is critical for the correct localisation of CaBP7 and CaBP8, however, the ER localisation of the 17 amino acid TMD fusion protein suggests it is sufficient for membrane insertion. An alternative viewpoint is that the short luminal tail of CaBP7 and CaBP8 may encode targeting information which is essential for their correct subcellular localisation. Further work will be required to distinguish between these possibilities.

Immunostaining with an anti-CaBP7 antibody confirmed observations from a recent high throughput siRNA screen (Neumann *et al*., 2010) that HeLa cells express CaBP7 endogenously. The localisation of CaBP7 and CaBP8 was therefore further examined in HeLa cells which are amenable to high-resolution subcellular localisation analyses. Co-localisation studies demostrated that both CaBP7 and CaBP8 localise to the same subcellular structures. In addition, the over-expressed and endogenous proteins also colocalised and the fluorescent tag variant used did not affect the localisation of either protein. As in N2A cells, CaBP7 and CaBP8 co-localised with a marker of the TGN, p230, in many cells, however in others little co-localisation at the TGN was observed with most of the protein localised to intracellular vesicles. Intracellular vesicles were also observed in N2A cells over-expressing CaBP7 or CaBP8, however the smaller cell bodies and more rounded morphology meant that these structures were less well distributed and appeared to accumulate near to the TGN.

The identity of CaBP7 and CaBP8 positive intracellular vesicles was investigated first by co-expression of CaBP7 and CaBP8 with colour tagged variants of three specific organelle markers. No co-localisation was observed with either the early endosome marker, Rab5a, or a marker of autophagosomes, LC3β. Extensive overlap was, however, observed in the distribution of CaBP7 and CaBP8 with the lysosomal marker LAMP1. To confirm this localisation, CaBP7 transfected cells were immunostained with antibodies for vesicle specific markers. No co-localisation with the endosome/MVB marker, HRS, the recycling endosome marker, Rab11, or the endosome marker, M6PR, was observed. Extensive co-localisation with the late endosome/lysosome markers, CD63 and LAMP1 was, however, observed.

Incubation of transfected cells with LysoTracker™ Blue demonstrated that there was complete co-localisation between CaBP7 and acidic compartments including lysosomes. HeLa cells immunostained for CaBP7 and either CD63 or LAMP1 confirmed that endogenous protein shares this localisation. Lysosomes are membrane-bound organelles containing hydrolytic enzymes which are most active at acidic pH and can be distinguished from endosomes due to the absence of M6PR (Luzio *et al*., 2001). Therefore the absence of co-localisation of exogenous CaBP7 with endogenous M6PR is consistent with a predominantly lysosomal localisation.

Lysosomes are generally regarded as the terminal degradation compartment of the endocytic pathway with important roles in phagocytosis, autophagy, crinophagy and the proteolysis of cytosolic proteins transported across the lysosomal membrane (Luzio *et al*., 2001). Advances in the understanding of how endocytosed material is delivered to lysosomes and the discovery of other important roles for lysosomes, for instance in secretion, have challenged the classical view of lysosomes simply as the waste disposal sites of the cell (Luzio *et al*., 2007). In mammalian cells, dynamic interactions between compartments of the late endocytic pathway results in heterogeneity between organelles constituting late endosomes and lysosomes. It has been suggested that late endosomes and lysosomes may fuse to form hybrid organelles allowing the degradation of components carried by the endosome before subsequent reformation of the lysosome (Luzio *et al*., 2000). Using markers of various compartments within the endo-lysosomal pathway, the data presented in this chapter demonstrate that CaBP7 does not localise to early endosomes (Rab5a), recycling endosomes (Rab11), MVBs (HRS), or M6PR positive late endosomes. Convincing co-localisation with LAMP1, CD63 and lysotracker™ blue and the absence of co-localisation with M6PR, suggests that the majority of CaBP7 resides specifically on lysosomes. In addition, extensive co-localisation of CaBP7 and the late-endosomal and lysosomal resident TA protein, VAMP7, was observed. VAMP7 (also known as TI-VAMP) is a v-SNARE which is involved in both exo- and endocytosis and in late-endosome-to-lysosome transport. Like, CaBP7, VAMP7 localisation to membranes requires its C-terminal tail anchor, however correct subcellular targeting of VAMP7, as with other VAMP

proteins (Zeng *et al*., 2003), relies on sequence information encoded in its cytosolic N-terminal domain – the longin domain (Martinez-Arca *et al*., 2003). The longin domain mediates VAMP7 localisation to late endosomes and lysosomes through an interaction with the adaptor protein, AP3 (Martinez-Arca *et al*., 2003), and correct localisation of other late endosomal and lysosmal markers including LAMP1 and CD63 are also dependent on AP3 (Nishimura *et al*., 2002, Dell'Angelica *et al*., 1999). It will be interesting to deduce whether CaBP7 traffics through a similar pathway in future work.

Extensive overlap of ts045 VSVG-GFP and CaBP7 was observed in both N2A and HeLa cells. Hradsky *et al.* also observed overlap in the localisation of CaBP8 with GFP-VSVG at the Golgi and in post-Golgi intermediates and suggest that CaBP8 trafficks to the PM via the same secretory pathway as VSVG (Hradsky *et al*., 2011). VSVG is commonly used as a marker of CSVs, however immunostaining of HeLa cells overexpressing ts045 VSVG-GFP with CD63 and LAMP1 demonstrated a late endosomsal and lysosomal distribution for this protein. In addition, no co-localisation was observed with SNAP29, a post-Golgi SNARE which has been shown to be important in constitutive secretion (Gordon *et al*., 2010). SNAP29 localised to the PM and PM ruffles which is consistent with previous observations (Wong *et al*., 1999, Su *et al*., 2001, Feldmann *et al*., 2009) and also localised to numerous small punctate structures which may be consistent with a pool of CSVs. The exact identity of these vesicles remains to be determined, however. Therefore these data demonstrate that both CaBP7 and VSVG reside on vesicles of the late endosomal and lysosomal pathway and that VSVG localisation is not specific to CSVs. Interestingly, export of both VSVG and LAMP1 from the TGN is mediated by AP3 and overexpression of VSVG was found to saturate the AP3 machinery and caused LAMP1 to traffic to lysosomes via an alternative pathway (Nishimura *et al*., 2002). Overexpression of VSVG can therefore cause undesirable trafficking artefacts when examining the subcellular localisation of proteins.

As some members of the NCS protein family have been shown to display Ca^{2+}-dependent membrane association via their *N*-myristoyl chains, the dependence of

CaBP7 and CaBP8 localisation upon Ca^{2+}-binding was assessed by creating a number of Ca^{2+}-binding defective mutants. Variants with mutations in one or both of the functional EF-hands of CaBP7 and CaBP8 were able to localise to the same subcellular compartments as wild-type protein illustrating that localisation to lysosomes is Ca^{2+}-independent. Similarly, treatment of HeLa cells overexpressing either CaBP7 or CaBP8 with the Ca^{2+} ionophore ionomycin, in the presence of extracellular Ca^{2+} to elevate $[Ca^{2+}]_i$, had no effect on the localisation of either protein (data not shown).

Lysosomal membrane proteins have been discovered to possess specific targeting motifs which are essential for their correct intracellular compartmentalization. These motifs are typically either tyrosine based of the form Y-X-X-Φ (where X is any amino acid and Φ is an amino acid with a hydrophobic side chain) or dileucine based in the form, L-X, where X can be L, I, M, V or F (Bonifacino and Traub, 2003). These motifs are recognized by the clathrin adaptor protein complexes AP-1, AP-2, AP-3 and AP-4, which bind to these sites on transmembrane proteins and direct their correct compartmentalization (Bonifacino and Traub, 2003). CaBP7 and CaBP8 possess motifs of both classes however only one appears at the same position in both proteins. As these proteins display 63% sequence identity (McCue *et al*., 2010a) and appear to traffic identically it was decided to study the effect of mutating this common motif only. No significant difference was observed in the localisation of the tyrosine motif mutants of CaBP7 and CaBP8 when compared in co-transfections with the wild-type proteins or when transfected cells were immunostained with the lysosomal markers, CD63 or LAMP1. As such, chimaeras of CaBP7 and CaBP8 TMDs fused to normally cytosolic proteins co-localised with endogenous CaBP7 indicating that motifs encoded in the N-terminus of the protein are not required for correct localisation. It is possible, however, that the numerous tyrosine and dileucine motifs found in the cytosolic domain of CaBP7 (two tyrosine and four dileucine motifs) and CaBP8 (one tyrosine and two dileucine motifs) may contribute more subtly to the localisation of these proteins. A detailed analysis of the trafficking dynamics of the tyrosine mutants would clarify this issue.

No lysosomal membrane proteins shown to require tyrosine or dileucine motifs for targeting are TA proteins. As CaBP7 and CaBP8 are TA proteins which are processed differently to other types of membrane protein, they may also require different motifs for lysosomal targeting. There do not appear to be strict rules governing how TA proteins are localised and examples exist showing the importance of numerous different domains depending on the individual protein. The length and hydrophobicity of the TMD has been shown to influence the targeting of TA proteins. Proteins with longer or more hydrophobic TMDs are more likely to be targeted to the cell surface and proteins with shorter or less hydrophobic TMDs are more likely to reside within the ER (Pedrazzini *et al*., 1996, Bulbarelli *et al*., 2002). The late endosome resident SNARE protein, VAMP7 has been shown to require its N-terminal domain for correct targeting to late endosomal vesicles (Martinez-Arca *et al*., 2003) whereas the luminal domain of cytochrome b5 has been shown to be essential for its retention within the ER (Honsho *et al*., 1998). A more detailed analysis of the domains required for CaBP7 and CaBP8 localisation is needed in order to understand how these proteins are able to specifically target to lysosomes.

As previously discussed a number of new roles for lysosomes have recently emerged. Of particular importance is the growing evidence that lysosomes can store Ca^{2+} at similar concentrations to that found in the lumen of the ER (Gerasimenko and Tepikin, 2005). Research to date indicates that NAADP stimulates Ca^{2+} release from highly localised and discrete areas of the cell through binding to a Ca^{2+}-releasing receptor on lysosomes (Galione *et al*., 2010). It has become apparent that NAADP-induced Ca^{2+} signals often act as a trigger for regenerative Ca^{2+} waves through stimulation of IP_3Rs or RyRs on the ER by a CICR mechanism (Brailoiu *et al*., 2010). Recent progress has identified the two pore channel (TPC) family of proteins as NAADP activated receptors which are resident in the membranes of acidic compartments (Zhu *et al*., 2010b). The TPCs are a family of Ca^{2+} release channels which are related to voltage dependent Ca^{2+} and Na^{+} channels. Three TPC genes, TPCN1-3, have been identified in vertebrate species but key findings indicate that TPC2 underpins NAADP-induced Ca^{2+} release from lysosomal stores (Ruas *et al*., 2010, Zhu *et al*., 2010a, Pitt *et al*., 2010). TPC1 and TPC3 are localised to endosomal

membranes, and have also been found to influence NAADP-dependent Ca^{2+} release from acidic stores (Ruas *et al*., 2010). Identification of CaBP7 and CaBP8 as late endosome and lysosome resident Ca^{2+}-sensing proteins further strengthens the view of these acidic organelles as important calcium signaling platforms.

CaBP7 and CaBP8 have been demonstrated to be important physiological regulators of vesicle trafficking through regulation of $PI(4,5)P_2$ production by PI4K (Mikhaylova *et al*., 2009). Another study (Shih *et al*., 2009) reported attenuation of N-type Ca^{2+}-channel activity upon overexpression of CaBP8 in bovine chromaffin cells. The same effect was not seen with a transmembrane deficient mutant suggesting correct localisation of the protein to membranes was essential for this function (Shih *et al*., 2009). The observed attenuation may have been due to a direct interaction between CaBP8 and the calcium channels, however, the possibility that CaBP8 overexpression may affect channel trafficking to the PM was not explored.

4.3.1. Conclusion

The data presented in this chapter provides evidence that CaBP7 and CaBP8 are unique Ca^{2+}-sensors which utilise a C-terminal tail anchor to localise to vesicles of the late endosomal and lysosomal pathway. This is the first observation of a CaM related EF-hand protein targeting to membranes via a tail anchor. The evolution of distinct mechanisms to target different types of Ca^{2+}-sensors allows them to localise to the specific subcellular domains required to mediate their dedicated physiological functions. To date, no other EF-hand containing Ca^{2+}-sensors that reside in the lysosomal membrane have been described which pinpoints CaBP7 and CaBP8 as potential regulators of essential Ca^{2+}-mediated processes within this compartment.

Chapter 5:

Examining the Role of CaBP7 in

Cytokinesis

5.1 Introduction

Proliferation and cell division are fundamental processes to the growth and maintenance of multicellular organisms, including mammals, and deregulation of the pathways involved can ultimately lead to cancer (Decordier *et al*., 2008). Although calcium signalling has been shown to regulate almost all cellular processes ranging from fertilisation to cell death, the role of Ca^{2+} at the various stages of the cell cycle has remained relatively unstudied. It has been shown that injection of cells with calcium chelators can block progression through the cell cycle (Tombes and Borisy, 1989) but the most convincing evidence for a role of Ca^{2+} in the cell cycle is the involvement of the ubiquitous Ca^{2+}-binding protein, CaM. CaM acts at multiple stages, stimulating the expression of genes and activating enzymes involved in DNA replication, nuclear envelope breakdown and cytokinesis (Takuwa *et al*., 1995). Furthermore, two of CaM's key interacting partners, Ca^{2+}/CaM-dependent kinase II and calcineurin are also implicated in cell growth regulation (Takuwa *et al*., 1995), demonstrating an important regulatory role for Ca^{2+} during mitosis. Despite this, measuring changes in $[Ca^{2+}]_i$ in the dividing cell has thus far proven problematic. The majority of studies detecting Ca^{2+} transients in the cell cycle have been carried out in sea urchin oocytes, however, transients marking the key phases of the cell cycle observed in these studies have not been replicated in other cell types (Hepler, 1994). It is speculated that Ca^{2+} signals may become highly spatially and temporally localised during division making them challenging targets for detection.

Calcium signalling has also been specifically implicated in the regulation of cytokinesis, although the mechanism of this control is only partially understood. Studies employing zebrafish embryos have detected transient Ca^{2+} signals at multiple stages of cytokinesis and Ca^{2+} elevation at the position of the cleavage furrow preceded furrow contraction (Webb *et al*., 2008). Ca^{2+} transients have also been observed in *Xenopus* oocytes, although these differ from those seen in zebrafish (Muto *et al*., 1996, Noguchi and Mabuchi, 2002). A role for Ca^{2+} signalling is further supported by the observation that treatment of cells with Ca^{2+} chelators such as BAPTA (Webb *et al*., 2008, Noguchi and Mabuchi, 2002) and EGTA (Baker and Warner, 1972) elicit cytokinesis failure and stimulation of Ca^{2+} release can induce the

formation of extra furrows (Mitsuyama *et al*., 1999, Schroeder and Strickland, 1974). A study using a permeabilised cell model for cytokinesis observed that incubation of the cell with both high or low concentrations of Ca^{2+} inhibited furrow ingression (Cande, 1980) suggesting that the precise levels of Ca^{2+} in the cell must be tightly regulated to ensure efficient completion of cytokinesis.

It is not clear what proteins are required for Ca^{2+} regulation during cytokinesis, however, CaM has been found to redistribute to interzonal microtubules and the intercellular bridge (Li *et al*., 1999). Loss of CaM or treatment with CaM inhibitors disrupts or prevents the completion of cytokinesis (Liu *et al*., 1992, Yu *et al*., 2005). MLCK (myosin light chain kinase), an effector of CaM, has also been implicated in the regulation of cytokinesis (Wong *et al*., 2007). Other Ca^{2+}-sensors that may play a role in cytokinesis include calpain II and Annexin XI. Calpain II redistributes to the midbody in telophase and injection of calpain II into metaphase cells caused premature disassembly of the mitotic spindle and onset of anaphase (Schollmeyer, 1988). Annexin XI is also recruited to the midbody during telophase in some cell types and appears to be necessary for formation of the midbody and completion of cytokinesis (Tomas *et al*., 2004).

A role for calcium signalling during cytokinesis is therefore very apparent but the precise mechanisms by which Ca^{2+} coordinates this process are not yet clear (Atilla-Gokcumen *et al*., 2010). In a recent high throughput RNAi screen in HeLa cells, designed to identify proteins with a mitotic phenotype, depletion of CaBP7 resulted in a binuclear phenotype (Neumann *et al*., 2010). CaBP7 was one of the few genes selected for more rigorous validation from the 572 genes identified in total. A binucleate phenotype was observed with 4 independent siRNA sequences, suggesting that this was not an off-target effect. Furthermore, complementation by stable expression of the RNAi-resistant mouse CaBP7 orthologue was able to prevent this phenotype. In detail examination of the CaBP7 knockdown phenotype using high resolution four-dimensional confocal microscopy showed that after normal chromosome segregation, CaBP7 knockdown cells failed to undergo cytokinesis resulting in cells with two nuclei and four centrosomes. Cells were able to undergo

subsequent rounds of division, however this resulted in the formation of multipolar spindles and aberrant chromosome segregation. This coupled to cytokinesis failure, gave rise to large polylobed nuclei. CaBP7 was therefore characterised as a *bona fide* regulator of cytokinesis and this could infer a novel role for the protein in calcium signalling during cell division.

The data presented by Neumann *et al.* more specifically suggested that CaBP7 knockdown cells were able to undergo furrow formation as normal but failed at the stage of abscission leading to eventual furrow regression and the generation of binucleate cells (Neumann *et al*., 2010). Abscission is generally the least well understood stage in cytokinesis (Atilla-Gokcumen *et al*., 2010). The severing process between the two daughter cells must be very carefully controlled in order to avoid the generation of a puncture in the PM. Various processes are involved in this final stage including vesicle trafficking, membrane remodelling and removal of the intercellular bridge. Vesicle transport is thought to play an important role generating a membrane barrier to seal the daughter cells before they sever (Atilla-Gokcumen *et al*., 2010). As such, membrane trafficking is known to play a vital role in plant cytokinesis. During division, plant cells form a structure called the phragmoplast which acts as a scaffold for vesicle delivery during cytokinesis. Vesicles fuse at the midpoint between the two daughter cells forming a cell plate which grows along the cell division plane until the two cells become completely separated (Van Damme *et al*., 2008).

The dependency of vesicle transport upon calcium signalling in other systems is well documented and, likewise, altering Ca^{2+} levels during cytokinesis has been shown to affect membrane remodelling and vesicle fusion (Li *et al*., 2008, Shuster and Burgess, 2002). Research examining membrane traffic during cytokinesis has focused on the involvement of recycling endosomes and secretory vesicles (McKay and Burgess, 2011, Neto *et al*., 2011). The involvement of lysosomes in mitosis has received very little attention to date, however, a redistribution of these organelles to the intercellular bridge has been reported (Bergeland *et al*., 2001).

Importantly, lysosomes have recently been demonstrated to act as Ca^{2+} release platforms which are stimulated by the second messenger NAADP (Galione *et al*., 2010). NAADP is the most potent Ca^{2+} releasing second messenger thus far characterised and NAADP-induced Ca^{2+} signals often act as a trigger for regenerative Ca^{2+} waves propagated by activation of IP_3Rs or RyRs on the ER through CICR (Brailoiu *et al*., 2010). The TPCs have recently been identified as NAADP-activated Ca^{2+} channels which are resident in the membranes of acidic compartments (Zhu *et al*., 2010a). Interestingly, in the same RNAi screen that identified CaBP7 as a regulator of cytokinesis, knockdown of TPC1 and TPC2 also resulted in mitotic defects. Cell death and binuclear phenotypes were observed in knockdowns of TPC1, whereas in the case of TPC2, metaphase delay, metaphase alignment defects and cell death were observed (www.mitocheck.org) (Neumann *et al*., 2010). This potentially indicates a more general requirement for endolysosomal calcium signalling machinery during key mitotic processes.

The aim of this chapter was to investigate the role of CaBP7 in mitosis and whether this could be linked to a novel role for calcium signalling from lysosomes during cytokinesis.

5.2. Results

5.2.1. Localisation of CaBP7 during mitosis

Figure 5.1 shows confocal images of HeLa cells at different stages in mitosis, immunostained with antibodies against CaBP7 and α-tubulin. In interphase, (Figure 5.1 A) CaBP7-positive vesicles distributed throughout the cytosol and, as discussed in chapter 4, often concentrated in a perinuclear region resembling the TGN. At metaphase (Figure 5.1 B), the vesicles appeared enlarged, were distributed around the periphery of the cell and were excluded from the central spindle region. At early anaphase (Figure 5.1 C), large CaBP7-positive vesicles were still visible at the periphery of the cells but during late anaphase (Figure 5.1 D) these vesicles began to redistribute. At early telophase (Figure 5.1 E), the vesicles had redistributed to opposite poles of the spindle and to the midzone, concentrating around the

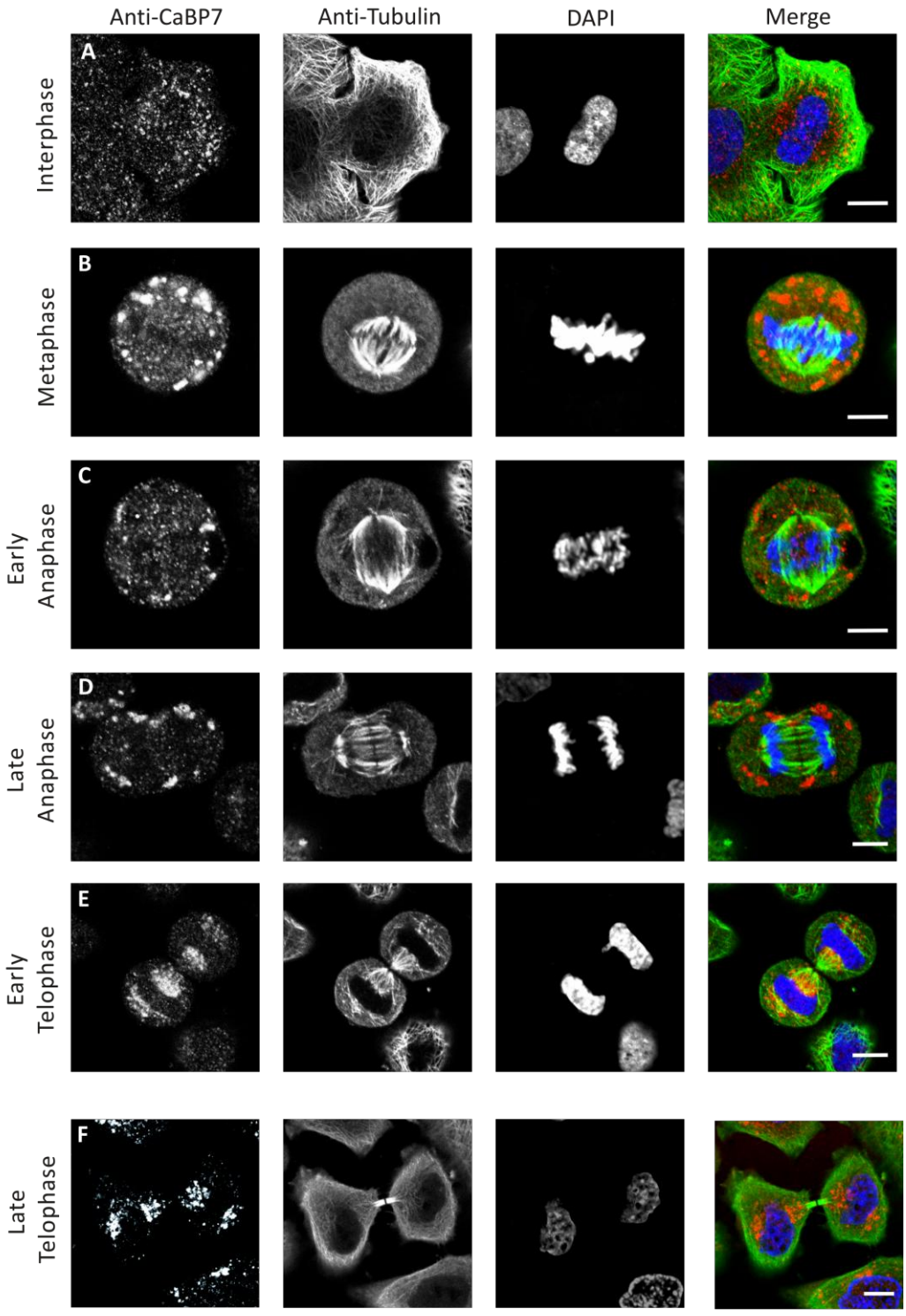

Figure 5.1. Distribution of endogenous CaBP7 in HeLa cells. A-F) HeLa cells immunostained with anti-CaBP7 (Alexa 568, red) and an α-tubulin antibody (Anti-DM1A, FITC, green), at various stages of mitosis. Nuclei are stained with DAPI (blue). Scale bars =10 µm.

intercellular bridge. In late telophase (Figure 5.1 F), as the intercellular bridge becomes thinner, CaBP7-positive vesicles remained in the vicinity of the midzone and also at the opposite poles of the cell. CaBP7-positive vesicles did not adopt their more dispersed interphase distribution until the two daughter cells had fully separated.

5.2.2. CaBP7 co-localises with lysosomes during mitosis

The data in chapter 4 illustrated that CaBP7 localised to vesicles which co-stained with markers specific for late endosomes and lysosomes. Co-localisation with the lysosomal integral membrane protein, CD63, was examined at different stages of the cell cycle (Figure 5.2). During all stages of the cell cycle there was extensive co-localisation of endogenous CaBP7 with CD63 implying that there is no redistribution of CaBP7 to other organelles in a cell-cycle dependent manner. The localisation of CaBP7 to lysosomes and the reported binucleate phenotype upon CaBP7 knockdown suggest a potentially important role for lysosomes during cytokinesis.

Figure 5.3 shows the localisation of CaBP7 during cytokinesis in HeLa cells compared to various vesicular markers. In accordance with localisation studies in interphase cells shown in chapter 4, endogenous CaBP7 showed complete co-localisation with ts045 VSVG-GFP during cytokinesis (Figure 5.3A). Cytokinetic cells overexpressing CaBP7 and immunostained for Rab11 as a marker of recycling endosomes (Figure 5.3B) showed no co-localisation. In agreement with previous studies (Wilson *et al*., 2005), Rab11 accumulated in the midzone during cytokinesis and coincided with anti-α-tubulin immunostaining of the interzonal microtubules (Figure 5.3B, merge). This is in contrast to CaBP7 localisation to vesicles around the cleavage furrow and at the opposite pole of the cell. No co-localisation of overexpressed CaBP7 was observed with anti-M6PR immunostaining suggesting that CaBP7 predominantly localises to lysosomes, rather than late endosomes, during cytokinesis. Finally, co-immunostaining of HeLa cells with antibodies to CaBP7 and VAMP7 showed extensive co-localisation as observed in interphase cells in Chapter 4. These observations support the conclusion that CaBP7 does not redistribute to an

alternative subcellular compartment during cytokinesis. CaBP7 localises to CD63- and VAMP7-positive vesicles, consistent with a predominantly lysosomal distribution during cytokinesis.

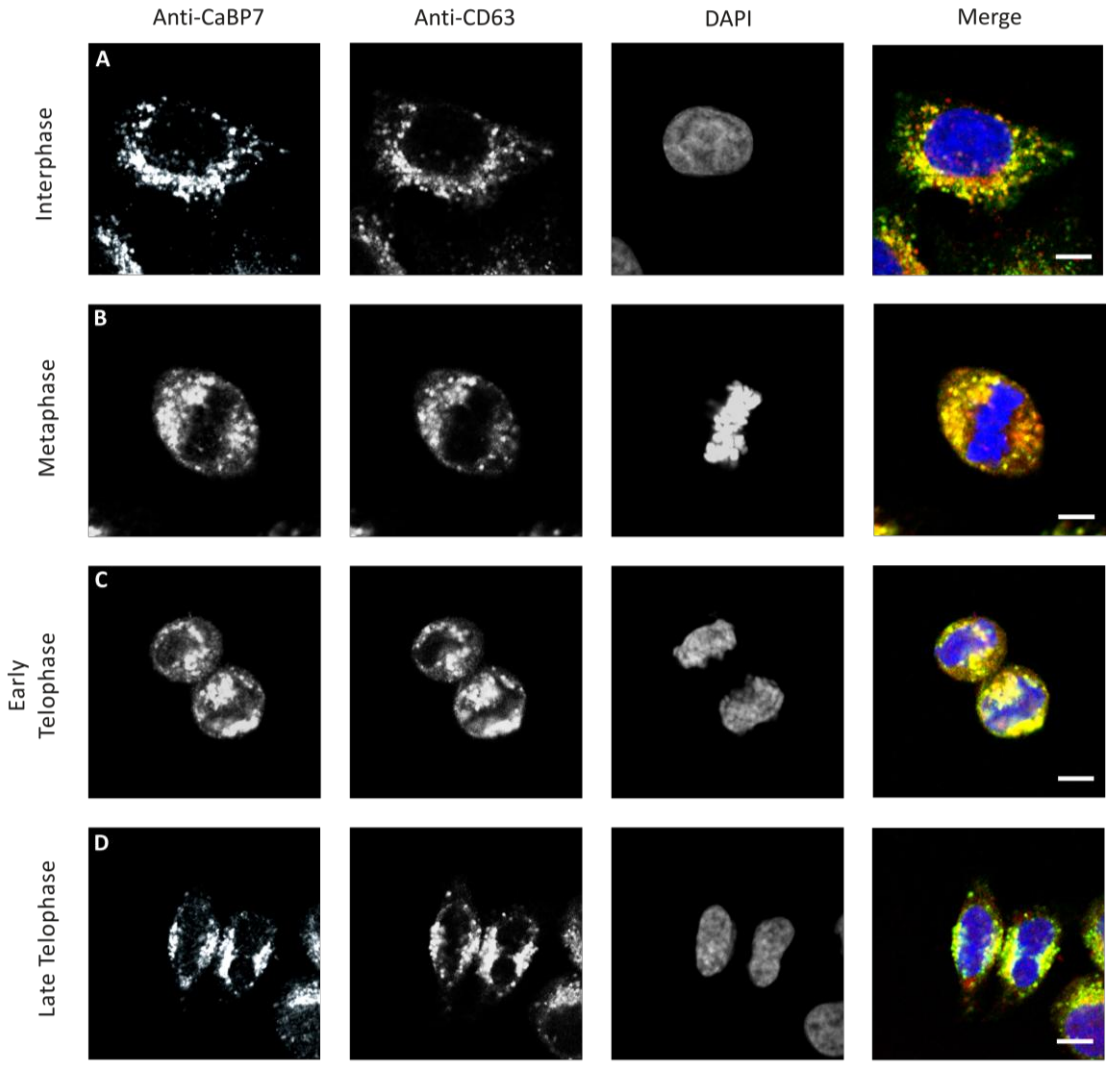

Figure 5.2. Co-localisation of endogenous CaBP7 with the lysosomal marker, CD63 in HeLa cells. A-D) HeLa cells immunostained with anti-CaBP7 (Alexa 568, red) and anti-CD63 (FITC, green), at various stages of mitosis. Nuclei are stained with DAPI (blue) and regions of co-localisation appear yellow in the merged images. Scale bars =10 µm.

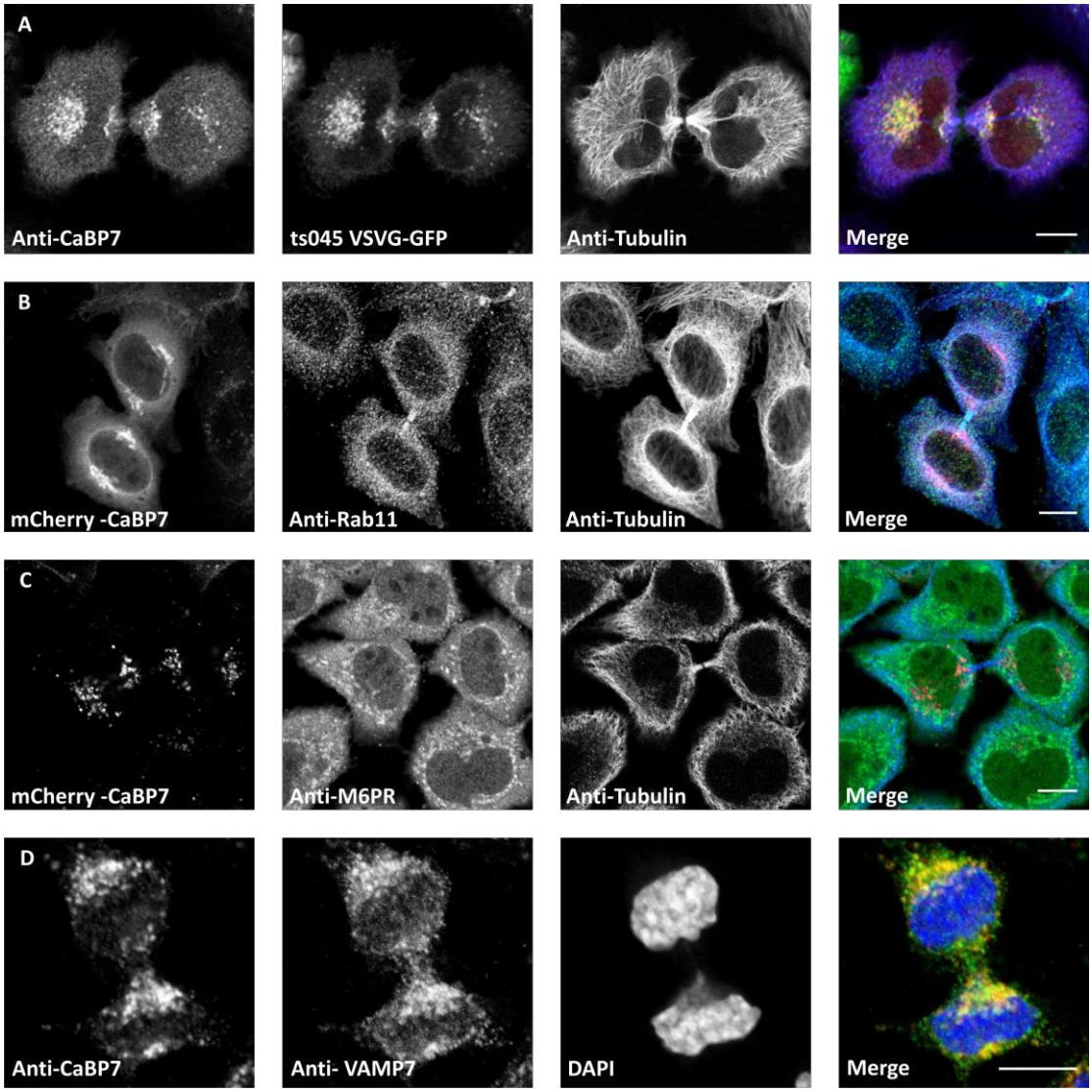

Figure 5.3. Localisation of CaBP7 at cytokinesis in HeLa cells with various antibody markers. A) HeLa cells co-transfected with mCherry-CaBP7 (red) and ts045 VSVG-GFP (Green) and immunostained with anti-α-tubulin (Anti-Tubulin, Alexa 405, blue). B) HeLa cells transfected with mCherry-CaBP7 (red) and immunostained with anti-Rab11 (FITC, green) and anti-α-tubulin (Anti-Tubulin, Alexa 405, blue). C) HeLa cells transfected with mCherry-CaBP7 (red) and immunostained with anti-M6PR (FITC, green) and anti-α-tubulin (Anti-Tubulin, Alexa 405, blue). D) HeLa cells co-immunostained with anti-CaBP7 (Alexa 568, red) and anti-VAMP7 (FITC, green) with DAPI-stained nuclei (Blue). Regions of co-localisation appear yellow (where red and green channels overlap) or aqua (where green and blue channels overlap) in the merged images. Scale bars =10 µm.

5.2.3. Knockdown of CaBP7 leads to an increase in the number of binucleate cells

To verify the reported defect in cytokinesis upon knockdown of CaBP7, HeLa cells were transfected with either a scrambled shRNA construct or an shRNA construct specifically targeting CaBP7. Figure 5.4A and 5.4B show western blot analysis of HeLa cell lysates from cells co-transfected with mCherry-CaBP7 or mCherry-CaBP8 and either of the two shRNA constructs for 72 hrs. Immunoblotting with an anti-RFP

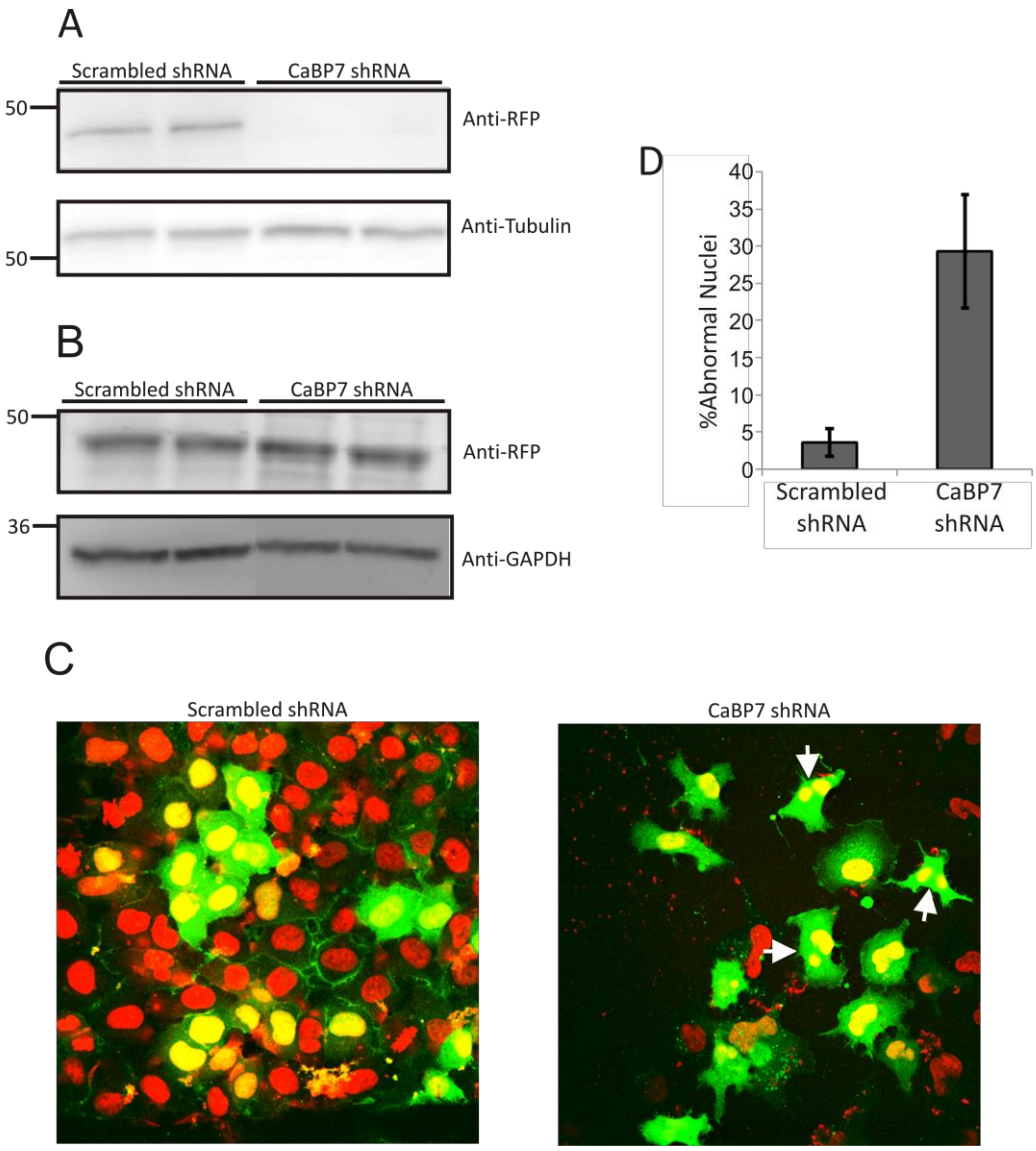

Figure 5.4. CaBP7 Knockdown in HeLa cells. A) Western blot showing reduction of exogenously expressed mCherry-CaBP7 protein through treatment with CaBP7-specific shRNA but not scrambled shRNA. B) Western blot showing resistance of exogenously expressed mCherry-CaBP8 protein to knockdown by CaBP7-specific shRNA and scrambled shRNA. Molecular weight standards (kDa) are shown on the left side of western blot images. C) Example images of HeLa cells treated with CaBP7-specific shRNA or scrambled shRNA. GFP (green) acts as a marker for shRNA-transfected cells. Nuclei are stained with DAPI (red in untransfected cells, yellow in transfected cells). White arrows indicated multinucleate cells. D) Histogram showing the average percentage of abnormal nuclei observed in multiple fields of view ± SEM (n=100 cells in two independent experiments).

antibody to detect the mCherry tag on exogenously expressed proteins showed efficient knockdown which was specific to CaBP7 and not CaBP8. Confocal microscopy was used to image cells transfected with shRNAs and the number of nuclei in transfected cells was quantified. The shRNA construct encoded free GFP under a separate promoter as a transfection marker (Figure 5.4C) and all cells were additionally stained with DAPI to examine their DNA content. Cells transfected with a CaBP7-specific shRNA exhibited an increase in the number of binucleate or polylobed nuclei as indicated by the white arrows in figure 5.4C. Approximately 100 cells were scored for each condition from two independent transfections and the number of abnormal nuclei quantified (Figure 5.4D). There was an approximate 3-fold increase in the number of abnormal nuclei in CaBP7 shRNA transfected cells compared to the scrambled control. This data confirms that there is an increase in the number of cells with abnormal nuclei upon depletion of CaBP7 protein levels.

A number of mCherry-tagged shRNA resistant variants of CaBP7 were generated to attempt to rescue the binucleate phenotype. Resistant variants included: wild type CaBP7; a mutant defective in Ca^{2+}-binding at both functional EF-hand motifs; and a mutant lacking the C-terminal domain containing the TMD. These variants were selected to assess the dependence of CaBP7 function in cytokinesis on Ca^{2+}-binding and normal subcellular localisation. Figure 5.5A-C show example images of HeLa cells transfected with each of these constructs and all three variants appear to localise similarly to their non-resistant counterparts (see chapter 4). Figure 5.5D shows a western blot of HeLa cells co-transfected with CaBP7 specific shRNA and each of the rescue constructs. Immunoblotting with an anti-RFP antibody to detect the mCherry colour tag illustrated that all three rescue constructs were indeed resistant to knockdown by CaBP7 specific shRNA. Cells co-transfected with CaBP7 shRNA and either mCherry as a control or the wild-type shRNA-resistant CaBP7 construct showed no significant differences in the number of abnormal nuclei counted (data not shown). A multinucleate phenotype is not, however, reversible (Uetake and Sluder, 2004) and therefore correction of the phenotype should ideally be shown by complementation rather than by rescue. There needs to be a high enough level of protein expressed from the resistant construct before the shRNA-driven depletion of

the endogenous protein is complete, otherwise the cytokinesis defects and multinucleate phenotype may occur before the rescue has taken effect. In transient transfections, both constructs will be expressed at the same time, however, there will be a period of time where the shRNA is being expressed, but protein synthesis from mRNA transcribed from the resistant construct has not started or is only at a low level. For this reason the use of stable cell lines expressing the resistant constructs, or inducible shRNA constructs would be necessary to truly examine the ability of the rescue constructs to correct the CaBP7 binucleate phenotype. Unfortunately this was not possible within the time limits of this project.

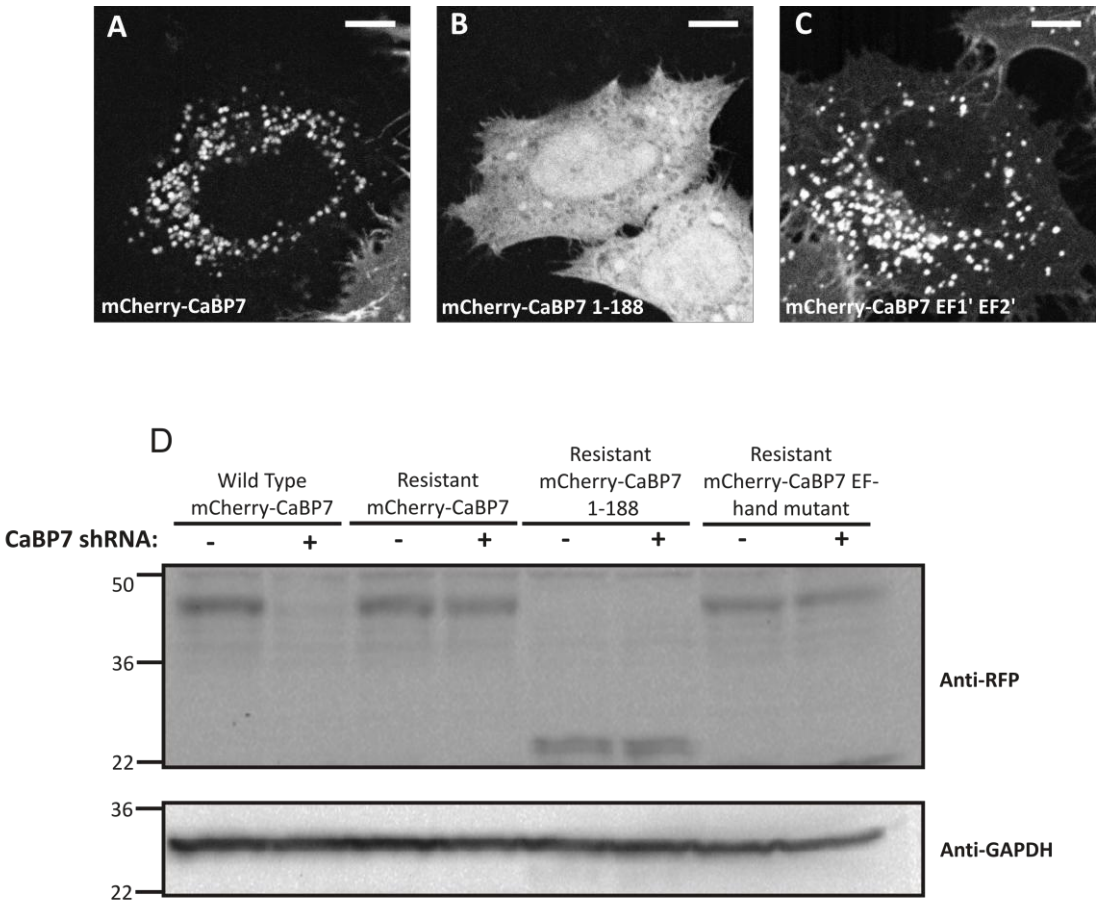

Figure 5.5. shRNA-resistant CaBP7 constructs. A) Localisation of shRNA-resistant mCherry-CaBP7 in HeLa cells. B) Localisation of shRNA resistant mCherry-CaBP7 1-188 in HeLa cells. C) Localisation of shRNA-resistant mCherry-CaBP7 Double EF hand mutant (mCherry-CaBP7 EF1' EF2') in HeLa cells. Scale bars =10 µm. D) Western blot showing that exogenous wild type mCherry-CaBP7 is knocked down by treatment with CaBP7-specific shRNA, whereas expression of the three shRNA-resistant constructs is not. '-' indicates samples with no shRNA treatment. '+' indicates samples treated with CaBP7 shRNA. Molecular weight standards (kDa) are shown on the left side of western blot images.

5.3. Discussion

Cellular depletion of CaBP7 by shRNA targeting has been previously shown to result in an increase in binucleate cells (Neumann *et al.*, 2010). The data presented in this chapter confirms this observation. Knockdown of CaBP7 in HeLa cells resulted in an approximately 3-fold increase in the number of abnormal nuclei, 72 hours after transfection with a CaBP7 specific shRNA construct. RNAi-resistant variants of CaBP7 were generated to use as rescue constructs and confirm that this was not an off-target effect. Unfortunately, transient co-transfection of cells with shRNA and resistant constructs was not suitable to assess the prevention of the binuclear phenotype as the shRNA may have been expressed and the phenotype generated before the resistant protein reached compensatory levels of expression. Complementation assays should be carried out using cells stably transfected with the resistant constructs to ensure that levels of exogenous protein are optimal before knockdown of endogenous CaBP7 is initiated. Alternatively, an inducible expression vector could be used to induce CaBP7 specific shRNA after the resistant protein has been transiently expressed for a number of days. Unfortunately this was not possible within the scope of the current project, however, in the original RNAi screen Neumann *et al.* were able to prevent the CaBP7 related binucleate phenotype by employing stable cell lines expressing the RNAi resistant mouse orthologue of CaBP7 (Neumann *et al.*, 2010). RNAi-resistant constructs encoding two mutants, one defective in Ca^{2+}-binding, and one lacking the TMD essential for correct localisation, were also generated. Creation of stable cell lines expressing these constructs in future work would permit an examination of how Ca^{2+}-binding and correct localisation contribute to the apparent role of CaBP7 in cytokinesis.

Examination of the localisation of CaBP7 at different stages of mitosis revealed that at the onset of cytokinesis, CaBP7-positive vesicles accumulated at opposite poles of the spindle and around the intercellular bridge. Co-localisation with CD63 confirmed that these vesicles were lysosomes and that there had been no redistribution of CaBP7 into other vesicular organelles during mitosis. Further investigation revealed that there was no co-localisation with the recycling endosome marker Rab11 or the late endosome marker M6PR. Extensive co-localisation was, however, observed with

ts045 VSVG-GFP and endogenous VAMP7 as also demonstrated in interphase cells in chapter 4. This localisation, coupled with the observed binucleate phenotype upon depletion of CaBP7, implies that lysosomes may play an important functional role in cytokinesis.

Numerous studies have reported a role for membrane trafficking and vesicle transport during cytokinesis, however this research has thus far focused on the role of the recycling endosome and secretory vesicle pathways (McKay and Burgess, 2011, Neto *et al*., 2011). The role of recycling endosomes was first discovered after the observation that Rab11 is required for cellularisation in *Drosophila* embryos (Pelissier *et al*., 2003) and knockdown of Rab11 in HeLa cells results in an increase in the number of binucleate cells (Wilson *et al*., 2005). Rab11-positive vesicles accumulate at the midbody (Wilson *et al*., 2005) and Rab11 mutants exhibit defects in both furrow ingression and in the contractile ring which either fails to contract or disassembles during late telophase (Giansanti *et al*., 2007).

The secretory pathway involves the sorting of protein at the Golgi apparatus and packaging into vesicles to be delivered to the PM (McKay and Burgess, 2011). SNARE proteins are essential for every vesicular fusion step along the secretory pathway (Yang *et al*., 2006b) and the importance of this pathway for normal cytokinesis is illustrated by the cytokinesis defects generated upon disruption of various SNARE proteins. In Madin-Darby Canine Kidney (MDCK) cells, syntaxin 2 is necessary for abscission but not for furrow ingression (Low *et al*., 2003). Inhibition of VAMP8 (Low *et al*., 2003) and depletion of syntaxin 16 (Song *et al*., 2009) lead to similar abscission defects. In addition, studies in *Drosophila* and *C. elegans* have demonstrated an essential role for syntaxins in the successful completion of cytokinesis (Xu *et al*., 2002, Jantsch-Plunger and Glotzer, 1999).

Such observations demonstrate an important role for membrane trafficking during cytokinesis and interestingly, proteomic analysis of isolated midbodies from Chinese hamster ovary (CHO) cells showed that the largest category of proteins (33% of 160 identified proteins) were associated with membrane trafficking or secretory

functions (Skop *et al*., 2004). The exact role of membrane trafficking during cytokinesis is poorly understood but a prevailing view is that the midbody forms a platform for the assembly of the protein complexes required for abscission (Neto *et al*., 2011). It is thought that the trafficking of vesicles into the midzone facilitates the delivery of key components to the midbody. Through fusion events with the PM, different species of vesicles are also thought to increase PM surface area allowing the intercellular bridge to thin prior to the final abscission event (Neto *et al*., 2011).

Interestingly, live cell imaging experiments in BSC1 cells overexpressing the temperature-sensitive VSVG mutant also demonstrated that Golgi-derived, VSVG-positive vesicles accumulate at the midbody during cytokinesis. Using total internal reflection fluorescence (TIRF) microscopy, direct docking and fusion of these vesicles at the midzone was observed (Goss and Toomre, 2008). Goss and Toomre suggested that this pool of VSVG-positive vesicles was distinct from both endosomal and lysosomal compartments (Goss and Toomre, 2008). Initially this observation appears contradictory to the observation that CaBP7 co-localises with both VSVG and markers of late endosomes and lysosomes, however, the use of LAMP1 as a marker for lysosomes casts some doubt on this conclusion. Both LAMP1 and VSVG have been shown to be dependent on the AP3 machinery for their subcellular trafficking from the TGN. Overexpression of VSVG has been shown to saturate the AP3 machinery and cause LAMP1 to traffic via an alternative pathway (Nishimura *et al*., 2002). Therefore, overexpression of VSVG in the experiments of Goss *et al.* could have resulted in the mistargeting of LAMP1 and therefore explain the conflict between their data and the results presented in this chapter.

To date, there have been few studies examining the contribution of lysosomes to membrane trafficking events during cytokinesis, however, lysosomes have been shown to redistribute to the midzone of dividing cells (Bergeland *et al*., 2001). The view of lysosomes merely as the waste disposal unit for the cell has begun to be challenged by the emergence of new and important roles for this organelle. In particular, lysosomes have been shown to behave as Ca^{2+}-regulated exocytotic vesicles in a number of cell lines (Gerasimenko *et al*., 2001). This process has been

shown to be important in PM repair and therefore is of interest when considering how, during cytokinesis, two daughter cells are able to separate without creating a hole in the PM (Finger and White, 2002). Wound healing by lysosomal exocytosis is triggered by the large influx of extracellular Ca^{2+} which accompanies damage to the PM, but lysosomal exocytosis can also be initiated when $[Ca^{2+}]_i$ is elevated to 1 μM (Martinez *et al*., 2000). Mediated by the Ca^{2+}-sensing protein synaptotagmin VII, the elevation in $[Ca^{2+}]_i$ leads to rapid homotypic fusion of lysosomes and their exocytic fusion with the PM thus repairing the damage through delivery of new membrane (Finger and White, 2002). This process represents an alternative mechanism for the donation of membrane during abscission in cytokinesis. Both wound healing and cytokinesis are sensitive to treatment with brefeldin A (BFA) which causes the tubulation of endosomes and lysosomes, and hence is consistent with a role for lysosomes in the successful abscission of two daughter cells (McNeil and Terasaki, 2001).

Although there is no direct evidence for an essential role of lysosomes during cytokinesis, proteins which are important for late endosome to lysosomal trafficking have been implicated. ESCRT (endosomal sorting complexes required for transport) proteins are involved in the sorting and trafficking of membrane proteins into MVBs (Dukes *et al*., 2008). ESCRT proteins such as charged MVB protein (CHMP) 2, 4 and 5 are localised to the midbody during the late stages of cytokinesis. A dominant negative mutant of CHMP3 which has been shown to alter endosome morphology and inhibit trafficking to the lysosomes was also shown to inhibit cytokinesis (Dukes *et al*., 2008). CHMP3 did not co-localise with Rab11 in recycling endosomes and this data suggested that proteins involved in late endosomal function are also important for the completion of cytokinesis (Dukes *et al*., 2008). Extensive co-localisation of CaBP7 and the late endosomal and lysosomal protein, VAMP7 was demonstrated in both interphase cells (chapter 4) and cytokinetic cells. Interestingly a dominant negative mutant of VAMP7 has also been shown to inhibit cytokinesis. Overexpression of the cytosolic longin domain of VAMP7 caused strong inhibition of cytokinesis inducing multiploidy of transfected cells. This was coupled with a significant reduction in both the recovery of PM surface area and the appearance of

LAMP1 at the cell surface (Boucrot and Kirchhausen, 2007). In accordance with this, overexpression of the VAMP7 longin domain has also been shown to inhibit lysosomal exocytosis (Proux-Gillardeaux *et al*., 2007). Normal VAMP7 function is therefore required for cytokinesis and is suggestive of an important role for CaBP7- and VAMP7-positive vesicles, of late endosome or lysosome origin, in exocytosis during cytokinesis.

A role for Ca^{2+}-stimulated lysosomal exocytosis in cytokinesis has not yet been explored in detail, however Boucrot *et al.* demonstrated the appearance of LAMP1-positive cell surface blebs during PM recovery in cytokinesis (Boucrot and Kirchhausen, 2007). A decrease in the number of blebs was observed upon treatment with the myosin II inhibitor, blebistatin which also caused a decrease in the internalisation of LAMP1. These observations were consistent with a role for PM fusion of late endosomes and lysosomes which is dependent on myosin II function (Boucrot and Kirchhausen, 2007). Importantly, myosin II has been shown to play an important role in Ca^{2+}-dependent exocytosis in membrane repair and wound healing (Togo and Steinhardt, 2004).

Localised elevations of $[Ca^{2+}]_i$ are associated with many stages of mitosis. It has been suggested that the highly localised spatio-temporal nature of mitotic Ca^{2+} signals is responsible for their elusiveness and underlies their lack of detection to date (Whitaker, 2006). As such the ER has been shown to cluster in close proximity to the spindle and forms a close association with microtubules (Terasaki and Jaffe, 1991, Zaal *et al*., 1999). In sea urchins the Ca^{2+} transient which occurs at the onset of mitosis is often confined to a small perinuclear region, consistent with the existence of Ca^{2+} microdomains (Wilding *et al*., 1996). The activation of CaM has also been shown to occur in discrete regions of the cell, first in a perinuclear region and then at the spindle poles (Torok *et al*., 1998). Unfortunately, there are very few reports where calcium signals have been detected from these putative Ca^{2+} microdomains (Whitaker, 2006).

There is growing evidence that lysosomes can store Ca^{2+} at concentrations comparable to those measured in the major Ca^{2+} storage organelle, the ER (Gerasimenko and Tepikin, 2005). Ca^{2+} release from lysosomes is stimulated by the potent second messenger, NAADP, which binds to receptors specifically found on acidic organelles (Galione *et al*., 2010). Recent research has revealed that the TPCs are a family of Ca^{2+} release channels located in the membranes of endosomes and lysosomes which are activated by NAADP binding (Zhu *et al*., 2010b). Interestingly, knockdown of TPC1 or TPC2 results in defects in mitosis suggestive of a role for Ca^{2+} signalling from acidic organelles during cell division (www.mitocheck.org and (Neumann *et al*., 2010)). The extremely localised nature of NAADP-mediated Ca^{2+} signals make lysosomal Ca^{2+} stores an attractive candidate for the generation of Ca^{2+} microdomains during cytokinesis. To date, no Ca^{2+}-sensor has been identified to interact with the TPCs or regulate the process of Ca^{2+} release at the lysosomes. As an integral membrane protein specifically targeted to the acidic compartments of the late endosomal and lysosomal pathway, CaBP7 represents a potential candidate for this role.

5.3.1. Conclusion

The data presented in this chapter provide evidence for a role of CaBP7 during cytokinesis. The observation that CaBP7 positive lysosomes redistribute to the intercellular bridge during cytokinesis infers an important role for lysosomal trafficking in the successful abscission of two daughter cells. Furthermore, extensive co-localisation of CaBP7 with both VSVG and VAMP7 is suggestive of an essential role for CaBP7-positive vesicles during cytokinesis. VSVG-positive vesicles have been shown to dock and fuse at the PM during cytokinesis (Goss and Toomre, 2008) and a dominant negative mutant of VAMP7, shown to impair lysosomal exocytosis (Proux-Gillardeaux *et al*., 2007), has also been shown to inhibit cytokinesis (Boucrot and Kirchhausen, 2007). Much more work is needed to deduce the exact role of CaBP7, the contribution of lysosomes during cytokinesis, and the Ca^{2+} dependency of these processes. Investigation of the emerging roles of lysosomes as important calcium

signalling platforms and their ability to undergo Ca^{2+}-regulated exocytosis in the context of cell division will be of particular interest.

Chapter 6:

Structural Characterisation of CaBP4 and CaBP7 using NMR

6.1. Introduction

NMR spectroscopy and X-ray crystallography are currently the only techniques which can provide the data required to determine atomic resolution protein structures. The use of these two techniques is not mutually exclusive and they are increasingly being used as complimentary approaches for structure determination (Snyder *et al*., 2005, Yee *et al*., 2005). X-ray crystallography allows a three-dimensional image of a molecule to be constructed based on its X-ray diffraction properties. To do this the molecule must first be crystallised, as scattering from an individual molecule is too weak to detect. The formation of suitable crystals concentrates the scattering in discrete directions to give a particular diffraction pattern. X-ray crystallography derives higher resolution structural data than NMR but requires that the protein form stable, well diffracting crystals (Yee *et al*., 2005, MacArthur *et al*., 1994). A limitation of this technique for some structural studies is the inability to monitor protein dynamics under changing conditions (MacArthur *et al*., 1994), however, discrete structural forms of a particular protein may be crystallised individually and the structures compared.

An important property of Ca^{2+}-sensors is their ability to undergo conformational changes in response to alterations in $[Ca^{2+}]_i$(Berridge *et al*., 2000). In addition, many Ca^{2+}-sensors have been shown to undergo unique conformational changes in response to the presence of Mg^{2+} ions (Wingard *et al*., 2005, Lusin *et al*., 2008). Depending on the exact cation binding status, the protein can exist in various conformations, which in turn allow the protein to interact with specific binding partners. The intrinsically dynamic nature of these proteins therefore represents an important consideration during structure determination. Despite the lower resolution structures generated by NMR, the ability to carry out experiments in solution means data can be obtained in a setting that more closely approximates a native protein environment, where protein dynamics can be monitored on molecular interaction timescales.

NMR works on the basis that protons have spin and can therefore generate a magnetic field (MacArthur *et al*., 1994). Certain atomic nuclei, usually those with an

odd mass number, possess a magnetic moment. If such nuclei are exposed to an external magnetic field, they will precess around an axis either parallel or anti-parallel to the direction of the applied magnetic field. This corresponds to upper and lower energy levels respectively. The energy difference between these two levels is characteristic of the particular type of nucleus and is modified by the small induced fields of neighboring atoms. Therefore by monitoring the shift in the resonance (known as chemical shift) of a particular type of atom, a characteristic spectrum of an atom's environment can be generated. Resonance between the two spin states is induced by applying electromagnetic radiation to a sample at an appropriate frequency and the transverse magnetisation is then detected as a unique NMR spectrum (MacArthur *et al*., 1994).

NMR is an intrinsically dynamic process and is therefore an extremely useful technique for monitoring structural changes as sample conditions are altered (Cooke, 1997, MacArthur *et al*., 1994). This allows simple screening of different buffer conditions for the optimisation of NMR spectra, and subsequently, titrations can be carried out to investigate the effect of different molecules and ions on protein conformation e.g. Ca^{2+} or Mg^{2+}. NMR is therefore amenable to the structural characterisation of Ca^{2+}-sensors.

As in X-ray crystallography, NMR sample preparation is critical. The target protein must exhibit certain key features including the capacity to remain soluble and stable for periods of weeks to allow the acquisition of the data required for structure determination (MacArthur *et al*., 1994). One of the biggest limitations of NMR spectroscopy is the size of the protein - generally proteins larger than 30 kDa can prove problematic (Snyder *et al*., 2005). The CaBP family of proteins, with the exception of caldendrin, fall below this molecular weight threshold and are therefore suitable candidates for NMR analysis.

The structure of CaBP1 has been recently solved by both NMR spectroscopy and X-ray crystallography and provides some potentially important insights into the structure of related CaBPs (Findeisen and Minor, 2010, Park *et al*., 2011). NMR

studies have determined that CaBP1 contains two independent domains separated by a flexible linker in its fully Ca^{2+}-bound form,. The first 18 residues of the N-terminus are structurally disordered and could not be assigned. The remainder of the N-terminal domain contains EF1 and EF2 in a closed conformation whereas the C-terminal domain contains EF3 and EF4 in the usual Ca^{2+}-bound open conformation as seen in CaM (Park *et al*., 2011).EF1 is assumed to be constitutively Mg^{2+}-bound under physiological conditions due to a glutamate to aspartate substitution at the 12^{th} position of the EF-hand loop which results in equal selectivity for both Mg^{2+} and Ca^{2+}. EF2 is unable to bind to Ca^{2+} due to a glycine at position 5 of the EF-hand loop. EF3 and EF4 both have a canonical glutamate at the 12^{th} position of the Ca^{2+}-binding loop and hence were found to bind to Ca^{2+} specifically with little affinity for Mg^{2+}. Mg^{2+} binding to the apo form of the protein induced a global shift in conformation from a molten globule state to a more folded conformation (Wingard *et al*., 2005). Subsequent addition of Ca^{2+} resulted in binding at EF3 and EF4 and a related shift in conformation localised to these two EF-hands. Mg^{2+} and Ca^{2+} therefore induce distinct conformational changes and markedly increase the folding stability of CaBP1 (Wingard *et al*., 2005). The crystal structure of CaBP1 generated partly contradictory results. Findeisen *et al*. described a more compact structure and a well-ordered interlobe linker (Findeisen and Minor, 2010). The largest discrepancies were seen in the N-terminal domain and can be explained by differences in the binding status of the EF-hands: in the crystal structure, EF1 was not Ca^{2+}-bound despite the presence of millimolar [Ca^{2+}] during crystallisation. A complete structural comparison would, therefore, require crystallographic data for the Mg^{2+}/Ca^{2+}-bound CaBP1 protein. The well ordered interlobe linker was unique to the crystal structure (Findeisen and Minor, 2010).

CaBP1 structural information has subsequently been applied to investigate and map regions which are important for interactions with IP_3Rs (Li *et al*., 2009) and $Ca_v1.2$ channels (Findeisen and Minor, 2010). In addition, comparisons with the structure of CaM have been made. The most striking difference was a solvent-exposed hydrophobic surface seen on the front face of the Ca^{2+}-bound C-terminal domain of CaBP1 which is more expansive than that present in CaM. This hydrophobic patch,

surrounded by charged residues, may form an important binding site for target proteins, and may explain the differences in interacting partners and modulatory effects of CaBP1 compared to CaM (Li *et al*., 2009, Park *et al*., 2011).

The NMR and crystal structures of CaBP1 have proven valuable for the elucidation of structure-function relationships and may serve as a model for predicting the structures of related CaBPs. There are, however, important differences in the sequence properties of the various CaBPs and it will be important to investigate how these differences affect the structure of the individual proteins. In particular, for reasons discussed in Chapter 3, CaBP7 and CaBP8 differ significantly in their domain properties compared to the rest of the CaBPs.

Unlike CaBP1, CaBP7 and CaBP8 have only two functional EF-hand motifs, EF1 and EF2, which, as determined by ITC, form high affinity Ca^{2+}-binding sites (Mikhaylova *et al*., 2006). Mikhaylova *et al.* reported that Ca^{2+} binding to CaBP7 or CaBP8 follows a one set of sites model with a Ca^{2+}-binding affinity of 0.2 - 0.5 µM, which is around ten-fold higher than that seen for caldendrin in similar experiments (Mikhaylova *et al*., 2006). ITC experiments also indicated that, unlike CaBP1, CaBP7 and CaBP8 do not bind to Mg^{2+} (Mikhaylova *et al*., 2009, Wingard *et al*., 2005). This data was supported by fluorimetry experiments examining CaBP8 with both Mg^{2+} and Ca^{2+} (Mikhaylova *et al*., 2009, Mikhaylova *et al*., 2006): Mg^{2+} did not induce a detectable conformational change in the protein whereas a large shift in fluorescence intensity was observed upon the addition of Ca^{2+}. The perturbation in fluorescence was more substantial than observed for caldendrin in similar experiments (Mikhaylova *et al*., 2006). These data indicate that CaBP7 and CaBP8 behave differently to caldendrin and CaBP1 when binding divalent cations. Moreover, the C-terminal regions of CaBP7 and CaBP8, containing their unique TMDs, share little sequence identity with other Ca^{2+}-sensors (McCue *et al*., 2011, McCue *et al*., 2009). As demonstrated in chapter 3, CaBP7 and CaBP8 appear to form a distinct group of proteins, unlike any other known Ca^{2+}-sensor family and likewise may exhibit divergent structures when compared with CaBP1 (McCue *et al*., 2010a).

Important differences also exist between the more closely related CaBPs 1-5 which might elicit structural diversity. In particular CaBP2 and CaBP4 are predicted to have different cation binding properties compared with CaBP1. Whereas CaBP1 constitutively binds Mg^{2+} at EF-1, this is predicted to form a high affinity Ca^{2+}-binding site in CaBP2 and CaBP4. This may have significant consequences for the structure and dynamics of these proteins in comparison to CaBP1. Most of the diversity between the CaBPs, however, resides within their N-termini. CaBP4 is the most divergent protein amongst CaBPs1-5 and possesses the most extended N-terminal region with the exception of caldendrin (McCue *et al*., 2010a, Haeseleer *et al*., 2000).

This chapter presents experimental efforts towards solving the NMR solution structures of both CaBP4 and CaBP7. These two proteins were selected due to their distinguishing features as discussed above and also because of their documented cellular physiological roles. CaBP4 is the most functionally characterised member of the CaBP family. It has been shown to interact with and regulate various VGCCs (Cui *et al*., 2007, Lee *et al*., 2007c, Haeseleer *et al*., 2004, Yang *et al*., 2006a) and plays a critical role in phototransduction in the mammalian retina (Maeda *et al*., 2005, Haeseleer *et al*., 2004, Zeitz *et al*., 2009, Littink *et al*., 2010, Haeseleer, 2008, Zeitz *et al*., 2006, Littink *et al*., 2009, Aldahmesh *et al*., 2010, Lee *et al*., 2007b). Various mutations have been identified in human CaBP4, which give rise to rod and cone synaptic disorders (Zeitz *et al*., 2009, Littink *et al*., 2010, Zeitz *et al*., 2006, Littink *et al*., 2009, Aldahmesh *et al*., 2010) and CaBP4 homozygous knockout mice exhibit a night blindness phenotype (Haeseleer *et al*., 2004). A role regulating Ca^{2+}-dependent inactivation of L-Type $Ca_V1.3$ channels in auditory inner hair cells has also been postulated for CaBP4 (Cui *et al*., 2007).

CaBP7 is less well-characterised but its implicated role in cytokinesis (Neumann *et al*., 2010), as discussed in chapter 5, marks CaBP7 as a potentially important candidate for structural characterisation. CaBP7 has also been shown to bind to and inhibit the activity of PI4KIIIβ and thus is important in the regulation of TGN to PM trafficking (Mikhaylova *et al*., 2009). It will be important to elucidate the key

structural differences between the Ca^{2+}-sensing protein families comprising CaBPs 1-5, and CaBP7 and CaBP8.

6.2. Results

6.2.1. Protein expression of CaBP4, CaBP7 and CaBP8

The sequences encoding human CaBP4, CaBP7 and CaBP8 were first cloned into a glutathione-S-transferase (GST) fusion vector for production of GST-tagged proteins in *E. coli*. The GST tag (26 kDa) must be cleaved following recombinant protein purification and this was accomplished using PreScision™ protease treatment.

Suitability of expression levels and purity of the GST fusion proteins for NMR analysis were trialled using BL21 (DE3) *E. coli* as a host organism (Table 6.1). *E. coli* is the most commonly used host organism for the expression of recombinant proteins and is particularly suited to the production of proteins for NMR due to its ability to synthesise amino acids from a simple carbon source and nitrogen salt. This facilitates the cost effective production of isotopically labelled proteins, which is vital for the generation of high resolution NMR spectra. The inherent signal overlap and unfavourable line widths associated with the typically large molecular weights of proteins are fundamental problems for protein NMR spectroscopy, but can be largely resolved through the use of multidimensional hetero-nuclear experiments (Hill, 2008, Cooke, 1997). High resolution NMR spectroscopy requires the use of nuclei with half integral spin (MacArthur *et al*., 1994). The most abundant isotopes of carbon (^{12}C) and nitrogen (^{14}N) are, therefore, unsuitable, but can be substituted relatively easily with stable isotopes (^{13}C and ^{15}N) which have a spin quantum number – ½. This is achieved by expressing proteins in minimal medium containing ^{13}C-labelled glucose and ^{15}N-labelled ammonium chloride as the sole carbon and nitrogen sources. This allows the acquisition of two dimensional (2D) and three dimensional (3D) NMR experiments which give the necessary information to perform backbone and side chain assignments and also allow structure calculations.

High purity (>90%) and concentration (>300 μM) is preferable for acquisition of structure quality NMR data. BL21 (DE3) *E. coli* grow rapidly and can produce large

amounts (>50 mg/litre culture) of recombinant protein, however, overexpression of exogenous protein can result in the formation of insoluble protein aggregates or inclusion bodies. Therefore, a balance must be struck between high expression and protein solubility. There are various parameters which may be altered in order to obtain a maximal yield of soluble protein. Slowing the expression rate, by reducing IPTG concentration, altering the induction temperature, or varying the length of induction was tested for each of the proteins investigated (Table 6.1).

The expression of GST-tagged CaBP4, CaBP7 and CaBP8 was insufficient under all induction conditions tested. As determined in chapter 4, CaBP7 and CaBP8 are TA membrane proteins and producing a high yield of full-length soluble protein is likely to prove problematic due to the hydrophobicity of their C-termini. As such, most of the expressed protein was insoluble and remained in the pellet fraction as visualised on SDS-PAGE (data not shown). In an attempt to improve the solubility of CaBP7 and CaBP8, truncations of both proteins, lacking their C-terminal TMDs, were generated (CaBP7 1-188 and CaBP8 1-192). This improved the solubility of both proteins, however, the expression yield remained too low to obtain sufficient quantities for NMR.

As changing the induction conditions and creating TMD deficient mutants did not sufficiently improve protein yield, alternative host expression strains were tested. Efficient production of heterologous protein in *E. coli* is often limited by the rarity of certain tRNAs which are more common in eukaryotes. Forced overexpression of heterologous proteins can deplete the limited pool of these rare tRNAs and stall translation, resulting in a poor expression yield of full-length protein. To overcome this, modified BL21 strains are commercially available that have been engineered to over-express rare tRNAs (Kleber-Janke and Becker, 2000). BL21-CodonPlus®(DE3)-RP, BL21-CodonPlus®(DE3)-RIL and Rosetta™ cells were tested for this reason. The process of testing induction conditions was repeated for each new BL21 strain. The use of BL21s encoding rare tRNAs generally improved the expression of CaBP7 1-188 and CaBP8 1-192, but once again the yield was not sufficient for NMR analysis.

Table 6.1. Summary of recombinant protein expression and conditions tested. Expression conditions are described for each of CaBP4, codon optimised CaBP4 (Opt CaBP4),full length CaBP7 (CaBP7 FL), full length CaBP8 (CaBP8 FL) and the truncations: CaBP8 1-192, CaBP7 1-188, codon optimised CaBP7 1-188 (Opt CaBP7 1-188) and codon optimised CaBP7 1-100 (Opt CaBP7 1-100). Different proteins are separated by alternating blocks of blue and white cells. Res. column indicates the antibiotic resistance encoded by the expression vector. Tag column lists the affinity tag encoded by the expression vector. Bact. Res column indicates the antibiotic resistance the expression bacteria. M9 = M9 minimal media, SB = superbroth media. Purification column lists the type of affinity resin used for purification of recombinant protein.

	Protein	Plasmid	Res.	Tag	Expression bacteria	Bact. Res.	Media	IPTG (mM)	Temp °C	Time, hrs	Purification	Yield	Additional Info
1	CaBP4	pGEX-6P1	Amp	GST	BL21	-	M9	0.50	22	Overnight	Glutathione Sepharose	Poor	Mainly insoluble
1	CaBP4	pGEX-6P1	Amp	GST	BL21	-	M9	0.05	18	Overnight	Glutathione Sepharose	Poor	Mainly insoluble
1	CaBP4	pGEX-6P1	Amp	GST	BL21	-	M9	0.20	18	Overnight	Glutathione Sepharose	Good	Low purity, poor cleavage
1	CaBP4	pOPIN-s	Amp	His-SUMO	RIL codon Plus	Cmp	SB	0.20	30	5	Talon	Very poor	Low purity
1	CaBP4	TrcHisTEV	Amp	His	RIL codon Plus	Cmp	SB	0.20	30	5	Talon	Poor	Improved cleavage
2	Opt CaBP4	SUMO-Pro	kan	His-SUMO	BL21	-	M9	1.00	37	3	Talon	Good	
2	Opt CaBP4	SUMO-Pro	kan	His-SUMO	BL21	-	M9	1.00	18	Overnight	Talon	Very good	Efficient cleavage, high purity
4	CaBP8 FL	pETM11	Amp	His	BL21	-	SB	0.10	30	5	Talon	Very poor	Insoluble
4	CaBP8 FL	pETM11	Amp	His	rosetta	Cmp	SB	0.10	30	5	Talon	Very poor	Insoluble
4	CaBP8 FL	pGEX-6P1	Amp	GST	BL21	-	M9	0.05	20	Overnight	Glutathione Sepharose	Very poor	Mainly insoluble
4	CaBP8 FL	pGEX-6P1	Amp	GST	RP codon Plus	Cmp	M9	0.10	20	Overnight	Glutathione Sepharose	Very poor	Mainly insoluble
4	CaBP8 FL	pGEX-6P1	Amp	GST	RP codon Plus	Cmp	SB	0.10	30	5	Glutathione Sepharose	Very poor	plus 0.5% tween, insoluble
4	CaBP8 FL	pGEX-6P1	Amp	GST	RP codon Plus	Cmp	SB	0.10	30	5	Glutathione Sepharose	Very poor	plus 0.5% CHAPS, insoluble
4	CaBP8 FL	TrcHisA	Amp	His	Rosetta	Cmp	M9	0.10	20	Overnight	Talon	Non	No bacterial growth
4	CaBP8 FL	TrcHisA	Amp	His	Rosetta	Cmp	SB	0.10	30	7	Talon	Non	Insoluble
4	CaBP8 FL	TrcHisA	Amp	His	RP codon Plus	Cmp	SB	0.10	18	Overnight	Talon	Poor	Low purity
4	CaBP8 FL	TrcHisA	Amp	His	RP codon Plus	Cmp	M9	0.50	30	Overnight	Talon	Poor	Low purity
5	CaBP7 FL	pGEX-6P1	Amp	GST	BL21	-	M9	0.05	20	Overnight	Glutathione Sepharose	Very poor	Mainly insoluble
5	CaBP7 FL	pGEX-6P1	Amp	GST	RP codon Plus	Cmp	M9	0.10	20	Overnight	Glutathione Sepharose	Very poor	Mainly insoluble
6	CaBP7 1-188	pETM11	Amp	His	Rosetta	Cmp	SB	0.10	30	7	Talon	Very poor	Low expression
6	CaBP7 1-188	pGEX-6P1	Amp	GST	BL21	-	M9	0.10	20	Overnight	Glutathione Sepharose	Poor	Mainly insoluble, double bands observed, poor cleavage
6	CaBP7 1-188	pGEX-6P1	Amp	GST	Rosetta	Cmp	SB	0.10	20	Overnight	Glutathione Sepharose	Good	
6	CaBP7 1-188	pGEX-6P1	Amp	GST	RP codon Plus	Cmp	M9	0.10	20	Overnight	Glutathione Sepharose	Poor	Mainly insoluble, cleavage inefficient
6	CaBP7 1-188	pGex-N2	Amp	GST	Arctic express RIL codon +	Cmp	SB	0.50	10	Overnight	Glutathione Sepharose	Non	
6	CaBP7 1-188	pGex-N2	Amp	GST	RIL codon Plus	Cmp	SB	0.50	30	5	Glutathione Sepharose	Very poor	
6	CaBP7 1-188	TrcHisA	Amp	His	RIL codon Plus	Cmp	M9	0.50	30	Overnight	Talon	Very good	Precipitation after dialysis or concentrating
6	CaBP7 1-188	TrcHisA	Amp	His	RIL codon Plus	Cmp	M9	0.50	22	Overnight	Talon	Very good	Double bands observed
6	CaBP7 1-188	TrcHisTEV	Amp	His	RIL codon Plus	Cmp	SB	0.20	30	5	Talon	Poor	Improved cleavage

Table 6.1 continued. Summary of recombinant protein expression and conditions tested. Expression conditions are described for each of CaBP4, codon optimised CaBP4 (Opt CaBP4), full length CaBP7 (CaBP7 FL), full length CaBP8 (CaBP8 FL) and the truncations: CaBP8 1-192, CaBP7 1-188, codon optimised CaBP7 1-188 (Opt CaBP7 1-188) and codon optimised CaBP7 1-100 (Opt CaBP7 1-100). Different proteins are separated by alternating blocks of blue and white cells. Res. column indicates the antibiotic resistance encoded by the expression vector. Tag column lists the affinity tag encoded by the expression vector. Bact. Res column indicates the antibiotic resistance the expression bacteria. M9 = M9 minimal media, SB = superbroth media. Purification column lists the type of affinity resin used for purification of recombinant protein.

	Protein	Plasmid	Res.	Tag	Expression bacteria	Bact. Res.	Media	IPTG (mM)	Temp °C	Time, hrs	Purification	Yield	Additional Info
7	CaBP8 1-192	pGEX-6P1	Amp	GST	BL21	-	M9	0.10	20	Overnight	Glutathione Sepharose	Poor	Mainly insoluble, double bands observed, poor cleavage
7	CaBP8 1-192	pGEX-6P1	Amp	GST	Rosetta	Cmp	SB	0.10	20	Overnight	Glutathione Sepharose	Good	Double bands observed
7	CaBP8 1-192	pGEX-6p-1	Amp	GST	RP codon Plus	Cmp	M9	0.10	20	Overnight	Glutathione Sepharose	Poor	Mainly insoluble, inefficient cleavage
7	CaBP8 1-192	pGex-N2	Amp	GST	Arctic express RIL codon +	Cmp	SB	0.50	10	Overnight	Glutathione Sepharose	Non	
7	CaBP8 1-192	pGex-N2	Amp	GST	RIL codon Plus	Cmp	SB	0.50	30	5	Glutathione Sepharose	Very poor	
7	CaBP8 1-192	TrcHisA	Amp	His	RIL codon Plus	Cmp	M9	0.50	30	Overnight	Talon	Very good	Precipitation after dialysis or concentrating
7	CaBP8 1-192	TrcHisA	Amp	His	RIL codon Plus	Cmp	M9	0.50	22	Overnight	Talon	Very good	Double bands observed
7	CaBP8 1-192	TrcHisA	Amp	His	RIL codon Plus	Cmp	M9	0.50	22	Overnight	Talon	Very good	Low purity
7	CaBP8 1-192	TrcHisA	Amp	His	RIL codon Plus	Cmp	M9	0.80	22	Overnight	Talon	Very good	Low purity
7	CaBP8 1-192	TrcHisA	Amp	His	Rosetta	Cmp	M9	0.10	20	Overnight	Talon	Very poor	No Bacterial growth
7	CaBP8 1-192	TrcHisA	Amp	His	Rosetta	Cmp	SB	0.10	30	7	Talon	Good	Double bands observed
7	CaBP8 1-192	TrcHisA	Amp	His	RP codon Plus	Cmp	SB	0.10	18	Overnight	Talon	Poor	Low purity
7	CaBP8 1-192	TrcHisA	Amp	His	RP codon Plus	Cmp	SB	0.50	18	Overnight	Talon	Very good	
7	CaBP8 1-192	TrcHisA	Amp	His	RP codon Plus	Cmp	M9	0.50	30	Overnight	Talon	Good	Low purity
8	Opt CaBP7 1-188	SUMO-Pro	kan	His-SUMO	BL22	-	SB	1.00	37	3	Talon	Excellent	Did not precipitate
8	Opt CaBP7 1-188	SUMO-Pro	kan	His-SUMO	BL22	-	M9	1.00	37	3	Talon	Very good	Precipitation after dialysis
8	Opt CaBP7 1-188	TrcHisA	Amp	His	RIL codon Plus	Cmp	SB	0.50	18	Overnight	Talon	Very poor	Low purity
9	Opt CaBP7 1-100	SUMO-Pro	kan	His-SUMO	BL22	-	SB	1.00	37	3	Talon	Excellent	Did not precipitate
9	Opt CaBP7 1-100	SUMO-Pro	kan	His-SUMO	BL22	-	M9	1.00	37	3	Talon	Good	Precipitation after dialysis

Production of a GST tag can be energetically costly for expression bacteria and the use of a smaller affinity tag can improve protein expression (Waugh, 2005). For this reason the use of hexa-histidine (His_6)-tagging vectors was investigated. Various His_6-tagging vectors were evaluated, each having unique properties (Appendix Table A1). Expression of CaBP4, CaBP7 1-188 and CaBP8 1-192 from the pTrcHisA vector improved recombinant protein yield. The His_6 tag encoded by pTrcHisA is removable by treatment with enterokinase. This protease is less efficient than other commercially available enzymes and therefore, in order to enhance the efficiency of tag removal, a TEV cleavage site was cloned into the vector. CaBP4 and CaBP7 1-188 were cloned into this new plasmid (pTrcHis-TEV) and efficient TEV protease cleavage of the recombinant proteins was acheived.

Despite the improved expression using the pTrcHisA expression plasmid, new problems were encountered. A protein doublet was frequently observed in eluates of CaBP7 1-188 and CaBP8 1-192, suggesting that either proteolysis or premature translation termination was occurring. In addition, when the proteins were dialysed to remove imidazole which is present in the elution buffers, the proteins exhibited a propensity to precipitate. Protein loss was also observed using ultrafiltration columns for buffer exchange and concentration, suggesting that the protein may have also precipitated during this process or was associating non-specifically with the ultrafiltration membrane.

The possible premature translation termination, and the observed improvement in expression upon transformation into modified *E. coli,* suggested that there was a potential issue with rare tRNA use in the gene encoded by these plasmids. For this reason synthetic, *E. coli* codon optimised, clones were generated. Codon optimised CaBP7 1-188, cloned into the pTrcHisA vector, exhibited reduced protein expression compared with the non-optimised sequence. For this reason, the codon optimised clones were cloned into an alternative expression plasmid – pE-SUMOPRO, which employs a His_6 affinity tag in conjunction with the yeast Small Ubiquitin-like Modifier (SUMO) protein, Smt3. Fusion of ubiquitin or ubiquitin-like proteins has been shown to exert chaperoning effects on fusion proteins made in yeast and

bacteria thereby improving yield and solubility (Zuo *et al*., 2005). It has been suggested that the increased solubility observed in these fusions is related to the outer hydrophillicity and inner hydrophobicity of SUMO, generating a detergent-like effect to solubilise the fusion protein (Malakhov *et al*., 2004).

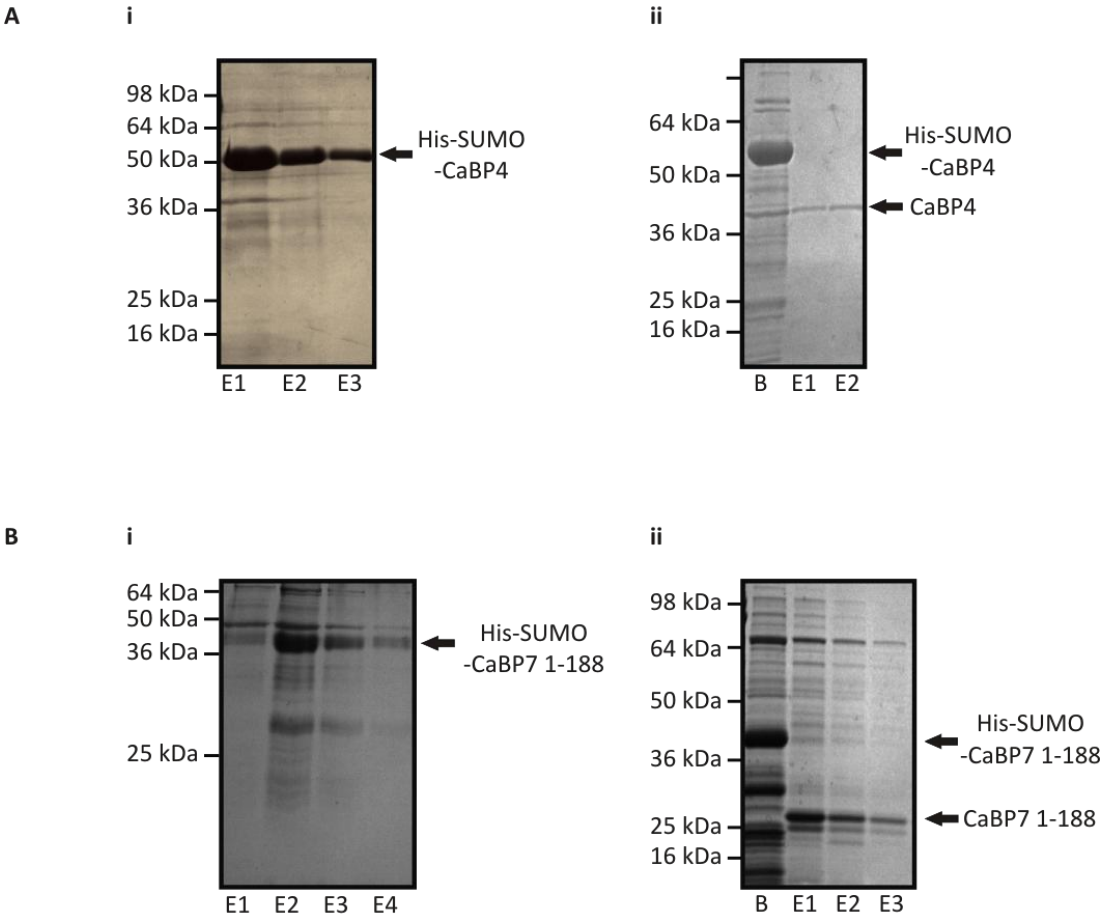

Figure 6.1. Example SDS-PAGE gels illustrating the expression and tag cleavage of ^{15}N - labelled His_6-SUMO-CaBP4 and His_6-SUMO-CaBP7 1-188. A i) His_6-SUMO-CaBP4; ii) His_6-SUMO-CaBP4 cleaved directly from affinity resin B i) His_6-SUMO-CaBP7 1-188; ii) His_6-SUMO-CaBP7 1-188 cleaved directly from beads. E1, E2, E3… etc. indicate succesive elutionsfrom either imidazole elutions (Ai and Bi) or from after sumo protease treatment of protein immobilized on affinity resin to remove SUMO tag (Aii and Bii). B = protein bound to affinity resin. Each lane represents the amount of protein in 5 µl of the indicated fraction.

Use of SUMO fusions is emerging as an efficient method for the optimisation of expression and solubility of difficult to express proteins (Butt *et al*., 2005). In addition, contrary to the other fusion tags discussed here, SUMO can be proteolytically removed without leaving residual amino acids (Malakhov *et al*., 2004). SUMO protease achieves this by primarily recognising the tertiary structure of the SUMO protein rather than a particular consensus amino acid sequence. The expression of both codon optimised CaBP4 and CaBP7 1-188 was greatly improved using this vector system in standard BL21 cells, increasing yields by up to 40-fold in rich media protein preparations, compared to recombinant protein expressed from pTrcHisA. Labelled minimal media protein preparations were therefore trialled using these constructs (Figure 6.1).

His_6-SUMO-tagged CaBP4 and CaBP7 1-188 also precipitated upon removal of imidazole by either dialysis or ultrafiltration. Imidazole must be removed in order to allow purification of the protein away from the SUMO tag following cleavage with SUMO protease. Multiple buffer conditions were tested, but all proved incapable of preventing protein precipitation. Although up to 50% of the protein was lost through precipitation, sufficient amounts of protein remained in solution to allow the generation of preliminary NMR spectra.

6.2.2. Optimisation of CaBP4 for NMR analysis

Prior to the collection of large amounts of NMR data, the protein sample should be optimised for concentration, ionic strength, pH and temperature to maximise NMR spectra quality (Muskett, 2011). Acquisition of the data required for backbone and side-chain assignments can take several weeks, therefore the sample must be stable over extended periods of time. A ^{15}N-labelled protein sample was, therefore, synthesised, then various buffer conditions were assessed by monitoring the improvement or deterioration of NMR spectra.

Initially, ^{1}H-^{15}N-heteronuclear single-quantum correlation (HSQC) spectra for uncleaved His_6-SUMO-CaBP4 were recorded. The fusion protein was left uncleaved

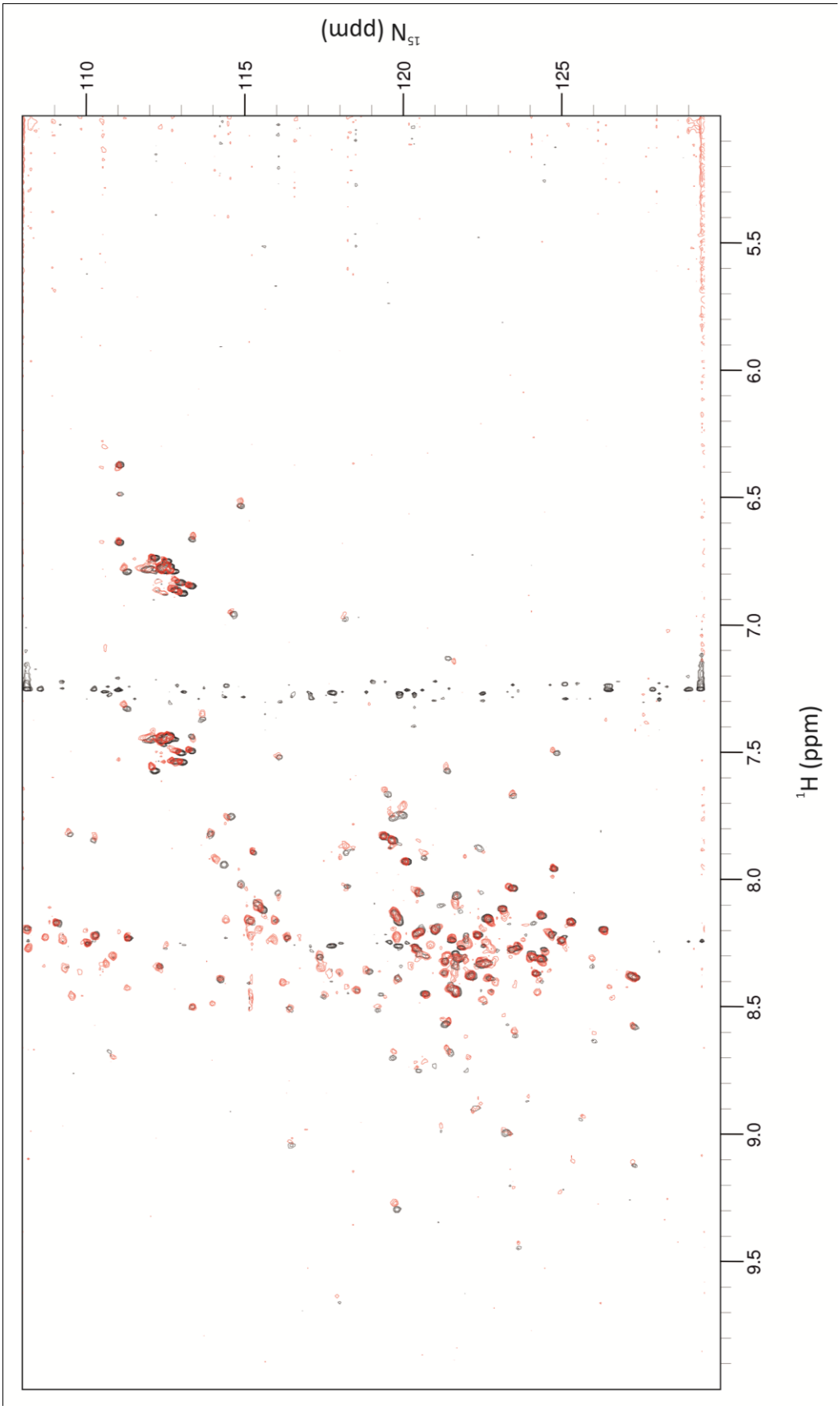

Figure 6.2. Overlay of 2D ^{1}H-^{15}N HSQC NMR spectra of His$_6$-SUMO-CaBP4. Black = His$_6$-SUMO-CaBP4 in 50 mM sodium phosphate buffer pH 7.0, 300 mM NaCl, 200 mM imidazole. Red = His$_6$-SUMO-CaBP4 in 25 mM Tris.HCl pH 6.5, 50 mM NaCl, 50 mM, arginine 50 mM glutamine.

to optimise buffer conditions, whilst minimising aggregation and precipitation by having the SUMO tag present to enhance fusion-protein solubility. HSQC spectra correlate the chemical shifts of the ^{1}H and ^{15}N nuclei for each amide group. The peaks in each spectrum therefore represent the main chain and side chain amide groups of the protein. This provides a residue specific fingerprint of an individual protein's conformation under a given set of conditions. Figure 6.2 shows two overlaid spectra for uncleaved CaBP4: one captured immediately after protein purification in 'Talon Buffer' with 200 mM imidazole, the other obtained from material dialysed into 'RE buffer' containing 50 mM arginine (R) and 50mM glutamine (E) (see table 6.2 for detailed descriptions of NMR buffer components). The addition of free amino acids such as glutamine and arginine has been shown to increase the stability and solubility of recombinant proteins (Golovanov *et al*., 2004). Addition of these amino acids failed to prevent precipitation of CaBP4, however, enough soluble protein (~ 150 µM) remained to permit acquisition of a ^{1}H-^{15}N-HSQC under these buffer conditions. Figure 6.2 highlights that there was little difference in NMR spectrum quality obtained under the two buffer conditions.

Protein dialysed into RE buffer was cleaved using SUMO protease and free SUMO removed by re-passing over affinity resin. An NMR spectrum of the cleaved material was then acquired (Figure 6.3, black). The ^{1}H-^{15}N-HSQC spectrum of cleaved CaBP4 is poorly resolved with narrow chemical shift dispersion in the amide proton dimension ranging between 8.5 and 7.5 ppm. The number of observed peaks is lower than expected (74 versus 275) and there is a mixture of very sharp and very weak peaks. The weak peaks may have low intensity due to exchange broadening caused by either dimerisation or conformational heterogeneity (Wingard *et al*., 2005, Cavanagh *et al*., 2007c). The poor chemical shift dispersion is indicative of an unstructured protein in a molten globule state. Sharp peaks often represent an unstructured, flexible peptide region and this spectrum exhibits features consistent with this. CaBP1 has been previously shown to possess a structurally disordered N-terminus (Park *et al*., 2011) and the sharp peaks observed in the CaBP4 spectrum may, likewise, represent the extended N-terminal region of the protein. In accordance with this, the PSIPRED protein secondary structure prediction server

(http://bioinf.cs.ucl.ac.uk/psipred/) predicted a region of coiled coil extending between residues 7 - 105.

Table 6.2. Table of Buffers used for preparation of NMR samples.

Buffer Name	**Buffer Components**
RE Buffer	25 mM Tris.HCl pH 6.5, 50 mM NaCl, 50 mM Arginine (R), 50 mM Glutamine (E)
Talon Buffer	50 mM sodium phosphate buffer pH 7.0, 300 mM NaCl
Low Octylglucoside Buffer	25 mM Tris.HCl pH 6.5, 150mM NaCl, 5 mM $CaCl_2$, 2 mM octylglucoside, 1 mM β-mercaptoethanol
High Salt Buffer	20 mM TrisHCl pH 6.5, 150 mM NaCl
Low Imidazole Buffer	25mM sodium phosphate buffer pH 7.0, 150 mM NaCl, 25 mM imidazole
HEPES Buffer	20 mM HEPES pH 7.5, 50 mM NaCl, 10 mM octylglucoside
EDTA/EGTA Buffer	20 mM HEPES pH 7.5, 50 mM NaCl, 2 mM octylglucoside 5 mM EDTA, 5 mM EGTA
Low Octylglucoside HEPES Buffer	20 mM HEPES pH 7.5, 50 mM NaCl, 2 mM octylglucoside

Structural studies of CaBP1 reported a poorly resolved structure suggestive of a molten globule conformation in the absence of Mg^{2+} and Ca^{2+} (Li *et al*., 2009). Addition of Mg^{2+} or Ca^{2+} dramatically changed the spectrum of CaBP1, with a greater number of peaks appearing and at a more uniform intensity (Li *et al*., 2009). Addition of these metal ions also substantially improved the chemical shift dispersion of peaks in the spectra. In particular, two downfield shifted peaks appeared in the Mg^{2+} spectra and three appeared in the Ca^{2+} spectra, which could be assigned to the glycine residues at the 6^{th} postion of the three functional EF-hands of CaBP1 (Li *et al*., 2009). This is a characteristic feature of NMR spectra

belonging to EF-hand containing Ca^{2+}-binding proteins (Lusin *et al*., 2008, Schwenk *et al*., 2008, Aravind *et al*., 2008, Wingard *et al*., 2005). In order to assess whether CaBP4 might behave in a similar fashion, 1 mM $CaCl_2$ was added to the cleaved sample (Figure 6.3, red). Figure 6.3 illustrates that the spectra with and without 1 mM $CaCl_2$ completely overlaid and no changes or improvements upon addition of Ca^{2+} were observed.

Up to 50% of CaBP4 recombinant protein was lost during the purification process due to a combination of precipitation and multiple purification steps. In an attempt to improve CaBP4 solubility and to obtain a more concentrated sample, recombinant protein was not eluted from the affinity resin. Instead, the resin-bound protein was washed directly in an appropriate NMR buffer followed by SUMO protease addition. This had the effect of simultaneously cleaving the SUMO tag from the protein while purifying both the tag and protease (which is itself a his_6-tagged protein) away from the free CaBP4 in a one step process. Most importantly, this method avoids dialysis where the majority of the expressed protein was lost through precipitation. An example SDS-PAGE image (Figure 6.1A) shows CaBP4, before and after cleavage directly from affinity resin, using this approach.

Buffer conditions were modified in an attempt to aid the solubility of the cleaved protein. NMR studies of the KChIP subfamily of NCS proteins (Schwenk *et al*., 2008, Lusin *et al*., 2008) reported that addition of octylglucoside stabilised these proteins and prevented aggregation. Therefore the effect of octylglusoside on CaBP4 NMR spectra was assessed. Cleavage directly from affinity resin was not efficient at high concentrations of octylglucoside (20 mM), therefore a concentration of 2 mM was used in the cleavage buffer ('Low Octylglucoside Buffer', Table 6.2). Addition of salts also increases the solubility of proteins and decreases aggregation, therefore 150 mM NaCl was included. This is the recommended maximum concentration of salt which can be used in NMR studies due to dielectric losses experienced at high ionic strength (Muskett, 2011). As addition of Ca^{2+} has generally been shown to improve the spectra of Ca^{2+}-binding proteins, 5 mM $CaCl_2$ was included in all buffers.

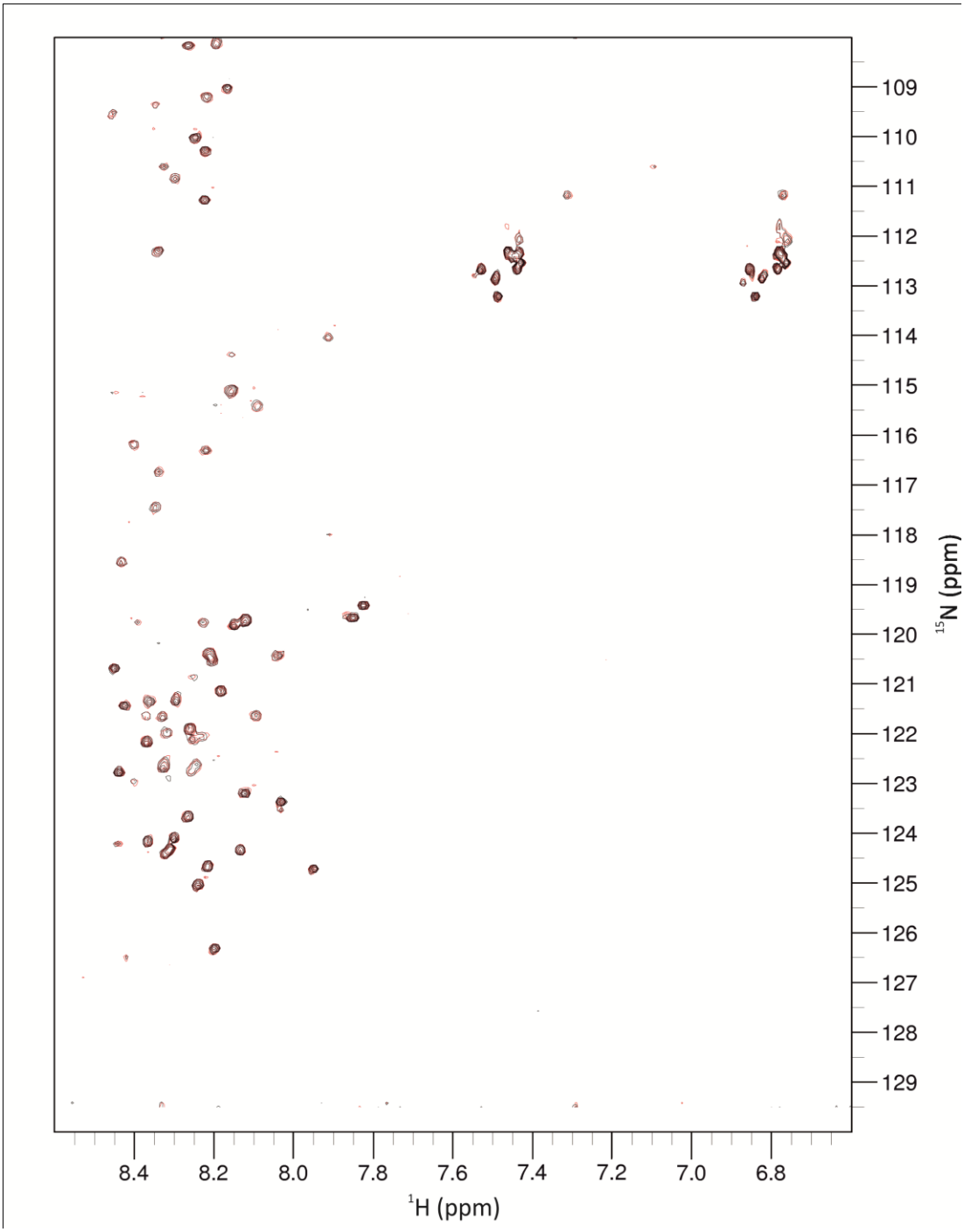

Figure 6.3. Overlay of 2D ^{1}H-^{15}N HSQC NMR spectra of cleaved CaBP4 in the presence and absence of $CaCl_2$. Black = 0 mM $CaCl_2$. Red = 1 mM $CaCl_2$. The sample was prepared in 25 mM Tris.HCl, pH 6.5, 50 mM NaCl, 50 mM arginine, 50 mM glutamine.

Although there is only one cysteine residue in CaBP4, β-mercaptoethanol was included to reduce disulphide bonds.

The spectrum obtained under these conditions was greatly improved compared to the original spectra (Figure 6.4A versus Figure 6.3). A greater number of structured peaks can be observed with wider chemical shift dispersion. Of particular note is the appearance of a downfield shifted peak in the region that is characteristic of an EF-hand glycine at the 6^{th} position (circled in green, Figure 6.4A). There were a greater number of weaker peaks and the sharp peaks originally observed in figure 6.3 intensified. The appearance of an increased number of weak peaks, representing an intermediate conformational exchange (Cavanagh *et al*., 2007c), may be due to either an increase in protein concentration, improved buffer conditions, or both. The remaining sharp peaks are again indicative of an unstructured region within the protein.

Elevation of sample temperature in NMR experiments can improve the signal to noise ratio provided the protein does not thermally denature over the temperature range employed. Figure 6.4C shows an overlay of five CaBP4 NMR spectra recorded at increasing temperatures. The initial spectrum discussed above was recorded at 298 K and the temperature was increased stepwise to 318 K (Figure 6.4B). Increasing the temperature increased signal to noise and many more widely dispersed weak peaks became visible, along with a drop in intensity of the original sharp peaks. The number of visible peaks is proportional to the increasing temperature (Figure 6.4D) with 126 peaks counted in the 298 K spectrum and 208 peaks in the 318 K spectrum. Importantly, three downfield shifted peaks can be seen in the 318 K spectrum in the characteristic region for EF-hand glycines (circled in green, Figure 6.4B). This is in agreement with the three active EF-hand motifs identified in CaBP4. Only one glycine is apparent in the 298 K spectrum, two at 303 K and 308 K, and three in the 313 K and 318 K spectra, indicating a gradual improvement in spectral resolution with increasing temperature. Despite the substantial enhancement of CaBP4 NMR spectra after sample optimisation, there remained insufficient peaks to represent all CaBP4 residues. The spectra quality, although improved, lacked the resolution to warrant expression of a $^{15}N/^{13}C$ double-labelled CaBP4 sample.

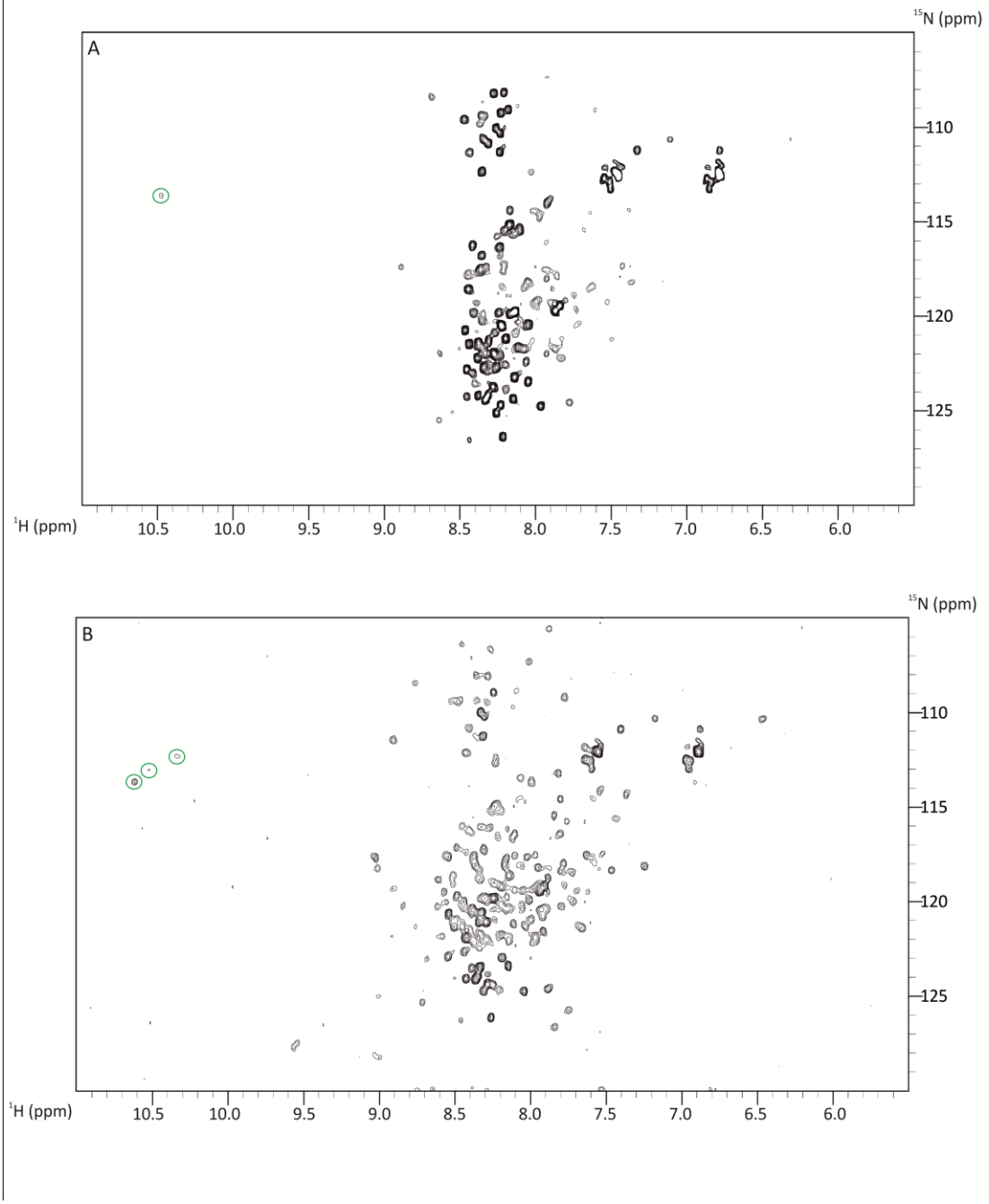

Figure 6.4 A and B.2D ^{1}H-^{15}N HSQC NMR spectra of cleaved CaBP4 at increasing temperatures. A) CaBP4 spectrum at 298 K; B) CaBP4 spectrum at 318 K. The peaks circled in green represent glycines at the 6th position of the three EF-hand Ca^{2+} binding loops in CaBP4. One is visible at 298 K (A) whereas three are visible at 318 K (B). The sample was prepared in 25 mM Tris.HCl pH 6.5, 150 mM NaCl, 5 mM $CaCl_2$, 2 mM octylglucoside, 1 mM β-mercaptoethanol.

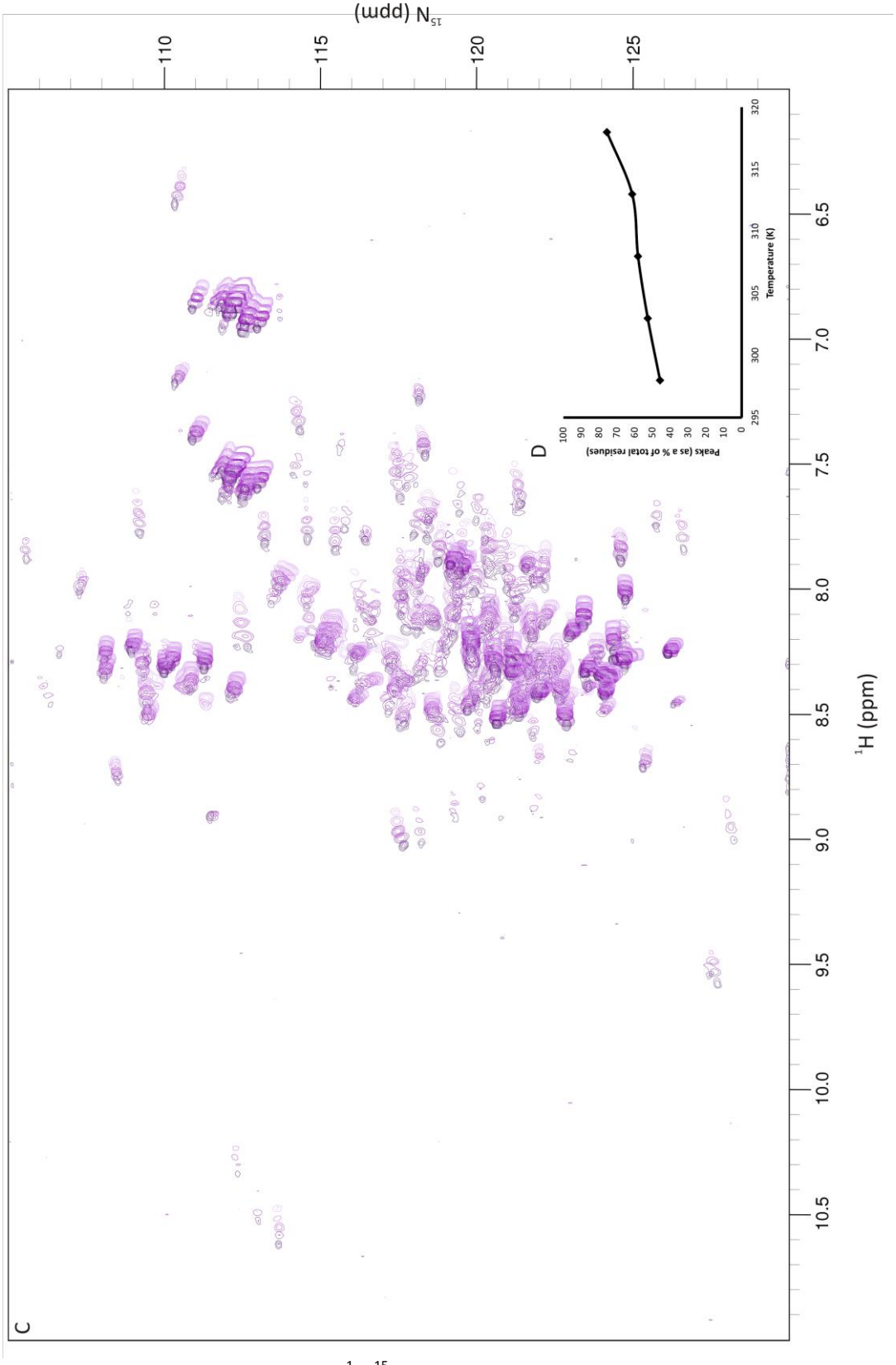

Figure 6.4 C and D. C) Overlay of ^{1}H-^{15}N HSQC NMR spectra of cleaved CaBP4 at increasing temperatures: 298 K, 303 K, 308 K, 313 K and 318 K. The colour changes from pale lilac to dark purple as temperature increases. D) Graph showing the increase in the number of peaks observed with increasing acquisition temperature as a percentage of the expected number of peaks. The sample was prepared in 25 mM Tris.HCl pH 6.5, 15 mM NaCl, 5 mM $CaCl_2$, 2 mM octyl-glucoside, 1 mM β-mercaptoethanol.

6.2.3. Optimisation of CaBP7 1-188 for NMR analysis

As observed with CaBP4, precipitation of recombinant CaBP7 1-188 was encountered. Therefore the SUMO tag was cleaved whilst immobilised on affinity resin to avoid dialysis steps which had proven costly for protein yield in CaBP4 preparations (Figure 6.1B). Figure 6.5A shows a ^{1}H-^{15}N HSQC spectrum of CaBP7 1-188 in 'High Salt buffer' (Table 6.2) with no added Ca^{2+}. Peaks arising from folded regions of the protein can be observed and there are two downfield shifted peaks (circled in green, Figure 6.5A and B) which likely represent glycines at the 6th position of the two functional EF-hands. These characteristic downfield shifted peaks are generally only seen when the EF-hands are occupied by Ca^{2+}. This, therefore, suggests this protein was not in the apo form. No defined peaks were present in the central region of the spectrum and substantial peak overlap was observed, characteristic of an aggregated protein. CaBP7 1-188 has five cysteine residues and this may increase the likelihood of aggregation through the formation of incorrect disulphide bonds between protein monomers.

Titrations of octylglucoside and $CaCl_2$ were performed on the sample to monitor any changes in the quality of the CaBP7 1-188 spectra. Figure 6.5C shows an overlay of the spectra obtained at increasing octylglucoside concentrations. When the 0 mM (Figure 6.5A) and the 30 mM (Figure 6.5B) spectra are compared, there is an increase in both the number and resolution of peaks at the higher concentration of detergent (circled in red, Figure 6.5B). A possible interpretation of this data is that the presence of octylglucoside reduced, but did not completely prevent protein aggregation.

A $CaCl_2$ titration was next performed to examine if this would further improve the spectra (Figure 6.6). Subtle changes were observed and some peaks became more defined and less overlapped (circled in red, Figure 6.6A and B) whilst others became weaker and less resolved (circled in green, Figure 6.6A and B). Preparation of CaBP7 1-188 cleaved directly in 'Low Octylglucoside Buffer' (Table 6.2) did not noticeably improve the ^{1}H-^{15}N HSQC spectrum (Figure 6.7).

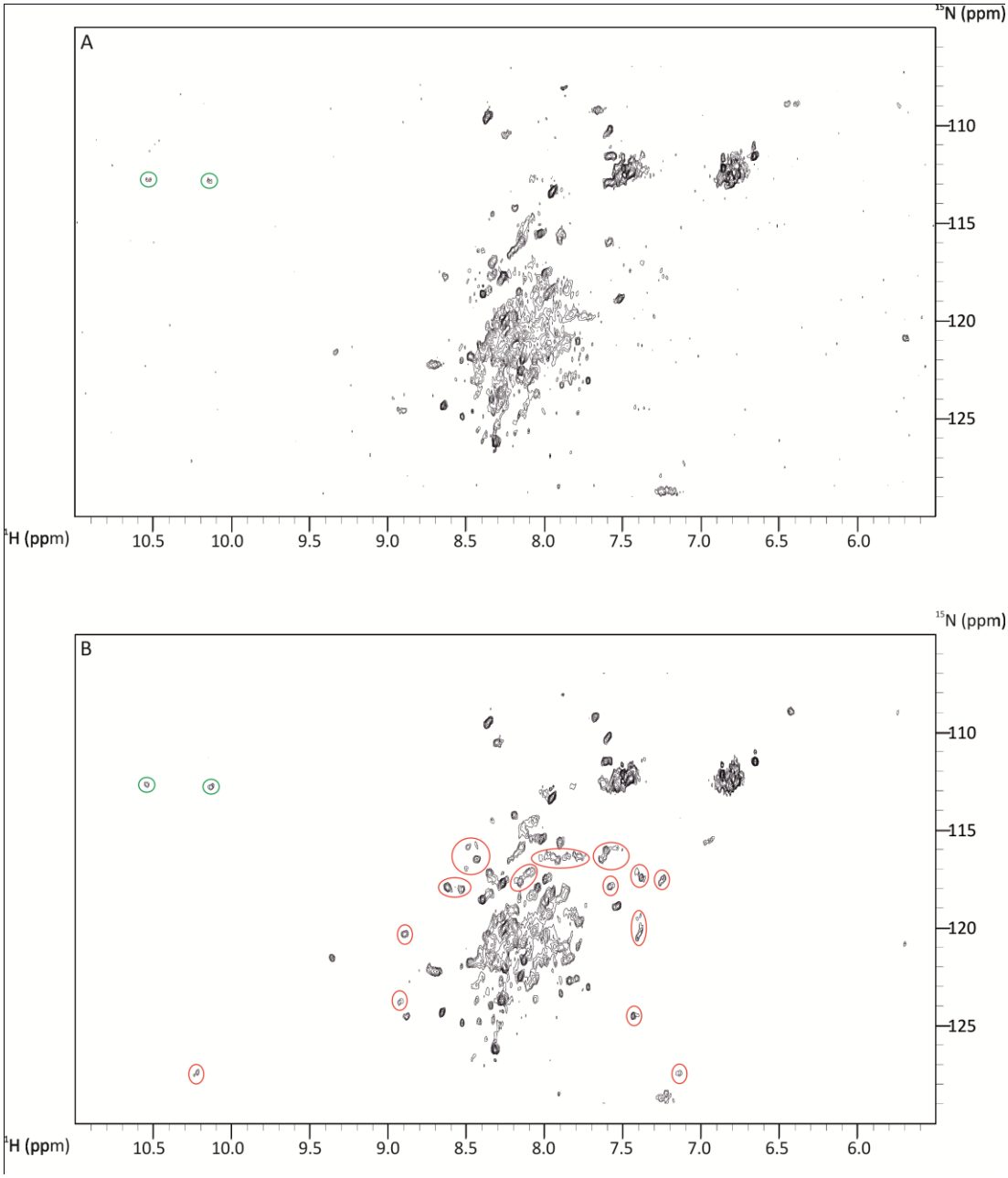

Figure 6.5 A and B. Two-dimensional ^{1}H-^{15}N HSQC NMR spectra of cleaved CaBP7 1-188 with increasing concentrations of octylglucoside. A) 0 mM octylglucoside; B) 30 mM octylglucoside. Peaks circled in green represent glycines at the 6th position of the two EF-hand Ca^{2+} binding loops. Peaks circled in red only appear in the spectra acquired in the presence of 30 mM octylglucoside. The sample was prepared in 20 mM Tris.HCl pH 6.5, 150 mM NaCl.

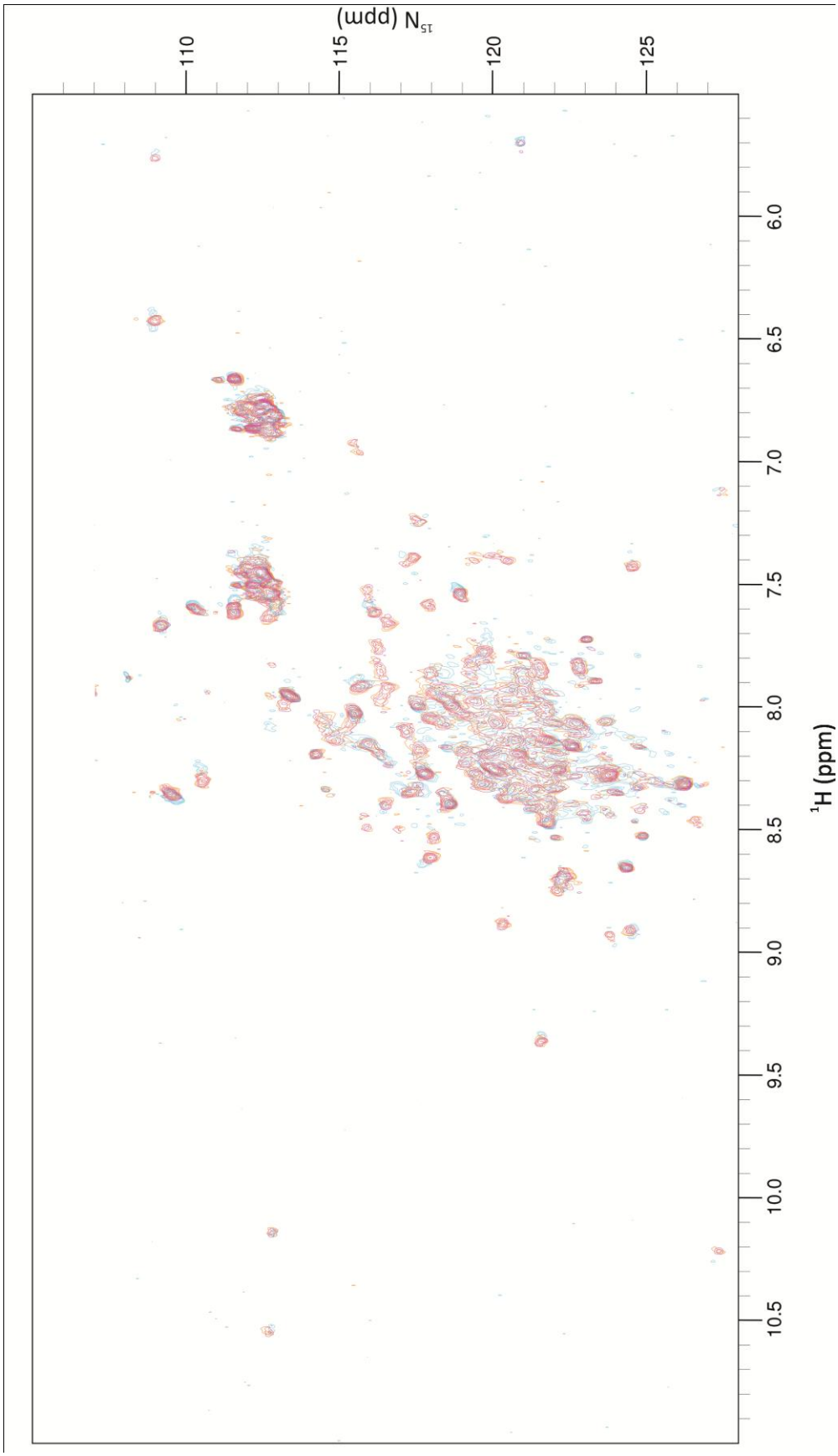

Figure 6.5 C. Overlay of ^{1}H-^{15}N HSQC NMR spectra of cleaved CaBP7 1-188 with increasing concentrations of octylglucoside: 0 mM (peach), 5 mM (blue), 10 mM (yellow), 20 mM (lilac) and 30 mM (pink) octylglucoside. The sample was prepared in 20 mM Tris.HCl pH 6.5, 150 mM NaCl.

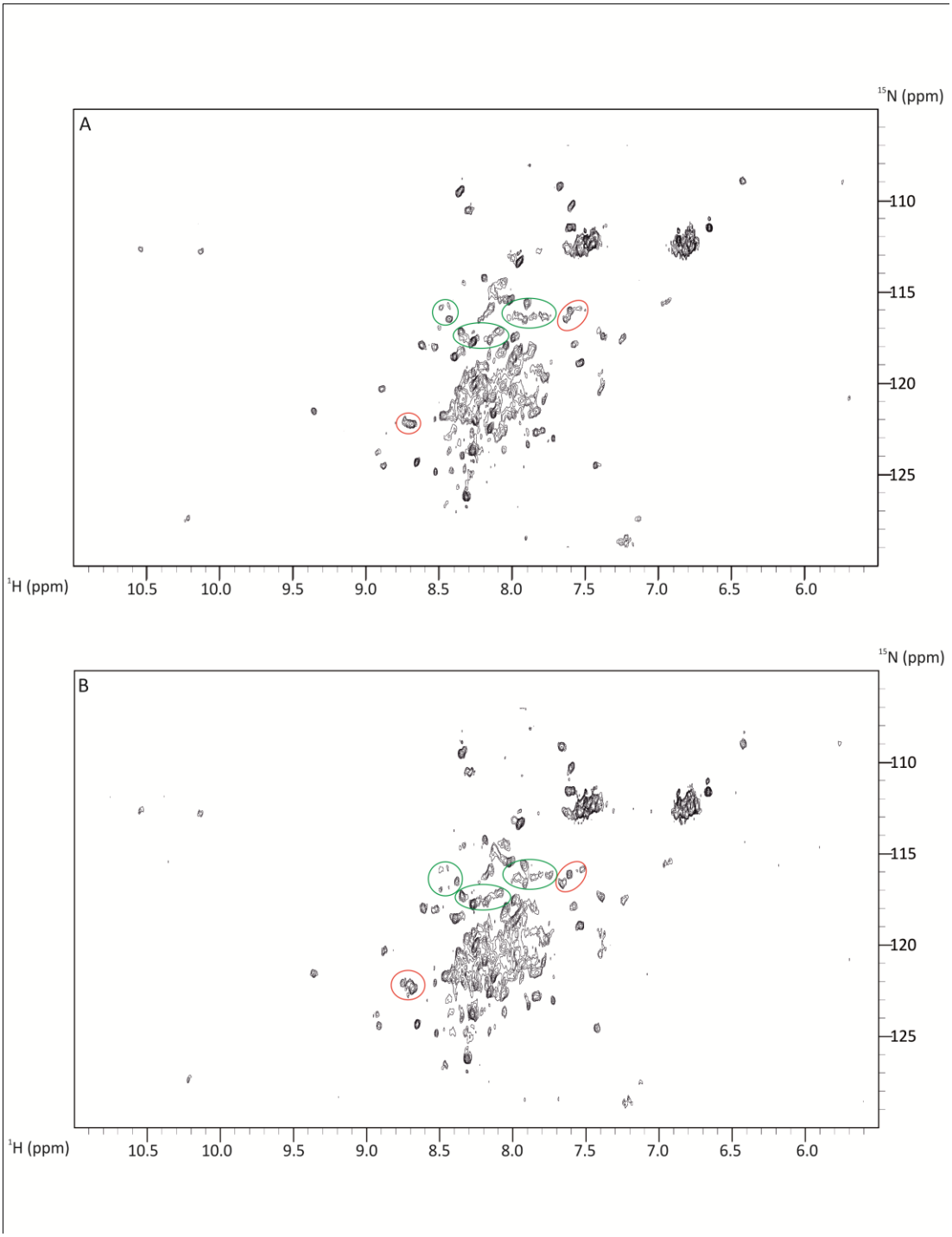

Figure 6.6 A and B. 2D ^{1H}-^{15}N HSQC NMR spectra of cleaved CaBP7 1-188 with increasing $CaCl_2$ concentration. A) 0 mM $CaCl_2$ B) 10 mM $CaCl_2$. Peaks which became more defined with increasing $CaCl_2$ are circled in red and peaks which became less defined and more overlapped are circled in green. The sample was prepared in 20 mM Tris.HCl pH 6.5, 150 mM NaCl, 30 mM octylglucoside.

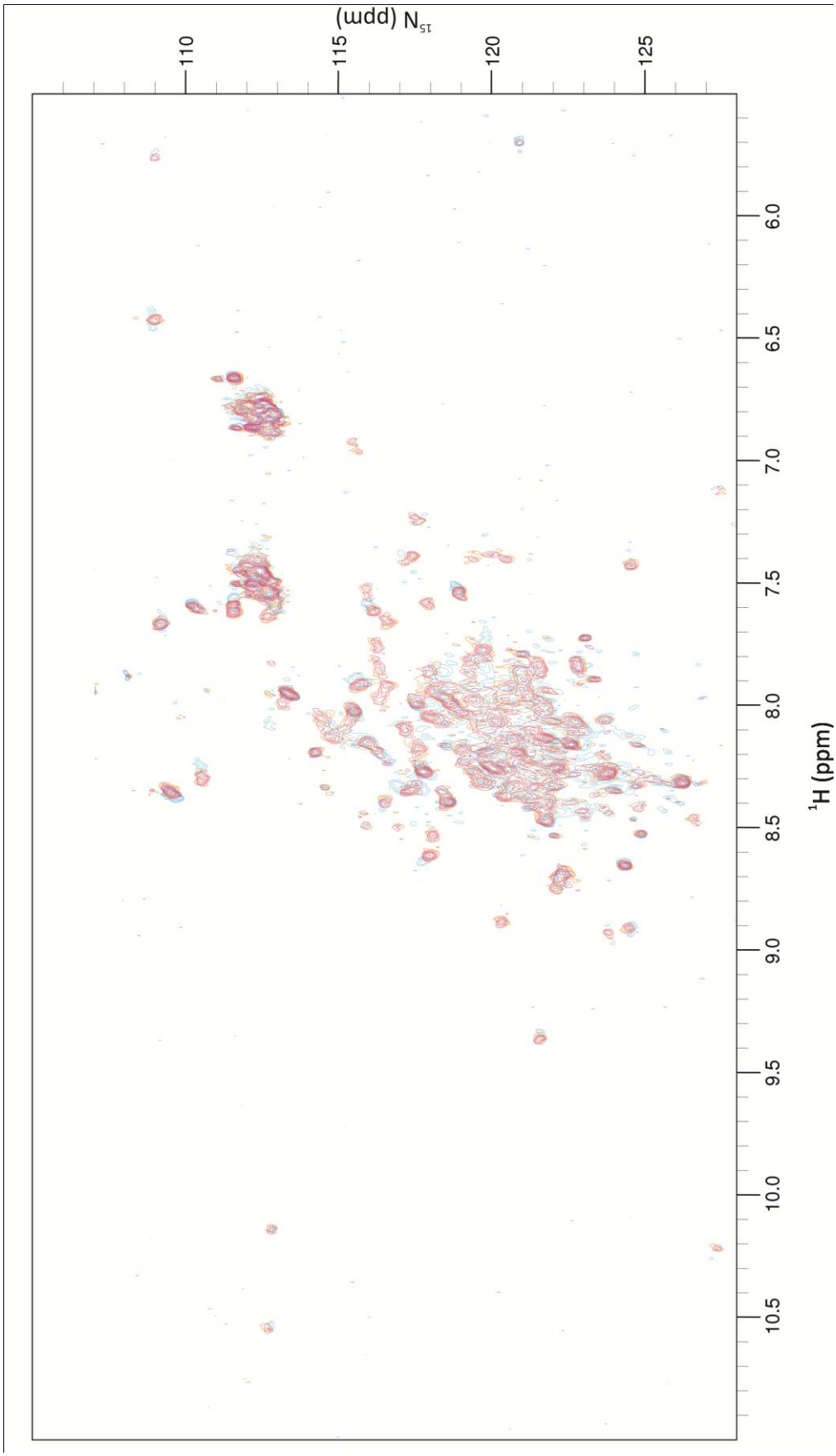

Figure 6.6 C. Overlay of ^{1}H-^{15}N HSQC NMR spectra of cleaved CaBP7 1-188 with increasing $CaCl_2$ concentration: 0 mM (blue), 2 mM (pink) and 5 mM (orange) $CaCl_2$. The sample was prepared in 20 mM Tris.HCl pH 6.5, 150 mM NaCl, 30 mM octylglucoside.

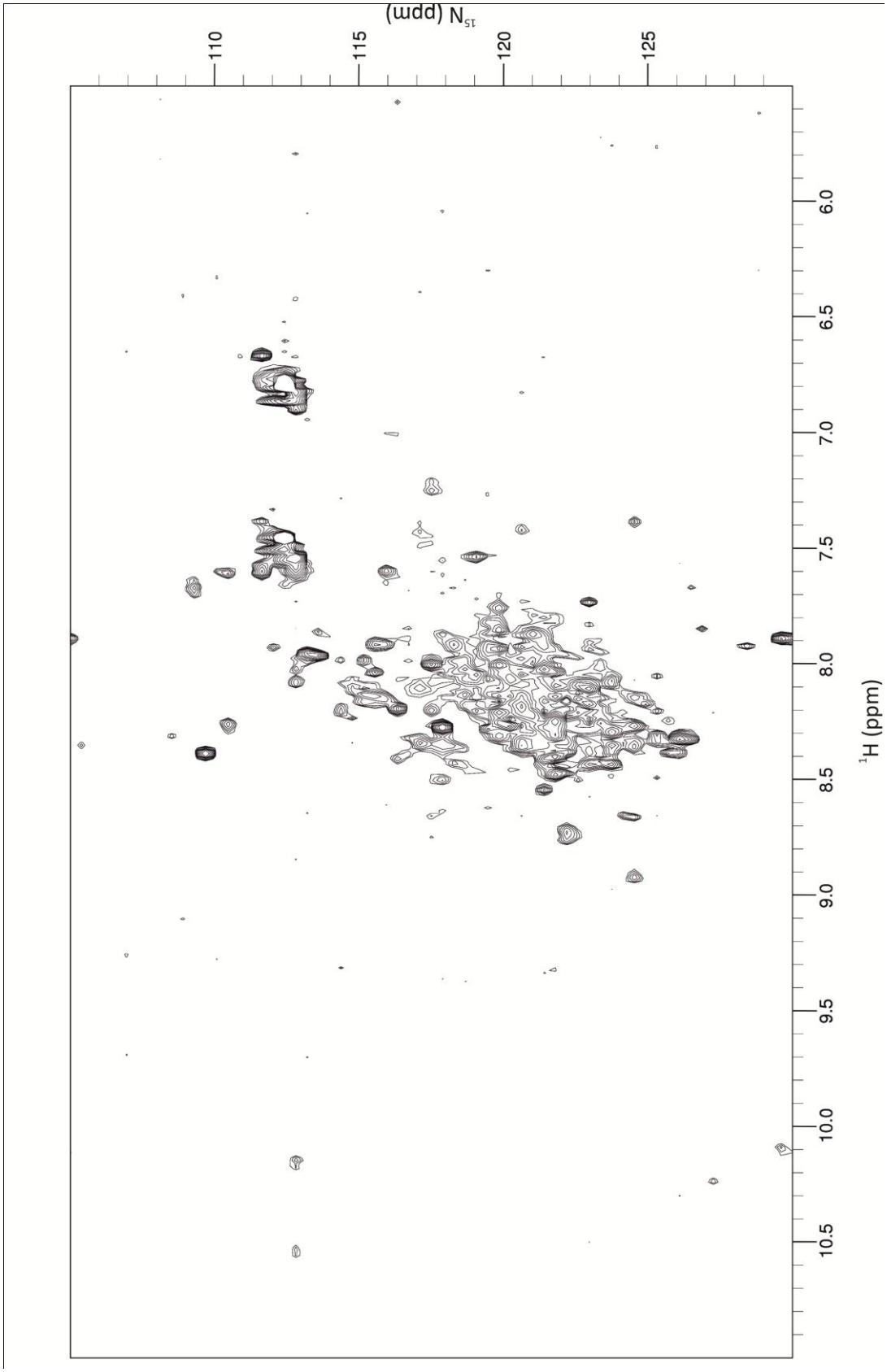

Figure 6.7. Two-dimensional ^{1}H-^{15}N HSQC NMR spectrum of cleaved CaBP7 1-188. The sample was prepared in 20 mM Tris.HCl pH 6.5, 150 mM NaCl, 5 mM $CaCl_2$, 2 mM octylglucoside, 1 mM β-mercaptoethanol.

The persistent aggregation of CaBP7 1-188 under all experimental conditions tested prevented structure determination within the timescale of this project. A potential explanation for the aggregation lies with the 5 cysteine residues found in the protein C-terminus. For this reason a new expression construct was generated by inserting a stop codon after the first 100 amino acids of CaBP7 1-188 in pE-SUMOPRO. This construct encoded the cysteine free N-terminus of CaBP7 (CaBP7 1-100) which exhibits higher sequence similarity with CaM and CaBP1S than the C-terminus and encompasses the two active EF-hands of CaBP7. This portion of the protein is therefore useful for comparison of the structure of the functional Ca^{2+}-binding motifs with related domains in other Ca^{2+}-sensors.

6.2.4. Optimisation of CaBP7 1-100 for NMR analysis

His_6-SUMO-CaBP7 1-100 expressed at levels comparable with His_6-SUMO-CaBP7 1-188 using standard BL21 *E. coli* (Figure 6.8A) and, like CaBP7 1-188, precipitated on removal of imidazole. Unlike CaBP4 (30.4 kDa) and CaBP7 1-188 (21.6 kDa), CaBP7 1-100 (11.4kDa) was more manageable in size even with His_6-SUMO (12.3 kDa) attached. Therefore, to avoid problems with precipitation, NMR optimisation was performed on the SUMO tagged protein.

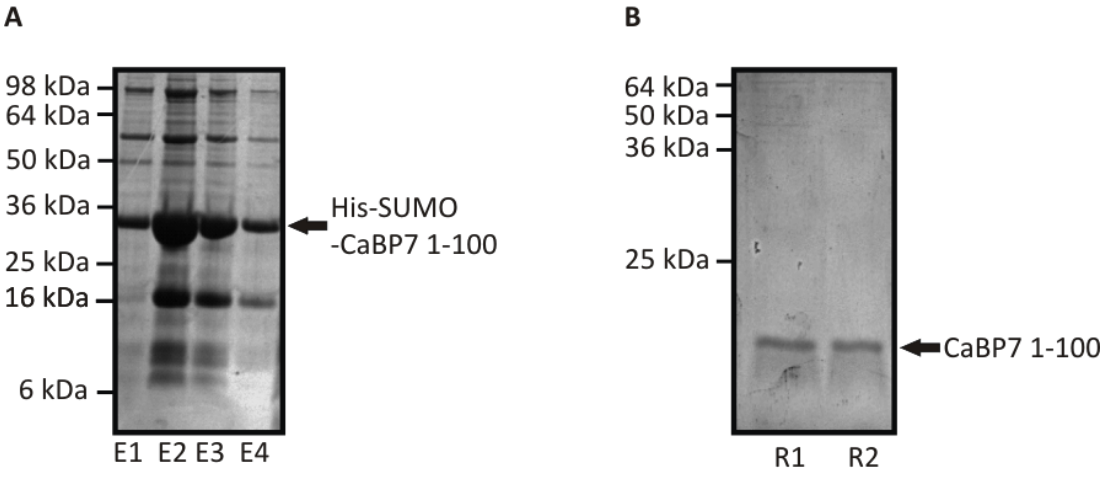

Figure 6.8. Example SDS-PAGE gels illustrating the expression and tag cleavage of ^{15}N - labelled His-SUMO-CaBP7 1-100. A) His_6-SUMO-CaBP7 1-100; B) CaBP7 1-100 cleaved and repassed over nickel resin. E = elution fraction, R = repass fraction (after cleavage). Each lane represents the amount of protein in 5 µl of the indicated fraction.

Figure 6.9 shows the ^{1}H-^{15}N HSQC spectrum of SUMO-CaBP7 1-100 in black, overlaid with the spectrum of SUMO in red. His_6-SUMO-CaBP7 1-100 was prepared in 'Low Imidazole Buffer' (Table 6.2) for the acquisition of this spectrum. Peaks in the black spectrum that are at similar positions to those in the red spectrum belong to the SUMO tag. Many non-overlapping peaks can also be seen, belonging to CaBP7 1-100. These peaks were well dispersed, suggesting that the protein was well structured. The two characteristic downfield shifted folded peaks of the EF-hand glycines were also visible, once again suggesting that the EF-hands were already occupied by Ca^{2+}.

An octylglucoside titration was carried out on this sample from 0 mM to 50 mM. Figure 6.10D shows an overlay of the spectra obtained. Increasing detergent concentration improved signal to noise, with many peaks gaining in intensity (circled in red, Figure 6.10B). At the highest concentration (Figure 6.10C), the spectrum deteriorated and exhibited increasing peak overlap in the centre of the spectrum causing poor resolution (circled in green, Figure 6.10C). This suggests that higher concentrations of octylglucoside caused protein aggregation. The spectrum with the greatest signal to noise and without significant loss of resolution in the central region was obtained at 30 mM octylglucoside (Figure 6.10B).

A calcium titration (data not shown) induced subtle improvements in the quality of the spectra. Peak sharpening was observed at 5 mM compared with 0 mM $CaCl_2$. These peaks weakened and there was more peak overlap when $CaCl_2$ was increased to 10 mM providing further evidence of oligomerisation/aggregation at this concentration.

A new sample of ^{15}N labelled CaBP7 1-100 was prepared and dialysed into 'HEPES Buffer' (Table 6.2). The octylglucoside concentration in the sample was increased to 30 mM by direct addition following protein dialysis. Protein precipitation under these conditions was minimal and this sample was used in subsequent NMR experiments to derive spectra for assignment of the CaBP7 1-100 backbone.

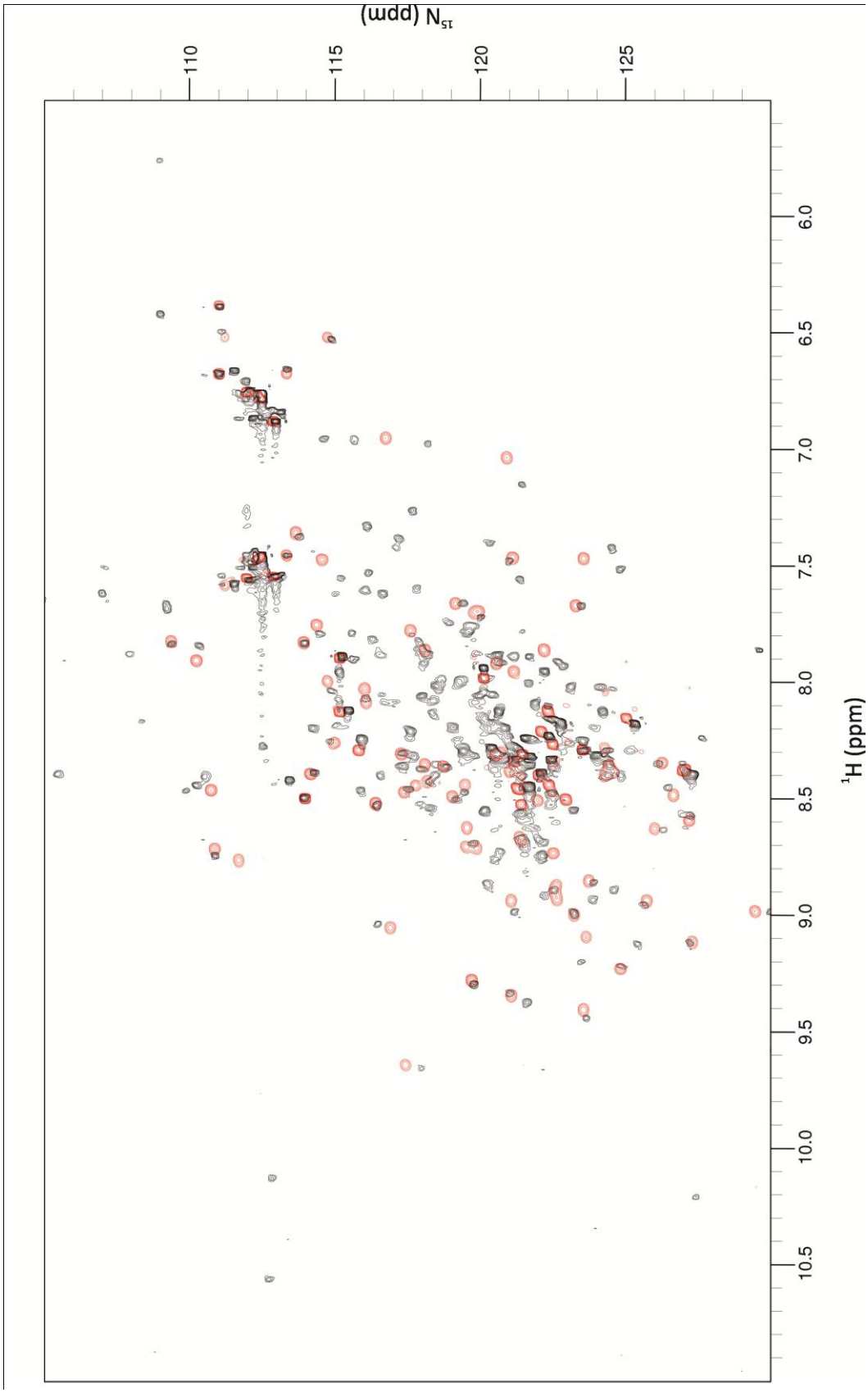

Figure 6.9. Two-dimensional ^{1}H-^{15}N HSQC NMR spectrum of SUMO- CaBP7 1-100 (Black) overlaid with the spectrum of SUMO (Red). SUMO-CaBP7 1-100 was prepared in 25 mM Na_2PO_4 pH 7.0, 150 mM NaCl, 25 mM imidazole. SUMO was prepared in 50 mM Tris.HCl pH 6.5, 50 mM NaCl.

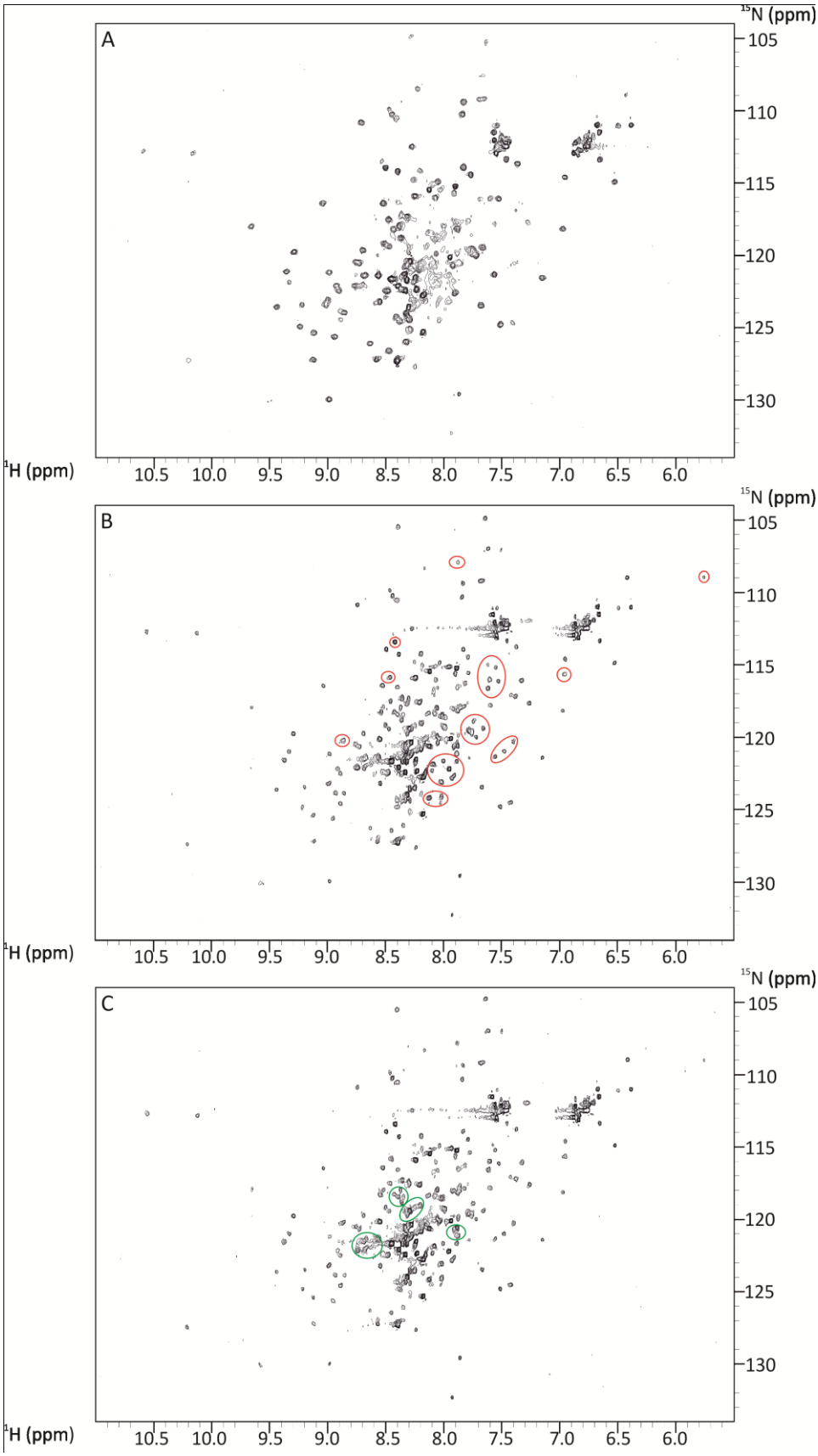

Figure 6.10 A-C. Two-dimensional ^{1}H-^{15}N HSQC NMR spectra of SUMO-CaBP7 1-100 with increasing concentrations of octylglucoside. A) 0 mM B) 30 mM C) 50 mM octylglucoside. Peaks which improved in intensity are circled in red. Peaks which decreased in resolution are circled in green. The sample was prepared in 25 mM Na_2PO_4 pH 7.0, 150 mM NaCl, 25 mM imidazole.

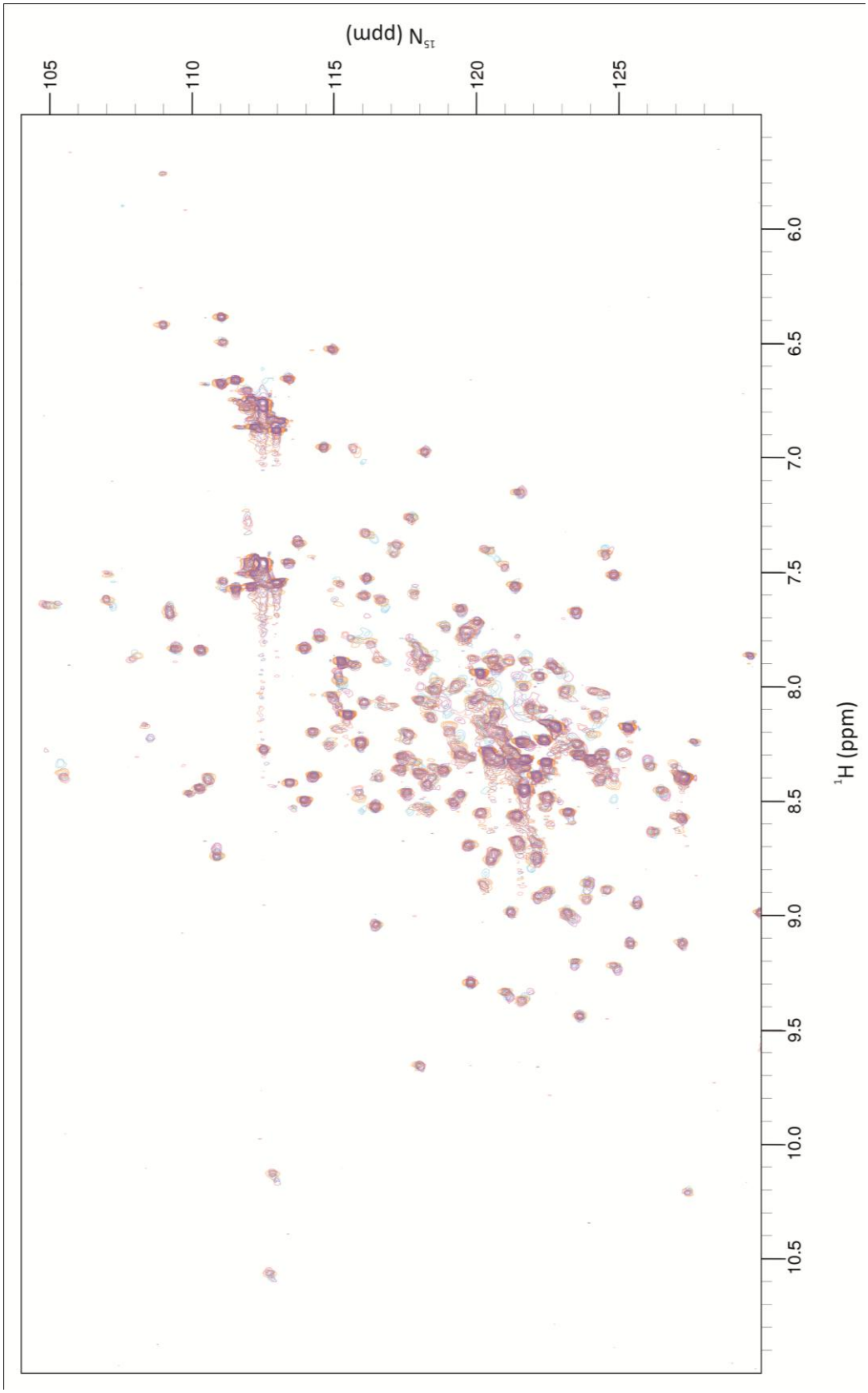

Figure 6.10 D. Overlay of ^1H-^{15}N HSQC NMR spectra of SUMO-CaBP7 1-100 with increasing octylglucoside concentration: 0 mM (pink), 10 mM (blue), 20 mM (orange), 30 mM (lilac), 50 mM (peach) octylglucoside. The sample was prepared in 25 mM Na_2PO_4 pH 7.0, 150 mM NaCl, 25 mM imidazole.

6.2.5. Backbone assignment of CaBP7 1-100

Assignment of resonances to the protein backbone is essential in order to carry out detailed structural studies of proteins by NMR. Complete proton assignments of both the backbone and side chains are required in order to determine a high-resolution structure, or less complete assignments can be sufficient for specific studies characterising the dynamics or interacting surfaces of a protein. A triple resonance approach is the most efficient method for both backbone and side chain assignment and requires a double $^{13}C/^{15}N$ labelled sample for the acquisition of 3D NMR data.

The triple-resonance experiments used to assign the backbone and side chains of a protein are described in table 6.3. These experiments correlate the ^{1}H and ^{15}N shifts of each residue's amide (NH) group with one or more carbon or proton resonances of the current residue (i) or the preceding residue (i-1) (Figure 6.11). In the assignment procedure, intra residue ^{13}C chemical shifts are first assigned to each detected NH group in the ^{1}H-^{15}N HSQC spectra and grouped within a spin-system. This information is then used to assemble the spin systems in sequential order by finding matching peaks from one spin system and those of the next (Figure 6.12). For instance a HNCO experiment provides the chemical shift of a particular amino acid's (i-1) carbonyl carbon ($^{13}C'$) atom, whereas a HN(CA)CO experiment provides the chemical shift for $^{13}C'$ for i and i-1. Therefore, the chemical shift of $^{13}C'$ for i in the HN(CA)CO experiment can be matched with that of the i-1 $^{13}C'$ in the HNCO experiment in order to establish a sequential link. The same approach applies to CBCA(CO)NH and HNCACB experiments which derive information concerning C_α and C_β for i and i-1 (Table 6.3 and Figures 6.11 and 6.12). These experiments are used in conjunction to find the best possible match out of all the identified spin systems.

A stretch of sequential spin systems is assigned to a particular region within the amino acid sequence by searching for spin systems with distinct chemical shifts that are characteristic of particular amino acids. Alanine, glycine, serine and threonine all give distinctive chemical shifts which can be used to verify the sequential links. If

the pattern of occurrence of these distinctive spin systems matches the expected sequence of the protein, this region can then be assigned (Figure 6.12).

Table 6.3NMR experiment definitions (Cavanagh *et al*., 2007a, Cavanagh *et al*., 2007b).

Experiment	Description	Detected chemical shifts
^{1}H-^{15}N-HSQC (2D)	Magnetisation is transferred from ^{1}H to the attached ^{15}N nuclei. The chemical shift is evolved on the nitrogen and transferred back to ^{1}H for detection.	$^{1}H_i$, $^{15}N_i$, (Backbone amide groups and Asn/ gln $^{15}N\delta$-$^{1}H\delta2$/$^{15}N\varepsilon$-$^{1}H\varepsilon2$ and Trp $^{15}N\varepsilon$-$^{1}H\varepsilon$ side chains.)
HNCO (3D)	Magnetisation is transferred from ^{1}H to the ^{15}N nuclei and then to the attached $^{13}C'$. The magnetization returns on the same path for detection.	$^{1}H_i$, $^{15}N_i$, $^{13}C'_i$
HN(CA)CO (3D)	Magnetisation is transferred from ^{1}H to the ^{15}N nuclei then to $^{13}C_\alpha$ of i and i-1. From there it is transferred to the attached $^{13}C'$. The magnetization returns on the same path for detection.	$^{1}H_i$, $^{15}N_i$, $^{13}C'_i$, $^{13}C'_{i-1}$ NOT $^{13}C_\alpha$
HNCACB (3D)	Magnetisation is transferred from $^{1}H_\alpha$ and $^{1}H_\beta$ to $^{13}C_\alpha$ and $^{13}C_\beta$ respectively and then from $^{13}C_\beta$ to $^{13}C_\alpha$. Subsequently, the magnetization is transferred to ^{15}N and ^{1}H of i-1 for detection.	$^{1}H_i$, $^{15}N_i$, $^{13}C_{\alpha i}$, $^{13}C_{\beta i}$, $^{13}C_{\alpha i-1}$, $^{13}C_{\beta i-1}$ NOT $^{1}H_\alpha$, $^{1}H_\beta$
CBCA(CO)NH (3D)	Magnetisation is transferred from $^{1}H_\alpha$ and $^{1}H_\beta$ to $^{13}C_\alpha$ and $^{13}C_\beta$ respectively and then from $^{13}C_\beta$ to $^{13}C_\alpha$. Subsequently the magnetization is transferred to $^{13}C'$ and then ^{15}N and ^{1}H of i-1 for detection.	$^{1}H_i$, $^{15}N_i$, $^{13}C_{\alpha i}$, $^{13}C_{\beta i}$, NOT $^{1}H_\alpha$, $^{1}H_\beta$, or $^{13}C'$
HBHA(CO)NH (3D)	Magnetisation is transferred from $^{1}H_\alpha$ and $^{1}H_\beta$ to $^{13}C_\alpha$ and $^{13}C_\beta$ respectively and then from $^{13}C_\beta$ to $^{13}C_\alpha$. Subsequently the magnetization is transferred to $^{13}C'$ and then ^{15}N and ^{1}H of i-1 for detection.	$^{1}H_i$, $^{15}N_i$, $^{1}H_{\alpha i}$, $^{1}H_{\beta i}$ NOT $^{13}C_\alpha$, $^{13}C_\beta$, or $^{13}C'$
HCCH-TOCSY (3D)	Magnetization is transferred from the side chain hydrogens to their attached carbons. Magnetisation is passed between the various carbon atoms and then back to the side chain hydrogens for detection	$^{13}C_\alpha$, $^{13}C_\beta$, $^{13}C_\gamma$etc. $^{1}H_\alpha$, $^{1}H_\beta$, $^{1}H_\gamma$ etc.
^{1}H-^{13}C-HSQC	Magnetisation is transferred from ^{1}H to the attached ^{13}C nuclei and back again for detection.	$^{13}C_\alpha$, $^{13}C_\beta$, $^{13}C_\gamma$etc. $^{1}H_\alpha$, $^{1}H_\beta$, $^{1}H_\gamma$ etc.

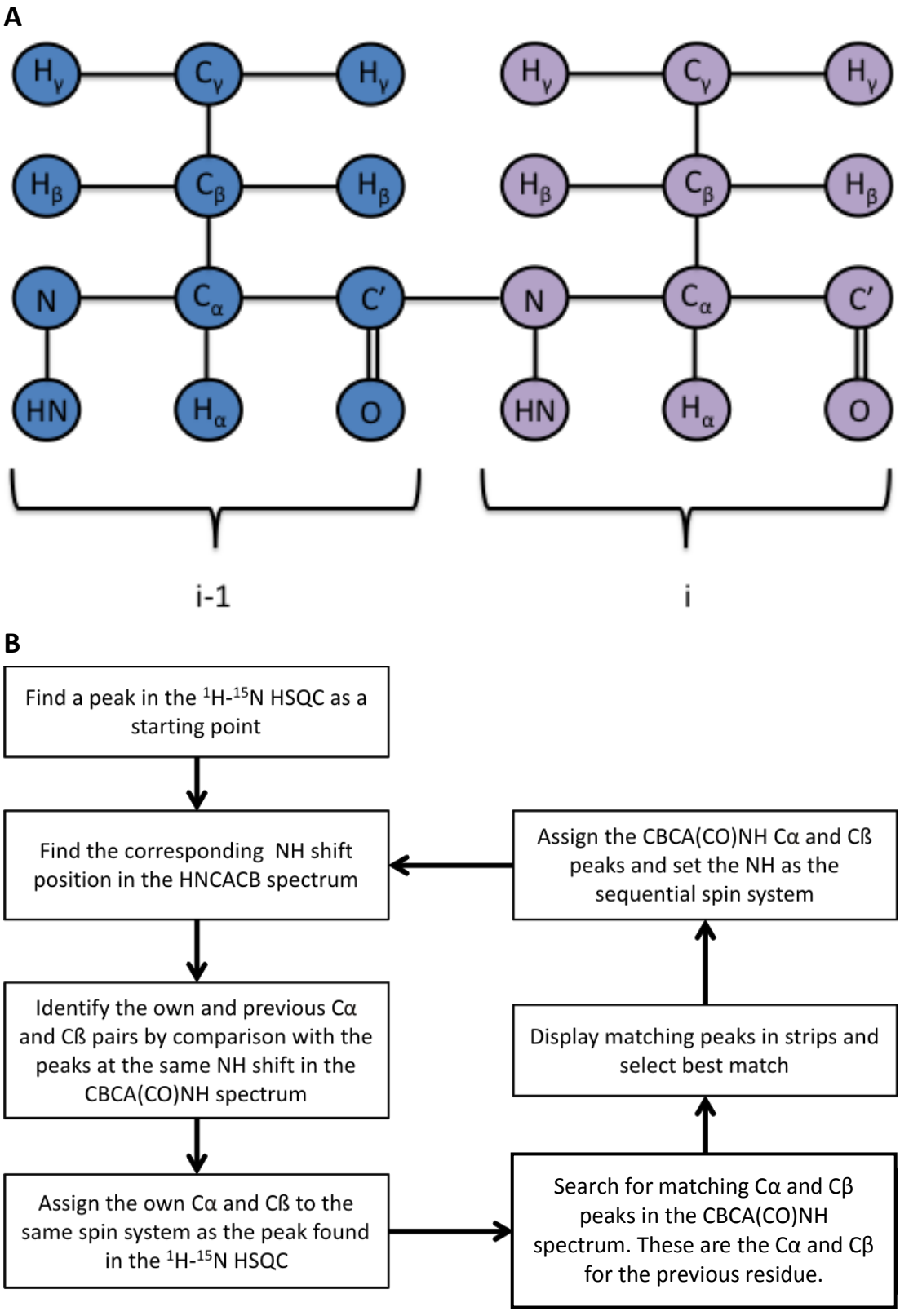

Figure 6.11. A) Schematic diagram showing the molecular structure of an amino acid illustrating how each atom is defined. B) Flow diagram showing the process involved in backbone assignment.

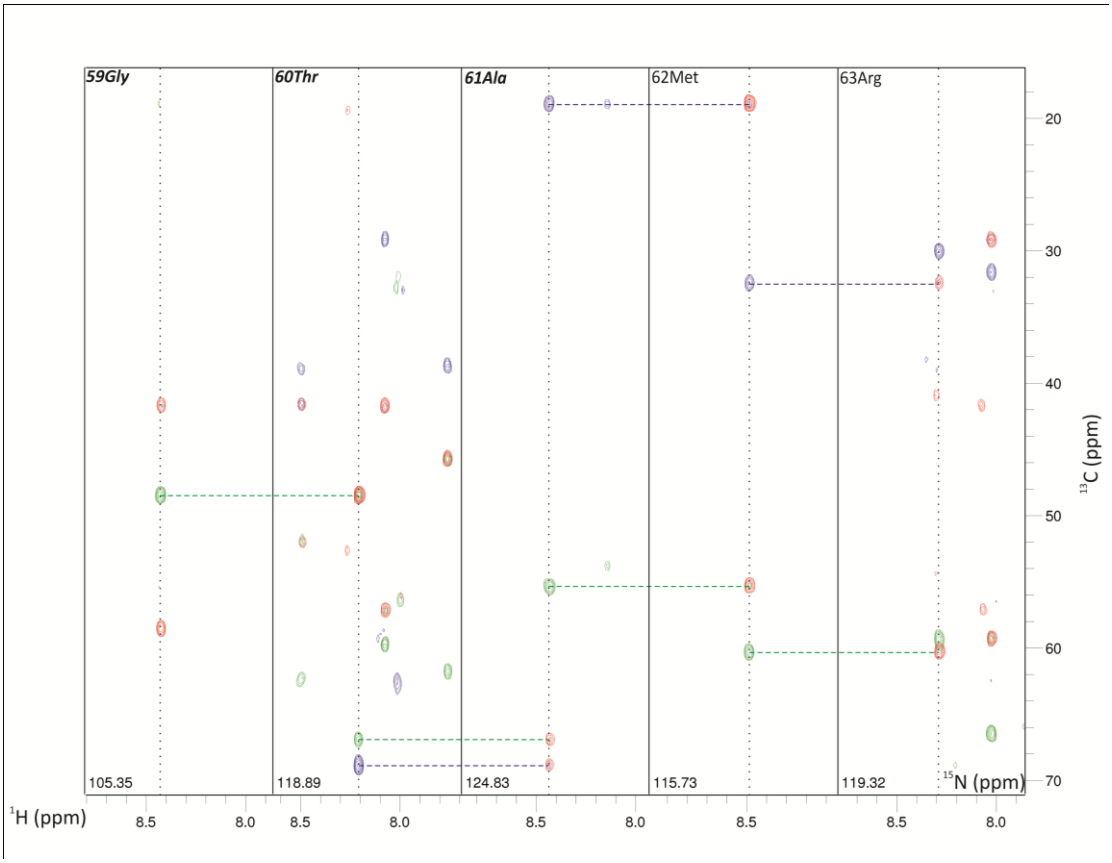

Figure 6.12. Strip-plot illustrating sequence-specific assignment of a stretch of five amino acids from CaBP7 1-100. Five spin systems are connected sequentially through chemical shift matches in the HNCACB and CBCA(CO)NH spectra. Chemical shifts of C_α and C_β for i are detected in the CBCA(CO)NH spectrum and are shown in red. Chemical shifts of C_α (green) and C_β (blue) for i and i-1 are detected in the HNCACB spectrum. Vertical dotted lines indicate the ^{1}H chemical shift of each spin system. The ^{15}N chemical shift is indicated in the bottom left corner of each strip. Horizontal dashed lines illustrate how the C_α (green dashed line) and C_β (blue dashed line) for i from the CBCA(CO)NH spectra (red peaks) can be matched with C_α and C_β (green and blue peaks) for i-1 of another spin system by searching for corresponding ^{13}C chemical shifts in the HNCACB spectrum. This process is used to make sequential links between spin systems. The three spin systems shown in bold italics have distinct chemical shifts and can therefore be matched to a corresponding sequence in the protein. Gly-Thr-Ala-X-X appears only once in CaBP7 1-100 therefore these spin systems, and sequentially attached spin systems, can be unambiguously assigned to the corresponding stretch of amino acids in the protein sequence. In this case the sequence is assigned as 59Gly-60Thr-61Ala-62Met-63Arg.

A cleaved double-labelled CaBP7 1-100 sample (Figure 6.8B) was produced in 'HEPES Buffer' (Table 6.2) supplemented with 30mM octylglucoside and 5mM $CaCl_2$. In NMR spectra for this sample, there was significant chemical shift dispersion and uniform peak intensities were observed suggesting that the protein was structurally homogeneous and stably folded. Figure 6.13 shows an overlay of the cleaved CaBP7 1-100 spectrum with the cleaved CaBP7 1-188 spectrum. Some of the dispersed peaks, indicating structured regions in the CaBP7 1-100 spectrum, also appear in the CaBP7 1-188 spectrum (circled in red, Figure 6.13) suggesting that the N-terminal domain was partly folded in CaBP7 1-188. There are also dispersed peaks in the CaBP7 1-188 spectrum (circled in green, Figure 6.13), which do not correlate with the CaBP7 1-100 spectrum, implying that at least some of the C-terminus was also folded in CaBP7 1-188.

More than 85% of the NMR resonances were assigned as indicated in Figure 6.14. Assignments were not obtained for residues 1-13 due to weak peak intensities which may be due to chemical exchange broadening (Cavanagh *et al*., 2007c). It is possible that this region may be unstructured as seen for the extreme N-termini of CaBP1 and DREAM (Lusin *et al*., 2008, Park *et al*., 2011, Wingard *et al*., 2005). Appendix Table A2 displays a summary table illustrating the percentage of the total backbone that was assigned. The side-chain assignments were also completed as far as the data obtained would allow (summarised in appendix table A2). Data from the HBHA(CO)NH experiment allowed determination of the chemical shifts of side chain $^{1}H_{\alpha}$ and $^{1}H_{\beta}$. Using this information in combination with data from the HCCH-TOCSY experiment, the side chains could be assigned. There was some ambiguity in the assignment of certain side chains, which should be resolved by the acquisition of NOESY experiments. Data from NOESY experiments provide information about resonances that are close together in space and can be used both to generate restraints for structure calculations and aid disambiguation of spectral overlap. Unfortunately, this was not possible within the time constraints of this project. The side chain assignments for CaBP7 1-100 can be found in Table A3 of the appendix.

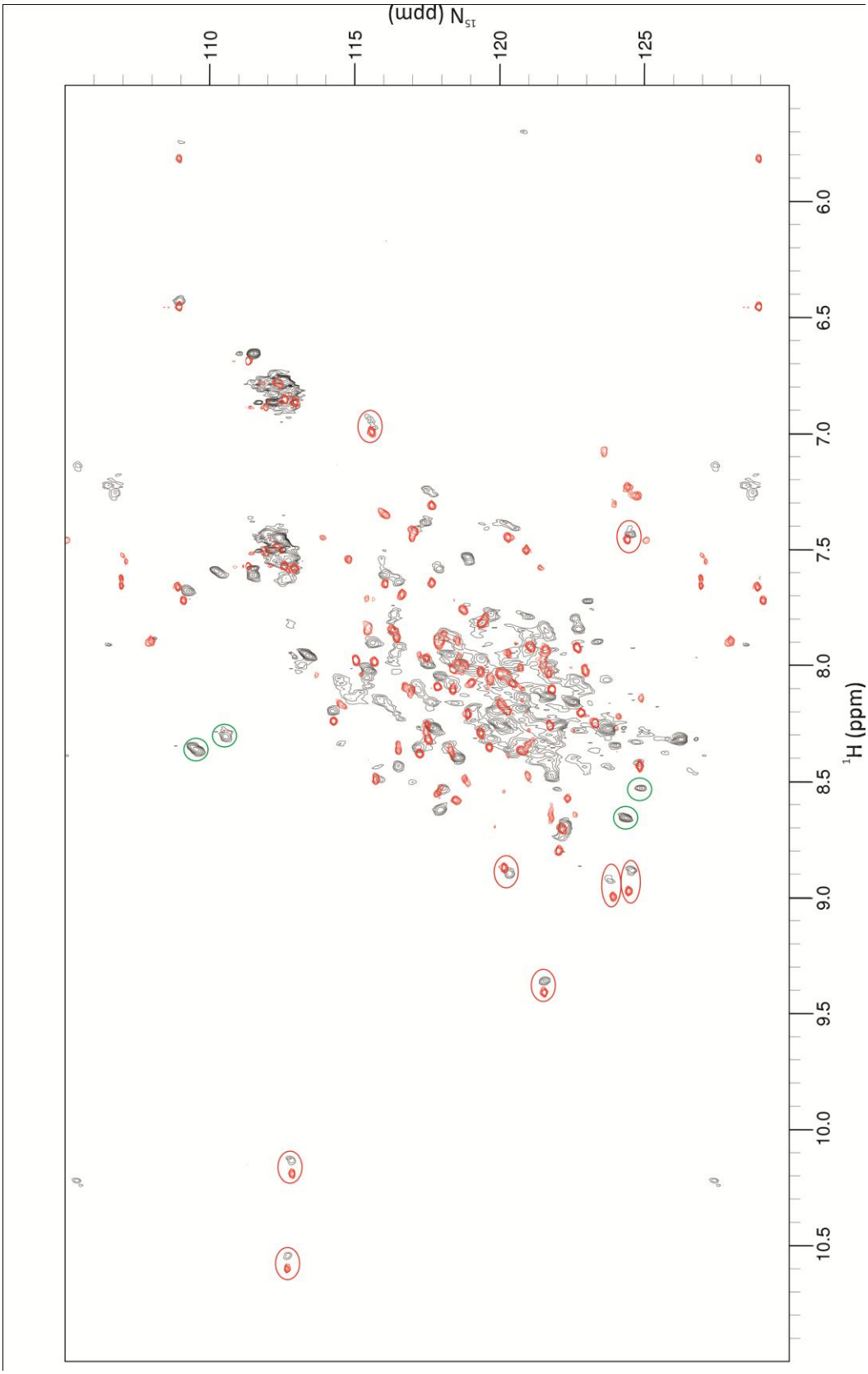

Figure 6.13. Overlay of ^{1}H-^{15}N HSQC NMR spectra for cleaved CaBP7 1-188 (Black) and cleaved CaBP7 1-100 (Red). CaBP7 1-188 was prepared in 20 mM Tris.HCl pH 6.5, 150 mM NaCl, 5 mM $CaCl_2$, 30 mM octylglucoside. CaBP7 1-100 was prepared in 20 mM HEPES pH 7.5, 50 mM NaCl, 5 mM $CaCl_2$, 30 mM octylglucoside. Peaks circled in red were found in both spectra. Peaks circled in green were unique to the CaBP7 1-188 spectra.

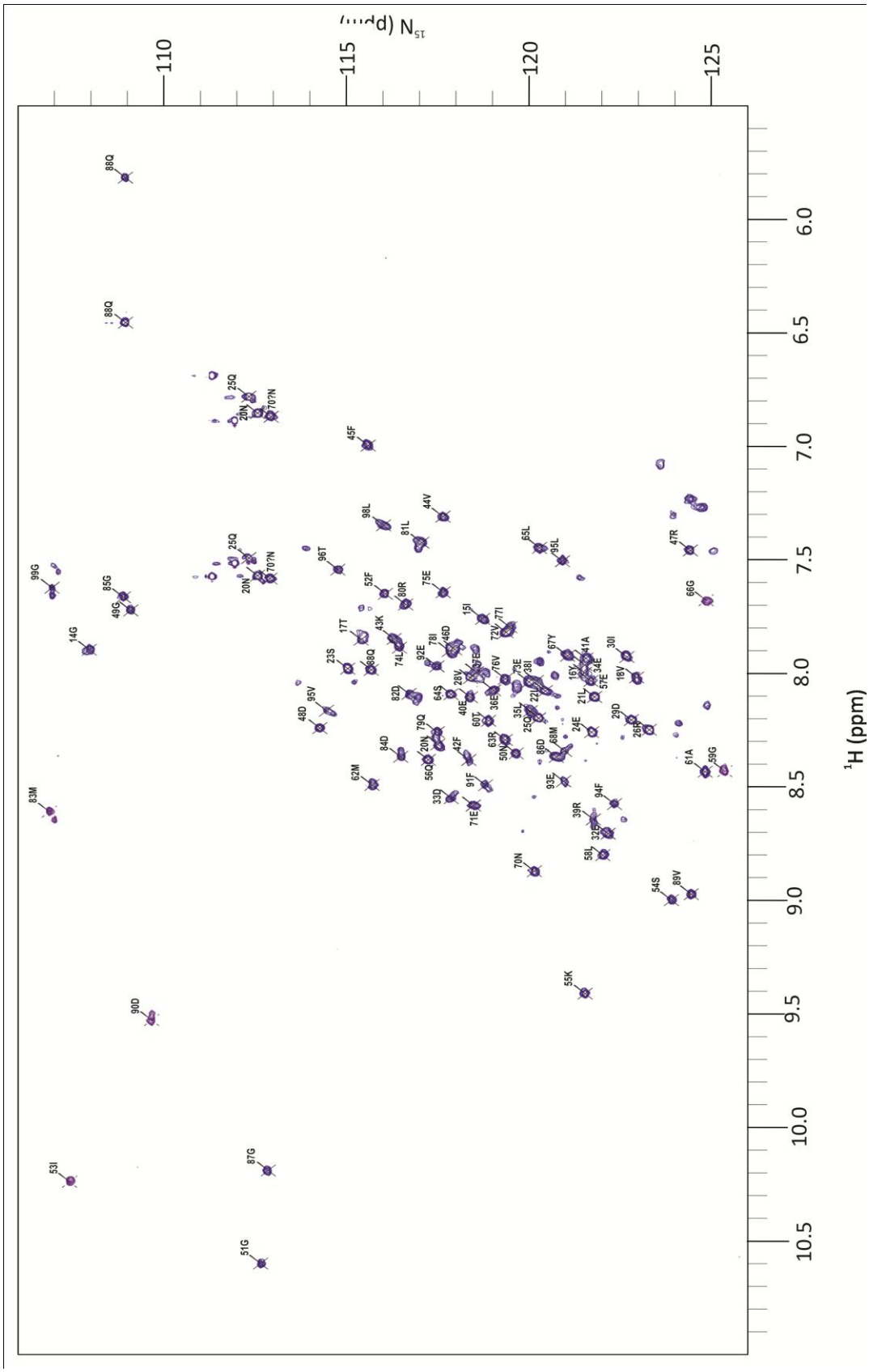

Figure 6.14. Assigned two-dimensional ^{1}H-^{15}N HSQC NMR spectra of cleaved CaBP7 1-100. The sample was prepared in 20 mM HEPES pH 7.5, 50 mM NaCl, 5 mM $CaCl_2$, 30 mM octylglucoside. '70?N': The side chain of 70N was only tentatively assigned due to peak overlap. Spectrum acquired at 303 K.

6.2.6. Calculation of CaBP7 1-100 secondary structure

Figure 6.15A shows a primary sequence alignment of CaBP7 with CaM and CaBP1S. This, along with the sequence identity table (Figure 6.15B), illustrates that CaBP7 shares 35% sequence similarity with the N-termini of CaM and CaBP1S, reducing to 10% sequence similarity across their C-termini. This makes the N-terminal domain the most informative in comparisons of similarity across the CaBPs and CaM. The secondary structure of CaBP7 1-100 was calculated using data obtained from NMR experiments. Chemical Shift Index (CSI) determines the secondary structure of a protein based on the chemical shifts of specific nuclei (C_α, C_β, C' and H_α) (Wishart and Sykes, 1994). DANGLE (Dihedral ANgles from Global Likelihood Estimate) calculates secondary structure based on chemical shift data and correlation to a database of known protein structures (Cheung *et al*., 2010).

Figure 6.15C shows the calculated secondary structure of CaBP7 1-100 from CSI and DANGLE, aligned with the known secondary structure of Ca^{2+}-bound CaM (PDB 1CLL (Chattopadhyaya *et al*., 1992)) and CaBP1S (Park *et al*., 2011) N-termini. The secondary structure of all three proteins appears relatively similar. Each protein has four helices that occur in approximately identical positions and all three proteins have short beta-strands in the same positions before the second helix in each EF-hand. This comparison reveals general structural similarities between these proteins and is consistent with both CaBP7 and CaBP1S being evolutionarily related to CaM. The two secondary structure calculations generated slightly differing results with the first defined helix extended by four amino acids in the CSI calculation compared to DANGLE, but overall the outputs were consistent.

6.2.7. Ca^{2+}-binding of CaBP7 1-100

Two downfield shifted peaks at ^1H 10.0 - 10.5 ppm in CaBP7 1-100 spectra were assigned to two glycines at the 6^{th} position of the two EF-hands (Figure 6.14). The characteristic chemical shift of these glycines indicated that the protein was already Ca^{2+}-bound when the spectra were acquired. Apo CaBP7 1-100 was prepared by dialysing protein into 'EGTA/EDTA buffer' (Table 6.2). No precipitation of the

A

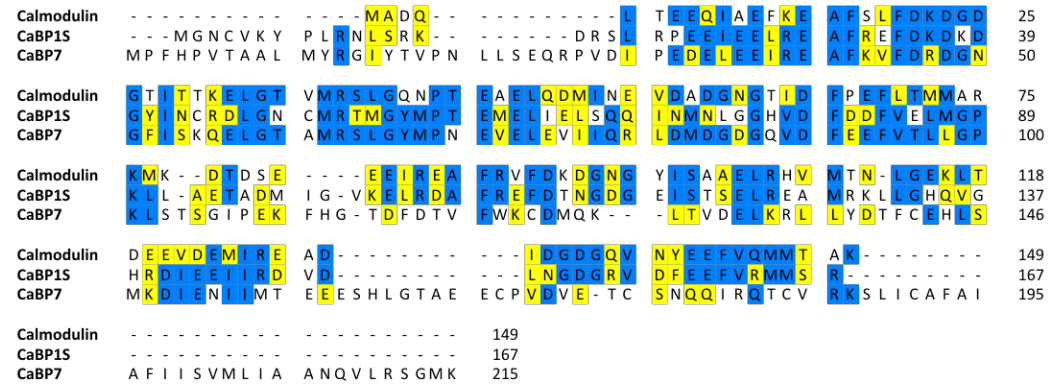

B

	Full	N-terminus	C-terminus
Calmodulin	20.5	34	9.2
CaBP1S	21.3	35	10

C

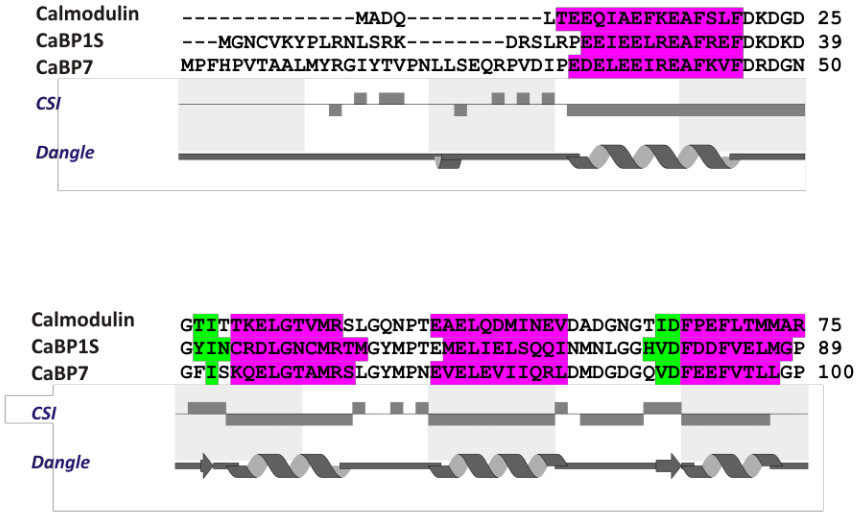

Figure 6.15. Secondary structure calculation of CaBP7 1-100. A) Multiple sequence alignment of full length CaM, CaBP1S and CaBP7. Residues highlighted in blue are identical and residues highlighted in yellow are similar across sequences. B) Percentage sequence identity of CaM and CaBP1S with CaBP7. C) Secondary structure of CaBP7 1-100 calculated with CSI and DANGLE and aligned with the known secondary structure of the Ca^{2+}-bound CaM (PDB 1CLL (Chattopadhyaya *et al*., 1992)) and CaBP1S (Park *et al*., 2011) N-termini. Residues highlighted in pink are found in regions of alpha-helix and residues highlighted in green are found in regions of beta-sheet. CaBP7 is highlighted based on the DANGLE prediction. In the CSI prediction bars above the line indicate beta sheet and bars below the line indicate alpha helix. In the DANGLE prediction, arrows indicate beta sheet and the helices represent alpha helix.

protein was observed during this process. The chelator concentration was subsequently reduced (<50 µM) by ultrafiltration into 'Low Octylglucoside HEPES Buffer' (Table 6.2). This permitted the sample to be cleaved and re-passed over a nickel affinity column to remove free SUMO tag, SUMO protease and any uncleaved material. During this stage precipitation was observed. 2mM octylglucoside was included in all buffers as a stabiliser.

Figure 6.16A depicts the spectrum obtained from this sample in the presence of 2 mM octylglucoside. Few peaks were visible and the signal intensities were weak. Addition of 30 mM octylglucoside (Figure 6.16B) led to a vast improvement in the quality of the spectrum with more peaks visible, exhibiting increased intensities. This further demonstrates the important role that the detergent played in stabilising the protein and preventing aggregation.

The downfield shifted glycines that were observed in the assigned ^{1}H-^{15}N-HSQC spectrum (Figure 6.14) were not visible in the apo spectrum (Figure 6.16B), but there were two previously unobserved peaks in the region typical for glycine residues, indicating that this is indeed the apo form of CaBP7 1-100. There was good peak dispersion in the apo spectrum indicating that the protein was folded in the absence of Ca^{2+}. Various EF-hand containing proteins have been shown to also bind to Mg^{2+} as well as Ca^{2+} ions and undergo Mg^{2+} induced conformational changes (Wingard *et al*., 2005, Lusin *et al*., 2008). As free Mg^{2+} levels in resting cells is estimated between 0.5 - 5 mM (Romani and Scarpa, 1992), it is thought that the protein conformation in the presence of Mg^{2+} is more physiologically relevant than the apo form. For this reason, the effect of adding 5 mM $MgCl_2$ to apo CaBP7 1-100 was tested. Unfortunately, the presence of $MgCl_2$ in the sample triggered protein precipitation.

A new sample of apo CaBP7 1-100 was prepared employing the above protocol with octylglucoside added to 30 mM (Figure 6.17A) and the effect of adding 5 mM $CaCl_2$ investigated (Figure 6.17B). The presence of Ca^{2+} did not cause the protein to precipitate and a shift from the apo form to the Ca^{2+}-bound form was observed. As

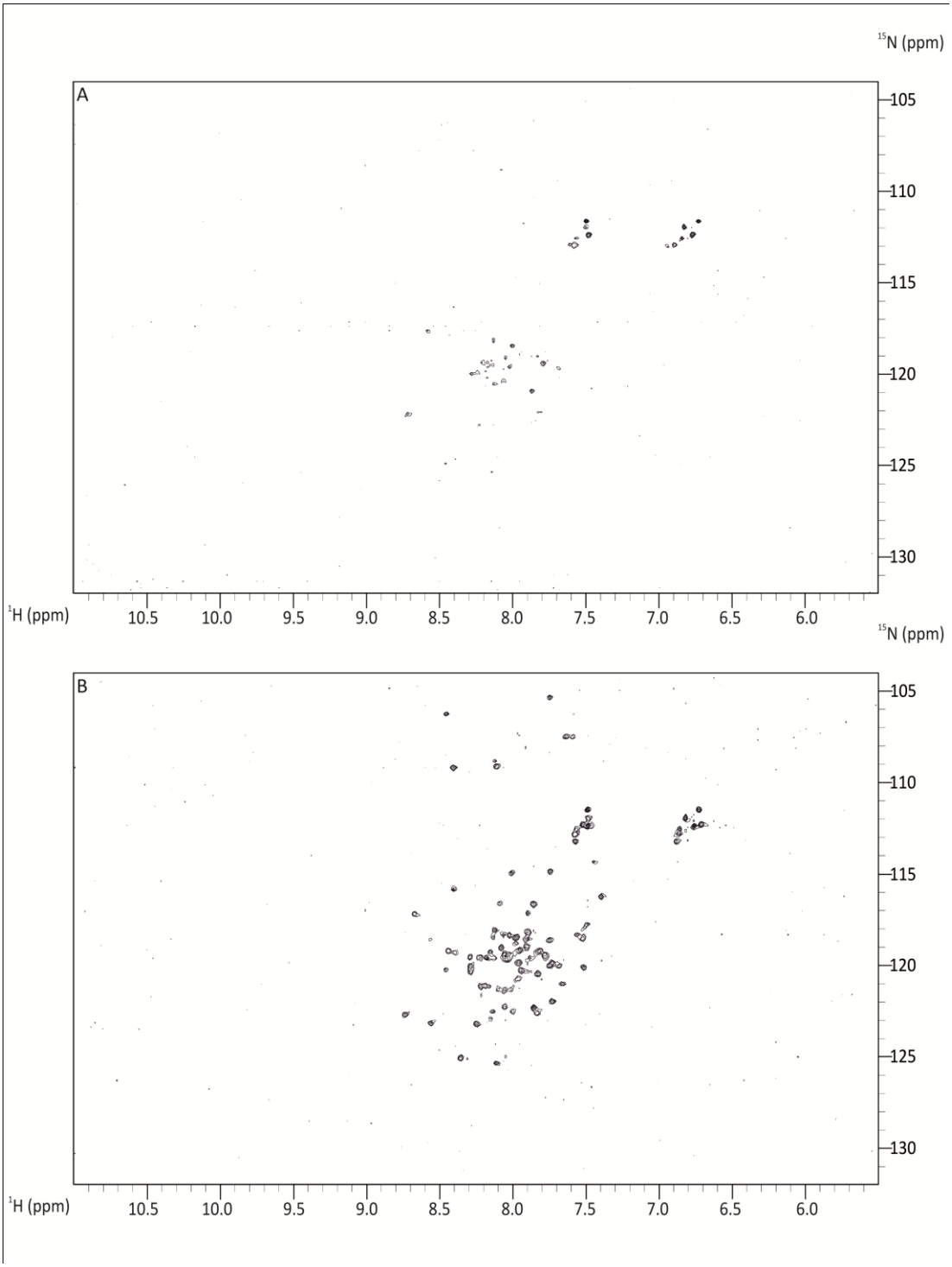

Figure 6.16. Two-dimensional ^{1}H-^{15}N HSQC NMR spectra of cleaved apo CaBP7 1-100. Apo CaBP7 1-100 was prepared by dialysis into 20 mM HEPES pH 7.5, 50 mM NaCl, 5 mM EDTA, 5 mM EGTA, 2 mM octylglucoside prior to SUMO-Protease treatment. Material was re-passed over affinity resin to remove free SUMO, SUMO-protease and uncleaved material, then buffer exchanged by ultrafiltration into 20 mM HEPES pH 7.5, 50 mM NaCl, 2 mM octylglucoside. A) Spectrum obtained from original sample with only 2 mM octylglucoside. B) spectrum obtained after addition of 30 mM octylglucoside.

expected this spectrum was extremely similar to the spectrum which was assigned (Figure 6.14) and the majority of the backbone amide assignments could be directly transferred.

The most notable difference between the apo and Ca^{2+}-bound spectra was the disappearance of two glycine peaks (circled in red, Figure 6.17A) and the appearance of the two downfield shifted 51G and 87G peaks (circled in red, Figure 6.17B). The spectrum of the apo form is completely different to that of the Ca^{2+} bound protein and very few of the apo resonances could be matched with those in the assigned, Ca^{2+}-bound, ^{1}H-^{15}N-HSQC (Figure 6.14). Therefore there is a Ca^{2+}-induced conformational change in the protein. 107 peaks were counted in the apo spectrum compared to 99 peaks in the Ca^{2+}-saturated spectrum. 93 peaks are expected due to the presence of 7 prolines in the sequence, which can not be detected in the ^{1}H-^{15}N-HSQC because they lack an amide proton. The discrepancy in the number of peaks is likely caused by overlapping peaks and peak broadening due to conformational heterogeneity (Wingard *et al*., 2005, Cavanagh *et al*., 2007c). An excess number of observed peaks can also arise due to protein degradation or the presence of other contaminants. The peaks in the spectrum for the Ca^{2+}-bound protein show improved chemical shift dispersion and reduced peak overlap. Many of the more dispersed peaks found in the spectrum for the Ca^{2+}-bound protein can be assigned to residues found within the Ca^{2+}-binding loops of the two EF-hand motifs. These include 47R, 48D, 49G, 51G, 53I, 54S, 55K, 83M, 85G, 87G, 89V, 90D (circled orange, Figure 6.17D) and the side chain of 88Q (circled pink, Figure 6.17D). In addition there were two glycines in the apo form which appeared to map onto 59G and 66G but which underwent significant shifts when the spectrum were compared (circled in purple, Figure 6.17D). 59G is found in the helix following the Ca^{2+}-binding loop of EF1 and 66G is found in the linker region between the two EF-hand motifs. Interestingly there are also conserved glycine residues at the corresponding positions in CaBP1S and CaM (Figure 6.15A).

As the addition of Ca^{2+} did not appear to negatively affect the stability of the protein, the effect of adding saturating Mg^{2+} was tested on the Ca^{2+}-bound form.

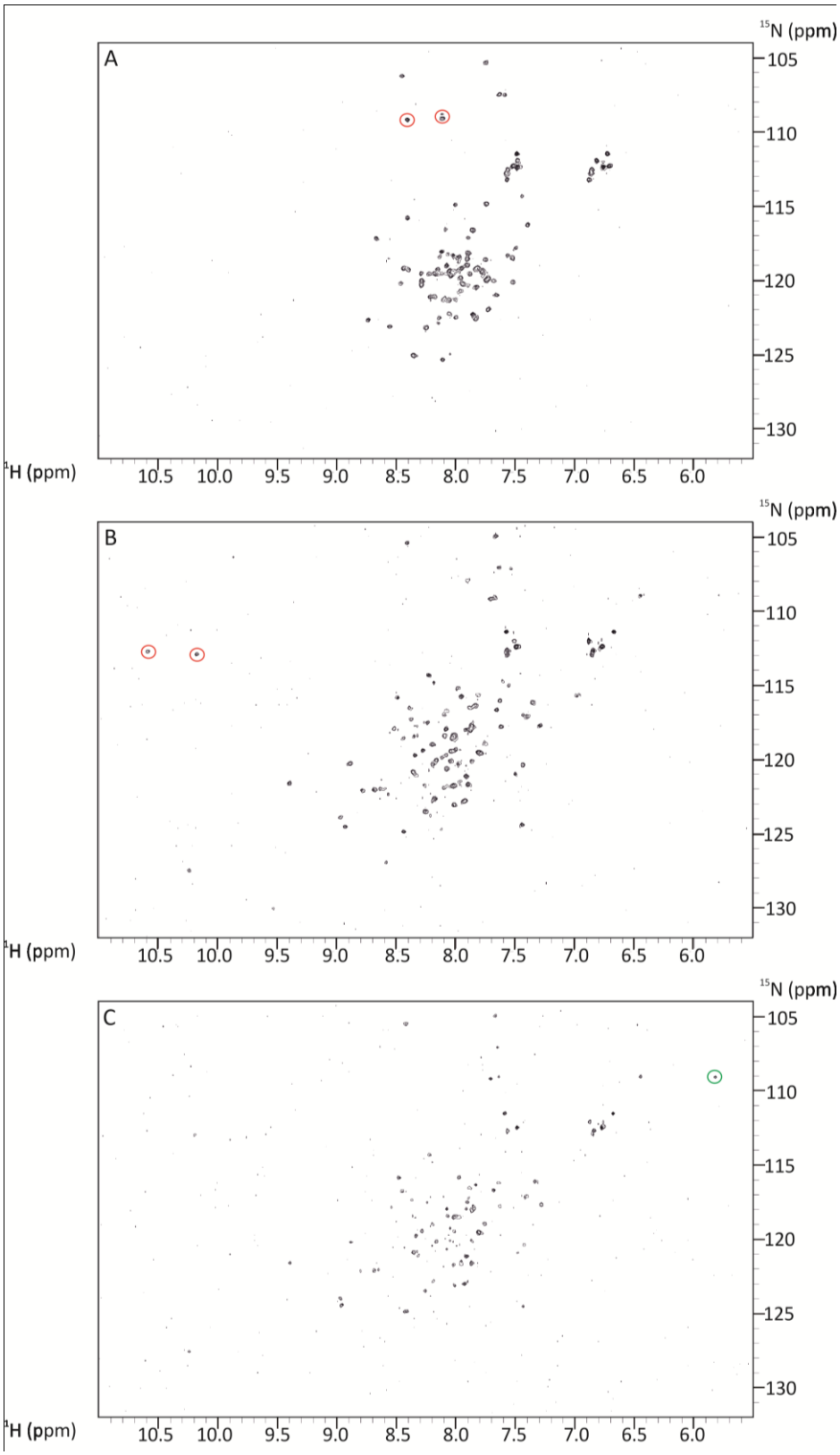

Figure 6.17 A-C. 2D ^{1}H-^{15}N HSQC NMR spectra of apo and Ca^{2+} saturated CaBP7 1-100. A) Apo CaBP7 1-100. B) CaBP7 1-100 after addition of 5 mM $CaCl_2$ C) CaBP7 1-100 after addition of 5 mM $CaCl_2$ and 5 mM $MgCl_2$. Peaks corresponding to the glycines at the 6th position of the two EF-hands are circled in red in A and B. The side chain peak which increased in intensity upon Mg^{2+} addition is circled in green in C. The sample was prepared as described in Figure 6.16.

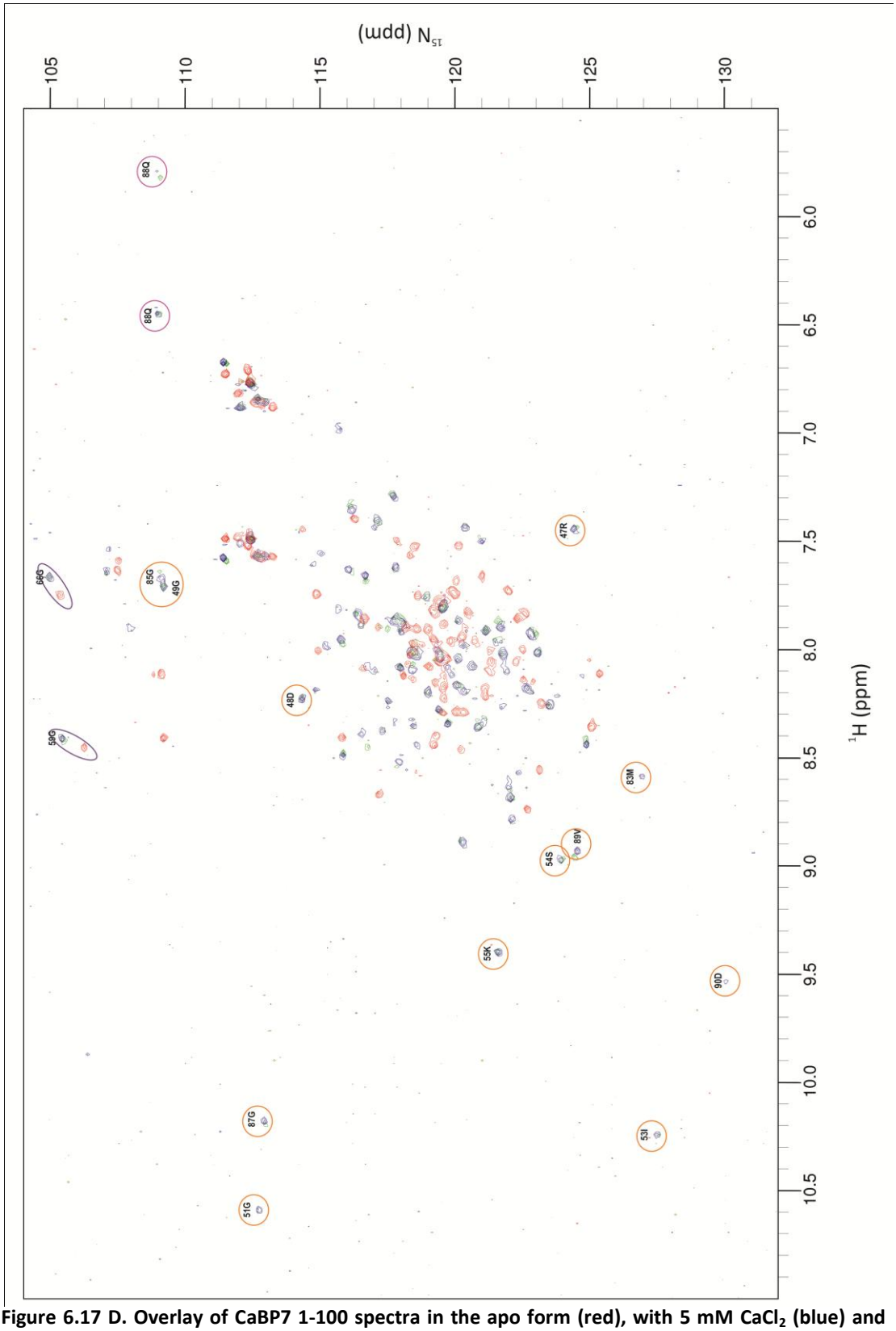

Figure 6.17 D. Overlay of CaBP7 1-100 spectra in the apo form (red), with 5 mM $CaCl_2$ (blue) and with 5 mM $CaCl_2$ and 5 mM $MgCl_2$ (Green). Residues circled in purple underwent significant shifts upon Ca^{2+} addition. Dispersed peaks from the Ca^{2+} saturated spectrum which are found in the Ca^{2+} binding loops of the two EF-hands are circled in orange. The side chains from 88Q are circled in pink. These peaks are labelled with their residue assignments as shown in Figure 6.14. The sample was prepared as described in Figure 6.16.

The presence of Mg^{2+} ions under these conditions again induced protein precipitation, therefore only a weak spectrum was obtained (Figure 6.17C). Most peaks reduced in intensity due to aggregation and precipitation of the protein, however subtle differences in the spectra were observed, which could not be ascribed to the effects of precipitation alone. There were minor shifts in some of the peaks, but the most notable difference was the increase in intensity of one of the side chain peaks for 88Q (circled in green, Figure 6.17C).

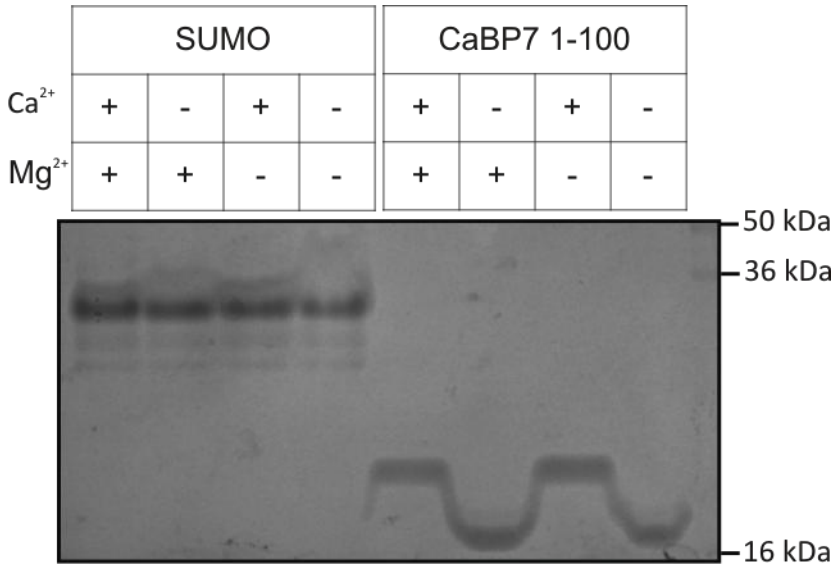

Figure 6.18. Native PAGE gel of SUMO and CaBP7 1-100 in the presence or absence of 10 mM Ca^{2+} or 10 mM Mg^{2+}.

Native PAGE was used to further investigate the effects of both Ca^{2+} and Mg^{2+} upon the conformation of CaBP7 1-100. Samples were prepared in a loading buffer containing 2 mM EGTA and 2 mM EDTA to strip the protein of all Ca^{2+} and Mg^{2+}. Ca^{2+} (10 mM), Mg^{2+} (10 mM) or both in combination were then added to these samples to examine any subsequent changes in the apparent protein molecular weight on native PAGE gels. Control SUMO protein exhibited no change in electrophoretic mobility under the conditions tested (Figure 6.18). Mg^{2+} alone failed to influence the migration of CaBP7 1-100 when compared to Ca^{2+}-free/Mg^{2+}-free conditions (Figure 6.18). Ca^{2+} alone induced a significant retardation in the migration rate of CaBP7 1-100 and this was unaffected by the presence of an

equimolar concentration of Mg^{2+} (Figure 6.18). Collectively, these data suggest that the protein does not bind Mg^{2+} or that Mg^{2+} binding causes no significant conformational change. Furthermore, this analysis demonstrates a Ca^{2+}-dependent shift in electrophoretic mobility of CaBP7 1-100, which is consistent with specific Ca^{2+}-binding to this protein. These data are in agreement with previously published ITC data demonstrating that CaBP7 does not bind to Mg^{2+}.

6.3. Discussion

Various protein expression systems were tested during the course of this project with the majority proving unsuitable for production of the amounts of pure protein necessary for NMR analysis. The use of codon optimised genes in conjunction with the pE-SUMOPRO vector improved the expression of soluble protein by up to 40-fold compared with other expression systems investigated. The SUMO tag has been proven to improve the solubility and stability of many difficult to express proteins and has the advantage that the tag can be efficiently cleaved without leaving any residual amino acids beyond those encoded by the gene of interest (Butt *et al*., 2005, Malakhov *et al*., 2004). Although expression of soluble CaBP4 and a TMD deficient CaBP7 1-188 mutant in this system was improved, optimisation for acquisition of NMR data proved problematic.

CaBP4 spectra contained insufficient peak resonances to represent the full length protein. Initial spectra acquired at ambient temperature displayed a mixture of sharp peaks in the unfolded region of the spectra and weaker more dispersed peaks, including a downfield shifted peak characteristic of an EF-hand glycine. The dispersed peaks were suggestive of partial protein folding, whereas the sharp peaks were indicative of an unstructured flexible region, which may correspond to the extended N-terminus of CaBP4. NMR analysis of CaBP1 has revealed that its short N-terminal extension (amino acids 1-18) forms a structurally disordered domain (Park *et al*., 2011, Li *et al*., 2009) and, likewise, secondary structure prediction of CaBP4 suggests that residues 7-105 form a region of random coil. Double $^{15}N/^{13}C$-labelling of CaBP4 would permit the acquisition of the data required to assign these

peaks in order to deduce if they form a contiguous stretch of amino acids that resides within the N-terminus of CaBP4. At 30.4 kDa, CaBP4 is at the upper size limit of proteins which are viable for study by NMR. If it could be proven that the N-terminus is unstructured, then a new expression construct could be designed to remove these residues and reduce the protein to a more manageable size for NMR. This modification would theoretically improve spectral quality for the folded C-terminus of the protein.

Increasing the temperature of acquisition from 298 K resulted in an increase in the number of peaks observed in the spectra and the intensity of the peaks became more uniform. In particular, the sharp peaks seen at 298 K became weaker and some disappeared entirely. Without assigning the sharp peaks observed in the 298 K spectrum the reason why the intensities of these resonances decreased cannot be deduced. The number of downfield shifted glycine peaks in CaBP4 spectra increased progressively from one at 298 K, to two at 303 K and 308 K, and finally three at 313 K and 318K. There are three Ca^{2+}-selective EF-hands in CaBP4 and as all spectra were acquired in the presence of 5 mM Ca^{2+}, it would be predicted that all three of the EF-hands should be Ca^{2+}-bound. Increasing the temperature therefore appears to increase the signal to noise ratio so that all three downfield shifted glycine residues of the Ca^{2+}-bound EF-hands became visible at temperatures above 313 K. It is also possible that the signal is weaker at 298 K due to protein aggregation, which is lost at higher temperatures hence, improving resonance intensity and peak dispersion.

Divalent cation binding properties of CaBP4 are predicted to differ from CaBP1. The first EF hand of CaBP1 is constitutively Mg^{2+} bound due to an glutamine to aspartate substitution at the 12^{th} position of the Ca^{2+}-binding loop that gives the motif equal selectivity for Mg^{2+} and Ca^{2+} (Wingard *et al*., 2005). In CaBP4 there is a glutamine at this position in EF1 indicating that this motif should display preferential selectivity for Ca^{2+} (Haeseleer *et al*., 2000, McCue *et al*., 2010a). Mg^{2+} binding to CaBP1 confers a global conformational change and subsequent Ca^{2+}-binding induces localised conformational changes at EF3 and EF4 (Wingard *et al*., 2005). The cation binding

properties of CaBP4 were not studied in detail here, but should prove interesting in future work.

CaBP7 1-188 spectra contained evidence of protein folding however there were a large number of overlapping peaks in the centre of the spectra which could not be resolved, suggestive of protein aggregation. The presence of two downfield shifted peaks in the region characteristic of EF-hand glycines, suggested that the EF-hands of the protein were at least partially folded and that they were Ca^{2+}-bound even without the addition of $Ca^{2+}$to the buffer. Minimal media contains $CaCl_2$ and it is possible that, since CaBP7 has a high affinity for Ca^{2+} (0.2 - 0.5 µM) (Mikhaylova *et al*., 2006, Mikhaylova *et al*., 2009), they may have been occupied from an early stage in the purification process. For this reason there was little change in the spectra upon addition of 5 mM $CaCl_2$. An octylglucoside titration was also performed and at higher concentrations more resonances could be distinguished, suggesting that it was potentially reducing protein aggregation. The improvement upon addition of octylglucoside was minor, however, and did not increase resolution sufficiently to facillitate further investigation of this protein.

A second truncation of CaBP7, encoding the first 100 amino acids, was generated in an attempt to overcome the problems encountered with expression of CaBP7 1-188. CaBP7 1-100 encompasses the two functional EF-hands of the protein and represents the most highly conserved portion of the protein when compared to other Ca^{2+}-binding proteins. This fragment expressed to a high level and generated well-resolved spectra with dispersed peaks indicative of a folded protein. Octylglucoside and $CaCl_2$ titrations were performed on the uncleaved protein in order to deduce optimal conditions for acquiring NMR spectra. Octylglucoside improved the spectra of CaBP7 1-100 at concentrations of up to 30 mM, but at 50 mM there were indications of increased protein aggregation. No significant conformational change was observed upon addition of $CaCl_2$. As the downfield shifted glycines were already visible in the spectra at 0 mM $CaCl_2$, the protein had likely become Ca^{2+}-bound at a prior stage of the purification process. The addition of $CaCl_2$ did, however, improve the quality of the spectra at concentrations up to 5

mM but induced spectral changes characteristic of aggregation when increased to 10 mM.

A double labelled, cleaved sample of CaBP7 1-100 was produced using the conditions determined to be optimal for acquiring structure quality NMR spectra. 87% of the CaBP7 1-100 backbone was assigned and it was verified that the two most downfield shifted peaks represented the glycines at the 6th position of the EF-hands (51G and 87G). Other downfield shifted peaks were also observed, which corresponded to residues within the two EF-hand Ca^{2+}-binding loops. These included 53I and 89V at the 8th position and 90D and 54S at the 9th position of the EF1 and EF2 loops, respectively.

Secondary structure calculations for CaBP7 1-100 gave a similar linear arrangement of alpha helices as found in CaM and CaBP1. The main difference between the calculations from CSI and DANGLE was the length of the first helix of the first EF-hand. CSI predicted this to be 4 amino acids longer than the DANGLE calculation. The DANGLE calculation appears to be consistent with the known secondary structures of Ca^{2+}-bound CaM and CaBP1S N-termini with the alpha helices and short regions of beta sheet occurring in approximately the same positions in all three proteins.

Further structural modelling of CaBP7 1-100 was not possible within the time constraints of this project, although the process of side chain assignment has been started. The secondary structure calculations imply that CaBP7 1-100 appears similar to Ca^{2+}-bound CaM and CaBP1S. This is in accordance with the calculated sequence homology between the three proteins (~35%). In contrast, the C-terminus has limited sequence homology to CaM or CaBP1S (< 10%). As described in chapter 3, CaBP7 is extremely well conserved through the evolution of vertebrates and there is 72% sequence conservation of the CaBP7 C-terminus, excluding the TMD, between elephant shark and human. This suggests that there is a conserved function for this region of the protein. Unlike in CaBPs 1-5, the C-terminus of CaBP7 does not contain functional EF-hands, and interestingly, in BLAST searches using this

region, no other Ca^{2+}-sensing proteins are retrieved. Using similar NMR analyses, it would be interesting to investigate if the C-terminus of CaBP7 exhibits structural homology to other Ca^{2+}-sensors or if a unqiue structural domain has evolved.

Extensive protein aggregation was evident in CaBP7 1-188 spectra which displayed a large degree of peak overlap. This was not observed in CaBP7 1-100 spectra suggesting that residues 101-188 may be key in determining the degree of precipitation. The C-terminus of CaBP7 1-188 contains 5 cysteine residues which could form incorrect disulphide bridges between monomers resulting in aggregation. Successful expression of CaBP7 101-188 might therefore require mutagenesis or alkylation (Crankshaw and Grant, 2001) of these residues in order to obtain stable, soluble protein. In accordance with the aggregation described in this chapter, Hradsky *et al.* have observed that CaBP7 and CaBP8 form soluble dimers and higher order oligomers when produced recombinantly in bacteria (Hradsky *et al*., 2011). In further investigations, pull down assays revealed that CaBP7 and CaBP8 can form both homo- and hetero-dimers with each other in a Ca^{2+}-independent manner. Using gel filtration and dynamic light scattering experiments, Hradsky *et al.* show that CaBP8 may have two dimerisation interfaces: the hydrophobic TMD and the cytosolic EF-hand containing domain. BRET and fluorescence complementation assays in HEK293T and COS-7 cells, respectively, confirmed that CaBP8 also forms parallel dimers *in vivo* (Hradsky *et al*., 2011). The propensity of the N-terminal domain to form dimers may explain the aggregation observed during the production of recombinant CaBP7 1-100 and CaBP7 1-188 as described in this chapter.

NMR spectra for apo CaBP7 1-100 were obtained and showed markedly different peak resonances compared with Ca^{2+}-bound CaBP7 1-100. This implies that the two forms have distinct conformations. There was less peak dispersion in the apo spectrum, however, the protein displayed signature characteristics of a natively folded protein. Upon binding to Ca^{2+},residues that underwent the most significant shifts in the spectrum generally resided within the Ca^{2+}-binding loops of the two EF-hand motifs. Native PAGE analysis confirmed that there is a Ca^{2+}-dependent shift in

electrophoretic mobility indicative of Ca^{2+}-binding. The apo form migrated quicker on the gel suggesting that it may have a more compact conformation than the Ca^{2+}-saturated protein or that the protein was forming dimers when Ca^{2+}-bound. A similar mobility shift on native PAGE has been reported for CaM and recoverin (Lambrecht and Koch, 1992, Burgess *et al*., 1980). Using semi-native SDS-PAGE Hradsky *et al.* observed that full length recombinant CaBP8 migrates as two bands corresponding to a monomer and a dimer. In addition, HeLa cell lysates subjected to native PAGE and immunoblotting with a CaBP7 specific antibody, detected bands corresponding to the molecular weights of monomeric, dimeric and higher order oligomeric forms of endogenous CaBP7. Ca^{2+} dependency was not investigated in these experiments, but data from gel filtration suggested that dimer formation is largely Ca^{2+}-independent (Hradsky *et al*., 2011). In contrast, only a single band was observed for both the apo and Ca^{2+}-bound forms of CaBP7 1-100 on native PAGE gels presented in this chapter. This suggests that the shift in mobility observed under these conditions was unlikely due to dimer formation.

As the secondary structure of CaBP7 1-100 approximates that of CaBP1S and CaM N-termini, it may undergo similar conformational changes upon Ca^{2+}-binding. In the Ca^{2+}-free form of CaBP1S the two helices of EF1 are almost perpendicular to the corresponding helices of EF2. In the Ca^{2+}-bound form, however, Ca^{2+}-binding to EF1 induces a 90° reorientation between the two EF-hands so that the two helices of EF1 are more parallel to those of EF2. This conformational change enables β-sheet formation and gives a more closed structure than that of the Ca^{2+}-free or Mg^{2+}-bound CaBP1S N-terminal domain (Park *et al*., 2011). In contrast, the apo form of the CaM N-terminal domain adopts a more closed conformation and shifts to a more open conformation upon Ca^{2+}-binding to both EF1 and EF2 (Chin and Means, 2000). It is therefore difficult to infer how Ca^{2+}-binding affects the conformation of CaBP7 1-100. The slower mobility of Ca^{2+}-bound CaBP7 1-100 compared to the apo form may suggest a shift from a more closed conformation to a more open conformation similar to CaM. The cation binding properties of CaBP7 1-100 are also more similar to CaM as both bind Ca^{2+} ions at EF1 and EF2 whereas CaBP1S binds Ca^{2+} at EF1 only. The global Ca^{2+} afinity of CaBP7 (~0.2 μM) (Mikhaylova *et al*., 2006)

is much higher than that of CaM (~4.0 – 20.0μM) (Schaad *et al*., 1996), however, suggesting there are likely important structural differences bewteen their EF-hands.

Native PAGE was also used to investigate whether Mg^{2+} is similarly able to influence the electrophoretic mobility of CaBP7 1-100. Samples prepared in the presence of excess Mg^{2+} exhibited no difference in migration rate when compared to the apo form of CaBP7 1-100 implying that, as previously published, CaBP7 does not bind to Mg^{2+} (Mikhaylova *et al*., 2009). The shift in mobility on native-PAGE gels is commonly believed to be due to a conformational change causing the protein to migrate at a different rate. As binding to Ca^{2+} would cause the protein to gain four extra positive charges this could also explain why the Ca^{2+}-bound form migrates slower on the gel. The fact that there is no change in the mobility of the protein in the presence of Mg^{2+} therefore suggests that the protein is not binding to Mg^{2+} under these conditions. This appears contradictory to the results obtained from NMR experiments, where CaBP7 1-100 precipitated upon the addition of Mg^{2+}, and suggests that the precipitation did not result as a consequence of Mg^{2+}-binding to the EF-hands. Interestingly, magnesium precipitation is a widely used method for the purification of proteins such as ribonclueoproteins (Palmiter, 1974), tubulins (Weisenberg and Timasheff, 1970), and also in the extraction of certain membrane proteins (Feric *et al*., 2011), although the exact mechanism of how this occurs is not clear. The precipitation of acidic proteins using divalent cations such as Mg^{2+} has also been documented (Takeuchi *et al*., 2008) and, with a pI of 4.21, CaBP7 1-100 may precipitate in a similar way.

6.3.1. Conclusion

This chapter documents the first steps toward solving the atomic resolution structures of CaBP4 and CaBP7. The NMR data acquired for CaBP4 indicates that this protein may become amenable to NMR analysis if the problems with aggregation are overcome. CaBP7 was truncated to the first 100 amino acids and secondary structure calculations based on initial NMR data suggest this peptide forms a domain which is similar to the N-termini of Ca^{2+}-bound CaM and CaBP1S.

Once the side chain assignments are completed and NOE data acquired, generation of a high quality 3D structural model may be possible. Due to the high sequence homology between CaBP7 and CaBP8 (63%), structural data obtained for CaBP7 may be used to infer the structure of CaBP8. As such, a prediction of the secondary structure of the N-terminus of CaBP8 using PSIPRED largely approximates the secondary structure of CaBP7 1-100 calculated using CSI and DANGLE. The sequence identity of the C-terminus of CaBP7 with other Ca^{2+}-sensors is very low with a maximum of 10% homology with CaM. The divergent nature of the C-termini of CaBP7 and CaBP8 compared to other CaBP proteins is unusual and further investigation into the structure of this domain will be critical in understanding functional differences that exist between these proteins and CaBPs 1-5 and CaM.

Solving the structures of CaBP4 and CaBP7 will facillitate further scientific investigation. Initially it will be important to characterise the conformational changes that occur upon cation binding. This will provide clues regarding the Ca^{2+}-dependencies of target interactions. It should be possible to locate specific binding sites for interacting proteins under both Ca^{2+}-dependent and -independent conditions and subsequently solve the structure of the complexes. Informed mutational studies could be carried out in order to map residues critical for such interactions. This may be of particular interest when considering the interactions of CaBP4 with VGCCs due to the various mutations which have been identified in human CaBP4. These mutations have been shown to result in cone-rod synaptic disorders of the retina. NMR could be used to screen for the structural effects of these mutations and how they affect CaBP4 binding to target proteins. Investigating the structure-function relationships of the CaBPs will reveal important mechanistic information about the physiological processes that they modulate.

Chapter 7:

Discussion

The CaBP family is a family of small EF hand containing Ca^{2+}-binding proteins with limited homology to CaM. The family comprises seven genes that can be divided into two groups, CaBPs 1-5 and CaBP7 & 8, based on differences in their domain structures (McCue *et al*., 2010a). CaBPs 1-5 interact with a number of known CaM target proteins but exert unique regulatory roles and have been shown to modulate the activity of numerous Ca^{2+} channels (Tippens and Lee, 2007, Zhou *et al*., 2004, Cui *et al*., 2007, Haeseleer *et al*., 2004, Few *et al*., 2005, Haynes *et al*., 2004, Kinoshita-Kawada *et al*., 2005). A number of interacting binding partners have also been identified which do not overlap with those of CaM (Dieterich *et al*., 2008, Nakajima, 2011, Seidenbecher *et al*., 2004) and knockout studies have revealed non-redundant roles for CaBP4 and CaBP5 (Maeda *et al*., 2005, Rieke *et al*., 2008). Much less is known about the functions of CaBP7 and CaBP8. Using a range of techniques, including bioinformatics analysis, confocal microscopy and NMR spectroscopy, the research presented in this thesis has focused on the characterisation of CaBP7 and CaBP8. A number of features, including a distinct pattern of EF-hand inactivation and the presence of a 38 amino acid hydrophobic domain at their C-termini, distinguish these proteins from other members in this protein family and prompted further investigation into the importance of these properties. In addition to a regulatory role in TGN to PM trafficking through an interaction with PI4KIIIβ (Mikhaylova *et al*., 2009), roles for CaBP7 in cytokinesis (Neumann *et al*., 2010) and for CaBP8 in the regulation of VGCCs (Shih *et al*., 2009) have also been suggested.

The first aim of this thesis was to perform a bioinformatics analysis of the CaBP family in order to deduce when these proteins first arose in evolution and the degree of sequence conservation they have retained. Phylogenomic analyses confirmed that CaBPs 1-5 and CaBP7 and CaBP8 form two separate families of Ca^{2+}-sensors that likely evolved independently of each other from a CaM-related ancestor. The first appearance of the CaBPs was evident in early vertebrate species. Partial sequences with homology to CaBP1 and CaBP8 were identified in the genome of the jawless fish, lamprey, the closest living species to the early

vertebrate ancestor. No orthologues of the CaBPs were found in invertebrates apart from CaM-like proteins.

A whole genome duplication (WGD) event occurring prior to the divergence of cartilaginous fish likely led to the expansion of the CaBP family. As such, at least four CaBP genes can be identified in the genome of the cartilaginous fish, the elephant shark: two corresponding to CaBP7 and CaBP8 and at least two corresponding to CaBPs 1-5. Another WGD event occurred specific to the bony fish, and accordingly, duplicate genes are found for the full complement of CaBP genes in the teleost fish, the zebrafish. This suggests that whereas the cartilaginous fish possess only four CaBP genes, ancestors of the bony fish lineage must have possessed the full complement of CaBP genes. The appearance of CaBP7 and CaBP8 is easily explained through the duplication of the primordial CaBP8 gene found in Lamprey. The expansion in the number of genes corresponding to CaBPs 1-5 from two in cartilaginous fish to four in the bony fish ancestor, however, cannot be explained by WGDs. This therefore suggests that there has been a transient expansion, between the emergence of cartilaginous fish and the divergence of the bony fish ancestor, in the number of genes corresponding to CaBPs 1-5. No genomes of species representing the sarcopterygian fish node have yet been fully sequenced and therefore the actual complement of CaBP genes in the tetrapod ancestor could not be examined. The genome project for the sarcopterygian fish, the coelacanth is currently underway, and once complete a clearer picture of how the full complement of CaBP genes arose can be obtained.

The CaBPs, particularly CaBP1S, CaBP7 and CaBP8, remain highly conserved throughout the evolution of vertebrates, suggestive of functionally important non-redundant roles for the CaBPs. To help understand the evolutionary pressures which have led this family of Ca^{2+}-sensors to remain highly evolutionarily conserved, an analysis of the emergence of known CaBP target proteins was also carried out. As such, a general expansion of both the VGCC and IP_3R families of Ca^{2+} channels coincided with the emergence of the vertebrate clade. It can therefore be reasoned that the sudden increase in complexity of these families provided the necessary

evolutionary pressures to select for new families of Ca^{2+}-sensing proteins. CaBP7 and CaBP8 have not, however, been shown to directly interact with VGCCs or IP_3Rs, although an effect of CaBP8 overexpression upon Ca^{2+} influx through VGCCs has been described (Shih *et al*., 2009). The evolutionary pressures controlling the remarkable degree of sequence conservation of these two proteins is therefore less easy to explain. There is 84% and 87% sequence identity between the elephant shark and human CaBP7 and CaBP8 proteins, respectively, indicating that these two proteins are unlikely to perform non-redundant roles. The remaining chapters of this thesis therefore focused on the cellular and biochemical characterisation of these two proteins in the hope of gaining a greater understanding of their function.

Initially the subcellular localisation and targeting mechanism of CaBP7 and CaBP8 was examined in both neuronal and non-neuronal cell types. CaBP7 and CaBP8 localise to cellular membranes via a distinct mechanism from CaBP1 and CaBP2, which associate with membranes through a post-translationally attached myristoyl group (Haeseleer *et al*., 2000). CaBP7 and CaBP8 do not possess a consensus sequence for *N*-myristoylation and were instead found to possess a single TMD, 10 amino acids from their extreme C-termini. Generation of a number of TMD mutants demonstrated that this TMD was essential and sufficient for correct subcellular localisation. The use of trypsin protection protease assays and antibody accessibility studies subsequently confirmed that the proteins maintained a topology typical of a special class of membrane protein, the tail anchored (TA) proteins. TA proteins have a cytosolic N-terminal domain, a short luminal C-terminal domain and a single membrane-spanning segment which is less than 30 amino acids from their extreme C-terminus (Kutay *et al*., 1993, Rabu *et al*., 2009). The positioning of the TMD in close proximity to the C-terminal end of a protein dictates that this type of protein must be inserted into membranes post-translationally. Insertion of TA proteins is therefore independent of the Sec61 translocon which is responsible for the co-translational insertion of typical type II membrane proteins (Brambillasca *et al*., 2006). At least three pathways have been identified for the post-translational insertion of TA proteins and the particular pathway engaged appears to be dictated by the overall hydrophobicity of the TMD (Borgese and Fasana, 2011, Kalbfleisch *et*

al., 2007). The hydrophobicity scores of CaBP7 and CaBP8 suggest that either the Asna1 or SRP pathways may facilitate membrane insertion of these proteins. As such, a direct interaction of CaBP8 with Asna1 and a weaker interaction with the SRP associated Sec61 translocon subunit, Sec61β, have been reported (Hradsky *et al*., 2011). Direct evidence that these proteins are required for CaBP7 and CaBP8 membrane insertion has not been demonstrated. Asna1 is an ATPase and has been demonstrated to mediate membrane insertion of VAMP4 and Sec61β in the absence of other cytosolic factors (Favaloro *et al*., 2010). This mechanism was shown to be dependent on the presence of ADP or ATP. In future work the dependence of CaBP7 and CaBP8 membrane insertion upon Asna1, and the presence of ADP or ATP, could also be assessed using reconstituted microsomes in a cell free system.

CaBP7 and CaBP8 were shown to co-localise with markers of the TGN in both neuronal and non-neuronal cell lines. In accordance with this Hradsky *et al.* performed protein-lipid overlay assays and demonstrated that CaBP8 strongly associates with PI4P, PI(4,5)P_2 and PI(3,4,5)P_3 which are lipids enriched at the TGN and PM (Hradsky *et al*., 2011). The TA protein topology and the observed TGN localisation is consistent with the known regulatory role of CaBP7 and CaBP8 in TGN to PM trafficking through an interaction with the cytosolic enzyme, PI4KIIIβ (Mikhaylova *et al*., 2009).

Further investigation into the subcellular localisation of CaBP7 and CaBP8 in HeLa cells revealed extensive co-localisation of CaBP7 with markers of late endosomal and lysosomal compartments. Heterogeneity is often observed between compartments of the late endosomal and lysosomal pathway with the fusion of late endosomes, lysosomes, autophagosomes and MVBs giving rise to the formation of hybrid organelles (Luzio *et al*., 2000, Fader *et al*., 2009, Mullock *et al*., 1998). Autophagosomes and MVBs fuse to form the amphisome, a prelysosomal hybrid organelle, and subsequent fusion of the amphisome with the lysosome allows the degradation of MVB and autophagosome contents (Fader *et al*., 2009). Likewise, late endosomes have been shown to transfer their contents to lysosomes by direct

fusion and hybrid organelle formation rather than vesicular transport (Mullock *et al*., 1998). The lysosome can then be subsequently reformed after the degradation process is complete (Luzio *et al*., 2000). This heterogeneity could therefore cause difficulty discerning the exact species of vesicle in which CaBP7 and CaBP8 are resident. As no co-localisation was observed between CaBP7 and markers of MVBs, autophagosomes, or M6PR-positive late endosomes, it can be reasoned that CaBP7 and CaBP8 reside predominantly on lysosomes.

Interestingly, almost complete overlap was also observed in the localisation of CaBP7 and with both VSVG and VAMP7. VSVG is a commonly used marker of the constitutive secretory pathway (Polishchuk *et al*., 2003). Data presented in this thesis, however, demonstrated that VSVG also co-localised extensively with markers of the late endosomes and lysosomes. This is consistent with CaBP7 co-localisation with the same markers and suggests that VSVG localisation is not specific for constitutive secretory vesicles. In accordance with this observation, no co-localisation was observed between CaBP7 and SNAP29, a post-Golgi SNARE which has been shown to be important in constitutive secretion (Gordon *et al*., 2010).

VAMP7 is a v-SNARE that is important for late endosome to lysosome fusion, amphisome to lysosome fusion and lysosomal exocytosis (Fader *et al*., 2009, Proux-Gillardeaux *et al*., 2007, Martinez-Arca *et al*., 2003). Interestingly, VAMP7 is also a TA protein and it will be interesting to examine whether the targeting of CaBP7 and CaBP8 to lysosomes utilises a similar post-Golgi pathway in future work. Correct localisation of VAMP7 to late endosomes and lysosomes not only requires an intact TMD but also the cytosolic longin domain. Trafficking of VAMP7 has been shown to be reliant on an interaction between the longin domain and the AP3 complex (Martinez-Arca *et al*., 2003).

The adaptor protein complexes, AP1, AP2, AP3 and AP4, are each involved in different trafficking pathways (Bonifacino and Traub, 2003). AP1 and AP4 deliver cargo from the TGN to the PM, AP2 is important for endocytosis and AP3 directs

lysosomal sorting. The μ subunit of each adaptor protein interacts with a distinct but similar type of tyrosine motif which determine the trafficking and turnover of many membrane proteins (Bonifacino and Traub, 2003). Analysis of the protein sequences of CaBP7 and CaBP8 identified a potential lysosomal tyrosine targeting motif residing at the same position in both proteins. The effect of mutating this tyrosine motif was therefore explored. No obvious difference between the tyrosine mutants and wild type proteins was noted, however, the possibility that these tyrosine motifs may contribute to the trafficking dynamics of the proteins cannot be discounted.

The dynamics of lysosomal trafficking can prove difficult to monitor and the most common approach employs ^{35}S methionine pulse chase experiments (Dell'Angelica *et al*., 1999). Subach *et al.* have described an alternative method to accurately measure the dynamics of protein trafficking (Subach *et al*., 2009). Through the use of monomeric fluorescent timers which mature and change colour over time, Subach *et al.* were able to monitor the dynamics of LAMP2A trafficking to lysosomes (Subach *et al*., 2009). A similar method could be employed to deduce the exact trafficking pathway of CaBP7 and CaBP8 and subsequently monitor the trafficking dynamics of various targeting mutants.

Correct localisation of chimaeras of the normally cytosolic CaBP5 fused to the C-terminal domain, encompassing the TMD of CaBP7 or CaBP8, suggests that the cytosolic N-terminal domain does not direct lysosomal targeting of these proteins. Compartmentalisation of CaBP7 and CaBP8 to lysosomes may therefore be dependent on information encoded in the luminal C-terminal domain or may rely solely on the TMD. Hradsky *et al.* generated a number of TMD mutants of CaBP8 fused to GFP and found that the isolated 17 amino acid TMD (as predicted by TMPRED) mislocalised the protein to the ER (Hradsky *et al*., 2011). A proposed longer 23 amino acid TMD was able to correctly localise the protein to the TGN, as was a C-terminal fragment encompassing both the TMD and the luminal domain (Hradsky *et al*., 2011). Although Hradsky *et al.* suggest this is an effect of TMD length, this was not formally proven. It is possible that the observed improvement

in subcellular localisation was due to the presence of targeting determinants encoded within the luminal domain which were not present in the 17 amino acid fusion. Future work should include an in depth analysis of all potential motifs required for correct lysosomal targeting. A mutagenesis approach may help to determine the actual length of the TMD and the contribution of the luminal domain for correct protein compartmentalisation.

CaBP7 and CaBP8 are the first reported instance of CaM-related Ca^{2+}-sensors that target to cellular membranes via a C-terminal tail anchor. Furthermore, no other lysosomal resident EF-hand containing proteins have been described to date. Coupled with the emerging evidence that lysosomes function as important calcium signalling platforms, this localisation is suggestive of a role for CaBP7 and CaBP8 regulating Ca^{2+}-mediated processes in acidic organelles. This is of particular interest when considering the observation that CaBP7 depletion causes failure of cytokinesis (Neumann *et al*., 2010).

The data presented in chapter 5 demonstrated that, as previously shown by Neumann *et al.* (Neumann *et al*., 2010), treatment of HeLa cells with shRNA targeting CaBP7 expression, caused an increase in the number of multinucleate cells. Using high-resolution four-dimensional confocal microscopy, Neumann *et al.* demonstrated that this phenotype arose as a consequence of cytokinesis failure after normal chromosome segregation. Cells were observed to undergo furrow formation but failed at the stage of abscission (Neumann *et al*., 2010). Neumann *et al.* were able to prevent the multinucleate phenotype through complementation with an RNAi resistant mouse CaBP7 orthologue, suggesting that the phenotype did not result from an off target effect. Unfortunately, due to time restraints, the results from these complementation assays were not replicated in this thesis. A number of RNAi resistant CaBP7 variants were generated however, and production of stable cell lines expressing these constructs will permit a more in depth analysis of the requirements for CaBP7 function during mitosis. Along with a wild type resistant construct, both a transmembrane deficient mutant and a mutant defective in Ca^{2+}-binding were also generated. Treatment of stable cell lines expressing these

constructs with CaBP7 specific shRNA will allow dissection of the localisation and Ca^{2+} dependency of this process.

Examination of the subcellular localisation of CaBP7 in dividing cells revealed a redistribution of CaBP7-positive vesicles to the vicinity of the midbody and to opposite poles of the spindle during cytokinesis. Co-immunostaining for endogenous CaBP7 and CD63 demonstrated that CaBP7 retains a late endosomal and lysosomal distribution. Likewise complete co-localisation with VSVG and VAMP7 was observed as also shown in interphase cells in chapter 4. No co-localisation was observed with M6PR-positive endosomes or Rab11-positive recycling endosomes.

The role of lysosomes in cytokinesis remains relatively unstudied with most research focusing on the roles of recycling endosomes and secretory vesicles (McKay and Burgess, 2011, Neto *et al*., 2011). Despite this there is strong evidence to suggest that membrane delivery from late endosomes and lysosomes is important for PM surface area recovery and abscission during cytokinesis. The appearance of LAMP1-positive cell surface blebs during PM surface area recovery in cytokinesis has been reported (Boucrot and Kirchhausen, 2007) and dominant negative mutants of CHMP3 and VAMP7, two proteins involved in late endosome to lysosome fusion, have been shown to induce cytokinesis failure and multiploidy (Dukes *et al*., 2008, Boucrot and Kirchhausen, 2007). Overexpression of the cytosolic longin domain of VAMP7 additionally causes a reduction in PM surface area recovery during cytokinesis and a reduction in the appearance of LAMP1 at the cell surface (Boucrot and Kirchhausen, 2007). Interestingly, the longin domain of VAMP7 was also shown to inhibit lysosomal secretion in an independent study (Proux-Gillardeaux *et al*., 2007). Together these observations are suggestive of a crucial involvement for the fusion of late endosomes and lysosomes with the PM during cytokinesis. The localisation of CaBP7 to VAMP7-positive vesicles infers that CaBP7 may be involved in calcium signalling events controlling membrane fusion, hence explaining the shared binucleate phenotype upon disruption of either protein. Interestingly, direct docking and fusion of VSVG-positive vesicles at the

midzone has also been demonstrated consistent with the presence of CaBP7 on VSVG containing vesicles (Goss and Toomre, 2008). The use of pHluorin tags may allow the fusion of CaBP7-positive vesicles at the cleavage furrow to be monitored in real time. pHluorins are commonly used to monitor the dynamics of proteins associated with endo- and exo-cytotic vesicles (Mahon, 2011). The technology is based on the pH sensitivity of GFP variants. pHluorin exhibits a bimodal excitation spectrum with peaks at 395 nm and 475 nm, and emission at 509 nm. In acidic environments, such as the lumen of the lysosome, excitation at 395 nm decreases, with a corresponding increase in excitation at 475 nm. This effect is reversed upon transfer to a more alkaline environment upon exocytosis (Mahon, 2011). Therefore by fusing a pHluorin tag to the luminal C-terminus of wild type CaBP7 and other variants, the dynamics of lysosomal exocytosis in cells at both interphase and during mitosis could be monitored.

Calcium signalling is fundamental for vesicle transport and likewise perturbations of Ca^{2+} levels during cytokinesis have been shown to affect membrane remodelling and vesicle fusion (Li *et al*., 1999, Shuster and Burgess, 2002). Importantly, PM recovery during cytokinesis has been shown to be perturbed upon treatment of cells with the myosin II inhibitor, blebistatin (Boucrot and Kirchhausen, 2007). Myosin II plays an important role in Ca^{2+} dependent exocytosis in membrane repair and wound healing (Togo and Steinhardt, 2004). Both wound healing and cytokinesis are also sensitive to treatment with BFA which causes the tubulation of endosomes and lysosomes (McNeil and Terasaki, 2001). This is consistent with a potential role for Ca^{2+} mediated lysosomal exocytosis for the efficient abscission of two daughter cells.

Although there is strong evidence to suggest an important role for calcium signalling during cytokinesis, Ca^{2+} transients during different stages of the cell cycle have proven difficult to record (Whitaker, 2006). It has been suggested that highly localised Ca^{2+} elevations may control the different stages in the cell cycle and this may underlie the elusive nature of mitotic Ca^{2+} signals (Whitaker, 2006). Lysosomes represent important platforms for the generation of highly localised Ca^{2+} signals

upon stimulation by NAADP in interphase cells (Galione *et al*., 2010). The NAADP-sensitive Ca^{2+}-release channel, TPC2, has been shown to underpin this process (Pitt *et al*., 2010). Interestingly, depletion of TPC2 was observed to cause mitotic defects in the same high throughput screen which identified a mitotic phenotype for CaBP7 (Neumann *et al*., 2010). Knockdown of TPC2 caused metaphase delay, metaphase alignment problems and cell death. Knockdown of the related protein, TPC1, which is resident on late endosomes, also induced mitotic defects causing a binuclear phenotype and cell death (Neumann *et al*., 2010). Acidic organelles therefore represent interesting candidates for the generation of localised Ca^{2+} signals during mitosis. The generation of a lysosomally targeted Cameleon may allow the detection of localised $[Ca^{2+}]_i$elevations at the surface of lysosomes during the process of cytokinesis. Cameleons are fluorescent Ca^{2+} indicators which function based on the Ca^{2+} dependent binding of CaM to a target binding peptide, M13 (Emmanouilidou *et al*., 1999). The indicator consists of a fusion of ECFP, CaM, M13, and EYFP and works on the basis that upon elevation of $[Ca^{2+}]_i$, CaM binds the M13 peptide bringing the two fluorescent proteins into close proximity and allowing fluorescence resonance energy transfer (FRET) to occur. Imaging of localised Ca^{2+} signals using a cameleon targeted to secretory granules has previously been described (Emmanouilidou *et al*., 1999).

Further investigation is therefore necessary to understand the molecular mechanisms underlying a role for CaBP7 in cytokinesis. Localisation analyses have demonstrated that CaBP7 co-localises with markers of vesicles previously shown to undergo fusion with the PM during cytokinesis. This could implicate CaBP7 in the regulation of Ca^{2+} signalling events involved in the process of lysosomal exocytosis during abscission. The only known function of CaBP7 is a role regulating PI4KIIIβ (Mikhaylova *et al*., 2009). Interestingly PI4K homologs in *Schizosaccharomyces pombe* and *Drosophilamelanogaster* have been shown to be important for the completion of cytokinesis (Park *et al*., 2009, Polevoy *et al*., 2009). Deletion of the yeast homolog PIK1 is lethal, however, ectopic expression of a loss of function allele in PIK1 null yeast allowed normal cell proliferation but exhibited a defect in septation (Park *et al*., 2009). Knockout of the *Drosophila* homolog, Fwd, is not

lethal, however, male flies are sterile and exhibit multinucleate cells characteristic of a meiotic cytokinesis defect (Polevoy *et al*., 2009). Expression of Fwd mutants in *Drosophila* spermatocytes cause defects in late cytokinesis resembling the phenotype observed for CaBP7: the cleavage furrow is able to constrict but becomes unstable and later regresses resulting in multinucleate cells. Interestingly, the cytokinesis defects in Fwd null drosophila have been attributed to loss of regulation of Rab11. Fwd is required for the localisation of Rab11 in dividing cells and is also required for the formation of PI4P containing secretory vesicles that localize to the midzone (Polevoy *et al*., 2009). CaBP7 inhibits the activity of PI4KIIIβ in mammalian cells (Mikhaylova *et al*., 2009) and does not appear to co-localise with Rab11 in interphase cells or in dividing cells. Additionally, CaBP7 is not expressed in yeast or *Drosophila*, and its role regulating PI4K is specific to vertebrate species. Although it therefore seems unlikely that the cytokinesis defects observed in CaBP7 deficient cells are due to deregulation of PI4K this mechanism cannot be discounted. CaBP7 mutants defective in PI4K binding could be generated and their ability to prevent the binucleate phenotype upon CaBP7 knockdown could be assessed in order to rule this possibility out.

The ability of Ca^{2+}-sensors to regulate essential Ca^{2+} dependent processes relies on their ability to undergo drastic conformational changes upon binding to Ca^{2+}. Different Ca^{2+}-sensors behave differently depending on their Ca^{2+}-binding affinities and structural properties. In order to better understand the differences between CaBPs 1-5 and CaBP7 & 8, NMR analyses of representative proteins from the two sub-families, CaBP4 and CaBP7, were attempted. Problems with aggregation hindered the progress of this project but preliminary steps were made towards solving the structures of these two proteins.

CaBP4 is at the upper size limit (≈ 30 kDa) for proteins which can be analysed by NMR. This was reflected in the NMR data obtained for this protein. An insufficient number of peaks were recorded in NMR spectra to represent the 275 amino acids in this protein. In addition, a relatively large number of sharp peaks characteristic of an unstructured region of the protein were observed. The N-termini of the CaBP

proteins are the most divergent region of this family of Ca^{2+}-sensors. NMR and X-ray crystallography have shown that this portion of the protein is unstructured in CaBP1. The N-terminal region of CaBP4, preceding the start of the first EF-hand motif, is greatly extended compared with the other CaBP proteins with the exception of caldendrin. Interestingly, in secondary structure predictions, the N-terminus of CaBP4 forms a region of random coil. It can be reasoned, therefore, that the sharp peaks observed in CaBP4 spectra may represent an unstructured extended N-terminus. In future work in may be possible to assign the sharp peaks in order to deduce if they correspond to a contiguous stretch of amino acids at the N-terminus of CaBP4. If this can be confirmed, a new construct encoding CaBP4 without the extended N-terminal region could be generated to produce a recombinant protein that is more amenable to NMR analysis.

CaBP4 represents an important member of the CaBP family of proteins due to its proven non-redundant role in photostransduction pathways of the retina (Maeda *et al*., 2005). CaBP4 is thought to mediate these roles through interactions with $Ca_v1.3$ and $Ca_v1.4$ VGCCs (Haeseleer *et al*., 2004, Lee *et al*., 2007b). It will be interesting to discover which regions are important for CaBP4 interactions with various VGCCs and whether they differ from interactions of CaBP1 with related VGCCs. It has been deduced that interactions between CaBP1 and $Ca_v1.2$ channels are mediated through interactions with the N-terminus, the S3-S4 linker and the IQ domain (Findeisen and Minor, 2010). CaBP4 is of particular interest due to the identification of various CaBP4 mutations in patients exhibiting cone-rod synaptic disorders of varying severity (Aldahmesh *et al*., 2010, Littink *et al*., 2009, Zeitz *et al*., 2006). By deducing the critical regions needed for CaBP4 interactions with VGCCs, and by examining the nature of the mutations detected in humans, the molecular basis for these visual disorders can be investigated. Using NMR the structure of CaBP4 in complex with interacting peptides could be solved and the effect of different mutations on peptide binding directly examined.

Problems encountered because of protein aggregation precluded NMR analysis of full length CaBP7 and a mutant lacking the TMD (CaBP7 1-188). A fragment

encoding the first 100 amino acids of CaBP7 (CaBP7 1-100) proved more amenable to analysis by this technique. Over 85% of the CaBP7 1-100 backbone assignment was completed and progress towards assigning the side chains of this fragment was made. The assigned NMR spectrum exhibited features characteristic of a Ca^{2+}-bound Ca^{2+}-sensor, namely the two downfield shifted peaks corresponding to the glycine residues at the 6^{th} position of each EF-hand. The peaks in the assigned spectrum were well dispersed, consistent with a well-folded protein and many of the more downfield shifted peaks corresponded to amino acids within the two EF-hand motifs. Assignment of the CaBP7 1-100 backbone and side chains allowed secondary structure calculations to be carried out using CSI and DANGLE. The output secondary structure closely approximated that of CaM and CaBP1S N-termini. In order to solve the tertiary structure of CaBP7 1-100 data from NOESY experiments will be required. NOESY experiments provide data about resonances that are close together in space and can be used to generate restraints for structure calculations and aid disambiguation of spectral overlap (Cavanagh *et al*., 2007b).

Spectra for the apo form of CaBP7 1-100 were also obtained and compared to spectra after addition of saturating Ca^{2+}. The two spectra were completely different suggesting a significant conformational change upon the addition of Ca^{2+}. This was in accordance with previously published data from fluorimetry assays (Mikhaylova *et al*., 2009). In addition a significant mobility shift was observed between Ca^{2+}-free and Ca^{2+}-bound CaBP7 1-100 on native PAGE gels. In the same experiment no shift in mobility was observed upon addition of Mg^{2+}. This data suggested that CaBP7 1-100 binds specifically to Ca^{2+} and not to Mg^{2+}.

Differences in the conformational changes of CaBP1 and CaM N-termini upon Ca^{2+} binding have been observed with CaBP1 adopting a more closed conformation and CaM adopting a more open conformation (Park *et al*., 2011, Chin and Means, 2000). These differences may be explained through the differences in cation binding properties of the two proteins. Whereas the N-terminal domain of CaM can co-ordinate a Ca^{2+} ion at each of its two EF-hands, CaBP1 has a non-functional EF2 motif and therefore binds Ca^{2+} only at EF1 (Chin and Means, 2000, Wingard *et al*.,

2005). Like CaM, CaBP7 has functional EF1 and EF2 motifs and therefore may be predicted to behave similarly. Differences in the Ca^{2+} affinities of CaBP7 (≈ 0.2 µm) (Mikhaylova *et al*., 2009) and CaM (≈ 4 - 20 µM) (Schaad *et al*., 1996) may, however, suggest there are likely to be structural differences between their EF-hand motifs. It will therefore be important to deduce the structures of both the Ca^{2+}-free and the Ca^{2+}-bound forms of CaBP7 1-100 in order to assess how the associated conformational change compares to that of related Ca^{2+}-sensors.

The N-terminal domain of CaBP7, containing the first pair of EF-hands and encoded by CaBP7 1-100, displays significantly higher homology to CaM and CaBP1 than the C-terminal domain. Despite a maximum of 10% sequence identity of the CaBP7 C-terminus with CaM, this region has remained remarkably conserved through evolution. The C-terminus of CaBP7 contains amino acid sequences loosely resembling a second pair of EF-hand motifs. Deletions, insertions and substitutions have, however, rendered these motifs inactive for cation binding. Although the domain does not participate in Ca^{2+} binding, the high sequence conservation through evolution implies that it imparts an important functional role. Elucidation of the structure of the C-terminus therefore represents an important task for the future to permit a full understanding of CaBP7 structure. NMR spectra of CaBP7 1-188 exhibited dispersed peaks which did not correspond to the spectra of CaBP7 1-100 suggesting that the C-terminal portion of this protein was at least partially folded. A large degree of overlap, characteristic of protein aggregation, was observed in the centre of CaBP7 1-188 spectra which was not observed in CaBP7 1-100 spectra. Therefore the C-terminus of CaBP7 may be critical in the formation of aggregates. Hradsky *et al.* have demonstrated that CaBP7, and the closely related CaBP8, are able to form dimers and higher order oligomers which may go some way toward explaining the aggregation problems encountered (Hradsky *et al*., 2011). In addition, the C-terminus of CaBP7 1-188 contains five cysteine residues. Cysteines can often cause problems with recombinant protein solubility due to the formation of incorrect disulphide bridges between monomers. Expression of sufficient levels of soluble CaBP7 1-188 or the CaBP7 C-terminal domain may therefore require mutation or modification of these residues.

Due to the limited information known about CaBP7 and CaBP8 function, identification of interacting binding partners should constitute a key area for future research. With this aim in mind, yeast-2-hybrid library screens were attempted during the course of this PhD project using CaBP7 and CaBP8 as bait proteins, with and without their respective TMDs (data not shown). The proteins displayed a propensity for autoactivation, therefore the data was not used in this thesis. Pull down assays, and subsequent mass spectroscopy, represent an alternative technique for the identification of unique binding partners of CaBP7 (Haynes *et al*., 2006).

Once more is known about the functions of CaBP7, NMR will prove useful for determining the interaction surfaces required for CaBP7 binding to target proteins. The demonstrated direct interaction of CaBP7 with PI4KIIIβ could be dissected in this way. Binding assays between different fragments of the two proteins will allow the binding interface(s) to be mapped. Once this is deduced, NMR can be used to monitor the dynamics of the binding process. Changes to the NMR spectra of CaBP7 upon addition of the binding peptide can be monitored and, if assigned, will allow the identification of critical amino acid residues. Reciprocal experiments, isotopically labelling either CaBP7 or the target peptide, would also enable the structure of the complex to be solved. NMR therefore represents a powerful tool for the analysis of protein-protein interactions.

Conclusion

A combination of bioinformatics, cell biology and structural biology techniques have been used to generate the data presented in this thesis which focused on the characterisation of CaBP7 and CaBP8. A number of distinct conclusions can be drawn from this data:

- Bioinformatics analyses revealed important information concerning the evolution of these proteins and categorised CaBP7 and CaBP8 into a group of Ca^{2+}-sensors distinct from CaBPs1-5.

- Studies examining the membrane association of CaBP7 and CaBP8 in neuronal and non-neuronal cell types revealed that they belong to the TA class of integral membrane proteins. Localisation of these proteins to the TGN and lysosomes was also reported – a distribution unique to this group of EF-hand containing Ca^{2+}-sensors.
- Depletion of CaBP7 in HeLa cells confirmed a previously reported mitotic phenotype for this protein: upon knockdown of CaBP7, an increase in the number of binucleate cells was observed. Closer examination of CaBP7 during different stages of the cell cycle demonstrated a redistribution of CaBP7-positive vesicles to the vicinity of the interzonal microtubules and opposite poles of the spindle during cytokinesis.
- CaBP7 remained associated with lysosomes during all stages of the cell cycle and colocalised with proteins previously implicated in membrane delivery to the cell surface during cytokinesis. Lysosomes are emerging as important platforms for calcium signalling, and therefore CaBP7 may play a role in the regulation of Ca^{2+} signalling processes at the lysosomal membrane, both during interphase and in dividing cells.
- Finally the use of NMR spectroscopy led to the partial backbone and side chain assignment of a 100 amino acid N-terminal fragment of CaBP7. The secondary structure of this fragment was calculated and closely resembled that of Ca^{2+}-bound CaM and CaBP1S N-termini. Spectra for apo CaBP7 were completely distinct from that of Ca^{2+}-saturated CaBP7 implying that the protein undergoes a significant conformational change upon Ca^{2+}-binding. Continued NMR analysis will hopefully lead to the deduction of a high-resolution structure for CaBP7.

Appendix

Table A1. Protein expression plasmids and descriptions.

Plasmid	Antibiotic Resistance	Tag	Description
pGEX-6P1	Amp	GST	PreScission Protease cleavage of GST tag
pGEX-N2	Amp	GST	Tag is at the C-terminus instead of the N-terminus
pTrcHisA	Amp	His	High level regulated expression from trc promoter. Enhanced translation efficiency of eukaryotic genes. Enterokinase cleavage of tag
pTrcHisTEV	Amp	His	Same as pTrcHisA except now encodes a TEV cleavage site
pETM11	Kan	His	TEV cleavage of tag
pOPIN-s	Amp	His-SUMO	SUMO fusion for increased solubility and stability of difficult to express proteins
pE-SUMOPRO	Kan	His-SUMO	SUMO fusion for increased solubility and stability of difficult to express proteins. Powerful T7 promoter.

Table A2. Assignment summary table.

Category	Available	Assigned	% Assigned	Min Shift	Mean Shift	Max Shift
Element C	490.00	322.00	65.71	11.28	77.95	181.32
Element H	593.00	415.00	69.98	0.13	3.75	10.60
Element N	129.00	85.00	65.89	104.89	118.30	129.65
Amide	192.00	164.00	85.42	None	None	None
Backbone	392.00	337.00	85.97	None	None	None
Backbone non-H	300.00	255.00	85.00	None	None	None
Side Chain H	501.00	333.00	66.47	0.13	2.66	7.57
Side Chain non-H	319.00	152.00	47.65	11.28	33.55	112.57
Type N	100.00	82.00	82.00	104.89	118.56	129.65
Type ND	4.00	1.00	25.00	112.57	112.57	112.57
Type NE	11.00	2.00	18.18	108.95	110.64	112.33
Type NZ	2.00	0.00	0.00	None	None	None
Type NH	12.00	0.00	0.00	None	None	None
Type H	92.00	82.00	89.13	7.00	8.20	10.60
Type HA	108.00	90.00	83.33	3.30	4.16	5.39
Type HB	162.00	132.00	81.48	1.27	2.29	4.47
Type HG	120.00	73.00	60.83	0.27	1.66	2.88
Type HD	72.00	30.00	41.67	0.13	1.65	7.57
Type HE	33.00	8.00	24.24	2.87	4.78	7.49
Type HZ	6.00	0.00	0.00	None	None	None
Type C	100.00	87.00	87.00	170.69	176.78	181.32
Type CA	100.00	86.00	86.00	44.97	57.61	66.90
Type CB	92.00	77.00	83.70	18.11	37.40	70.03
Type CG	99.00	46.00	46.46	17.07	26.75	37.26
Type CD	67.00	24.00	35.82	11.28	23.84	43.41
Type CE	17.00	2.00	11.76	41.88	42.06	42.25
Type CZ	15.00	0.00	0.00	None	None	None
Residue Ala	4.00	2.00	50.00	None	None	None
Residue Arg	6.00	6.00	100.00	None	None	None
Residue Asn	3.00	3.00	100.00	None	None	None
Residue Asp	8.00	8.00	100.00	None	None	None
Residue Gln	4.00	4.00	100.00	None	None	None
Residue Glu	12.00	12.00	100.00	None	None	None
Residue Gly	8.00	8.00	100.00	None	None	None
Residue His	1.00	0.00	0.00	None	None	None
Residue Ile	6.00	6.00	100.00	None	None	None
Residue Leu	10.00	9.00	90.00	None	None	None
Residue Lys	2.00	2.00	100.00	None	None	None
Residue Met	5.00	3.00	60.00	None	None	None
Residue Phe	6.00	5.00	83.33	None	None	None
Residue Pro	7.00	4.00	57.14	None	None	None
Residue Ser	3.00	3.00	100.00	None	None	None
Residue Thr	4.00	3.00	75.00	None	None	None
Residue Tyr	3.00	2.00	66.67	None	None	None
Residue Val	8.00	7.00	87.50	None	None	None
All Residues	100.00	87.00	87.00	None	None	None
Spin Systems	137.00	103.00	75.18	None	None	None

Table A3. Side chain assignments for CaBP7 1-100.

	H	N	C	CA							
2 Pro	-	-	-	-							
3 Phe	-	-	-	-							
4 His	-	-	-	-							
5 Pro	-	-	-	-							
6 Val	-	-	-	-							
7 Thr	-	-	-	-							
8 Ala	-	-	-	-							
9 Ala	-	-	-	-							
10 Leu	-	-	-	-							
11 Met	-	-	-	-							
12 Tyr	-	-	-	-							
13 Arg	-	-	176.67	-	4.20:Ha	1.76:Hb2	1.76:Hb3				
14 Gly	7.90	107.94	174.06	45.63	3.86:Ha2	3.88:Ha3					
15 Ile	7.76	118.74	175.59	61.65	4.10:Ha	1.74:Hb	1.02:Hg12	1.22:Hg13	0.77:Hg2*	0.77:Hd1*	38.78:Cb 26.83:Cg1 17.42:Cg2 13.03:Cd1
16 Tyr	7.99	121.50	175.51	57.67	4.64:Ha	2.82:Hb2	3.05:Hb3	38.96:Cb			
17 Thr	7.84	115.43	173.81	61.57	4.31:466	4.09:467	70.03:Cb				
18 Val	8.02	122.97	174.44	60.58	32.29:Cb						
19 Pro	-	-	176.54	63.54	4.33:Ha	1.83:Hb2	2.25:Hb3	31.96:Cb			
20 Asn	8.32	117.54	175.40	53.45	4.61:Ha	2.77:Hb2	2.80:Hb3	6.85:Hd21	7.57:Hd22	38.59:Cb	112.57:[949]
21 Leu	8.10	121.80	177.33	55.89	4.26:Ha	1.60:Hb2	1.60:Hb3	42.34:Cb			
22 Leu	8.08	120.46	177.44	55.37	4.33:Ha	1.63:Hb2	1.63:Hb3	42.06:Cb			
23 Ser	7.98	115.05	174.61	58.69	4.35:Ha	3.82:Hb2	3.87:Hb3	63.85:Cb			
24 Glu	8.26	121.74	176.21	56.69	4.27:Ha	1.96:Hb2	2.04:Hb3	2.23:Hg2	2.23:Hg3	30.25:Cb	36.27:Cg
25 Gln	8.20	120.28	175.43	55.72	4.29:Ha	1.96:Hb2	2.04:Hb3	2.32:Hg2	2.31:Hg3	6.78:He21	7.49:He22 29.42:Cb 33.87:Cg 112.33:[956]
26 Arg	8.25	123.29	174.14	54.01	4.60:Ha	1.71:Hb2	1.82:Hb3	1.64:Hg2	1.64:Hg3	3.18:Hd2	3.18:Hd3 30.35:Cb 26.90:Cg 43.41:Cd
27 Pro	-	-	176.70	63.14	4.44:Ha	1.90:Hb2	2.26:Hb3	31.94:Cb			
28 Val	8.02	118.44	175.53	62.21	4.07:Ha	2.04:Hb	0.91:Hg1*	0.91:Hg2*	32.89:Cb	20.39:Cg1	21.25:Cg2
29 Asp	8.20	122.82	175.32	53.99	4.63:Ha	2.56:Hb2	2.60:Hb3	41.27:Cb			
30 Ile	7.92	122.68	174.05	58.63	4.42:Ha	1.77:Hb	1.07:Hg12	1.50:Hg13	0.93:Hg2*	0.78:Hd1*	39.49:Cb 27.26:Cg1 17.21:Cg2 13.21:Cd1
31 Pro	-	-	177.39	63.06	32.49:Cb						
31 Pro	-	-	-	-	4.43:Ha	1.99:Hb2	2.39:Hb3				
32 Glu	8.70	122.17	177.50	59.02	4.03:Ha	2.04:Hb2	2.04:Hb3	29.83:Cb			
33 Asp	8.55	117.87	177.86	55.66	4.48:Ha	2.68:Hb2	2.74:Hb3	40.20:Cb			
34 Glu	7.96	121.51	177.91	58.31	4.27:Ha	2.01:Hb2	2.11:Hb3	2.29:Hg2	2.33:Hg3	29.53:Cb	36.25:Cg
35 Leu	8.17	120.05	178.66	57.14	4.22:Ha	1.73:Hb2	1.79:Hb3	1.67:Hg	0.95:Hd1*	1.02:Hd2*	41.92:Cb 27.15:Cg 24.52:Cd1 24.54:Cd2
36 Glu	8.08	119.00	178.81	59.69	4.14:Ha	2.12:Hb2	2.24:Hb3	2.36:Hg2	2.47:Hg3	29.20:Cb	36.23:Cg
37 Glu	7.99	118.56	179.25	59.71	29.14:Cb						
38 Ile	8.04	120.21	178.26	64.97	3.97:Ha	2.20:Hb	1.92:Hg12	1.92:Hg13	1.19:Hg2*	0.87:Hd1*	37.86:Cb 29.59:Cg1 19.04:Cg2 13.64:Cd1
39 Arg	8.64	121.77	178.96	60.26	4.05:Ha	1.83:Hb2	1.83:Hb3	29.86:Cb			
40 Glu	8.10	118.40	179.09	59.17	29.01:Cb						

Table A3 Continued. Side chain assignments for CaBP7 1-100.

	H	N	C	CA							
41 Ala	7.93	121.60	178.59	55.19	4.12:Ha	1.74:Hb*	18.11:Cb				
42 Phe	8.38	118.35	177.20	62.18	3.30:Ha	2.89:Hb2	3.26:Hb3	39.56:Cb			
43 Lys	7.84	116.28	177.83	59.28	3.82:Ha	1.90:Hb2	1.90:Hb3	1.53:Hg2	1.77:Hg3	1.66:Hd2	1.66:Hd3 2.87:He2 2.90:He3 32.67:Cb 25.67:Cg 29.71:Cd 42.25:Ce
44 Val	7.31	117.67	177.09	65.62	3.44:Ha	2.05:Hb	0.53:Hg1*	0.98:Hg2*	31.13:Cb	20.93:Cg1	22.82:Cg2
45 Phe	7.00	115.60	176.99	59.59	4.13:Ha	2.58:Hb2	2.67:Hb3	40.67:Cb			
46 Asp	7.89	117.97	177.09	52.28	4.53:Ha	1.42:Hb2	2.28:Hb3	38.76:Cb			
47 Arg	7.46	124.43	177.99	58.74	3.92:Ha	1.84:Hb2	1.96:Hb3	3.25:Hd2	3.26:Hd3	30.38:Cb	27.21:Cg 42.95:Cd
47 Arg	-	-	176.67	-	4.20:Ha	1.71:Hg2	1.80:Hg3				
48 Asp	8.24	114.26	177.80	53.02	4.59:Ha	2.66:Hb2	3.10:Hb3	39.67:Cb			
49 Gly	7.72	109.09	175.10	47.17	3.85:Ha2	3.85:Ha3					
50 Asn	8.35	119.64	175.95	52.76	4.64:Ha	2.69:Hb2	3.43:Hb3	38.20:Cb			
51 Gly	10.60	112.65	172.49	45.06	3.42:Ha2	4.04:Ha3					
52 Phe	7.65	116.06	174.80	56.05	5.11:Ha	2.61:Hb2	2.61:Hb3	43.75:Cb			
53 Ile	10.24	127.42	175.63	61.00	4.68:Ha	1.83:Hb	0.87:Hg12	1.22:Hg13	0.27:Hg2*	0.13:Hd1*	38.74:Cb 17.42:Cg2 15.11:Cd1
54 Ser	8.99	123.92	175.24	56.02	4.87:Ha	4.00:Hb2	4.47:Hb3	66.78:Cb			
55 Lys	9.41	121.52	178.34	61.11	3.83:Ha	1.87:Hb2	1.92:Hb3	1.39:Hg2	1.43:Hg3	1.76:Hd2	1.76:Hd3 2.96:He2 2.96:He3 32.23:Cb 25.80:Cg 28.95:Cd 41.88:Ce
56 Gln	8.38	117.23	179.73	59.34	4.11:Ha	2.03:Hb2	2.10:Hb3	2.45:Hg2	2.45:Hg3	28.19:Cb	34.22:Cg
57 Glu	8.03	121.69	179.71	59.31	3.99:Ha	2.56:Hb2	2.56:Hb3	29.30:Cb			
58 Leu	8.80	122.03	178.79	58.57	4.10:Ha	1.54:Hb2	2.03:Hb3	1.59:Hg	0.83:Hd1*	0.86:Hd2*	41.71:Cb 41.79:Cb 26.35:Cd1 23.80:Cd2
59 Gly	8.43	105.35	175.60	48.46	4.04:Ha2	3.66:Ha3					
60 Thr	8.21	118.89	176.85	66.90	3.90:Ha	4.23:Hb	1.24:Hg2*	68.83:Cb	21.64:Cg2		
61 Ala	8.43	124.83	180.28	55.32	3.99:Ha	1.27:Hb*	18.89:Cb				
62 Met	8.49	115.73	178.69	60.31	4.04:Ha	2.17:Hb2	2.22:Hb3	2.40:Hg2	2.88:Hg3	32.45:Cb	34.17:Cg
63 Arg	8.29	119.32	181.32	59.30	4.66:Ha	1.96:Hb2	1.96:Hb3	29.97:Cb			
64 Ser	8.09	117.86	174.97	61.70	4.31:Ha	4.03:Hb2	4.05:Hb3	62.97:Cb			
65 Leu	7.45	120.32	176.36	54.91	4.40:Ha	1.83:Hb2	1.97:Hb3	1.83:Hg	0.90:Hd1*	0.89:Hd2*	42.82:Cb 26.80:Cg 22.89:Cd1 25.74:Cd2
66 Gly	7.68	104.89	173.84	45.13	3.63:Ha2	4.23:Ha3					
67 Tyr	7.92	121.07	173.80	57.39	4.61:Ha	2.62:Hb2	2.88:Hb3	40.62:Cb			
68 Met	8.34	120.94	173.31	52.10							
69 Pro	-	-	176.99	62.24	4.72:Ha	2.02:Hb2	2.02:Hb3	32.10:Cb			
70 Asn	8.88	120.15	175.52	51.50	4.87:Ha	2.87:Hb2	3.19:Hb3	39.22:Cb			
71 Glu	8.58	118.48	178.85	60.32	3.93:Ha	2.06:Hb2	2.06:Hb3	2.35:Hg2	2.35:Hg3	29.58:Cb	36.29:Cg
72 Val	7.82	119.35	178.07	65.90	3.78:Ha	2.11:Hb	0.94:Hg1*	1.00:Hg2*	31.59:Cb	22.22:Cg2	
73 Glu	8.04	120.01	179.00	59.34	3.89:Ha	1.86:Hb2	2.25:Hb3	2.22:Hg2	2.43:Hg3	29.90:Cb	37.26:Cg
74 Leu	7.88	116.45	178.17	57.92	3.96:Ha	1.38:Hb2	1.90:Hb3	1.78:Hg	0.81:Hd1*	0.87:Hd2*	42.34:Cb 26.78:Cg 23.74:Cd1 25.35:Cd2
75 Glu	7.64	117.66	178.73	59.33	3.97:Ha	2.15:Hb2	2.15:Hb3	2.28:Hg2	2.39:Hg3	29.21:Cb	36.11:Cg
76 Val	8.03	119.35	178.49	66.50	3.63:Ha	2.19:Hb	0.91:Hg1*	1.07:Hg2*	31.63:Cb	21.42:Cg1	22.82:Cg2
77 Ile	7.80	119.50	177.68	65.86,	66.00 3.49	:Ha 1.87	:Hb 1.88	:Hg12 1.88:	Hg13 0.78	:Hg2* 0.78	:Hd1* 37.94:Cb 29.46:Cg1 18.17:Cg2 13.81:Cd1
78 Ile	7.90	117.84	177.46	64.34	3.48:Ha	1.96:Hb	1.29:Hg12	1.43:Hg13	0.80:Hg2*	0.69:Hd1*	36.65:Cb 29.06:Cg1 17.07:Cg2 11.28:Cd1

Table A3 Continued. Side chain assignments for CaBP7 1-100.

	H	N	C	CA							
79 Gln	8.26	117.47	178.45	58.96	4.04:Ha	2.15:Hb2	2.15:Hb3	2.45:Hg2	2.60:Hg3	28.20:Cb	34.31:Cg
80 Arg	7.69	116.64	177.39	57.58	4.10:Ha	1.93:Hb2	1.93:Hb3	30.01:Cb			
81 Leu	7.42	117.06	176.85	55.47	4.31:Ha	1.43:Hb2	1.44:Hb3	1.81:Hg	0.77:Hd1*	0.77:Hd2*	44.91:Cb 26.11:Cd1 26.11:Cd2
82 Asp	8.10	116.74	176.39	54.39	4.51:Ha	2.41:Hb2	2.83:Hb3	40.65:Cb			
83 Met	-	-	-	-	4.42:Ha	2.14:Hb2	2.19:Hb3				
83 Met	8.61	126.87	177.55	57.06	2.60:Hg2	2.79:Hg3	34.35:Cb	32.35:Cg			
84 Asp	8.36	116.49	178.17	53.30	4.66:Ha	2.68:Hb2	3.06:Hb3	40.38:Cb			
85 Gly	7.66	108.89	175.23	47.38	3.83:Ha2	3.96:Ha3					
86 Asp	8.37	120.73	177.71	53.56	4.49:Ha	2.49:Hb2	2.91:Hb3	40.23:Cb			
87 Gly	10.19	112.84	172.84	45.90	3.43:Ha2	4.02:Ha3					
88 Gln	7.98	115.68	174.92	53.09	108.95:Ne2	4.92:Ha	1.79:Hb2	1.99:Hb3	1.92:Hg2	1.99:Hg3	5.82:He21 6.46:He22 32.55:Cb 33.37:Cg
89 Val	8.97	124.43	175.78	61.42	5.27:Ha	2.22:Hb	0.84:Hg1*	1.24:Hg2*	34.12:Cb	22.04:Cg1	22.02:Cg2
90 Asp	9.52	129.65	176.16	52.06	5.39:Ha	3.00:Hb2	3.05:Hb3	41.68:Cb			
91 Phe	8.50	118.81	176.18	62.27	3.48:Ha	2.10:Hb2	2.48:Hb3	38.85:Cb			
92 Glu	7.96	117.42	179.94	60.00	3.70:Ha	2.02:Hb2	2.11:Hb3	2.28:Hg2	2.28:Hg3	28.80:Cb	37.07:Cg
93 Glu	8.47	120.97	178.50	58.94	4.00:Ha	2.27:Hb2	2.27:Hb3	29.60:Cb			
94 Phe	8.57	122.34	176.39	61.65	3.96:Ha	3.16:Hb2	3.24:Hb3	40.86:Cb			
95 Val	8.17	114.49	178.02	65.59	3.32:Ha	1.74:Hb	0.53:Hg1*	0.64:Hg2*	31.34:Cb	22.78:Cg1	21.68:Cg2
96 Thr	7.55	114.77	176.09	65.98	3.90:Ha	4.25:Hb	1.29:Hg2*	68.88:Cb	21.47:Cg2		
97 Leu	7.50	120.92	177.23	56.93	1.48:654	1.48:655	4.03:Ha	1.43:Hb2	1.54:Hb3	1.59:Hg	0.66:Hd1* 0.73:Hd2* 42.16:Cb 27.05:Cg 24.86:Cd1 24.31:Cd2
98 Leu	7.35	116.06	177.05	55.26	0.66:730	4.16:Ha	1.50:Hb2	1.50:Hb3	1.42:Hg	0.56:Hd1*	0.66:Hd2* 42.13:Cb 27.23:Cg 25.44:Cd1 23.32:Cd2
99 Gly	7.63	106.92	170.69	44.97	3.88:Ha2	4.09:Ha3					

Bibliography

ABELL, B. M., POOL, M. R., SCHLENKER, O., SINNING, I. & HIGH, S. 2004. Signal recognition particle mediates post-translational targeting in eukaryotes. *The EMBO journal,* 23**,** 2755-64.

ALDAHMESH, M. A., AL-OWAIN, M., ALQAHTANI, F., HAZZAA, S. & ALKURAYA, F. S. 2010. A null mutation in CABP4 causes Leber's congenital amaurosis-like phenotype. *Mol Vis,* 16**,** 207-12.

AMES, J. B., GORDON, J. I., IKURA, M. & STRYER, L. 1997. NMR studies of calcium-bound recoverin containing a polar mvristoyl analog. *FASEB Journal,* 11.

AMES, J. B., TANAKA, T., STRYER, L. & IKURA, M. 1996. Portrait of a myristoyl switch protein. *Current opinion in structural biology,* 6**,** 432-438.

ARAVIND, P., CHANDRA, K., REDDY, P. P., JEROMIN, A., CHARY, K. V. & SHARMA, Y. 2008. Regulatory and structural EF-hand motifs of neuronal calcium sensor-1: Mg 2+ modulates Ca 2+ binding, Ca 2+ -induced conformational changes, and equilibrium unfolding transitions. *J Mol Biol,* 376**,** 1100-15.

ASHWORTH, R., DEVOGELAERE, B., FABES, J., TUNWELL, R. E., KOH, K. R., DE SMEDT, H. & PATEL, S. 2007. Molecular and functional characterization of inositol trisphosphate receptors during early zebrafish development. *The Journal of biological chemistry,* 282**,** 13984-13993.

ASMARA, H., MINOBE, E., SAUD, Z. A. & KAMEYAMA, M. 2010. Interactions of calmodulin with the multiple binding sites of Cav1.2 Ca2+ channels. *Journal of pharmacological sciences,* 112**,** 397-404.

ATILLA-GOKCUMEN, G. E., CASTORENO, A. B., SASSE, S. & EGGERT, U. S. 2010. Making the cut: the chemical biology of cytokinesis. *ACS chemical biology,* 5**,** 79-90.

AUGUSTINE, G. J., SANTAMARIA, F. & TANAKA, K. 2003. Local calcium signaling in neurons. *Neuron,* 40**,** 331-346.

BAHI, N., FRIOCOURT, G., CARRIE, A., GRAHAM, M. E., WEISS, J. L., CHAFEY, P., FAUCHEREAU, F., BURGOYNE, R. D. & CHELLY, J. 2003. IL1 receptor accessory protein like, a protein involved in X-linked mental retardation, interacts with Neuronal Calcium Sensor-1 and regulates exocytosis. *Hum Mol Genet,* 12**,** 1415-25.

BAKER, P. F. & WARNER, A. E. 1972. Intracellular calcium and cell cleavage in early embryos of Xenopus laevis. *The Journal of cell biology,* 53**,** 579-81.

BALLA, A. & BALLA, T. 2006. Phosphatidylinositol 4-kinases: old enzymes with emerging functions. *Trends in cell biology,* 16**,** 351-61.

BARRITT, G. J. 1999. Receptor-activated Ca2+ inflow in animal cells: a variety of pathways tailored to meet different intracellular Ca2+ signalling requirements. *The Biochemical journal,* 337**,** Pt 2/.

BATISTIC, O. & KUDLA, J. 2009. Plant calcineurin B-like proteins and their interacting protein kinases. *Biochimica et biophysica acta,* 1793**,** 985-992.

BAYLOR, D. 1996. How photons start vision. *Proceedings of the National Academy of Sciences of the United States of America,* 93**,** 560-565.

BAZHIN, A. V., SAVCHENKO, M. S., BELOUSOV, E. V., JAQUES, G. & PHILIPPOV, P. P. 2004. Stimulation of the aberrant expression of a paraneoplastic antigen, recoverin, in small cell lung cancer cell lines. *Lung Cancer,* 45**,** 299-305.

BEAR, M. F. & MALENKA, R. C. 1994. Synaptic plasticity: LTP and LTD. *Current opinion in neurobiology,* 4**,** 389-99.

BEECH, D. J. 2007. Canonical transient receptor potential 5. *Handb Exp Pharmacol***,** 109-23.

BEILHARZ, T., EGAN, B., SILVER, P. A., HOFMANN, K. & LITHGOW, T. 2003. Bipartite signals mediate subcellular targeting of tail-anchored membrane proteins in Saccharomyces cerevisiae. *The Journal of biological chemistry,* 278**,** 8219-23.

BERGELAND, T., WIDERBERG, J., BAKKE, O. & NORDENG, T. W. 2001. Mitotic partitioning of endosomes and lysosomes. *Current biology : CB,* 11**,** 644-51.

BERNSTEIN, H. G., SAHIN, J., SMALLA, K. H., GUNDELFINGER, E. D., BOGERTS, B. & KREUTZ, M. R. 2007. A reduced number of cortical neurons show increased Caldendrin protein levels in chronic schizophrenia. *Schizophr Res,* 96**,** 246-56.

BERRIDGE, M. J. 1998. Neuronal calcium signaling. *Neuron,* 21**,** 13-26.

BERRIDGE, M. J. 2009. Inositol trisphosphate and calcium signalling mechanisms. *Biochimica et biophysica acta,* 1793**,** 933-40.

BERRIDGE, M. J., LIPP, P. & BOOTMAN, M. D. 2000. The versatility and universality of calcium signalling. *Nature reviews. Molecular cell biology,* 1**,** 11-21.

BICHET, D., CORNET, V., GEIB, S., CARLIER, E., VOLSEN, S., HOSHI, T., MORI, Y. & DE WAARD, M. 2000. The I-II loop of the Ca2+ channel alpha1 subunit contains an endoplasmic reticulum retention signal antagonized by the beta subunit. *Neuron,* 25**,** 177-90.

BONIFACINO, J. S. & TRAUB, L. M. 2003. Signals for sorting of transmembrane proteins to endosomes and lysosomes. *Annual review of biochemistry,* 72**,** 395-447.

BOOTMAN, M. D., COLLINS, T. J., PEPPIATT, C. M., PROTHERO, L. S., MACKENZIE, L., DE SMET, P., TRAVERS, M., TOVEY, S. C., SEO, J. T., BERRIDGE, M. J., CICCOLINI, F. & LIPP, P. 2001. Calcium signalling--an overview. *Seminars in cell & developmental biology,* 12**,** 3-10.

BORGESE, N., BRAMBILLASCA, S. & COLOMBO, S. 2007. How tails guide tail-anchored proteins to their destinations. *Current opinion in cell biology,* 19**,** 368-75.

BORGESE, N., COLOMBO, S. & PEDRAZZINI, E. 2003. The tale of tail-anchored proteins: coming from the cytosol and looking for a membrane. *The Journal of cell biology,* 161**,** 1013-9.

BORGESE, N. & FASANA, E. 2011. Targeting pathways of C-tail-anchored proteins. *Biochimica et biophysica acta,* 1808**,** 937-46.

BORGESE, N., GAZZONI, I., BARBERI, M., COLOMBO, S. & PEDRAZZINI, E. 2001. Targeting of a tail-anchored protein to endoplasmic reticulum and mitochondrial outer membrane by independent but competing pathways. *Molecular biology of the cell,* 12**,** 2482-96.

BORGESE, N. & RIGHI, M. 2010. Remote origins of tail-anchored proteins. *Traffic,* 11**,** 877-85.

BOUCROT, E. & KIRCHHAUSEN, T. 2007. Endosomal recycling controls plasma membrane area during mitosis. *Proceedings of the National Academy of Sciences of the United States of America,* 104**,** 7939-44.

BOULWARE, M. J. & MARCHANT, J. S. 2008. Timing in Cellular Ca2+ Signaling. *Current Biology,* 18**,** R769-R776.

BRAILOIU, E., RAHMAN, T., CHURAMANI, D., PROLE, D. L., BRAILOIU, G. C., HOOPER, R., TAYLOR, C. W. & PATEL, S. 2010. An NAADP-gated two-pore channel

targeted to the plasma membrane uncouples triggering from amplifying Ca2+ signals. *The Journal of biological chemistry,* 285**,** 38511-6.

BRAMBILLASCA, S., YABAL, M., MAKAROW, M. & BORGESE, N. 2006. Unassisted translocation of large polypeptide domains across phospholipid bilayers. *The Journal of cell biology,* 175**,** 767-77.

BRAMBILLASCA, S., YABAL, M., SOFFIENTINI, P., STEFANOVIC, S., MAKAROW, M., HEGDE, R. S. & BORGESE, N. 2005. Transmembrane topogenesis of a tail-anchored protein is modulated by membrane lipid composition. *The EMBO journal,* 24**,** 2533-42.

BRAUNEWELL, K. H. 2005. The darker side of Ca2+ signaling by neuronal Ca2+-sensor proteins: from Alzheimer's disease to cancer. *Trends Pharmacol Sci,* 26**,** 345-51.

BRAUNEWELL, K. H. & KLEIN-SZANTO, A. J. 2009. Visinin-like proteins (VSNLs): interaction partners and emerging functions in signal transduction of a subfamily of neuronal Ca2+ -sensor proteins. *Cell Tissue Res,* 335**,** 301-16.

BROWN, J. R. & AUGER, K. R. 2011. Phylogenomics of phosphoinositide lipid kinases: perspectives on the evolution of second messenger signaling and drug discovery. *BMC evolutionary biology,* 11**,** 4.

BRUNET, F. G., ROEST CROLLIUS, H., PARIS, M., AURY, J. M., GIBERT, P., JAILLON, O., LAUDET, V. & ROBINSON-RECHAVI, M. 2006. Gene loss and evolutionary rates following whole-genome duplication in teleost fishes. *Molecular biology and evolution,* 23**,** 1808-1816.

BULBARELLI, A., SPROCATI, T., BARBERI, M., PEDRAZZINI, E. & BORGESE, N. 2002. Trafficking of tail-anchored proteins: transport from the endoplasmic reticulum to the plasma membrane and sorting between surface domains in polarised epithelial cells. *Journal of cell science,* 115**,** 1689-702.

BURGESS, W. H., JEMIOLO, D. K. & KRETSINGER, R. H. 1980. Interaction of calcium and calmodulin in the presence of sodium dodecyl sulfate. *Biochimica et biophysica acta,* 623**,** 257-70.

BURGOYNE, R. 2004. The neuronal calcium-sensor proteins. *Biochim Biophys Acta,* 1742**,** 59-68.

BURGOYNE, R. D. 2007. Neuronal calcium sensor proteins: Generating diversity in neuronal Ca 2+ signalling. *Nature Reviews Neuroscience,* 8**,** 182-193.

BURGOYNE, R. D., O'CALLAGHAN, D. W., HASDEMIR, B., HAYNES, L. P. & TEPIKIN, A. V. 2004. Neuronal Ca2+-sensor proteins: multitalented regulators of neuronal function. *Trends Neurosci,* 27**,** 203-9.

BURGOYNE, R. D. & WEISS, J. L. 2001. The neuronal calcium sensor family of Ca2+-binding proteins. *Biochem J,* 353**,** 1-12.

BUTT, T. R., EDAVETTAL, S. C., HALL, J. P. & MATTERN, M. R. 2005. SUMO fusion technology for difficult-to-express proteins. *Protein expression and purification,* 43**,** 1-9.

BUXBAUM, J. D., CHOI, E. K., LUO, Y., LILLIEHOOK, C., CROWLEY, A. C., MERRIAM, D. E. & WASCO, W. 1998. Calsenilin: A calcium-binding protein that interacts with the presenilins and regulates the levels of a presenilin fragment. *Nature medicine,* 4**,** 1177-1181.

CALCRAFT, P. J., RUAS, M., PAN, Z., CHENG, X., ARREDOUANI, A., HAO, X., TANG, J., RIETDORF, K., TEBOUL, L., CHUANG, K. T., LIN, P., XIAO, R., WANG, C., ZHU, Y., LIN, Y., WYATT, C. N., PARRINGTON, J., MA, J., EVANS, A. M., GALIONE, A. & ZHU, M. X. 2009. NAADP mobilizes calcium from acidic organelles through two-pore channels. *Nature,* 459**,** 596-600.

CANDE, W. Z. 1980. A permeabilized cell model for studying cytokinesis using mammalian tissue culture cells. *The Journal of cell biology,* 87**,** 326-35.

CATTERALL, W. A. 2000. Structure and regulation of voltage-gated Ca2+ channels. *Annual review of cell and developmental biology,* 16**,** 521-55.

CATTERALL, W. A. & FEW, A. P. 2008. Calcium channel regulation and presynaptic plasticity. *Neuron,* 59**,** 882-901.

CAVANAGH, J., FAIRBROTHER, W. J., PALMER III, A. G., RANCE, M. & SKELTON, N. J. 2007a. Classical NMR spectroscopy. *Protein NMR Spectroscopy (Second Edition).* Burlington: Academic Press.

CAVANAGH, J., FAIRBROTHER, W. J., PALMER III, A. G., RANCE, M. & SKELTON, N. J. 2007b. Multidimensional NMR spectroscopy. *Protein NMR Spectroscopy (Second Edition).* Burlington: Academic Press.

CAVANAGH, J., FAIRBROTHER, W. J., PALMER III, A. G., RANCE, M. & SKELTON, N. J. 2007c. Relaxation and dynamic processes. *Protein NMR Spectroscopy (Second Edition).* Burlington: Academic Press.

CHANDRA, K., RAMAKRISHNAN, V., SHARMA, Y. & CHARY, K. V. 2011. N-terminal myristoylation alters the calcium binding pathways in neuronal calcium sensor-1. *J Biol Inorg Chem,* 16**,** 81-95.

CHATTOPADHYAYA, R., MEADOR, W. E., MEANS, A. R. & QUIOCHO, F. A. 1992. Calmodulin structure refined at 1.7 A resolution. *Journal of molecular biology,* 228**,** 1177-92.

CHEN, C. K., INGLESE, J., LEFKOWITZ, R. J. & HURLEY, J. B. 1995a. Ca2+-dependent interaction of recoverin with rhodopsin kinase. *Journal of Biological Chemistry,* 270**,** 18060-18066.

CHEN, J., MAKINO, C. L., PEACHEY, N. S., BAYLOR, D. A. & SIMON, M. I. 1995b. Mechanisms of rhodopsin inactivation in vivo as revealed by a COOH-Terminal truncation mutant. *Science,* 267**,** 374-377.

CHEUNG, M. S., MAGUIRE, M. L., STEVENS, T. J. & BROADHURST, R. W. 2010. DANGLE: A Bayesian inferential method for predicting protein backbone dihedral angles and secondary structure. *Journal of magnetic resonance,* 202**,** 223-33.

CHIN, D. & MEANS, A. R. 2000. Calmodulin: A prototypical calcium sensor. *Trends in cell biology,* 10**,** 322-328.

CHOI, D. W. 1988. Calcium-mediated neurotoxicity: Relationship to specific channel types and role in ischemic damage. *Trends in neurosciences,* 11**,** 465-469.

CLAPHAM, D. E. 2007. Calcium Signaling. *Cell,* 131**,** 1047-1058.

COOKE, R. M. 1997. Protein NMR extends into new fields of structural biology. *Current opinion in chemical biology,* 1**,** 359-64.

COUKELL, B., CAMERON, A., PERUSINI, S. & SHIM, K. 2004. Disruption of the NCS-1/frequenin-related ncsA gene in Dictyostelium discoideum accelerates development. *Dev Growth Differ,* 46**,** 449-58.

CRANKSHAW, M. W. & GRANT, G. A. 2001. Modification of cysteine. *Current protocols in protein science / editorial board, John E. Coligan ... [et al.],* Chapter 15**,** Unit15 1.

CUI, G., MEYER, A. C., CALIN-JAGEMAN, I., NEEF, J., HAESELEER, F., MOSER, T. & LEE, A. 2007. Ca2+-binding proteins tune Ca2+-feedback to Cav1.3 channels in mouse auditory hair cells. *J Physiol,* 585**,** 791-803.

DE BARRY, J., JANOSHAZI, A., DUPONT, J. L., PROCKSCH, O., CHASSEROT-GOLAZ, S., JEROMIN, A. & VITALE, N. 2006. Functional implication of neuronal calcium sensor-1 and phosphoinositol 4-kinase-beta interaction in regulated exocytosis of PC12 cells. *J Biol Chem,* 281**,** 18098-111.

DECORDIER, I., CUNDARI, E. & KIRSCH-VOLDERS, M. 2008. Mitotic checkpoints and the maintenance of the chromosome karyotype. *Mutation research,* 651**,** 3-13.

DELL'ANGELICA, E. C., SHOTELERSUK, V., AGUILAR, R. C., GAHL, W. A. & BONIFACINO, J. S. 1999. Altered trafficking of lysosomal proteins in Hermansky-Pudlak syndrome due to mutations in the beta 3A subunit of the AP-3 adaptor. *Molecular cell,* 3**,** 11-21.

DIETERICH, D. C., KARPOVA, A., MIKHAYLOVA, M., ZDOBNOVA, I., KONIG, I., LANDWEHR, M., KREUTZ, M., SMALLA, K. H., RICHTER, K., LANDGRAF, P., REISSNER, C., BOECKERS, T. M., ZUSCHRATTER, W., SPILKER, C., SEIDENBECHER, C. I., GARNER, C. C., GUNDELFINGER, E. D. & KREUTZ, M. R. 2008. Caldendrin-Jacob: a protein liaison that couples NMDA receptor signalling to the nucleus. *PLoS Biol,* 6**,** e34.

DIZHOOR, A. M., RAY, S., KUMAR, S., NIEMI, G., SPENCER, M., BROLLEY, D., WALSH, K. A., PHILIPOV, P. P., HURLEY, J. B. & STRYER, L. 1991. Recoverin: A calcium sensitive activator of retinal rod guanylate cyclase. *Science,* 251**,** 915-918.

DONATO, R. 2001. S100: a multigenic family of calcium-modulated proteins of the EF-hand type with intracellular and extracellular functional roles. *The international journal of biochemistry & cell biology,* 33**,** 637-668.

DUKES, J. D., RICHARDSON, J. D., SIMMONS, R. & WHITLEY, P. 2008. A dominant-negative ESCRT-III protein perturbs cytokinesis and trafficking to lysosomes. *The Biochemical journal,* 411**,** 233-9.

DUNDR, M. & MISTELI, T. 2001. Functional architecture in the cell nucleus. *The Biochemical journal,* 356**,** 297-310.

EMMANOUILIDOU, E., TESCHEMACHER, A. G., POULI, A. E., NICHOLLS, L. I., SEWARD, E. P. & RUTTER, G. A. 1999. Imaging Ca2+ concentration changes at the secretory vesicle surface with a recombinant targeted cameleon. *Current biology : CB,* 9**,** 915-8.

FADER, C. M., SANCHEZ, D. G., MESTRE, M. B. & COLOMBO, M. I. 2009. TI-VAMP/VAMP7 and VAMP3/cellubrevin: two v-SNARE proteins involved in specific steps of the autophagy/multivesicular body pathways. *Biochimica et biophysica acta,* 1793**,** 1901-16.

FALCONE, D., HENDERSON, M. P., NIEUWLAND, H., COUGHLAN, C. M., BRODSKY, J. L. & ANDREWS, D. W. 2011. Stability and function of the Sec61 translocation complex depends on the Sss1p tail-anchor sequence. *The Biochemical journal,* 436**,** 291-303.

FATIMATHAS, L. & MOSS, S. E. 2010. Annexins as disease modifiers. *Histology and histopathology,* 25**,** 527-32.

FAUROBERT, E., CHEN, C. K., HURLEY, J. B. & TENG, D. H. 1996. Drosophila neurocalcin, a fatty acylated, Ca2+-binding protein that associates with membranes and inhibits in vitro phosphorylation of bovine rhodopsin. *The Journal of biological chemistry,* 271**,** 10256-62.

FAVALORO, V., VILARDI, F., SCHLECHT, R., MAYER, M. P. & DOBBERSTEIN, B. 2010. Asna1/TRC40-mediated membrane insertion of tail-anchored proteins. *Journal of cell science,* 123**,** 1522-30.

FELDMANN, A., WINTERSTEIN, C., WHITE, R., TROTTER, J. & KRAMER-ALBERS, E. M. 2009. Comprehensive analysis of expression, subcellular localization, and cognate pairing of SNARE proteins in oligodendrocytes. *Journal of neuroscience research,* 87**,** 1760-72.

FERIC, M., ZHAO, B., HOFFERT, J. D., PISITKUN, T. & KNEPPER, M. A. 2011. Large-scale phosphoproteomic analysis of membrane proteins in renal proximal and distal tubule. *American journal of physiology. Cell physiology,* 300**,** C755-70.

FEW, A. P., LAUTERMILCH, N. J., WESTENBROEK, R. E., SCHEUER, T. & CATTERALL, W. A. 2005. Differential regulation of CaV2.1 channels by calcium-binding protein 1 and visinin-like protein-2 requires N-terminal myristoylation. *J Neurosci,* 25**,** 7071-80.

FINDEISEN, F. & MINOR, D. L., JR. 2010. Structural basis for the differential effects of CaBP1 and calmodulin on Ca(V)1.2 calcium-dependent inactivation. *Structure,* 18**,** 1617-31.

FINGER, F. P. & WHITE, J. G. 2002. Fusion and fission: membrane trafficking in animal cytokinesis. *Cell,* 108**,** 727-30.

FITZGERALD, D. J., BURGOYNE, R. D. & HAYNES, L. P. 2008. Neuronal calcium sensor proteins are unable to modulate NFAT activation in mammalian cells. *Biochim Biophys Acta,* 1780**,** 240-8.

FLAHERTY, K. M., ZOZULYA, S., STRYER, L. & MCKAY, D. B. 1993. Three-dimensional structure of recoverin, a calcium sensor in vision. *Cell,* 75**,** 709-716.

FRANKLIN, J. L. & JOHNSON JR, E. M. 1992. Suppression of programmed neuronal death by sustained elevation of cytoplasmic calcium. *Trends in neurosciences,* 15**,** 501-508.

FRANSSON, S., RUUSALA, A. & ASPENSTROM, P. 2006. The atypical Rho GTPases Miro-1 and Miro-2 have essential roles in mitochondrial trafficking. *Biochemical and biophysical research communications,* 344**,** 500-10.

FRIEDBERG, F. & RHOADS, A. R. 2001. Evolutionary aspects of calmodulin. *IUBMB life,* 51**,** 215-221.

FRIES, R., REDDY, P. P., MIKHAYLOVA, M., HAVERKAMP, S., WEI, T., MULLER, M., KREUTZ, M. R. & KOCH, K. W. 2010. Dynamic cellular translocation of caldendrin is facilitated by the Ca2+-myristoyl switch of recoverin. *J Neurochem,* 113**,** 1150-62.

GALIONE, A., MORGAN, A. J., ARREDOUANI, A., DAVIS, L. C., RIETDORF, K., RUAS, M. & PARRINGTON, J. 2010. NAADP as an intracellular messenger regulating lysosomal calcium-release channels. *Biochemical Society transactions,* 38**,** 1424-31.

GERASIMENKO, J. V., GERASIMENKO, O. V. & PETERSEN, O. H. 2001. Membrane repair: Ca(2+)-elicited lysosomal exocytosis. *Current biology : CB,* 11**,** R971-4.

GERASIMENKO, O. & TEPIKIN, A. 2005. How to measure Ca2+ in cellular organelles? *Cell calcium,* 38**,** 201-11.

GHOSH, A. & GREENBERG, M. E. 1995. Calcium signalling in neurons: Molecular mechanisms and cellular consequences. *Science,* 268**,** 239-247.

GIANSANTI, M. G., BELLONI, G. & GATTI, M. 2007. Rab11 is required for membrane trafficking and actomyosin ring constriction in meiotic cytokinesis of Drosophila males. *Molecular biology of the cell,* 18**,** 5034-47.

GIFFORD, J. L., ISHIDA, H. & VOGEL, H. J. 2011. Fast methionine-based solution structure determination of calcium-calmodulin complexes. *Journal of biomolecular NMR,* 50**,** 71-81.

GIFFORD, J. L., WALSH, M. P. & VOGEL, H. J. 2007. Structures and metal-ion-binding properties of the Ca2+-binding helix-loop-helix EF-hand motifs. *Biochemical Journal,* 405**,** 199-221.

GOLOVANOV, A. P., HAUTBERGUE, G. M., WILSON, S. A. & LIAN, L. Y. 2004. A simple method for improving protein solubility and long-term stability. *Journal of the American Chemical Society,* 126**,** 8933-9.

GOMEZ, M., DE CASTRO, E., GUARIN, E., SASAKURA, H., KUHARA, A., MORI, I., BARTFAI, T., BARGMANN, C. I. & NEF, P. 2001. Ca2+ signaling via the neuronal calcium sensor-1 regulates associative learning and memory in C. elegans. *Neuron,* 30**,** 241-8.

GORDON, D. E., BOND, L. M., SAHLENDER, D. A. & PEDEN, A. A. 2010. A targeted siRNA screen to identify SNAREs required for constitutive secretion in mammalian cells. *Traffic,* 11**,** 1191-204.

GOSS, J. W. & TOOMRE, D. K. 2008. Both daughter cells traffic and exocytose membrane at the cleavage furrow during mammalian cytokinesis. *The Journal of cell biology,* 181**,** 1047-54.

GRABAREK, Z. 2006. Structural Basis for Diversity of the EF-hand Calcium-binding Proteins. *Journal of Molecular Biology,* 359**,** 509-525.

GRAHAM, T. R. & BURD, C. G. 2011. Coordination of Golgi functions by phosphatidylinositol 4-kinases. *Trends in cell biology,* 21**,** 113-21.

HAESELEER, F. 2008. Interaction and colocalization of CaBP4 and Unc119 (MRG4) in photoreceptors. *Invest Ophthalmol Vis Sci,* 49**,** 2366-75.

HAESELEER, F., IMANISHI, Y., MAEDA, T., POSSIN, D. E., MAEDA, A., LEE, A., RIEKE, F. & PALCZEWSKI, K. 2004. Essential role of Ca2+-binding protein 4, a Cav1.4 channel regulator, in photoreceptor synaptic function. *Nat Neurosci,* 7**,** 1079-87.

HAESELEER, F., IMANISHI, Y., SOKAL, I., FILIPEK, S. & PALCZEWSKI, K. 2002. Calcium-binding proteins: intracellular sensors from the calmodulin superfamily. *Biochemical and biophysical research communications,* 290**,** 615-623.

HAESELEER, F., SOKAL, I., VERLINDE, C. L., ERDJUMENT-BROMAGE, H., TEMPST, P., PRONIN, A. N., BENOVIC, J. L., FARISS, R. N. & PALCZEWSKI, K. 2000. Five members of a novel Ca(2+)-binding protein (CABP) subfamily with similarity to calmodulin. *J Biol Chem,* 275**,** 1247-60.

HALESTRAP, A. P. 2009. What is the mitochondrial permeability transition pore? *Journal of Molecular and Cellular Cardiology,* 46**,** 821-831.

HASDEMIR, B., FITZGERALD, D. J., PRIOR, I. A., TEPIKIN, A. V. & BURGOYNE, R. D. 2005. Traffic of Kv4 K+ channels mediated by KChIP1 is via a novel post-ER vesicular pathway. *The Journal of cell biology,* 171**,** 459-69.

HAYNES, L. P. & BURGOYNE, R. D. 2008. Unexpected tails of a Ca2+ sensor. *Nature chemical biology,* 4**,** 90-1.

HAYNES, L. P., FITZGERALD, D. J., WAREING, B., O'CALLAGHAN, D. W., MORGAN, A. & BURGOYNE, R. D. 2006. Analysis of the interacting partners of the neuronal calcium-binding proteins L-CaBP1, hippocalcin, NCS-1 and neurocalcin delta. *Proteomics,* 6**,** 1822-32.

HAYNES, L. P., SHERWOOD, M. W., DOLMAN, N. J. & BURGOYNE, R. D. 2007. Specificity, promiscuity and localization of ARF protein interactions with NCS-1 and phosphatidylinositol-4 kinase-III beta. *Traffic,* 8**,** 1080-92.

HAYNES, L. P., TEPIKIN, A. V. & BURGOYNE, R. D. 2004. Calcium-binding protein 1 is an inhibitor of agonist-evoked, inositol 1,4,5-trisphosphate-mediated calcium signaling. *J Biol Chem,* 279**,** 547-55.

HAYNES, L. P., THOMAS, G. M. & BURGOYNE, R. D. 2005. Interaction of neuronal calcium sensor-1 and ADP-ribosylation factor 1 allows bidirectional control of phosphatidylinositol 4-kinase beta and trans-Golgi network-plasma membrane traffic. *J Biol Chem,* 280**,** 6047-54.

HENDRICKS, K. B., WANG, B. Q., SCHNIEDERS, E. A. & THORNER, J. 1999. Yeast homologue of neuronal frequenin is a regulator of phosphatidylinosrtol-4-OH kinase. *Nature cell biology,* 1**,** 234-241.

HEPLER, P. K. 1994. The role of calcium in cell division. *Cell calcium,* 16**,** 322-30.

HILFIKER, S. 2003. Neuronal calcium sensor-1: a multifunctional regulator of secretion. *Biochem Soc Trans,* 31**,** 828-32.

HILL, J. M. 2008. NMR screening for rapid protein characterization in structural proteomics. *Methods in molecular biology,* 426**,** 437-46.

HOBSON, K. F., HOUSLEY, N. A. & PEDIGO, S. 2005. Ligand-linked stability of mutants of the C-domain of calmodulin. *Biophysical chemistry,* 114**,** 43-52.

HONG, W. 2005. SNAREs and traffic. *Biochimica et biophysica acta,* 1744**,** 120-44.

HONSHO, M., MITOMA, J. Y. & ITO, A. 1998. Retention of cytochrome b5 in the endoplasmic reticulum is transmembrane and luminal domain-dependent. *The Journal of biological chemistry,* 273**,** 20860-6.

HOOK, S. S. & MEANS, A. R. 2001. Ca2+/CaM-Dependent kinases: From activation to function.

HOPKINS JR, H. P. & GAYDEN, R. H. 1989. Comparison of Ca2+ and Mg2+ binding to calmodulin. An enthalpy, entropy, and gibbs free energy analysis. *Journal of Solution Chemistry,* 18**,** 743-757.

HORNE, W. A., ELLINOR, P. T., INMAN, I., ZHOU, M., TSIEN, R. W. & SCHWARZ, T. L. 1993. Molecular diversity of Ca2+ channel alpha 1 subunits from the marine ray Discopyge ommata. *Proceedings of the National Academy of Sciences of the United States of America,* 90**,** 3787-3791.

HRADSKY, J., RAGHURAM, V., REDDY, P. P., NAVARRO, G., HUPE, M., CASADO, V., MCCORMICK, P. J., SHARMA, Y., KREUTZ, M. R. & MIKHAYLOVA, M. 2011. Posttranslational membrane insertion of the tail anchored transmembrane EF-hand Ca2+-sensors Calneurons requires the TRC40/Asna1 chaperone. *The Journal of biological chemistry*.

HUBBARD, M. J. & KLEE, C. B. 1987. Calmodulin binding by calcineurin. Ligand-induced renaturation of protein immobilized on nitrocellulose. *Journal of Biological Chemistry,* 262**,** 15062-15070.

IKURA, M. & AMES, J. B. 2006. Genetic polymorphism and protein conformational plasticity in the calmodulin superfamily: Two ways to promote multifunctionality. *Proceedings of the National Academy of Sciences of the United States of America,* 103**,** 1159-1164.

IWASAKI, H., CHIBA, K., UCHIYAMA, T., YOSHIKAWA, F., SUZUKI, F., IKEDA, M., FURUICHI, T. & MIKOSHIBA, K. 2002. Molecular characterization of the starfish inositol 1,4,5-trisphosphate receptor and its role during oocyte maturation and fertilization. *The Journal of biological chemistry,* 277**,** 2763-2772.

JAILLON, O., AURY, J. M., BRUNET, F., PETIT, J. L., STANGE-THOMANN, N., MAUCELI, E., BOUNEAU, L., FISCHER, C., OZOUF-COSTAZ, C., BERNOT, A., NICAUD, S., JAFFE, D., FISHER, S., LUTFALLA, G., DOSSAT, C., SEGURENS, B., DASILVA, C., SALANOUBAT, M., LEVY, M., BOUDET, N., CASTELLANO, S., ANTHOUARD, V., JUBIN, C., CASTELLI, V., KATINKA, M., VACHERIE, B., BIEMONT, C., SKALLI, Z., CATTOLICO, L., POULAIN, J., DE BERARDINIS, V., CRUAUD, C., DUPRAT, S., BROTTIER, P., COUTANCEAU, J. P., GOUZY, J., PARRA, G., LARDIER, G., CHAPPLE, C., MCKERNAN, K. J., MCEWAN, P., BOSAK, S., KELLIS, M., VOLFF, J. N., GUIGO, R., ZODY, M. C., MESIROV, J., LINDBLAD-TOH, K., BIRREN, B., NUSBAUM, C., KAHN, D., ROBINSON-RECHAVI, M., LAUDET, V., SCHACHTER, V., QUETIER, F., SAURIN, W., SCARPELLI, C., WINCKER, P., LANDER, E. S., WEISSENBACH, J. & ROEST CROLLIUS, H. 2004. Genome duplication in the teleost fish Tetraodon nigroviridis reveals the early vertebrate proto-karyotype. *Nature,* 431**,** 946-957.

JANTSCH-PLUNGER, V. & GLOTZER, M. 1999. Depletion of syntaxins in the early Caenorhabditis elegans embryo reveals a role for membrane fusion events in cytokinesis. *Current biology : CB,* 9**,** 738-45.

JEZIORSKI, M. C., GREENBERG, R. M. & ANDERSON, P. A. 2000. The molecular biology of invertebrate voltage-gated Ca(2+) channels. *The Journal of experimental biology,* 203**,** 841-856.

JO, D. G., LEE, J. Y., HONG, Y. M., SONG, S., INHEE, M. J., KOH, J. Y. & JUNG, Y. K. 2004. Induction of pro-apoptotic calsenilin/DREAM/KChIP3 in Alzheimer's disease and cultured neurons after amyloid-Œ≤ exposure. *Journal of neurochemistry,* 88**,** 604-611.

KABBANI, N., NEGYESSY, L., LIN, R., GOLDMAN-RAKIC, P. & LEVENSON, R. 2002. Interaction with neuronal calcium sensor NCS-1 mediates desensitization of the D2 dopamine receptor. *J Neurosci,* 22**,** 8476-86.

KABBANI, N., WOLL, M. P., NORDMAN, J. C. & LEVENSON, R. 2011. Dopamine Receptor Interacting Proteins: Targeting Neuronal Calcium Sensor-1/D2 Dopamine Receptor Interaction for Antipsychotic Drug Development. *Curr Drug Targets*.

KALBFLEISCH, T., CAMBON, A. & WATTENBERG, B. W. 2007. A bioinformatics approach to identifying tail-anchored proteins in the human genome. *Traffic,* 8**,** 1687-94.

KARABINOS, A. & BHATTACHARYA, D. 2000. Molecular evolution of calmodulin and calmodulin-like genes in the cephalochordate Branchiostoma. *Journal of Molecular Evolution,* 51**,** 141-148.

KASRI, N. N., HOLMES, A. M., BULTYNCK, G., PARYS, J. B., BOOTMAN, M. D., RIETDORF, K., MISSIAEN, L., MCDONALD, F., DE SMEDT, H., CONWAY, S. J., HOLMES, A. B., BERRIDGE, M. J. & RODERICK, H. L. 2004. Regulation of InsP3 receptor activity by neuronal Ca2+-binding proteins. *EMBO J,* 23**,** 312-21.

KASRI, N. N., SIENAERT, I., PARYS, J. B., CALLEWAERT, G., MISSIAEN, L., JEROMIN, A. & DE SMEDT, H. 2003. A novel Ca2+-induced Ca2+ release mechanism in A7r5 cells regulated by calmodulin-like proteins. *The Journal of biological chemistry,* 278**,** 27548-55.

KIM, P. K., JANIAK-SPENS, F., TRIMBLE, W. S., LEBER, B. & ANDREWS, D. W. 1997. Evidence for multiple mechanisms for membrane binding and integration via carboxyl-terminal insertion sequences. *Biochemistry,* 36**,** 8873-82.

KINOSHITA-KAWADA, M., TANG, J., XIAO, R., KANEKO, S., FOSKETT, J. K. & ZHU, M. X. 2005. Inhibition of TRPC5 channels by Ca2+-binding protein 1 in Xenopus oocytes. *Pflugers Arch,* 450**,** 345-54.

KLEBER-JANKE, T. & BECKER, W. M. 2000. Use of modified BL21(DE3) Escherichia coli cells for high-level expression of recombinant peanut allergens affected by poor codon usage. *Protein expression and purification,* 19**,** 419-24.

KLENCHIN, V. A., CALVERT, P. D. & BOWNDS, M. D. 1995. Inhibition of rhodopsin kinase by recoverin. Further evidence for a negative feedback system in phototransduction. *Journal of Biological Chemistry,* 270**,** 16147-16152.

KOH, P. O., UNDIE, A. S., KABBANI, N., LEVENSON, R., GOLDMAN-RAKIC, P. S. & LIDOW, M. S. 2003. Up-regulation of neuronal calcium sensor-1 (NCS-1) in the

prefrontal cortex of schizophrenic and bipolar patients. *Proc Natl Acad Sci U S A,* 100**,** 313-7.

KORDEL, J., SKELTON, N. J., AKKE, M. & CHAZIN, W. J. 1993. High-resolution solution structure of calcium-loaded calbindin D(9k). *Journal of Molecular Biology,* 231**,** 711-734.

KOURIE, J. I. & WOOD, H. B. 2000. Biophysical and molecular properties of annexin-formed channels. *Progress in biophysics and molecular biology,* 73**,** 91-134.

KUO, H. C., CHENG, C. F., CLARK, R. B., LIN, J. J., LIN, J. L., HOSHIJIMA, M., NGUYEN-TRAN, V. T., GU, Y., IKEDA, Y., CHU, P. H., ROSS, J., GILES, W. R. & CHIEN, K. R. 2001. A defect in the Kv channel-interacting protein 2 (KChIP2) gene leads to a complete loss of I(to) and confers susceptibility to ventricular tachycardia. *Cell,* 107**,** 801-13.

KURODA, R., KINOSHITA, J., HONSHO, M., MITOMA, J. & ITO, A. 1996. In situ topology of cytochrome b5 in the endoplasmic reticulum membrane. *Journal of biochemistry,* 120**,** 828-33.

KUTAY, U., AHNERT-HILGER, G., HARTMANN, E., WIEDENMANN, B. & RAPOPORT, T. A. 1995. Transport route for synaptobrevin via a novel pathway of insertion into the endoplasmic reticulum membrane. *The EMBO journal,* 14**,** 217-23.

KUTAY, U., HARTMANN, E. & RAPOPORT, T. A. 1993. A class of membrane proteins with a C-terminal anchor. *Trends in cell biology,* 3**,** 72-5.

KYTE, J. & DOOLITTLE, R. F. 1982. A simple method for displaying the hydropathic character of a protein. *Journal of molecular biology,* 157**,** 105-32.

LAMBRECHT, H. G. & KOCH, K. W. 1992. Recoverin, a novel calcium-binding protein from vertebrate photoreceptors. *Biochimica et biophysica acta,* 1160**,** 63-6.

LAUBE, G., SEIDENBECHER, C. I., RICHTER, K., DIETERICH, D. C., HOFFMANN, B., LANDWEHR, M., SMALLA, K. H., WINTER, C., BOCKERS, T. M., WOLF, G., GUNDELFINGER, E. D. & KREUTZ, M. R. 2002. The neuron-specific Ca2+-binding protein caldendrin: gene structure, splice isoforms, and expression in the rat central nervous system. *Mol Cell Neurosci,* 19**,** 459-75.

LAUDE, A. J. & SIMPSON, A. W. M. 2009. Compartmentalized signalling: Ca2+ compartments, microdomains and the many facets of Ca2+ signalling. *FEBS Journal,* 276**,** 1800-1816.

LEE, A., JIMENEZ, A., CUI, G. & HAESELEER, F. 2007a. Phosphorylation of the Ca2+-binding protein CaBP4 by protein kinase C Œð in photoreceptors. *Journal of Neuroscience,* 27**,** 12743-12754.

LEE, A., JIMENEZ, A., CUI, G. & HAESELEER, F. 2007b. Phosphorylation of the Ca2+-binding protein CaBP4 by protein kinase C zeta in photoreceptors. *J Neurosci,* 27**,** 12743-54.

LEE, A., WESTENBROEK, R. E., HAESELEER, F., PALCZEWSKI, K., SCHEUER, T. & CATTERALL, W. A. 2002. Differential modulation of Ca(v)2.1 channels by calmodulin and Ca2+-binding protein 1. *Nat Neurosci,* 5**,** 210-7.

LEE, S., BRIKLIN, O., HIEL, H. & FUCHS, P. 2007c. Calcium-dependent inactivation of calcium channels in cochlear hair cells of the chicken. *J Physiol,* 583**,** 909-22.

LI, C., CHAN, J., HAESELEER, F., MIKOSHIBA, K., PALCZEWSKI, K., IKURA, M. & AMES, J. B. 2009. Structural insights into Ca2+-dependent regulation of inositol 1,4,5-trisphosphate receptors by CaBP1. *J Biol Chem,* 284**,** 2472-81.

LI, C., LU, P. & ZHANG, D. 1999. Using a GFP-gene fusion technique to study the cell cycle-dependent distribution of calmodulin in living cells. *Science in China. Series C, Life sciences / Chinese Academy of Sciences,* 42**,** 517-28.

LI, W. M., WEBB, S. E., CHAN, C. M. & MILLER, A. L. 2008. Multiple roles of the furrow deepening Ca2+ transient during cytokinesis in zebrafish embryos. *Developmental biology,* 316**,** 228-48.

LILLIEHOOK, C., BOZDAGI, O., YAO, J., GOMEZ-RAMIREZ, M., ZAIDI, N. F., WASCO, W., GANDY, S., SANTUCCI, A. C., HAROUTUNIAN, V., HUNTLEY, G. W. & BUXBAUM, J. D. 2003. Altered Abeta formation and long-term potentiation in a calsenilin knock-out. *The Journal of neuroscience : the official journal of the Society for Neuroscience,* 23**,** 9097-106.

LITTINK, K. W., KOENEKOOP, R. K., VAN DEN BORN, L. I., COLLIN, R. W., MORUZ, L., VELTMAN, J. A., ROOSING, S., ZONNEVELD, M. N., OMAR, A., DARVISH, M., LOPEZ, I., KROES, H. Y., VAN GENDEREN, M. M., HOYNG, C. B., ROHRSCHNEIDER, K., VAN SCHOONEVELD, M. J., CREMERS, F. P. & DEN HOLLANDER, A. I. 2010. Homozygosity mapping in patients with cone-rod dystrophy: novel mutations and clinical characterizations. *Invest Ophthalmol Vis Sci,* 51**,** 5943-51.

LITTINK, K. W., VAN GENDEREN, M. M., COLLIN, R. W., ROOSING, S., DE BROUWER, A. P., RIEMSLAG, F. C., VENSELAAR, H., THIADENS, A. A., HOYNG, C. B., ROHRSCHNEIDER, K., DEN HOLLANDER, A. I., CREMERS, F. P. & VAN DEN BORN, L. I. 2009. A novel homozygous nonsense mutation in CABP4 causes congenital cone-rod synaptic disorder. *Invest Ophthalmol Vis Sci,* 50**,** 2344-50.

LIU, T., WILLIAMS, J. G. & CLARKE, M. 1992. Inducible expression of calmodulin antisense RNA in Dictyostelium cells inhibits the completion of cytokinesis. *Molecular biology of the cell,* 3**,** 1403-13.

LORENZ, H., HAILEY, D. W. & LIPPINCOTT-SCHWARTZ, J. 2006. Fluorescence protease protection of GFP chimeras to reveal protein topology and subcellular localization. *Nature methods,* 3**,** 205-10.

LOW, S. H., LI, X., MIURA, M., KUDO, N., QUINONES, B. & WEIMBS, T. 2003. Syntaxin 2 and endobrevin are required for the terminal step of cytokinesis in mammalian cells. *Developmental cell,* 4**,** 753-9.

LUKYANETZ, E. A. 1997. Development of the concepts on voltage-operated calcium channels. *Neurophysiology,* 29**,** 45-56.

LUSIN, J. D., VANAROTTI, M., LI, C., VALIVETI, A. & AMES, J. B. 2008. NMR structure of DREAM: Implications for Ca(2+)-dependent DNA binding and protein dimerization. *Biochemistry,* 47**,** 2252-64.

LUZIO, J. P., MULLOCK, B. M., PRYOR, P. R., LINDSAY, M. R., JAMES, D. E. & PIPER, R. C. 2001. Relationship between endosomes and lysosomes. *Biochemical Society transactions,* 29**,** 476-80.

LUZIO, J. P., PRYOR, P. R. & BRIGHT, N. A. 2007. Lysosomes: fusion and function. *Nature reviews. Molecular cell biology,* 8**,** 622-32.

LUZIO, J. P., ROUS, B. A., BRIGHT, N. A., PRYOR, P. R., MULLOCK, B. M. & PIPER, R. C. 2000. Lysosome-endosome fusion and lysosome biogenesis. *Journal of cell science,* 113 (Pt 9)**,** 1515-24.

MACARTHUR, M. W., DRISCOLL, P. C. & THORNTON, J. M. 1994. NMR and crystallography--complementary approaches to structure determination. *Trends in biotechnology,* 12**,** 149-53.

MAEDA, T., LEM, J., PALCZEWSKI, K. & HAESELEER, F. 2005. A critical role of CaBP4 in the cone synapse. *Invest Ophthalmol Vis Sci,* 46**,** 4320-7.

MAHLOOGI, H., GONZAÃÅLEZ-GUERRICO, A. M., DE CICCO, R. L., BASSI, D. E., GOODROW, T., BRAUNEWELL, K. H. & KLEIN-SZANTO, A. J. P. 2003. Overexpression of the calcium sensor visinin-like protein-1 leads to a cAMP-mediated decrease of in vivo and in vitro growth and invasiveness of squamous cell carcinoma cells. *Cancer research,* 63**,** 4997-5004.

MAHON, M. J. 2011. pHluorin2: an enhanced, ratiometric, pH-sensitive green florescent protein. *Advances in bioscience and biotechnology,* 2**,** 132-137.

MALAKHOV, M. P., MATTERN, M. R., MALAKHOVA, O. A., DRINKER, M., WEEKS, S. D. & BUTT, T. R. 2004. SUMO fusions and SUMO-specific protease for efficient expression and purification of proteins. *Journal of structural and functional genomics,* 5**,** 75-86.

MARTINEZ, I., CHAKRABARTI, S., HELLEVIK, T., MOREHEAD, J., FOWLER, K. & ANDREWS, N. W. 2000. Synaptotagmin VII regulates Ca(2+)-dependent exocytosis of lysosomes in fibroblasts. *The Journal of cell biology,* 148**,** 1141-49.

MARTINEZ-ARCA, S., RUDGE, R., VACCA, M., RAPOSO, G., CAMONIS, J., PROUX-GILLARDEAUX, V., DAVIET, L., FORMSTECHER, E., HAMBURGER, A., FILIPPINI, F., D'ESPOSITO, M. & GALLI, T. 2003. A dual mechanism controlling the localization and function of exocytic v-SNAREs. *Proceedings of the National Academy of Sciences of the United States of America,* 100**,** 9011-6.

MCCUE, H. V., BURGOYNE, R. D. & HAYNES, L. P. 2009. Membrane targeting of the EF-hand containing calcium-sensing proteins CaBP7 and CaBP8. *Biochem Biophys Res Commun,* 380**,** 825-31.

MCCUE, H. V., BURGOYNE, R. D. & HAYNES, L. P. 2011. Determination of the membrane topology of the small EF-hand Ca2+-sensing proteins CaBP7 and CaBP8. *PLoS One,* 6**,** e17853.

MCCUE, H. V., HAYNES, L. P. & BURGOYNE, R. D. 2010a. Bioinformatic analysis of CaBP/calneuron proteins reveals a family of highly conserved vertebrate Ca2+-binding proteins. *BMC Res Notes,* 3**,** 118.

MCCUE, H. V., HAYNES, L. P. & BURGOYNE, R. D. 2010b. The diversity of calcium sensor proteins in the regulation of neuronal function. *Cold Spring Harb Perspect Biol,* 2**,** a004085.

MCFERRAN, B. W., GRAHAM, M. E. & BURGOYNE, R. D. 1998. Neuronal Ca2+ sensor 1, the mammalian homologue of frequenin, is expressed in chromaffin and PC12 cells and regulates neurosecretion from dense-core granules. *J Biol Chem,* 273**,** 22768-72.

MCKAY, H. F. & BURGESS, D. R. 2011. 'Life is a highway': membrane trafficking during cytokinesis. *Traffic,* 12**,** 247-51.

MCNEIL, P. L. & TERASAKI, M. 2001. Coping with the inevitable: how cells repair a torn surface membrane. *Nature cell biology,* 3**,** E124-9.

MICHALAK, M., GROENENDYK, J., SZABO, E., GOLD, L. I. & OPAS, M. 2009. Calreticulin, a multi-process calcium-buffering chaperone of the endoplasmic reticulum. *Biochemical Journal,* 417**,** 651-666.

MIKHAYLOVA, M., HRADSKY, J. & KREUTZ, M. R. 2011. Between promiscuity and specificity: novel roles of EF-hand calcium sensors in neuronal Ca(2+) signalling. *Journal of neurochemistry,* 118**,** 695-713.

MIKHAYLOVA, M., REDDY, P. P., MUNSCH, T., LANDGRAF, P., SUMAN, S. K., SMALLA, K. H., GUNDELFINGER, E. D., SHARMA, Y. & KREUTZ, M. R. 2009. Calneurons provide a calcium threshold for trans-Golgi network to plasma membrane trafficking. *Proc Natl Acad Sci U S A,* 106**,** 9093-8.

MIKHAYLOVA, M., SHARMA, Y., REISSNER, C., NAGEL, F., ARAVIND, P., RAJINI, B., SMALLA, K. H., GUNDELFINGER, E. D. & KREUTZ, M. R. 2006. Neuronal Ca2+ signaling via caldendrin and calneurons. *Biochim Biophys Acta,* 1763**,** 1229-37.

MIKOSHIBA, K. 2007. The IP3 receptor/Ca2+ channel and its cellular function. *Biochemical Society symposium***,** 9-22.

MINOR, D. L., JR. & FINDEISEN, F. 2010. Progress in the structural understanding of voltage-gated calcium channel (CaV) function and modulation. *Channels,* 4**,** 459-74.

MITSUYAMA, F., SAWAI, T., CARAFOLI, E., FURUICHI, T. & MIKOSHIBA, K. 1999. Microinjection of Ca2+ store-enriched microsome fractions to dividing newt

eggs induces extra-cleavage furrows via inositol 1,4,5-trisphosphate-induced Ca2+ release. *Developmental biology,* 214**,** 160-7.

MONCRIEF, N. D., KRETSINGER, R. H. & GOODMAN, M. 1990. Evolution of EF-hand calcium-modulated proteins. I. Relationships based on amino acid sequences. *Journal of Molecular Evolution,* 30**,** 522-562.

MULLOCK, B. M., BRIGHT, N. A., FEARON, C. W., GRAY, S. R. & LUZIO, J. P. 1998. Fusion of lysosomes with late endosomes produces a hybrid organelle of intermediate density and is NSF dependent. *The Journal of cell biology,* 140**,** 591-601.

MUSKETT, F. W. 2011. Sample Preparation, Data Collection and Processing. *In:* ROBERTS, L.-Y. L. A. G. (ed.) *Protein NMR Spectroscopy: Practical Techniques and Applications.* Chichester, UK: John Wiley & Sons, Ltd.

MUTO, A., KUME, S., INOUE, T., OKANO, H. & MIKOSHIBA, K. 1996. Calcium waves along the cleavage furrows in cleavage-stage Xenopus embryos and its inhibition by heparin. *The Journal of cell biology,* 135**,** 181-90.

NAKAJIMA, Y. 2011. Ca(2+)-dependent binding of calcium-binding protein 1 to presynaptic group III metabotropic glutamate receptors and blockage by phosphorylation of the receptors. *Biochemical and biophysical research communications*.

NAKAMURA, T. Y., JEROMIN, A., MIKOSHIBA, K. & WAKABAYASHI, S. 2011. Neuronal calcium sensor-1 promotes immature heart function and hypertrophy by enhancing Ca2+ signals. *Circulation research,* 109**,** 512-23.

NELSON, M. R. & CHAZIN, W. J. 1998. Structures of EF-hand Ca2+-binding proteins: Diversity in the organization, packing and response to Ca2+ binding. *BioMetals,* 11**,** 297-318.

NETO, H., COLLINS, L. L. & GOULD, G. W. 2011. Vesicle trafficking and membrane remodelling in cytokinesis. *The Biochemical journal,* 437**,** 13-24.

NEUMANN, B., WALTER, T., HERICHE, J. K., BULKESCHER, J., ERFLE, H., CONRAD, C., ROGERS, P., POSER, I., HELD, M., LIEBEL, U., CETIN, C., SIECKMANN, F., PAU, G., KABBE, R., WUNSCHE, A., SATAGOPAM, V., SCHMITZ, M. H., CHAPUIS, C., GERLICH, D. W., SCHNEIDER, R., EILS, R., HUBER, W., PETERS, J. M., HYMAN, A. A., DURBIN, R., PEPPERKOK, R. & ELLENBERG, J. 2010. Phenotypic profiling

of the human genome by time-lapse microscopy reveals cell division genes. *Nature,* 464**,** 721-7.

NIKI, I., YOKOKURA, H., SUDO, T., KATO, M. & HIDAKA, H. 1996. Ca2+ signaling and intracellular Ca2+ binding proteins. *Journal of Biochemistry,* 120**,** 685-698.

NISHIMURA, N., PLUTNER, H., HAHN, K. & BALCH, W. E. 2002. The delta subunit of AP-3 is required for efficient transport of VSV-G from the trans-Golgi network to the cell surface. *Proceedings of the National Academy of Sciences of the United States of America,* 99**,** 6755-60.

NOGUCHI, T. & MABUCHI, I. 2002. Localized calcium signals along the cleavage furrow of the Xenopus egg are not involved in cytokinesis. *Molecular biology of the cell,* 13**,** 1263-73.

O'CALLAGHAN, D. W., HASDEMIR, B., LEIGHTON, M. & BURGOYNE, R. D. 2003. Residues within the myristoylation motif determine intracellular targeting of the neuronal Ca2+ sensor protein KChIP1 to post-ER transport vesicles and traffic of Kv4 K+ channels. *J Cell Sci,* 116**,** 4833-45.

OBERMULLER, S., KIECKE, C., VON FIGURA, K. & HONING, S. 2002. The tyrosine motifs of Lamp 1 and LAP determine their direct and indirect targetting to lysosomes. *Journal of cell science,* 115**,** 185-94.

OHKI, S. Y., IKURA, M. & ZHANG, M. 1997. Identification of Mg2+-binding sites and the role of Mg2+ on target recognition by calmodulin. *Biochemistry,* 36**,** 4309-4316.

OHYA, S. & HOROWITZ, B. 2002. Differential transcriptional expression of Ca2+ BP superfamilies in murine gastrointestinal smooth muscles. *American journal of physiology. Gastrointestinal and liver physiology,* 283**,** G1290-7.

OLAFSSON, P., WANG, T. & LU, B. 1995. Molecular cloning and functional characterization of the Xenopus Ca2+- binding protein frequenin. *Proceedings of the National Academy of Sciences of the United States of America,* 92**,** 8001-8005.

ON, C., MARSHALL, C. R., CHEN, N., MOYES, C. D. & TIBBITS, G. F. 2008. Gene structure evolution of the Na+-Ca2+ exchanger (NCX) family. *BMC evolutionary biology,* 8**,** 127.

OSAWA, M., DACE, A., TONG, K. I., VALIVETI, A., IKURA, M. & AMES, J. B. 2005. Mg2+ and Ca2+ differentially regulate DNA binding and dimerization of DREAM. *The Journal of biological chemistry,* 280**,** 18008-14.

OZ, S., TSEMAKHOVICH, V., CHRISTEL, C. J., LEE, A. & DASCAL, N. 2011. CaBP1 regulates voltage-dependent inactivation and activation of Ca(V)1.2 (L-type) calcium channels. *J Biol Chem,* 286**,** 13945-53.

PALCZEWSKI, K., SOKAL, I. & BAEHR, W. 2004. Guanylate cyclase-activating proteins: Structure, function, and diversity. *Biochemical and biophysical research communications,* 322**,** 1123-1130.

PALMITER, R. D. 1974. Magnesium precipitation of ribonucleoprotein complexes. Expedient techniques for the isolation of undergraded polysomes and messenger ribonucleic acid. *Biochemistry,* 13**,** 3606-15.

PANKRATOVA, E. V., SYTINA, E. V. & STEPCHENKO, A. G. 1994. Cell differentiation in vitro and the expression of Oct-2 protein and oct-2 RNA. *FEBS letters,* 338**,** 81-4.

PARK, J. S., STEINBACH, S. K., DESAUTELS, M. & HEMMINGSEN, S. M. 2009. Essential role for Schizosaccharomyces pombe pik1 in septation. *PloS one,* 4**,** e6179.

PARK, S., LI, C. & AMES, J. B. 2011. Nuclear magnetic resonance structure of calcium-binding protein 1 in a Ca(2+) -bound closed state: Implications for target recognition. *Protein Sci*.

PAULS, T. L., COX, J. A. & BERCHTOLD, M. W. 1996. The Ca2+-binding proteins parvalbumin and oncomodulin and their genes: New structural and functional findings. *Biochimica et Biophysica Acta - Gene Structure and Expression,* 1306**,** 39-54.

PECHERE, J. F., DERANCOURT, J. & HAIECH, J. 1977. The participation of parvalbumins in the activation relaxation cycle of vertebrate fast skeletal muscle. *FEBS letters,* 75**,** 111-114.

PEDRAZZINI, E., VILLA, A. & BORGESE, N. 1996. A mutant cytochrome b5 with a lengthened membrane anchor escapes from the endoplasmic reticulum and reaches the plasma membrane. *Proceedings of the National Academy of Sciences of the United States of America,* 93**,** 4207-12.

PELHAM, H. R. 2001. Traffic through the Golgi apparatus. *The Journal of cell biology,* 155**,** 1099-101.

PELISSIER, A., CHAUVIN, J. P. & LECUIT, T. 2003. Trafficking through Rab11 endosomes is required for cellularization during Drosophila embryogenesis. *Current biology : CB,* 13**,** 1848-57.

PERSECHINI, A. & STEMMER, P. M. 2002. Calmodulin is a limiting factor in the cell. *Trends in cardiovascular medicine,* 12**,** 32-37.

PETERSEN, O. H., MICHALAK, M. & VERKHRATSKY, A. 2005. Calcium signalling: Past, present and future. *Cell Calcium,* 38**,** 161-169.

PETKO, J. A., KABBANI, N., FREY, C., WOLL, M., HICKEY, K., CRAIG, M., CANFIELD, V. A. & LEVENSON, R. 2009. Proteomic and functional analysis of NCS-1 binding proteins reveals novel signaling pathways required for inner ear development in zebrafish. *BMC Neurosci,* 10**,** 27.

PITT, S. J., FUNNELL, T. M., SITSAPESAN, M., VENTURI, E., RIETDORF, K., RUAS, M., GANESAN, A., GOSAIN, R., CHURCHILL, G. C., ZHU, M. X., PARRINGTON, J., GALIONE, A. & SITSAPESAN, R. 2010. TPC2 is a novel NAADP-sensitive Ca2+ release channel, operating as a dual sensor of luminal pH and Ca2+. *The Journal of biological chemistry,* 285**,** 35039-46.

POLANS, A., BAEHR, W. & PALCZEWSKI, K. 1996. Turned on by Ca2+! The physiology and pathology of Ca2+-binding proteins in the retina. *Trends in neurosciences,* 19**,** 547-554.

POLANS, A. S., BUCZYLKO, J., CRABB, J. & PALCZEWSKI, K. 1991. A photoreceptor calcium binding protein is recognized by autoantibodies obtained from patients with cancer-associated retinopathy. *Journal of Cell Biology,* 112**,** 981-989.

POLEVOY, G., WEI, H. C., WONG, R., SZENTPETERY, Z., KIM, Y. J., GOLDBACH, P., STEINBACH, S. K., BALLA, T. & BRILL, J. A. 2009. Dual roles for the Drosophila PI 4-kinase four wheel drive in localizing Rab11 during cytokinesis. *The Journal of cell biology,* 187**,** 847-858.

POLISHCHUK, E. V., DI PENTIMA, A., LUINI, A. & POLISHCHUK, R. S. 2003. Mechanism of constitutive export from the golgi: bulk flow via the formation, protrusion,

and en bloc cleavage of large trans-golgi network tubular domains. *Molecular biology of the cell,* 14**,** 4470-85.

PONGS, O., LINDEMEIER, J., ZHU, X. R., THEIL, T., ENGELKAMP, D., KRAH-JENTGENS, I., LAMBRECHT, H. G., KOCH, K. W., SCHWEMER, J., RIVOSECCHI, R., MALLART, A., GALCERAN, J., CANAL, I., BARBAS, J. A. & FERRUS, A. 1993. Frequenin - A novel calcium-binding protein that modulates synaptic efficacy in the Drosophila nervous system. *Neuron,* 11**,** 15-28.

PROUX-GILLARDEAUX, V., RAPOSO, G., IRINOPOULOU, T. & GALLI, T. 2007. Expression of the Longin domain of TI-VAMP impairs lysosomal secretion and epithelial cell migration. *Biology of the cell / under the auspices of the European Cell Biology Organization,* 99**,** 261-71.

PRUUNSILD, P. & TIMMUSK, T. 2005. Structure, alternative splicing, and expression of the human and mouse KCNIP gene family. *Genomics,* 86**,** 581-593.

RABU, C., SCHMID, V., SCHWAPPACH, B. & HIGH, S. 2009. Biogenesis of tail-anchored proteins: the beginning for the end? *Journal of cell science,* 122**,** 3605-12.

REBELLO, M. R., AKTAS, A. & MEDLER, K. F. 2011. Expression of calcium binding proteins in mouse type II taste cells. *J Histochem Cytochem,* 59**,** 530-9.

REISCH, N., AESCHLIMANN, A., GAY, S. & SPROTT, H. 2006. The DREAM of pain relief. *Current Rheumatology Reviews,* 2**,** 69-82.

RENNER, M., DANIELSON, M. A. & FALKE, J. J. 1993. Kinetic control of Ca(II) signaling: Tuning the ion dissociation rates of EF-hand Ca(II) binding sites. *Proceedings of the National Academy of Sciences of the United States of America,* 90**,** 6493-6497.

RIEKE, F., LEE, A. & HAESELEER, F. 2008. Characterization of Ca2+-binding protein 5 knockout mouse retina. *Invest Ophthalmol Vis Sci,* 49**,** 5126-35.

RIZO, J. & SUDHOF, T. C. 1998. C2-domains, structure and function of a universal Ca2+-binding domain. *Journal of Biological Chemistry,* 273**,** 15879-15882.

ROMANI, A. & SCARPA, A. 1992. Regulation of cell magnesium. *Archives of biochemistry and biophysics,* 298**,** 1-12.

RUAS, M., RIETDORF, K., ARREDOUANI, A., DAVIS, L. C., LLOYD-EVANS, E., KOEGEL, H., FUNNELL, T. M., MORGAN, A. J., WARD, J. A., WATANABE, K., CHENG, X., CHURCHILL, G. C., ZHU, M. X., PLATT, F. M., WESSEL, G. M., PARRINGTON, J. &

GALIONE, A. 2010. Purified TPC Isoforms Form NAADP Receptors with Distinct Roles for Ca(2+) Signaling and Endolysosomal Trafficking. *Current biology : CB,* 20**,** 703-9.

SAMPATH, A. P., STRISSEL, K. J., ELIAS, R., ARSHAVSKY, V. Y., MCGINNIS, J. F., CHEN, J., KAWAMURA, S., RIEKE, F. & HURLEY, J. B. 2005. Recoverin improves rod-mediated vision by enhancing signal transmission in the mouse retina. *Neuron,* 46**,** 413-420.

SCHAAD, N. C., DE CASTRO, E., NEF, S., HEGI, S., HINRICHSEN, R., MARTONE, M. E., ELLISMAN, M. H., SIKKINK, R., RUSNAK, F., SYGUSH, J. & NEF, P. 1996. Direct modulation of calmodulin targets by the neuronal calcium sensor NCS-1. *Proc Natl Acad Sci U S A,* 93**,** 9253-8.

SCHNURRA, I., BERNSTEIN, H. G., RIEDERER, P. & BRAUNEWELL, K. H. 2001. The neuronal calcium sensor protein VILIP-1 is associated with amyloid plaques and extracellular tangles in Alzheimer's disease and promotes cell death and tau phosphorylation in vitro: a link between calcium sensors and Alzheimer's disease? *Neurobiol Dis,* 8**,** 900-9.

SCHOLLMEYER, J. E. 1988. Calpain II involvement in mitosis. *Science,* 240**,** 911-3.

SCHRODER, T., LILIE, H. & LANGE, C. 2011. The myristoylation of guanylate cyclase-activating protein-2 causes an increase in thermodynamic stability in the presence but not in the absence of Ca(2+). *Protein Sci,* 20**,** 1155-65.

SCHROEDER, T. E. & STRICKLAND, D. L. 1974. Ionophore A23187, calcium and contractility in frog eggs. *Experimental cell research,* 83**,** 139-42.

SCHWALLER, B. 2009. The continuing disappearance of "pure" Ca2+ buffers. *Cellular and Molecular Life Sciences,* 66**,** 275-300.

SCHWENK, J., ZOLLES, G., KANDIAS, N. G., NEUBAUER, I., KALBACHER, H., COVARRUBIAS, M., FAKLER, B. & BENTROP, D. 2008. NMR analysis of KChIP4a reveals structural basis for control of surface expression of Kv4 channel complexes. *The Journal of biological chemistry,* 283**,** 18937-46.

SEIDENBECHER, C. I., LANDWEHR, M., SMALLA, K. H., KREUTZ, M., DIETERICH, D. C., ZUSCHRATTER, W., REISSNER, C., HAMMARBACK, J. A., BOCKERS, T. M., GUNDELFINGER, E. D. & KREUTZ, M. R. 2004. Caldendrin but not calmodulin binds to light chain 3 of MAP1A/B: an association with the microtubule

cytoskeleton highlighting exclusive binding partners for neuronal Ca(2+)-sensor proteins. *J Mol Biol,* 336**,** 957-70.

SEIDENBECHER, C. I., LANGNAESE, K., SANMARTI-VILA, L., BOECKERS, T. M., SMALLA, K. H., SABEL, B. A., GARNER, C. C., GUNDELFINGER, E. D. & KREUTZ, M. R. 1998. Caldendrin, a novel neuronal calcium-binding protein confined to the somato-dendritic compartment. *J Biol Chem,* 273**,** 21324-31.

SHIH, P. Y., LIN, C. L., CHENG, P. W., LIAO, J. H. & PAN, C. Y. 2009. Calneuron I inhibits Ca(2+) channel activity in bovine chromaffin cells. *Biochem Biophys Res Commun,* 388**,** 549-53.

SHU, D. G., LUO, H. L., CONWAY MORRIS, S., ZHANG, X. L., HU, S. X., CHEN, L., HAN, J., ZHU, M., LI, Y. & CHEN, L. Z. 1999. Lower Cambrian vertebrates from south China. *Nature,* 402**,** 42-46.

SHUSTER, C. B. & BURGESS, D. R. 2002. Targeted new membrane addition in the cleavage furrow is a late, separate event in cytokinesis. *Proceedings of the National Academy of Sciences of the United States of America,* 99**,** 3633-8.

SKOP, A. R., LIU, H., YATES, J., 3RD, MEYER, B. J. & HEALD, R. 2004. Dissection of the mammalian midbody proteome reveals conserved cytokinesis mechanisms. *Science,* 305**,** 61-6.

SMALLA, K. H., SEIDENBECHER, C. I., TISCHMEYER, W., SCHICKNICK, H., WYNEKEN, U., BOCKERS, T. M., GUNDELFINGER, E. D. & KREUTZ, M. R. 2003. Kainate-induced epileptic seizures induce a recruitment of caldendrin to the postsynaptic density in rat brain. *Brain Res Mol Brain Res,* 116**,** 159-62.

SMYTH, J. T., DEHAVEN, W. I., JONES, B. F., MERCER, J. C., TREBAK, M., VAZQUEZ, G. & PUTNEY JR, J. W. 2006. Emerging perspectives in store-operated Ca2+ entry: Roles of Orai, Stim and TRP. *Biochimica et Biophysica Acta - Molecular Cell Research,* 1763**,** 1147-1160.

SNYDER, D. A., CHEN, Y., DENISSOVA, N. G., ACTON, T., ARAMINI, J. M., CIANO, M., KARLIN, R., LIU, J., MANOR, P., RAJAN, P. A., ROSSI, P., SWAPNA, G. V., XIAO, R., ROST, B., HUNT, J. & MONTELIONE, G. T. 2005. Comparisons of NMR spectral quality and success in crystallization demonstrate that NMR and X-ray crystallography are complementary methods for small protein structure determination. *Journal of the American Chemical Society,* 127**,** 16505-11.

SONG, M. Y. & YUAN, J. X. 2010. Introduction to TRP channels: structure, function, and regulation. *Advances in experimental medicine and biology,* 661**,** 99-108.

SONG, S. J., KIM, S. J., SONG, M. S. & LIM, D. S. 2009. Aurora B-mediated phosphorylation of RASSF1A maintains proper cytokinesis by recruiting Syntaxin16 to the midzone and midbody. *Cancer research,* 69**,** 8540-4.

STEFANOVIC, S. & HEGDE, R. S. 2007. Identification of a targeting factor for posttranslational membrane protein insertion into the ER. *Cell,* 128**,** 1147-59.

STEFER, S., REITZ, S., WANG, F., WILD, K., PANG, Y. Y., SCHWARZ, D., BOMKE, J., HEIN, C., LOHR, F., BERNHARD, F., DENIC, V., DOTSCH, V. & SINNING, I. 2011. Structural basis for tail-anchored membrane protein biogenesis by the Get3-receptor complex. *Science,* 333**,** 758-62.

STEPHEN, R., BERETA, G., GOLCZAK, M., PALCZEWSKI, K. & SOUSA, M. C. 2007. Stabilizing function for myristoyl group revealed by the crystal structure of a neuronal calcium sensor, guanylate cyclase-activating protein 1. *Structure,* 15**,** 1392-402.

SU, Q., MOCHIDA, S., TIAN, J. H., MEHTA, R. & SHENG, Z. H. 2001. SNAP-29: a general SNARE protein that inhibits SNARE disassembly and is implicated in synaptic transmission. *Proceedings of the National Academy of Sciences of the United States of America,* 98**,** 14038-43.

SUBACH, F. V., SUBACH, O. M., GUNDOROV, I. S., MOROZOVA, K. S., PIATKEVICH, K. D., CUERVO, A. M. & VERKHUSHA, V. V. 2009. Monomeric fluorescent timers that change color from blue to red report on cellular trafficking. *Nature chemical biology,* 5**,** 118-26.

SUN, L., GOROSPE, J. R., HOFFMAN, E. P. & RAO, A. K. 2007. Decreased platelet expression of myosin regulatory light chain polypeptide (MYL9) and other genes with platelet dysfunction and CBFA2/RUNX1 mutation: insights from platelet expression profiling. *J Thromb Haemost,* 5**,** 146-54.

TAKEUCHI, T., SARASHINA, I., IIJIMA, M. & ENDO, K. 2008. In vitro regulation of CaCO(3) crystal polymorphism by the highly acidic molluscan shell protein Aspein. *FEBS letters,* 582**,** 591-6.

TAKIMOTO, K., YANG, E. K. & CONFORTI, L. 2002. Palmitoylation of KChIP splicing variants is required for efficient cell surface expression of Kv4.3 channels. *The Journal of biological chemistry,* 277**,** 26904-11.

TAKUWA, N., ZHOU, W. & TAKUWA, Y. 1995. Calcium, calmodulin and cell cycle progression. *Cellular signalling,* 7**,** 93-104.

TANG, N., LIN, T., YANG, J., FOSKETT, J. K. & OSTAP, E. M. 2007. CIB1 and CaBP1 bind to the myo1c regulatory domain. *J Muscle Res Cell Motil,* 28**,** 285-91.

TAVERNA, E., FRANCOLINI, M., JEROMIN, A., HILFIKER, S., RODER, J. & ROSA, P. 2002. Neuronal calcium sensor 1 and phosphatidylinositol 4-OH kinase beta interact in neuronal cells and are translocated to membranes during nucleotide-evoked exocytosis. *J Cell Sci,* 115**,** 3909-22.

TENG, F. Y., WANG, Y. & TANG, B. L. 2001. The syntaxins. *Genome biology,* 2**,** REVIEWS3012.

TERASAKI, M. & JAFFE, L. A. 1991. Organization of the sea urchin egg endoplasmic reticulum and its reorganization at fertilization. *The Journal of cell biology,* 114**,** 929-40.

THEISGEN, S., THOMAS, L., SCHRODER, T., LANGE, C., KOVERMANN, M., BALBACH, J. & HUSTER, D. 2011. The presence of membranes or micelles induces structural changes of the myristoylated guanylate-cyclase activating protein-2. *European biophysics journal : EBJ,* 40**,** 565-76.

THOMAS, A. P., BIRD, G. S., HAJNOCZKY, G., ROBB-GASPERS, L. D. & PUTNEY, J. W., JR. 1996. Spatial and temporal aspects of cellular calcium signaling. *The FASEB journal : official publication of the Federation of American Societies for Experimental Biology,* 10**,** 1505-17.

TIPPENS, A. L. & LEE, A. 2007. Caldendrin, a neuron-specific modulator of Cav/1.2 (L-type) Ca2+ channels. *J Biol Chem,* 282**,** 8464-73.

TOGO, T. & STEINHARDT, R. A. 2004. Nonmuscle myosin IIA and IIB have distinct functions in the exocytosis-dependent process of cell membrane repair. *Molecular biology of the cell,* 15**,** 688-95.

TOMAS, A., FUTTER, C. & MOSS, S. E. 2004. Annexin 11 is required for midbody formation and completion of the terminal phase of cytokinesis. *The Journal of cell biology,* 165**,** 813-22.

TOMBES, R. M. & BORISY, G. G. 1989. Intracellular free calcium and mitosis in mammalian cells: anaphase onset is calcium modulated, but is not triggered by a brief transient. *The Journal of cell biology,* 109**,** 627-36.

TOROK, K., THOROGATE, R. & HOWELL, S. 2002. Studying the spatial distribution of Ca(2+)-binding proteins. How does it work for calmodulin? *Methods in molecular biology,* 173**,** 383-407.

TOROK, K., WILDING, M., GROIGNO, L., PATEL, R. & WHITAKER, M. 1998. Imaging the spatial dynamics of calmodulin activation during mitosis. *Current biology : CB,* 8**,** 692-9.

TOUTENHOOFD, S. L. & STREHLER, E. E. 2000. The calmodulin multigene family as a unique case of genetic redundancy: Multiple levels of regulation to provide spatial and temporal control of calmodulin pools? *Cell Calcium,* 28**,** 83-96.

UETAKE, Y. & SLUDER, G. 2004. Cell cycle progression after cleavage failure: mammalian somatic cells do not possess a "tetraploidy checkpoint". *The Journal of cell biology,* 165**,** 609-15.

VAN DALEN, A. & DE KRUIJFF, B. 2004. The role of lipids in membrane insertion and translocation of bacterial proteins. *Biochimica et biophysica acta,* 1694**,** 97-109.

VAN DAMME, D., INZE, D. & RUSSINOVA, E. 2008. Vesicle trafficking during somatic cytokinesis. *Plant physiology,* 147**,** 1544-52.

VIJAY-KUMAR, S. & COOK, W. J. 1992. Structure of a sarcoplasmic calcium-binding protein from Nereis diversicolor refined at 2.0 A resolution. *Journal of molecular biology,* 224**,** 413-26.

VRANKEN, W. F., BOUCHER, W., STEVENS, T. J., FOGH, R. H., PAJON, A., LLINAS, M., ULRICH, E. L., MARKLEY, J. L., IONIDES, J. & LAUE, E. D. 2005. The CCPN data model for NMR spectroscopy: development of a software pipeline. *Proteins,* 59**,** 687-96.

WALCH-SOLIMENA, C. & NOVICK, P. 1999. The yeast phosphatidylinositol-4-OH kinase pik1 regulates secretion at the Golgi. *Nature cell biology,* 1**,** 523-525.

WANG, K. 2008. Modulation by clamping: Kv4 and KChIP interactions. *Neurochem Res,* 33**,** 1964-9.

WATSON, R. T. & PESSIN, J. E. 2001. Transmembrane domain length determines intracellular membrane compartment localization of syntaxins 3, 4, and 5. *American journal of physiology. Cell physiology,* 281**,** C215-23.

WAUGH, D. S. 2005. Making the most of affinity tags. *Trends in biotechnology,* 23**,** 316-20.

WEBB, S. E., LI, W. M. & MILLER, A. L. 2008. Calcium signalling during the cleavage period of zebrafish development. *Philosophical transactions of the Royal Society of London. Series B, Biological sciences,* 363**,** 1363-9.

WEIDBERG, H., SHVETS, E., SHPILKA, T., SHIMRON, F., SHINDER, V. & ELAZAR, Z. 2010. LC3 and GATE-16/GABARAP subfamilies are both essential yet act differently in autophagosome biogenesis. *The EMBO journal,* 29**,** 1792-802.

WEINL, S. & KUDLA, J. 2009. The CBL-CIPK Ca(2+)-decoding signaling network: function and perspectives. *The New phytologist,* 184**,** 517-528.

WEISENBERG, R. C. & TIMASHEFF, S. N. 1970. Aggregation of microtubule subunit protein. Effects of divalent cations, colchicine and vinblastine. *Biochemistry,* 9**,** 4110-6.

WEISS, J. L., ARCHER, D. A. & BURGOYNE, R. D. 2000. Neuronal Ca2+ sensor-1/frequenin functions in an autocrine pathway regulating Ca2+ channels in bovine adrenal chromaffin cells. *J Biol Chem,* 275**,** 40082-7.

WEISS, J. L., HUI, H. & BURGOYNE, R. D. 2010. Neuronal calcium sensor-1 regulation of calcium channels, secretion, and neuronal outgrowth. *Cell Mol Neurobiol,* 30**,** 1283-92.

WHITAKER, M. 2006. Calcium microdomains and cell cycle control. *Cell calcium,* 40**,** 585-92.

WILDING, M., WRIGHT, E. M., PATEL, R., ELLIS-DAVIES, G. & WHITAKER, M. 1996. Local perinuclear calcium signals associated with mitosis-entry in early sea urchin embryos. *The Journal of cell biology,* 135**,** 191-9.

WILSON, G. M., FIELDING, A. B., SIMON, G. C., YU, X., ANDREWS, P. D., HAMES, R. S., FREY, A. M., PEDEN, A. A., GOULD, G. W. & PREKERIS, R. 2005. The FIP3-Rab11 protein complex regulates recycling endosome targeting to the cleavage furrow during late cytokinesis. *Molecular biology of the cell,* 16**,** 849-60.

WINGARD, J. N., CHAN, J., BOSANAC, I., HAESELEER, F., PALCZEWSKI, K., IKURA, M. & AMES, J. B. 2005. Structural analysis of Mg2+ and Ca2+ binding to CaBP1, a neuron-specific regulator of calcium channels. *J Biol Chem,* 280**,** 37461-70.

WISHART, D. S. & SYKES, B. D. 1994. The 13C chemical-shift index: a simple method for the identification of protein secondary structure using 13C chemical-shift data. *Journal of biomolecular NMR,* 4**,** 171-80.

WONG, R., FABIAN, L., FORER, A. & BRILL, J. A. 2007. Phospholipase C and myosin light chain kinase inhibition define a common step in actin regulation during cytokinesis. *BMC cell biology,* 8**,** 15.

WONG, S. H., XU, Y., ZHANG, T., GRIFFITHS, G., LOWE, S. L., SUBRAMANIAM, V. N., SEOW, K. T. & HONG, W. 1999. GS32, a novel Golgi SNARE of 32 kDa, interacts preferentially with syntaxin 6. *Molecular biology of the cell,* 10**,** 119-34.

WOODS, A. S., MARCELLINO, D., JACKSON, S. N., FRANCO, R., FERRE, S., AGNATI, L. F. & FUXE, K. 2008. How calmodulin interacts with the adenosine A(2A) and the dopamine D(2) receptors. *Journal of proteome research,* 7**,** 3428-34.

WU, Y. Q., LIN, X., LIU, C. M., JAMRICH, M. & SHAFFER, L. G. 2001. Identification of a human brain-specific gene, calneuron 1, a new member of the calmodulin superfamily. *Mol Genet Metab,* 72**,** 343-50.

XIONG, H., XIA, K., LI, B., ZHAO, G. & ZHANG, Z. 2009. KChIP1: A potential modulator to GABAergic system. *Acta Biochimica et Biophysica Sinica,* 41**,** 295-300.

XU, H., BRILL, J. A., HSIEN, J., MCBRIDE, R., BOULIANNE, G. L. & TRIMBLE, W. S. 2002. Syntaxin 5 is required for cytokinesis and spermatid differentiation in Drosophila. *Developmental biology,* 251**,** 294-306.

YAKOVLEVA, T., BAZOV, I., CEBERS, G., MARINOVA, Z., HARA, Y., AHMED, A., VLASKOVSKA, M., JOHANSSON, B., HOCHGESCHWENDER, U., SINGH, I. N., BRUCE-KELLER, A. J., HURD, Y. L., KANEKO, T., TERENIUS, L., EKSTROM, T. J., HAUSER, K. F., PICKEL, V. M. & BAKALKIN, G. 2006. Prodynorphin storage and processing in axon terminals and dendrites. *The FASEB journal : official publication of the Federation of American Societies for Experimental Biology,* 20**,** 2124-6.

YAMAGATA, K., GOTO, K., KUO, C. H., KONDO, H. & MIKI, N. 1990. Visinin: a novel calcium binding protein expressed in retinal cone cells. *Neuron,* 4**,** 469-476.

YANG, J., MCBRIDE, S., MAK, D. O., VARDI, N., PALCZEWSKI, K., HAESELEER, F. & FOSKETT, J. K. 2002a. Identification of a family of calcium sensors as protein ligands of inositol trisphosphate receptor Ca(2+) release channels. *Proc Natl Acad Sci U S A,* 99**,** 7711-6.

YANG, J., MCBRIDE, S., MAK, D. O. D., VARDI, N., PALCZEWSKI, K., HAESELEER, F. & FOSKETT, J. K. 2002b. Identification of a family of calcium sensors as protein ligands of inositol trisphosphate receptor Ca2+ release channels. *Proceedings of the National Academy of Sciences of the United States of America,* 99**,** 7711-7716.

YANG, P. S., ALSEIKHAN, B. A., HIEL, H., GRANT, L., MORI, M. X., YANG, W., FUCHS, P. A. & YUE, D. T. 2006a. Switching of Ca2+-dependent inactivation of Ca(v)1.3 channels by calcium binding proteins of auditory hair cells. *J Neurosci,* 26**,** 10677-89.

YANG, X., XU, P., XIAO, Y., XIONG, X. & XU, T. 2006b. Domain requirement for the membrane trafficking and targeting of syntaxin 1A. *The Journal of biological chemistry,* 281**,** 15457-63.

YEE, A. A., SAVCHENKO, A., IGNACHENKO, A., LUKIN, J., XU, X., SKARINA, T., EVDOKIMOVA, E., LIU, C. S., SEMESI, A., GUIDO, V., EDWARDS, A. M. & ARROWSMITH, C. H. 2005. NMR and X-ray crystallography, complementary tools in structural proteomics of small proteins. *Journal of the American Chemical Society,* 127**,** 16512-7.

YU, Y. Y., DAI, G., PAN, F. Y., CHEN, J. & LI, C. J. 2005. Calmodulin regulates the post-anaphase reposition of centrioles during cytokinesis. *Cell research,* 15**,** 548-52.

ZAAL, K. J., SMITH, C. L., POLISHCHUK, R. S., ALTAN, N., COLE, N. B., ELLENBERG, J., HIRSCHBERG, K., PRESLEY, J. F., ROBERTS, T. H., SIGGIA, E., PHAIR, R. D. & LIPPINCOTT-SCHWARTZ, J. 1999. Golgi membranes are absorbed into and reemerge from the ER during mitosis. *Cell,* 99**,** 589-601.

ZEITZ, C., KLOECKENER-GRUISSEM, B., FORSTER, U., KOHL, S., MAGYAR, I., WISSINGER, B., MATYAS, G., BORRUAT, F. X., SCHORDERET, D. F., ZRENNER,

E., MUNIER, F. L. & BERGER, W. 2006. Mutations in CABP4, the gene encoding the Ca2+-binding protein 4, cause autosomal recessive night blindness. *Am J Hum Genet,* 79**,** 657-67.

ZEITZ, C., LABS, S., LORENZ, B., FORSTER, U., UKSTI, J., KROES, H. Y., DE BAERE, E., LEROY, B. P., CREMERS, F. P., WITTMER, M., VAN GENDEREN, M. M., SAHEL, J. A., AUDO, I., POLOSCHEK, C. M., MOHAND-SAID, S., FLEISCHHAUER, J. C., HUFFMEIER, U., MOSKOVA-DOUMANOVA, V., LEVIN, A. V., HAMEL, C. P., LEIFERT, D., MUNIER, F. L., SCHORDERET, D. F., ZRENNER, E., FRIEDBURG, C., WISSINGER, B., KOHL, S. & BERGER, W. 2009. Genotyping microarray for CSNB-associated genes. *Invest Ophthalmol Vis Sci,* 50**,** 5919-26.

ZENG, Q., TRAN, T. T., TAN, H. X. & HONG, W. 2003. The cytoplasmic domain of Vamp4 and Vamp5 is responsible for their correct subcellular targeting: the N-terminal extenSion of VAMP4 contains a dominant autonomous targeting signal for the trans-Golgi network. *The Journal of biological chemistry,* 278**,** 23046-54.

ZHANG, D., BOULWARE, M. J., PENDLETON, M. R., NOGI, T. & MARCHANT, J. S. 2007. The inositol 1,4,5-trisphosphate receptor (Itpr) gene family in Xenopus: identification of type 2 and type 3 inositol 1,4,5-trisphosphate receptor subtypes. *The Biochemical journal,* 404**,** 383-391.

ZHAO, X., VARNAI, P., TUYMETOVA, G., BALLA, A., TOTH, Z. E., OKER-BLOM, C., RODER, J., JEROMIN, A. & BALLA, T. 2001. Interaction of neuronal calcium sensor-1 (NCS-1) with phosphatidylinositol 4-kinase beta stimulates lipid kinase activity and affects membrane trafficking in COS-7 cells. *J Biol Chem,* 276**,** 40183-9.

ZHENG, Q., BOBICH, J. A., VIDUGIRIENE, J., MCFADDEN, S. C., THOMAS, F., RODER, J. & JEROMIN, A. 2005. Neuronal calcium sensor-1 facilitates neuronal exocytosis through phosphatidylinositol 4-kinase. *J Neurochem,* 92**,** 442-51.

ZHOU, H., KIM, S. A., KIRK, E. A., TIPPENS, A. L., SUN, H., HAESELEER, F. & LEE, A. 2004. Ca2+-binding protein-1 facilitates and forms a postsynaptic complex with Cav1.2 (L-type) Ca2+ channels. *J Neurosci,* 24**,** 4698-708.

ZHOU, H., YU, K., MCCOY, K. L. & LEE, A. 2005. Molecular mechanism for divergent regulation of Cav1.2 Ca2+ channels by calmodulin and Ca2+-binding protein-1. *J Biol Chem,* 280**,** 29612-9.

ZHU, M. X., EVANS, A. M., MA, J., PARRINGTON, J. & GALIONE, A. 2010a. Two-pore channels for integrative Ca signaling. *Communicative & integrative biology,* 3**,** 12-7.

ZHU, M. X., MA, J., PARRINGTON, J., GALIONE, A. & EVANS, A. M. 2010b. TPCs: Endolysosomal channels for Ca2+ mobilization from acidic organelles triggered by NAADP. *FEBS letters,* 584**,** 1966-74.

ZUO, X., LI, S., HALL, J., MATTERN, M. R., TRAN, H., SHOO, J., TAN, R., WEISS, S. R. & BUTT, T. R. 2005. Enhanced expression and purification of membrane proteins by SUMO fusion in Escherichia coli. *Journal of structural and functional genomics,* 6**,** 103-11.